CARBONATE LEACHING OF URANIUM FROM INDIAN ALKALINE HOST ROCKS USING OXYGEN: MATHEMATICAL MODELING AND EXPERIMENTAL VALIDATION

By

K. Anand Rao

Registration No.: ENGG01200904032

BHABHA ATOMIC RESEARCH CENTRE

A thesis submitted to the
Board of Studies in Engineering Sciences Discipline

In partial fulfillment of requirements
For the Degree of

DOCTOR OF PHILOSOPHY
of
HOMI BHABHA NATIONAL INSTITUTE

September, 2015

HOMI BHABHA NATIONAL INSTITUTE

Recommendations of the Viva Voce Board

As members of the Viva Voce Board, we certify that we have read the dissertation prepared by **Mr. K. Anand Rao** entitled **"Carbonate leaching of uranium from Indian alkaline host rocks using oxygen: mathematical modelling and experimental validation"** and recommend that it may be accepted as fulfilling the dissertation requirement for the Degree of Doctor of Philosophy.

---Date: 27/4/2016
Chairman: **Dr. P.K. Vijayan**

---Date: 27/4/2016
Guide/Convener: **Dr. A.K. Suri**

---Date: 27/4/16
Co-Guide: **Dr. MadhuVinjamur**

---Date: 27-04-2016
Member 1: **Prof. J.C. Mandal, IITB, Mumbai**

* ---Date: 10/5/2016
Member 2: **Dr. K. Velusamy, IGCAR, Kalpakkam**

---Date: 27-04-2016
Member 3: **Dr. A.K. Nayak, RED, BARC**

---Date: 27/4/16
Technology Advisor: **Dr. T. Sreenivas, MinD, BARC, Hyderabad**

---Date: 27-4-2016
External Examiner: **Prof. S. Subramanian, IISc, Bangalore**

Final approval and acceptance of this dissertation is contingent upon the candidate's submission of the final copies of dissertation to HBNI.

I hereby certify that I have read this dissertation prepared under my direction and recommend that it may be accepted as fulfilling the dissertation requirement.

Date: 27/4/2016
Place: HomiBhabha National Institute, Mumbai

Dr. A.K. Suri
Bhabha Atomic Research Centre, Mumbai **(Guide)**

Dr. MadhuVinjamur
Indian Institute of Technology, Mumbai **(Co-Guide)**

* Though I could not attend the viva voce of Shri K. Anand Rao, I agree with the decision of the committee.

STATEMENT BY AUTHOR

This dissertation has been submitted in partial fulfillment of requirements for an advanced degree at Homi Bhabha National Institute (HBNI) and is deposited in the library to be made available to borrowers under rules of the HBNI.

Brief quotations from this dissertation are allowable without special permission, provided that accurate acknowledgement of source is made. Requests for permission for extended quotation from or reproduction of this manuscript in whole or in part may be granted by the Competent Authority of HBNI when in his or her judgment the proposed use of the material is in the interests of scholarship. In all other instances, however, permission must be obtained from the author.

K. Anand Rao

[K. Anand Rao]

DECLARATION

I, hereby declare that the investigation presented in the thesis has been carried out by me. The work is original and has not been submitted earlier as a whole or in part for a degree / diploma at this or any other Institution / University.

K. Anand Rao

[K. Anand Rao]

List of Publications arising from the thesis

Journals

1. Continuous leaching of uranium from an Indian ore: Residence time scale up and heat effects. **K. Anand Rao**, T. Sreenivas, Madhu Vinjamur, A.K. Suri, *Hydrometallurgy*, 146 (2014) 119-127. (**http://dx.doi.org/10.1016/j.hydromet.2014.03.014**).

2. Application of a topochemical reaction model to predict leaching behavior of high carbonate uranium ores in alkaline solutions: An experimental case study. **K. Anand Rao** and A.K. Suri, *Hydrometallurgy*, 141 (2014) 67–75. (**http://dx.doi.org/10.1016/j.hydromet.2013.10.005**).

3. Kinetics of alkaline leaching of UO_2 and FeS_2 in co-existing system. **K. Anand Rao**, T. Sreenivas, Madhu Vinjamur, A.K. Suri, *Transactions of the Indian Institute of Metals*, 69(1) (2016) 23-31. **(http://dx.doi.org/10.1007/s12666-015-0615-8)**.

Conferences

1. Statistical modelling and optimization of alkaline leaching of uranium from synthetic mixture of minerals, **K. Anand Rao**, T. Sreenivas, Madhu Vinjamur and A.K. Suri, Proceedings of International Seminar on Mineral Processing Technology (MPT2 015) held at Visakhapatnam, India during 11-13 Mar'2015.

2. Leaching kinetics of UO_2 and FeS_2 in co-existing systems under oxidative alkaline conditions. **K. Anand Rao**, T. Sreenivas and Madhu Vinjamur, Proceedings of 52nd National Metallurgists Day and 68th Annual Technical Meeting of the Indian Institute of Metals (NMD-ATM-2014) held at Pune, India during 12-15 Nov'2014.

3. Pore diffusion controlled leaching model incorporating particle size distribution: A case study. **K Anand Rao** and T. Sreenivas, Proceedings of International Seminar on Mineral Processing Technology (MPT 2013) held at IMMT, Bhubaneswar, India during December 10 – 13, 2013 **(Received Mishra Award of Indian Institute of Mineral Engineers (IIME) in the session on 'Hydro and Electrometallurgy')**.

4. Kinetic model coupling particle size distribution for alkaline leaching of uranium, **K. Anand Rao**, N.P.H. Padmanabhan and A.K. Suri, Proceedings of XXVI International Mineral Processing Congress (IMPC) 2012 held at New Delhi, India during September 24-28, 2012. – **A peer reviewed paper.**

5. Kinetics of Batch leaching of low grade uranium ore using distributed rate constant model, **K. Anand Rao**, N.P.H. Padmanabhan and A.K. Suri, Proceedings of International Seminar on Mineral Processing Technology (MPT 2011), October 2011, Udaipur.

6. A kinetic model for alkaline leaching of uranium from dolomitic limestone ore, **K. Anand Rao**, T. Sreenivas, R.R. Venkitakrishnan, Md. Serajuddin, P. Karthikayini and N.P.H. Padmanabhan, Proceedings of XI International seminar on MPT 2010 held at NML, Jamshedpur during 15-17 December 2010.

7. Studies on enhancement of leachability of refractory uranium minerals in autoclave reactor, T. Sreenivas, **K. Anand Rao**, M. Manmadha Rao, K.C. Rajan, Md. Serajuddin, P. Karthikayini and N.P.H. Padmanabhan, Proceedings of XI International seminar on MPT 2010 held at NML, Jamshedpur during 15-17 December 2010.

8. Process development studies for low-grade uranium deposit in alkaline host rocks of Tummalapalle. A.K. Suri, N.P.H Padmanabhan, T. Sreenivas, **K. Anand Rao**, A.K. Singh, K.T. Shenoy, T. Mishra and S.K. Ghosh. Proceedings of IAEA Technical Meeting on Low-grade uranium deposits at Vienna, March 2010.

Course work completed

1. "Colloids and Interfacial Engineering – CL656" by Prof. Rochish Thaokar & Prof. Rajdip Bandopadhyay, Dept. of Chemical Engineering, IIT-Mumbai, Jan-June 2010. (Grade: AA).

2. "Experimental Methods – CL610" by Prof. Juvekar and Prof. Rajdip Bandyopadhyay, Dept. of Chemical Engineering, IIT-Mumbai, Jan-June 2010. (Grade: BB).

3. “Optimization – CL603” by Prof. Santosh Naronha, Dept. of Chemical Engineering, IIT-Mumbai, Jan-June 2010. (Grade: CC).

Credit seminars

1. “Design and Analysis of Experiments” presented on 3rd January, 2014 at HBNI.

Comprehensive viva

Held on 3rd January 2014 at HBNI, Mumai.

Pre-synopsis viva

Held on 28th January 2015 at Hall 7, BARC, Mumbai

Dedicated to

My Beloved Parents, Kacham Bala Krishna Rao & Kodipyaka Rajya Laxmi and my wife Bysani Shilpa

A space for

My children Kacham Anish Kumar and Kacham Amartya

Acknowledgements

The author expresses deep and sincere gratitude to his guide **Prof. A. K. Suri**, Raja Ramanna Fellow, Bhabha Atomic Research Centre for his constant support, encouragement, and invaluable guidance. The author would like to extend his heartfelt gratitude to his co-guide **Prof. Madhu Vinjamur**, Department of Chemical Engineering, Indian Institute of Technology, Mumbai for the fruitful discussions, advice and the kind reviews from time to time. He will be forever indebted to his technical advisor, **Prof. T. Sreenivas**, Head, Mineral Processing Division, Bhabha Atomic Research Centre (BARC), for the consistent and invaluable encouragement, timely discussions and suggestions throughout the period of doctoral studies. The author conveys his sincere thanks to **Dr. J.K. Chakravartty**, Director, Materials Group, BARC, for his kind support, permissions as and when required, and encouragement during the course of PhD studies.

The author expresses his sincere gratitude to **Shri R.N. Jayaraj**, Ex Chief Executive, and **Dr. N. Saibaba**, Chief Executive of Nuclear Fuel Complex, Hyderabad for providing pure UO_2 samples on which part of the studies were carried out. Thanks are conveyed to **Shri Ramendra Gupta**, Ex C&MD, Uranium Corporation of India Limited, Jaduguda for providing uranium ore samples from Tummalapalle in Andhra Pradesh and Gogi in Karnataka. The author also thanks **Shri Parihar**, Director, Atomic Minerals Directorate for Exploration and Research, for extending the services and facilities of Petrological, XRF, XRD and Chemical laboratories. The author owes a special thanks to **Dr. A.K. Sahoo**, Glass Ceramics Division, BARC, for porosimetry and **Dr. Bhaskar Pal**, Materials Science Division, BARC, for exhaustive Scanning Electron Microscopic studies. Sincere thanks are conveyed to **Dr. (Smt.) Sulekha Mukhopadhyay**, Chemical Engineering Division of BARC for her friendly support and advice.

The author wishes to thank **Dr. N.P.H. Padmanabhan**, Ex Head, Mineral Processing Division and all the members of Mineral Processing Division for their help at various stages of his doctoral work. Finally, the author would like to express gratitude to his parents, parents-in-law, wife, children and friends for their understanding and support during the course of the work.

K. Anand Rao

K. Anand Rao

SYNOPSIS

1. INTRODUCTION

Uranium is the chief nuclear fuel used for generating eco-friendly electricity with carbon footprint as low as 28 tons of CO_2 e/GWh [1]. At present, about 11% of the world's total electricity (373 GWe) is produced through nuclear power plants. It is expected to grow to about 511 GWe by 2030 according to a low-case projection by International Atomic Energy Agency (IAEA) [1]. The contribution of nuclear energy to the overall electricity generation in India is about 3%. India also envisages raise in nuclear power to 63 GWe by 2032 from the current level of 5.3 GWe. The growth forecast of nuclear power, globally as well as in India, has led to increased interest in extraction of uranium from complex ores with characteristics like low tenor (<0.1% U_3O_8), refractory nature and high carbonate content (>10%), all of which make them expensive for exploitation.

Leaching is at the heart of processes for extraction of uranium from its ores. Chemical nature of gangue minerals rather than uranium minerals often dictate the type of leachant (acidic/alkaline) used for extraction of uranium. Cheaper acid leachant is preferred for the ores containing siliceous minerals as main gangue; expensive alkali leachant is necessary to extract uranium for ores having > 10% carbonate gangue.

The focus of this thesis is on modeling and measuring the kinetics of alkaline leaching of uranium from lean tenor, high carbonate content synthetic mixture as well as Indian uranium ores available at: Tummalapalle in Andhra Pradesh and Gogi in Karnataka.

1.1. URANIUM RESOURCES, PRODUCTION AND DEMAND

Uranium is recovered from ores containing 0.01 to 23% U_3O_8. The chief economic minerals are: uraninite (U_3O_8 / UO_2), pitchblende (UO_2) and coffinite $U(SiO_4)_{1-x}(OH)_{4x}$ [2,3]. Total known resources of uranium, as reported in early 2013, amount to 76,35,200 tons [4]. About 50% of the world's uranium resources occur in three countries namely, Australia (highest, about 22%), Kazakhstan (13%) and Russian Federation (11%). India has about 1,19,900 tons (1.6%) of uranium resources.

Based on the 2013 uranium production statistics, about 400 tons of uranium were produced in India and about 59,673 tons of uranium were produced worldwide [1]. The current annual demand of uranium in India is ≈715 tons, and across the world, is ≈66883 tons. The supply demand gap of uranium is speculated to increase all over the world in general and India in particular [4].

1.2. MOTIVATION

The commercial importance of alkaline leaching of uraniferous ores in India has increased due to the discovery of two uranium ore deposits: Tummalapalle (Andhra Pradesh) and Gogi (Karnataka). The host rock of former deposit is Phosphatic Silicious Calcitic Dolostone (PSCD) and that of the latter is brecciated Limestone. The uranium resource at Tummalapalle is a low grade one (≈ 0.04% U_3O_8), with proven estimates of 81,000 tons of uranium in 9.5 km strike length. It is the single largest deposit found in India so far and has the potential to become the world's largest uranium deposit with probable estimates of 8,00,000 tons of uranium over a total strike length of 160 km [5]. A commercial mill with a throughput of 3000 tons of ore per day has been recently commissioned at Tummalapalle. A number of satellite deposits are envisaged in this belt of uranium resource, the characteristics of which may vary in mineralogy including tenor of the ore, pyrite content etc. from pocket to pocket. Hence, studies to understand the leaching behavior of Tummalapalle ore including the effects of the variations in ore characteristics will be of utmost use in maximizing the recovery of uranium in the existing / under expansion / new mills in and around this deposit. Another small deposit at Gogi in the Karnataka state of India also has high calcium carbonate content with 4000 tons of estimated uranium reserves with a medium grade of 0.2% U_3O_8. A uranium plant is being designed for this deposit. Utilization of the above two important resources of uranium in India at Tummalapalle and Gogi is essential for reducing the gap between demand and supply of uranium required for indigenous nuclear reactors.

With the imminent need for increasing uranium production in India, the present work is focused on understanding the fundamentals of leaching of uranium, the heart of the uranium extraction process, from two newly discovered lean grade Indian uranium ores of high carbonate content.

1.3. OBJECTIVES AND SCOPE OF THE THESIS

The objectives of the thesis include: (1) development of kinetic models for dissolution of uranium dioxide (UO_2), the chief uranium mineral of economic interest, and iron pyrite (FeS_2), the common reactive gangue mineral in uranium ores (under basic studies), (2) development of kinetic models for leaching efficiencies of uranium in actual Indian ores, namely, Tummalapalle in Andhra Pradesh and Gogi in Karnataka (under applied studies), (3) determination of the optimum values of leaching parameters like reagent concentration, pressure, temperature, particle size for mixture of minerals, as well as for uranium ores, (4) comparison of alkaline leaching behavior of synthetic mixture (Ideal system) with actual uranium ores, (5) unveiling beneficial and deleterious effects of presence of the reactive gangue mineral, iron pyrite, on leaching of uranium, (6) characterization and corroboration of the feed and leach residues with regard to underlying microscopic phenomenon in alkaline leaching of pure minerals and low grade Indian alkaline host rock deposits, (7) quantification of the role of oxygen in alkaline leaching of uranium from Indian ores containing uraninite (U_3O_8) mineral, (8) scale up of the alkaline leaching process from batch level to continuous pilot level, using residence time distribution, and (9) validation of heat effects in the continuous leaching model on pilot scale for extrapolation to commercial alkaline leaching plant data of an Indian uranium ore.

Understanding the dissolution of pure uranium dioxide and iron pyrite minerals is essential for the understanding of the leaching of more complex natural ores. Hence, initial experiments were carried out on the leaching of pure minerals both as individual and in the form of synthetic mixture followed by the experiments on actual low grade Indian uranium ores. Kinetic models were developed for leaching of synthetic mixture as well as the actual uranium ores as a function of process parameters, including temperature, pressure, leaching reagent concentrations, and particle size. Interference effects of the reactive gangue mineral (iron pyrite) on the leaching performance, were analyzed, initially based on the synthetic mixture, and subsequently corroborated with the data from Indian uranium ores. The investigations were supported by extensive and detailed characterization using techniques such as X-ray diffraction, X-ray Fluorescence, wet chemical analyses, optical microscopy, and scanning electron microscopy. Finally, batch kinetic data of uranium leaching from a lean Indian uranium ore from

Tummalapalle, was applied to multiple continuous stirred tank reactors using the Residence Time Distribution (RTD) model. The model was used to predict leaching efficiencies and rise in temperature of the reactor, which happen mostly due to conversion of iron pyrites present in the ore. A good comparison is obtained for several different operating conditions of the pilot and commercial scale reactors. Figure.1. summarizes the components of the research work conducted.

2. LITERATURE SURVEY

2.1. Extraction Technology of Uranium

Mining of uranium bearing ores is carried out by open-pit and underground techniques. The uranium is generally extracted by hydrometallurgical route which includes the following steps (1) crushing (2) grinding (3) acid / alkaline leaching (4) concentration and purification by ion exchange / solvent extraction and (5) precipitation as intermediate concentrate, commonly known as ‘yellow cake’ [6,7,8]. The 4th step of concentration and purification is generally not found necessary when alkaline leaching is adopted as the alkaline leach liquors are purer in comparison to the acid leach liquors.

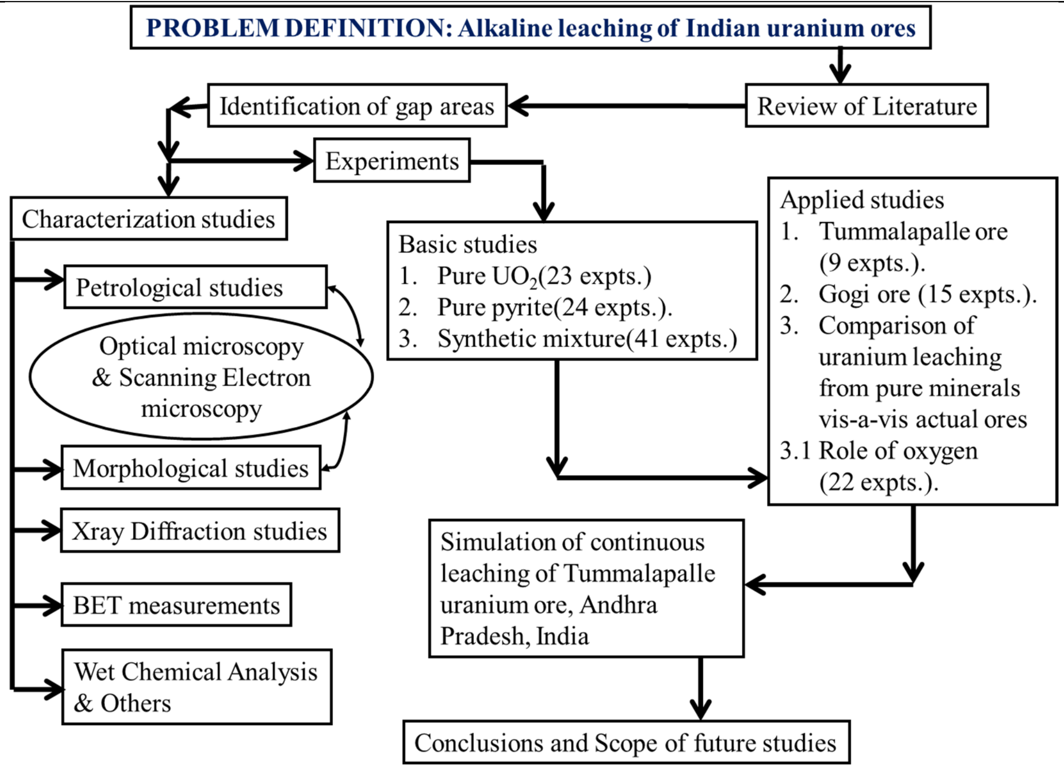

Fig.1. The research layout

The intermediate uranium concentrate is then refined by solvent extraction, followed by precipitation as Ammonium Diuranate, which is calcined to nuclear fuel, the pure UO_2.

2.2. Operating Uranium Mills based on Alkaline Leaching Technology

At present, there are only four uranium plants operating all over the world using alkaline leaching technology as reported in the Red Book published every year by International Atomic Energy Agency [4]. (1) The Rozna uranium mill in the Czech Republic is the oldest plant, operating since 1957, based on alkaline leaching technology. It produces about 300 tons Uranium/annum from Metamorphite type of deposit with an average grade of 0.251% U, (2) Langer Heinrich in Namibia processes calcrete type of ore deposit (ROM grade = 0.045% U), (3) Azelik – Teguidda in Niger processes sandstone type with 0.2% U ore grade, and (4) Tummalapalle in India processes carbonate type of ore deposit (ROM grade = 0.034% U) using pressurized alkaline leaching technology. This chapter in the thesis gives details of all the above operating plants, and those of a few other committed plants based on alkaline leaching technology.

2.3. Modeling of Alkaline Leaching Process

Uranium is oxidized from +4 oxidation state to +6 oxidation state followed by complexation with carbonate ions during carbonate leaching of uranium according to chemical reactions given below.

$$2UO_2 + O_2 \rightarrow 2UO_3 \qquad [1]$$

$$UO_3 + Na_2CO_3 + 2NaHCO_3 \rightarrow Na_4UO_2(CO_3)_3 + H_2O \qquad [2]$$

$$UO_3 + 3Na_2CO_3 + H_2O \rightarrow Na_4UO_2(CO_3)_3 + 2NaOH \qquad [2a]$$

$$NaOH + NaHCO_3 \rightarrow Na_2CO_3 + H_2O \qquad [2b]$$

$$2Na_4UO_2(CO_3)_3 + 6NaOH \rightarrow Na_2U_2O_7 + 6Na_2CO_3 + 3H_2O \qquad [3]$$

Chemical reaction (3) precipitates uranium as $Na_2U_2O_7$ if NaOH formed in reaction (2a) is not neutralized by reaction (2b). If any pyrite (FeS_2) is present in the ore, the following reaction also takes place during alkaline leaching with Na_2CO_3-$NaHCO_3$ leachants.

$$4FeS_2 + 15O_2 + 16Na_2CO_3 + 14H_2O \rightarrow 16NaHCO_3 + 4Fe(OH)_3 + 8Na_2SO_4 \qquad [4]$$

The chemical reactions during extraction of uranium into the fluid phase from ground ore are controlled by various factors, of which, main ones are: (1) degree of liberation of uranium mineral in the ore, (2) grain size of uranium mineral, (3) porosity of host rock including gangue as well as uranium minerals, (4) type of leachant, (5) type of oxidant, and (6) system properties like temperature, pressure, stirring speed and type of stirrer. Various mathematical models available in literature for fitting the experimental kinetic data of leaching are summarized in Figure.2.

Dissolution of UO_2 in carbonate or acid medium was suggested to take place in two consecutive steps [9]: (1) Oxidation of UO_2 to UO_3, followed by, (2) Dissolution of UO_3 by complexing with CO_3^{-2} ions. Habashi and Thurston have first proposed that the dissolution of UO_2 is driven by an electrochemical mechanism similar to the corrosion of metals [10]. Schortmann and Desesa deduced a Michaelis–Menten type kinetic rate equation using an electrochemical mechanism which was validated with exhaustive kinetic data of leaching of pure UO_2 using Na_2CO_3 and $NaHCO_3$ [11]. Several authors have studied the dissolution of pyrite in alkaline media from coal and systems other than uranium ores [12, 13]. A number of publications are available on alkaline leaching kinetics of uranium dioxide from ores that contain low pyrite [14, 15].

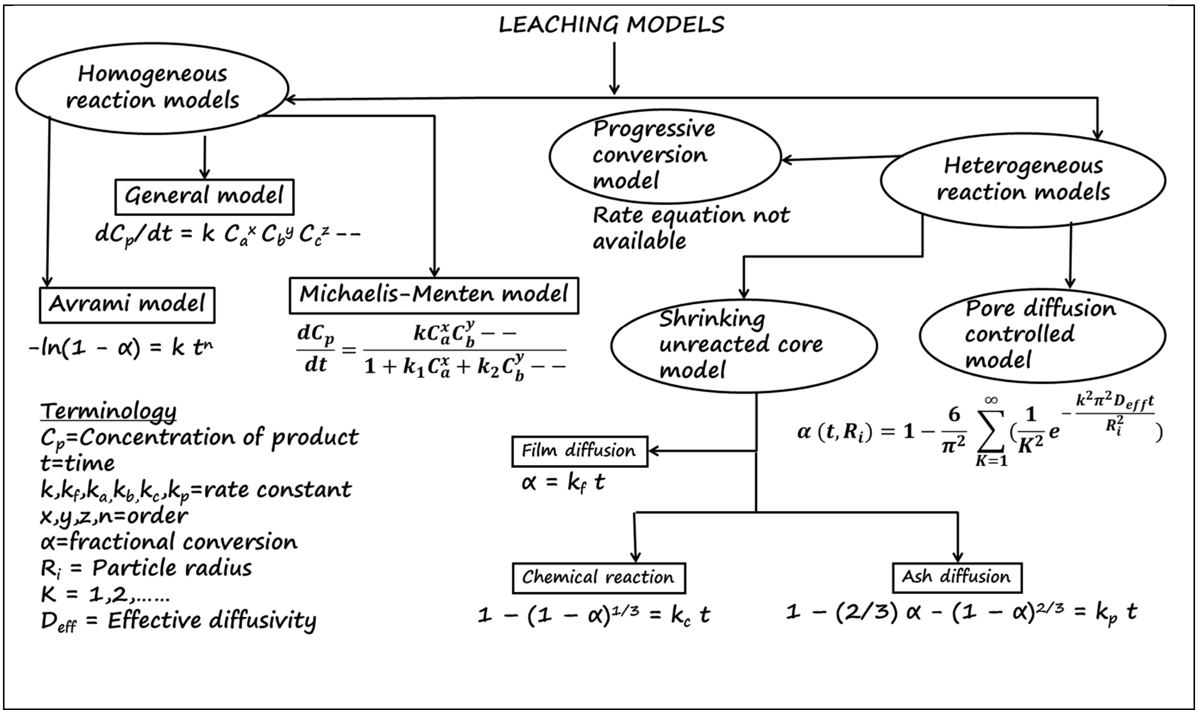

Fig.2. Various leaching models available for fitting experimental kinetic data and their governing rate equations

2.4. Gap Areas in Alkaline Leaching of Uranium

The following areas were identified, after exhaustive literature review, as those needing significant enhancement of technical knowledge, and have therefore been taken up in the present study.

Sulphide minerals, particularly iron pyrite, are commonly found gangue in uranium ores. They react with alkaline reagents used for leaching of uranium. Many authors have reported the kinetics of dissolution of pure UO_2 and pure pyrite separately in carbonate solutions. However, there is no focused study published on alkaline leaching of coexistent (Uranium Dioxide + Pyrite) system. Hence, the present attempt at combined leaching of uranium dioxide and pyrite in the present studies should help in enhancing the understanding of the leaching behavior of uranium ores containing pyrite. Pyrite under alkaline conditions of different temperature, pressure, CO_3^{2-} concentration, etc., oxidizes to one or more of the compounds: FeO, Fe_2O_3, $Fe(CO_3)$ and $Fe(OH)_2$ and $Fe(OH)_3$. There do not appear to be any reported studies on identification of the iron oxide phase formed under the alkaline leaching conditions specific to Indian uranium ores.

Most of the uranium leaching models reported in literature are developed for widely practiced insitu leaching, which accounted for 47% of the world's uranium production in the year 2013 [1]. These models are based on film diffusion controlling mechanism as in situ leaching involves dissolving uranium by circulating the acidic/alkaline reagent in a porous ore body (forming a film over the solid phase), and pumping the pregnant solution to the surface. Limited data is available on heterogeneous models for extraction of uranium by agitation leaching which is controlled by either surface chemical reaction or ash diffusion, but not film diffusion. Moreover, variations in particle size and its distribution likely to occur in heterogeneous systems are not incorporated in the heterogeneous models cited in literature for uranium leaching from the ores.

There is no reference to any previous work on modeling of leaching of prominent Indian deposits like Tummalapalle and Gogi. Engineering scale up of batch leaching to continuous industrial scale autoclave for Indian uranium ores based on alkaline leaching is also not dealt with. Hence, exhaustive studies on leaching of the two Indian uranium ores (referenced above) were conducted eliciting the effect of temperature, pressure, reagent concentrations, particle size and its distribution.

The leaching process is essentially a microscopic phenomenon controlled by diffusion and/or reaction of solvent molecules with those of solid. Morphological changes that occur during leaching of pure UO_2 and Pyrite minerals vis-à-vis the two Indian uranium ores (Gogi and Tummalapalle) have not been reported in literature so far. Therefore, an in-depth morphological study, using optical and scanning electron microscopes, formed an integral part of the current work.

3. MATERIALS USED AND THEIR CHARACTERIZATION

The leaching experiments were carried out on synthetic mixtures of pure minerals, as well as on actual uranium ores. The synthetic mixtures included one or more of the following pure materials that constitute the bulk of Indian alkaline host rocks (1) Uranium Dioxide (UO_2), (2) Iron Pyrite (FeS_2), (3) Calcite ($CaCO_3$), and (4) Silica (SiO_2). Separate leaching experiments were conducted on two Indian uranium ores: (1) Tummalapalle in Andhra Pradesh and (2) Gogi in Karnataka. Na_2CO_3 and $NaHCO_3$ of L.R. grade (99.5% pure) were used to prepare the solutions of leachant in required concentrations in various experiments. Distilled water was used for leaching of pure mineral samples and normal tap water was used for leaching of actual uranium ores. The preselected commercial grade (99.6% pure) gas (O_2 / N_2 / Ar), drawn from a pressurized cylinder, was used to maintain the required total pressure in the reaction vessel. This chapter on materials and their characterization is divided into five sections.

3.1. Physical Properties

This section presents results of the measured specific gravities of all the solid feed materials, specific surface areas of different size fractions determined by Brunauer, Emmett and Teller (BET) method and the porosimetry of two uranium ores used in the studies.

3.3. Chemical Analyses

The purity of calcite, pyrite and UO_2 specimen was found to be >99% from the analyses carried out by volumetry (permanganometry), gravimetry and Davies-Gray titration methods respectively.

Silica was found to be 99.6% pure by molybdenum blue method using UV-visible spectrophotometer. The whole rock analyses of the Tummalapalle and Gogi uranium ores were also carried out by chemical analyses, from which the U_3O_8 assays were found to be 0.048% and 0.193% respectively.

3.4. X-ray Diffraction Analyses

The mineral phases in pure materials and in the two ore samples were ascertained by their unit cell parameters and the characteristic peaks identified in the respective Xray-diffractograms.

3.5. Optical and Scanning Electron Microscopy

The observation of leaching phenomena at microscopic scale, being the direct evidence of what has occurred during leaching, would be of immense use in understanding the leaching of uranium. Hence, the grain mounts of pure mineral samples were prepared using glass slides and observed under an optical microscope.

Sieve fractions of ground ore samples of Tummalapalle and Gogi uranium ores were partitioned into different density fractions using heavy media like bromoform and methylene iodide. Methylene iodide heavies were further separated by magnetic separation in two stages for removal of magnetite and concentration of uranium minerals. Microscopic grain counting of all the mass fractions was carried out using Reflected light (RL) for identifying opaque (ore / metallic) minerals and Transmitted light (TL) for identifying gangue (nonmetallic) minerals. Auto-radiography by Solid State Nuclear Tract Detection (SSNTD) technique using alpha sensitive cellulose nitrate 85 film was also carried out on all fractions to estimate the distribution of radioactive phases in various mineral fractions. The results and details of the above procedure followed for estimating the complete mineralogical analyses of two uranium ore samples are given in this section of the thesis.

Optical micrographs shown in Figure.3. revealed that the two ores have high content of carbonate minerals as gangue and uraninite/pitchblende/coffinite as main uranium minerals. Figure. 3[A] shows intimate association of uraninite with pyrite in Tummalapalle ore and Figure.3[B] shows the Coffinite mineral with alpha tracks in Gogi ore. Several other authors also reported occurrence of uranium minerals such as coffinite, uraninite / pitchblende and brannerite in association with sulphide minerals, in Tummalapalle ore and Coffinite mineral in Gogi ore [16, 17, 18].

To get more insight into the morphology, the powdered samples of pure materials or specific ore samples were sprinkled on a double sided carbon tape pasted to a brass disk (1” dia. x 1” height). They were examined under Scanning Electron Microscope (SEM) attached with Energy Dispersive X-ray spectroscope (EDX) model CAMSCAN MB 2300 CT/100 (United Kingdom make) with a 5 nm resolution and 10 to 5,00,000 times magnification. The EDX analysis showing characteristic peaks of Mg, Ca, Fe and S in scanning electron micrographs confirmed the presence of dolostone and pyrite minerals in Tummalapalle ore. Scanning electron micrograph of Gogi ore shows crystallized pyrite embedded in calcite and dolomite, and free and liberated vein type pyrite.

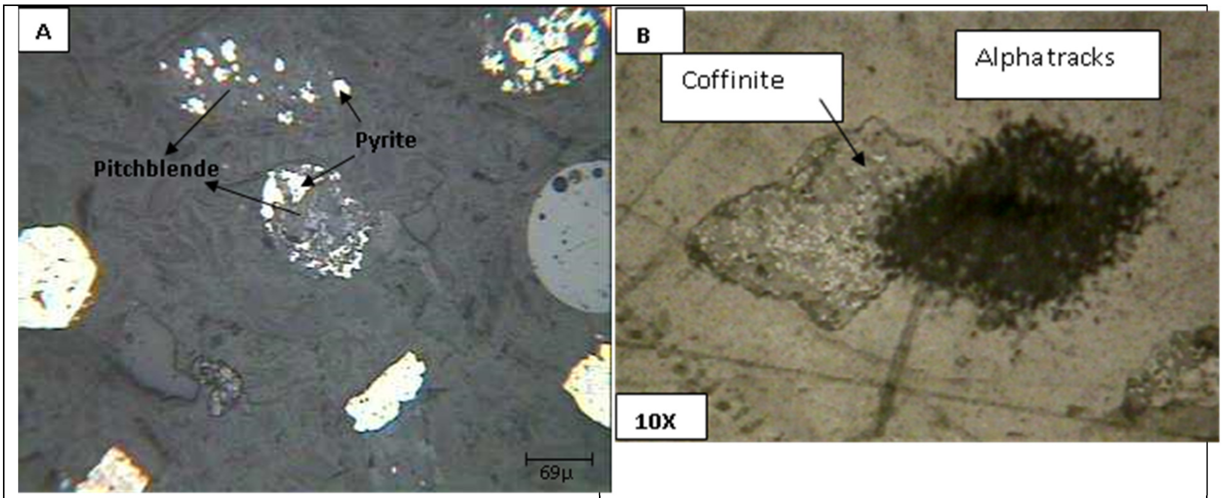

Fig.3. Optical micrographs obtained with Reflected Light, 1 Nicol [A] Discrete finer pitchblende grains in intimate association with pyrite in Tummalapalle Ore [B] Coffinite with alpha tracks in Gogi Uranium Ore

4. EQUIPMENT AND EXPERIMENTAL METHODS

Details of the equipment and method of leaching are presented in section 4.1, followed by the chemical analyses and procedures are described in section 4.2.

4.1. Leaching Experiments

The powdered feed samples were wet sieved into required sizes for use in leaching experiments. Autoclaves of 1-litre (twin autoclaves of glass and stainless steel (SS)) and 5-litre capacity (SS) were used for leaching experiments with pure minerals and uranium ores, respectively. Both the autoclaves are similar and have the same features to control temperature, pressure, and rotation speed of the impeller. The features of the autoclaves are described below.

The 1-litre autoclave consists of two separate interchangeable cylindrical cells, one made of glass and the other made of SS. Each of these cells are 0.1 m in internal diameter and 0.16 m in height. The system is designed for use of any one vessel at a time. The borosilicate glass vessel is used for leaching below 423 K and 6 bar, SS vessel is used for conditions up to 473 K and 50 bar pressure. Both vessels have a common SS top lid coupled to a motor with a magnetic seal. The lid is equipped with a two-stage gas induction, pitched blade turbine type impeller of 0.04 m diameter, a thermo well for thermocouple, a tube for oxygen feed, sample addition device for charging samples to the autoclaves under high temperature and pressure, cooling water coil, pressure sensor, rupture disk and solenoid valve to release pressure when it exceeds the set point inside the reactor. The oxygen inlet tube is connected to oxygen cylinder through oxygen gas mass flow controller, which permits flow when the pressure inside the reactor is below the set value. Electrical heating pads are wrapped all around outside the SS vessel and insulated. For glass vessel, however, the electrical heater was provided only at the bottom to visualize the leaching process inside the reactor. Heaters of both the vessels were connected to a common temperature indicator and controller. Cooling water tank with pump was provided with an auto mechanism of starting the pump whenever temperature in the vessel rises due to exothermicity of the reactions. A separate autoclave reactor system of 5-litre capacity (made of stain less steel), provided with all the above features of 1-litre autoclave reactor, was used for leaching of natural uranium ores. The reactor height, reactor diameter and the impeller (two stage gas induction pitched blade turbine type) diameter of 5-litre autoclave are 0.32 m and 0.15 m and 0.05 m respectively.

Predetermined amounts of pure minerals (7 g / 35 g) of single mineral or mixture of minerals was accurately weighed and taken in a beaker. A volume of 700 ml of water was mixed with these minerals and loaded into the autoclave. The reactor vessel was closed and agitated to suspend the solids. The contents were heated and when the set temperature was attained, the vessel was pressurized up to the desired level with preselected gas (O_2/N_2/Ar) drawn from a cylinder. A solution containing predetermined amounts of Na_2CO_3 and $NaHCO_3$ was added to the reactor under pressure using a pressure pot. The agitation speed was controlled using a Variable Frequency Drive (VFD). The time of reaction was considered as zero at this point. Leaching continued for pre-set time of 6 h for most of the experiments. Samples of leach liquor were drawn periodically for chemical analyses to monitor the kinetics of leaching. Leaching tests were repeated to check the reproducibility of results.

Experiments on Indian uranium ores were conducted in 5-L autoclave using 1 kg dry ore of specific size distribution obtained by grinding the ore in a batch ball mill for suitable time period. Required amount of water mixed with ore was loaded into the autoclave subsequently following the procedures adopted for the case of pure minerals described above.

4.2. Chemical Analysis Procedures

Leach liquor samples of 3 – 5 ml were drawn through the sample draining port, fitted with a filter; at the following times in minutes: 10, 20, 30, 60, 90, 120, 150, 180, 240, 300 and 360. The samples were analysed for dissolved uranium (as U_3O_8 equivalent) by spectrofluorimetry and for dissolved sulphate, if pyrite is present in the feed solids, by gravimetry. Solid samples at the end of 360 min were also analysed for uranium (as U_3O_8 equivalent) and sulfur (for pyrite containing feed samples) contents by pellet fluorimetry and gravimetry respectively. These values were used for computing back U_3O_8 and FeS_2 in the feed. The Back Calculated Feed (BCF) values and the concentrations of U_3O_8 and SO_4^{2-} in leach liquor were used to calculate conversion either or both of uranium and pyrite, as the case may be, with time in each leaching test. Carbonate and bicarbonate concentrations in the leach liquor samples were analysed by volumetry. For all experiments, the sodium balance was checked using concentrations of Na_2CO_3 and $NaHCO_3$ in the input and the concentrations of Na_2SO_4, Na_2CO3 and $NaHCO_3$ in the output leach liquor.

5. MODELING OF KINETICS OF DISSOLUTION OF SINGLE AND BINARY MIXTURES OF URANIUM DIOXIDE AND PYRITE (BASIC STUDIES)

The details of experimental results are presented in five sections; Section 5.1 describes results obtained with pure UO_2 (19 experiments), Section 5.2 for pure iron pyrite (23 experiments) and Section 5.3 for synthetic mixture of UO_2, iron pyrite, silica and calcite (32 experiments). Scanning electron micrographs of pure minerals before and after leaching are compared in section 5.4. Results of the decomposition of pure sodium bicarbonate in solution are discussed in the last section 5.5.

5.1. Pure Uranium dioxide

Dissolution behaviour of UO_2 in alkaline media was studied and a kinetic model was developed in the 'window' of conditions under which the specific ores of Indian origin are to be processed. Several authors published Michaelis–Menten type of rate equation for representing dissolution of pure UO_2. However, the models either do not have all the empirical constants (shows only the trends of dissolution with respect to particular leaching parameter) or have not been developed in the range of leaching parameters adopted for the two uranium ores dealt in the present study. The kinetic rate equation developed through experiments using Na_2CO_3 and $NaHCO_3$ leachants conducted in 1 litre autoclave is: $\frac{\mathrm{dC}}{\mathrm{dt}} = \frac{99.1\times[\mathrm{Na}^2\mathrm{CO}^3]^{0.24}\times[\mathrm{NaHCO_3}]^{0.09}\times \mathrm{Po_2}^{0.58}\times d^{-0.2762}\times e^{-\frac{4440.8}{T}}}{(3\text{ x }10^{-7}\times \mathrm{Na_2CO_3}^{0.24})+(1.5\text{x}10^{-4}\times \mathrm{NaHCO_3}^{0.09})+(1.9\text{x}10^{-5}\times \mathrm{Po_2}^{0.58})}$, where C is the mg of UO_2 dissolved per litre per minute of leaching period, P_{O2} is partial pressure of oxygen in the range 0 to 10 atm., concentrations of Na_2CO_3 and $NaHCO_3$ varied from 0.05 to 0.7 M, average particle sizes, d changed from 41 to 172 μm and temperature from 353 to 413 K. The details of complete methodology of developing above equation are given in the thesis. The predicted leaching rates and the Arrhenius activation energy are comparable with those reported in literature [10, 11].

5.2. Pure Iron pyrite

In this section, results of the study on dissolution of a common gangue mineral, iron pyrite, that occur in uranium ores have been discussed. It is important to study the dissolution of this mineral as it is the reactive gangue which consumes oxidant as well as the leachants and compete with uranium minerals. Exhaustive literature is available on reaction kinetics of pyrite in acidic systems but only limited information is available on pyrite reaction under alkaline solutions. The following rate equations are developed for dissolution of pure pyrite on the basis of shrinking core leaching model [19].

$$1-(1-X)^{\frac{1}{3}} = 3x10^{7}x\, p_{O_2}^{0.2}\, d^{-0.2} e^{-\frac{7006}{T}}\, [CO_3]^{0.8}\, [HCO_3]^{0.2}\, t\,, for$$

$$[Na_2CO_3]\ and\ [NaHCO_3]\ between\ 0\ to\ 0.7\ M$$

$$1-(1-X)^{\frac{1}{3}} = 2x10^{6}xp_{O_2}^{0.2}d^{-0.2}e^{-\frac{7006}{T}}\, [CO_3]^{-2.9}\, [HCO_3]^{-2.1}\, t\,, for$$

$$[Na_2CO_3]\ and\ [NaHCO_3] between\ 0.7\ to\ 1M$$

where, X is the fractional conversion of pyrite in time t (h). Partial pressure of oxygen (P_{O2}) was studied in the range 0.5 to 3 atm., particle size (d) from 6 to 253 μ and temperature 343 to 393 K. The base experiments were conducted at 363 K and 0.5 atm. oxygen partial pressure in these set of experiments. The hypothesis of chemical reaction control is supported by the high activation energy (13.87 kcal/mol) and the fractional reaction orders with respect to oxygen partial pressure, sodium carbonate concentration, sodium bicarbonate concentration, particle size. Fractional order (0.5) of pyrite oxidation with respect to partial pressure of oxygen and about 14.6 k-cal/mol of activation energy are reported in literature [12,13], which are in agreement with those deduced in the present study.

5.3. Synthetic mixture

This section is further divided into three sub sections.

5.3.1 Sequential experiments: The common gangue minerals in carbonate host rocks are: calcite, dolomite, silica and pyrite. Pyrite is the only reactive gangue mineral; all the others are inert in carbonate medium. Since calcite and dolomite have similar chemical nature, only calcite (85 wt%) is used along with pure UO_2 (0.2 wt%), iron pyrite (5 wt%) and silica (9.8 wt%) for preparing synthetic mixture of minerals. The composition of the synthetic mixture used for experiments is chosen close / intermediate to the compositions of the two alkaline rock hosted Indian uranium ores, Tummalapalle and Gogi. The base case experiments were conducted at 413 K, pO_2 of 10 atm., d = 87 µm and $[Na_2CO_3]$ and $[NaHCO_3]$ = 0.5 M. Following rate equations have been found up to 2 h time period.

$$1\text{-}(1-X_{\mathrm{Py}})^{\frac{1}{3}} = 3489\, p_{O_2}{}^{0.5669}\, [Na_2CO_3]^{-0.31}\, [NaHCO_3]^{-0.4802}\, d^{-0.126}\, e^{-\frac{4465}{T}}\, \mathrm{t}$$

$$1-(1-X_{UO_2})^{\frac{1}{3}} = 0.1147\, p_{O_2}{}^{1.9149}\, [Na_2CO_3]^{0.3647}\, [NaHCO_3]^{0.4255}\, d^{-0.1735}\, e^{-\frac{1637}{T}}\, \mathrm{t}$$

The Arrhenius activation energy of dissolution of pyrite and uranium were found to be 8.75 kcal/mol and 3.2 kcal/mol respectively.

Effect of pyrite content on leaching of UO_2 and pyrite: A separate study was conducted to determine the effect of pyrite content on the dissolution of both UO_2 and iron pyrite under given leaching conditions (T = 398 K and P_{O2} = 5.2 atm., the optimum values of Tummalapalle ore leaching). The specific rates of dissolution of FeS_2 and UO_2 were calculated from specific surface areas of the mineral samples reported in section 3.1 and fractional dissolution of FeS_2 and UO_2 obtained in the experiments. These rates are plotted in Figure.4.

Increase in pyrite content from 1 to 3% promoted the rate of dissolution of UO_2 due to neutralization of NaOH (formed during dissolution of uranium by reaction 2(a)) by the $NaHCO_3$ generated in dissolution reaction of pyrite (reaction 4). However, further rise in pyrite lowered these rates due to lowering of pH to < 9 because of higher dissolution of pyrite, generating excessive $NaHCO_3$ and Na_2SO_4. pH values < 9 lower leachability of UO_2. Several other studies reported similar effect of pyrite for uranium ores [6, 7]. The rate of dissolution of the competing mineral, pyrite, increased monotonically as pyrite content rose from 1 to 6% due to increase in surface area of the pyrite mineral.

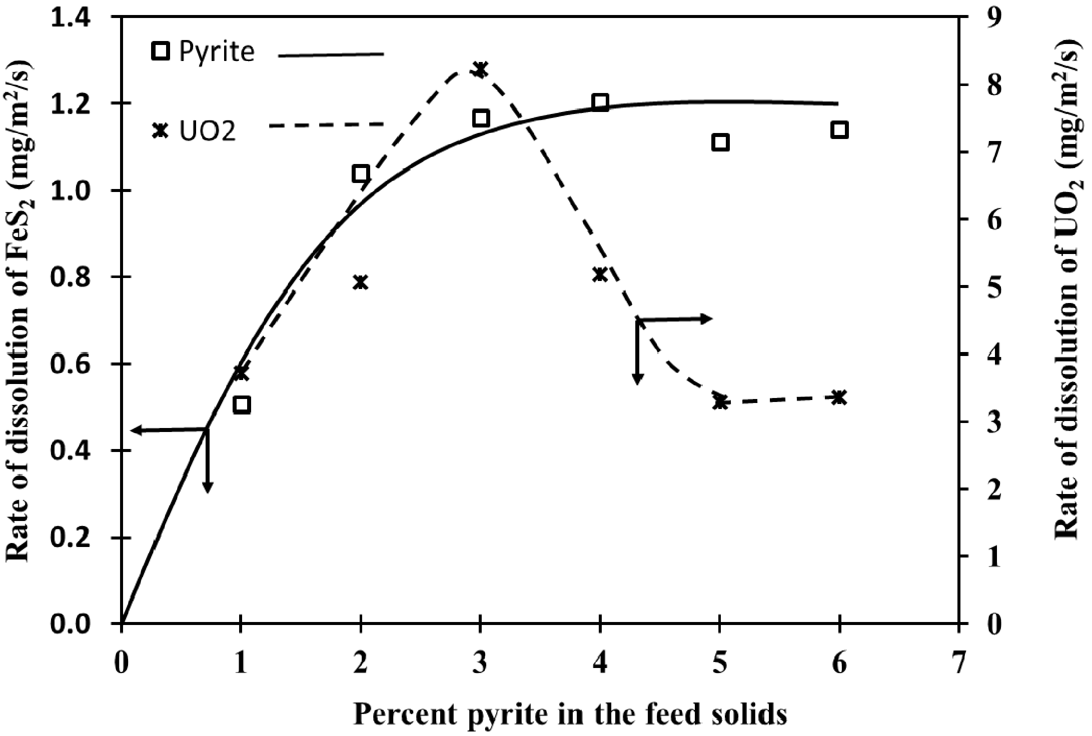

Fig.4. Rate of leaching of Iron pyrite and UO_2 from synthetic mixtures with varying pyrite content

5.3.3. Statistical modeling and optimization of alkaline leaching of uranium: Statistical modeling has been used to delineate effects of operating variables on leaching of uranium without dwelling into the details of rate controlling mechanisms of non-elementary reactions of the two competing minerals, uraninite and pyrite, in alkaline media. Batch leaching experiments were carried out, each of 6 h duration, according to a two-factor central composite design using synthetic mixture. Temperature was varied from 353 K to 403 K and total pressure from 1 to 10 bar using oxygen. The quadratic polynomial functions in terms of temperature (T, expressed in K) and pressure (P, bar) for percent leaching of uranium dioxide (Y_{UO2}) and that of pyrite (Y_{py}), developed by the analysis of variance method (ANOVA) using DOE++ software, are as follows:

$$Y_{py} = -829.7093 + 14.3148(T - 273) + 17.1348(P) - 0.0267(T - 273)(P) - 0.0586(T - 273)^2 - 0.7742(P)^2$$

$$Y_{UO2} = -191.8001 + 4.154(T - 273) + 18.2415(P) - 0.0544(T - 273)(P) - 0.0217(T - 273)^2 - 0.622(P)^2$$

Predicted and experimental values of leaching efficiency of both uranium dioxide and pyrite after 6 h were in good agreement with an R^2 value (coefficient of determination) of 0.98. Multi-objective optimization of the two equations gave 353 K and 6.5 bar as optimum levels to achieve maximum uranium dissolution of 65.4% and minimum undesirable pyrite dissolution of 5.4%.

5.4. Morphological studies

Scanning electron micrographs (along with EDX analyses) of all the four minerals used in the synthetic mixture before and after leaching at high temperature and pressure (398 K, 7.5 bar - the optimum conditions of Tummalapalle ore leaching) were obtained. Typical scanning electron micrographs are given in Figures.5.1. and 5.2.

Figure.5.1 suggests that pure UO_2 feed particles are 75 - 100 µ in size, have smooth surface and irregular shape. The SEM image of leached UO_2 particles show a rough surface, with a significant number of pits and micro cracks around them indicating the dissolution of uranium dioxide. Since uranium reaction product is soluble (as given by reactions (1) and (2) in section 2.3), it has not formed any new solid phase. Figure.5.2 suggests that iron pyrite is chemically altered to (mainly) iron oxide (inferred from EDX analyses) and present in ultra-fine sizes. The new solid phase formed in leaching is confirmed to be $Fe(OH)_3$ by X-ray diffraction studies, as expected to be formed by reaction (4) given in Section 2.3.

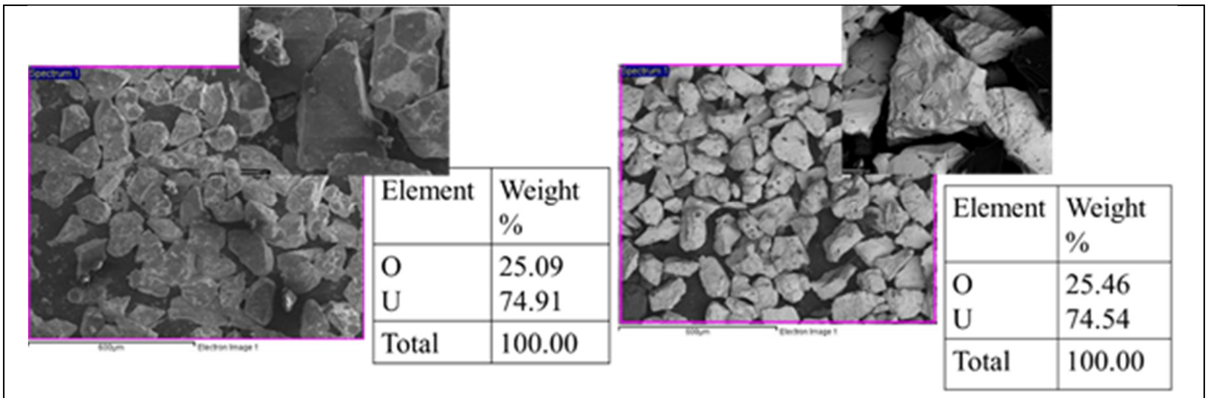

Element	Weight %
O U	25.09 74.91
Total	100.00

Element	Weight %
O U	25.46 74.54
Total	100.00

Fig.5.1. Scanning Electron Micrographs of Uranium dioxide before and after leaching

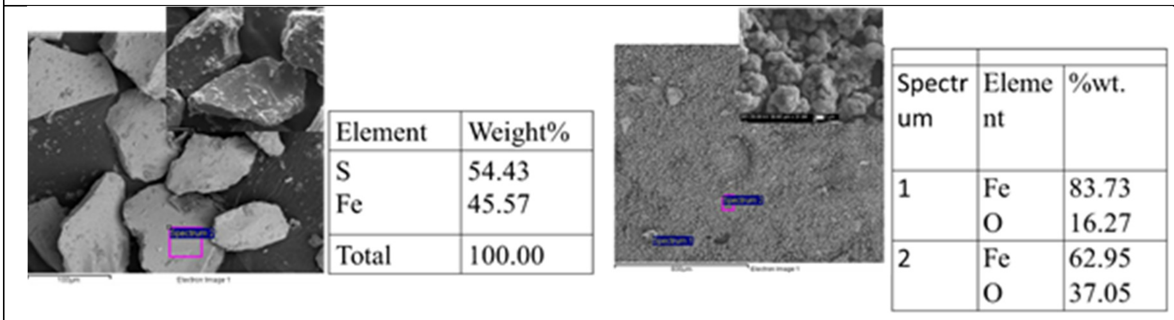

Element	Weight%
S Fe	54.43 45.57
Total	100.00

Spectrum	Element	%wt.
1	Fe O	83.73 16.27
2	Fe O	62.95 37.05

Fig.5.2. Scanning Electron Micrographs of Iron pyrite before and after leaching

6. MODELING OF KINETICS OF BATCH LEACHING OF INDIAN URANIUM ORES (APPLIED STUDIES)

This chapter has been divided in to three sections. Section 6.1 presents the results of experiments on Tummalapalle uranium ore and section 6.2 on Gogi uranium ore. Section 6.3 compares uranium leaching from pure minerals with its leaching from Indian ores. The role of oxygen in uranium leaching is established through experiments.

If uranium minerals are fully liberated, the popular shrinking core model mechanisms, mass transport through the boundary layer fluid film surrounding each particle or internal surface chemical reaction or the product layer diffusion are applicable. Usually, the uranium minerals in the ground ore are fully / partially liberated by grinding. In the case of high grade ores, even if uranium is partially liberated, the above mechanisms of shrinking core model generally fit the kinetic data due to high rock permeability to the leachants, examples of which are available in literature. But in case of low-grade uranium ores with very fine dissemination of uranium minerals, the rate controlling step is observed to be the diffusion process of dissolved ions in liquid within pores of rock particles.

6.1. Tummalapalle uranium ore

Nine leaching experiments were conducted sequentially varying partial pressure of oxygen from 4.5 to 6.5 kg/cm^2, stirring speed from 573 to 900 rpm (tip speed = 1.5 to 2.4 m/s), reaction temperature from 398 to 438 K and particle size from 18 to 150µ (mean volume surface diameter from 25.8 to 34.76 µ) in a 5-litre autoclave.

The experimental kinetic data obtained was first fitted to two homogeneous rate models using fractional conversion of U_3O_8, α, at time t in different experiments: (1) First order pseudo homogeneous model according to the equation $-ln(1-\alpha)=kt$ was tested. No linear relationship between $-ln(1-\alpha)$ and t could be obtained. (2) Avrami model, given by equation $-ln(1-\alpha)=kt^n$ was fitted to the data. Linear relation could not be obtained for the data of all the experiments when $ln[-ln(1-\alpha)]\ Vs\ ln(t)$ was plotted. The leaching data was then analysed with three heterogeneous rate equations of well-known shrinking core model. (1) Film diffusion controlled model given by equation, $\alpha = k\,t$, (2) Surface chemical reaction controlled model, whose rate equation is given by $1-(1-\alpha)^{\frac{1}{3}}=k_c t$ (3) Diffusion of reactants through particle pore alone is rate limiting (control through ash or product layer) whose rate equation is given by $1-\frac{2}{3}\alpha-(1-\alpha)^{\frac{2}{3}}=k_D t$. Film diffusion kinetics does not adequately represent physical system, due to absence of constant film layer over the particles, as the slurry is subjected to high agitation. Hence the data was not tested for this rate equation. Experimental data did not fit both of the latter rate equations independently. However, the data fit a mixed control model (both surface chemical reaction and diffusion together) of shrinking core model. This type of model is reported in literature by Shaohua et al, for leaching of ulexite mineral [20]. The overall rate equation developed is given by $1-\frac{2}{3}\alpha-(1-\alpha)^{\frac{2}{3}}+\beta[1-(1-\alpha)^{\frac{1}{3}}]=kt$ and $k=40570\,(p_{O_2})^{2.5}\,s^{0.21}\,d^{-5.7}\exp(-4.5/RT)$. The rate of leaching is least affected by the stirring speed, in the range studied, decreases significantly with increase in particle size, and increases with increase in partial pressure of oxygen and temperature. The Arrhenius activation energy was found to be low at 4.5 k cal/mole.

As an alternative approach, search for a kinetic model that could represent the physical system more closely was attempted. The fact that a single mechanism of shrinking core model could not be fitted is due to low rock permeability of the Tummalapalle rock. Low permeability is evident from the low average specific surface area (0.42 m^2/g) and low pore volume (0.002 cm^3/g). In the case of low grade ores, transport of dissolved metal in liquid within pores of rock particles is likely to be the rate controlling step in the overall leaching process, especially for low grade ores. Counter current diffusion of anionic complexes of uranyl carbonate out of the particle with CO_3^{-2} and O^{-2} ions of the fluid phase diffusing into the particle is involved. The diffusivity in turn is a function of porosity and tortuosity of the ground ore particles. Hence, a pore diffusion rate controlling kinetic model is presented herein for the case of low grade uranium ore from Tummalapalle, Andhra Pradesh, India. Further, Gates-Gaudin-Schumann size distribution was incorporated and the effective diffusivity was computed for different combinations of experimental conditions of Tummalapalle ore leaching according to pore diffusion controlled rate equation, $\alpha(t, R_i) = 1 - \frac{6}{\pi^2} \sum_{K=1}^{\infty} (\frac{1}{K^2} e^{-K^2 \pi^2 D_{eff} t / R_i^2})$. The effective diffusivity was found to be between 0.61 cm^2/s to 5.67 cm^2/s. It was observed to be increasing with increase in partial pressure of oxygen, increase in stirring speed, increase in temperature and decrease in average particle size. An Arrhenius plot of **log(D_{eff}) Vs *1/T*** yielded activation energy of 3.27 kcal/mole, which verifies the assumption of diffusion controlled mechanism [21].

6.2. Gogi uranium ore

Fifteen experiments were conducted. Leaching parameters studied include partial pressure of oxygen (0.15 - 3 atm.), temperature of the reaction mixture (343 – 383 K), concentration of leachant (0.47 - 0.94 g mol/l), average particle size (61 – 136 μ) and stirring speed (573 - 900 rpm). The results of kinetic experiments were analysed with shrinking core model rate equations. Film diffusion is not considered as sufficiently high agitation is maintained during leaching, due to which the film layer on the particles is continuously replaced leading to fast diffusion of solutes in the film. Also, since all the reaction products are soluble in lixiviant and leave no ash product, ash diffusion controlled mechanism is also ignored. Hence, the experimental data of rate of leaching was analysed on the basis of surface chemical reaction control mechanism governed by equation, $\mathbf{1-(1-\alpha)^{\frac{1}{3}} = k\,t}$, where α= conversion at time t (min), and k = overall rate constant (min^{-1}) which is a function of concentrations of reactants, temperature, stirring speed, size of particles and many other properties of the leaching system. Particle size distribution is incorporated into the above shrinking core model equation using the procedure adopted by Gbor and Jia, as the particles participating in leaching actually are not identical but do vary in size [22]. However, variation of the particle shape is not included in the present study owing to the difficulty of obtaining detailed knowledge of the shape distribution. Hence, one of the limitations of the model presented here is that particulate matter do not possess a distribution of shapes i.e. particles are all assumed to be spherical. The overall rate equation developed is given by, $\boldsymbol{Fraction\,reacted} = \int_0^{D_t}(m\frac{D^{m-1}}{D_{max}^m})dD + \int_{D_t}^{D_{max}}\left(1-(1-\frac{k_n}{D}t)^3\right)(m\frac{D^{m-1}}{D_{max}^m})dD$ and **k**$_{\mathbf{n}}$ **where** $\boldsymbol{k_n} = \mathbf{17198}\,\boldsymbol{M^{1.28}e^{-\ln(p_{O_2})(0.37\ln(p_{O_2})+0.23)}e^{-\frac{7}{RT}}}$ and $\boldsymbol{D_t = k_n t}$. The kinetic model fit is in close agreement with the experimental data and the model can be applied to ores with low silica, high pyrite content and mineralogy similar to Gogi uranium ore. The high activation energy of 7 kcal/mol supports a reaction controlled mechanism [23]. The rate of leaching of uranium from Gogi ore increased with increasing concentration of sodium carbonate and temperature. However, there is an optimum oxygen partial pressure. The extraction of uranium is >90% and dissolution of pyrite is <40% at <1 atm. oxygen pressure and 363 K. This phenomenon is due to increased dissolution of pyrite at oxygen pressures > 1 atm. Morphological studies using scanning electron microscope with EDX of unleached and leached Gogi ore samples affirmed near complete leaching of uranium and partial leaching of pyrite mineral at 363 K and below 1 atm. oxygen pressure. The higher dissolution rate of uranium, in the initial periods, from Gogi ore in comparison with that of pure UO_2 is attributed to the UO_3 content of pitchblende present in the ore.

Alternatively, a first order kinetic model with distributed rate constant was also tested for leaching of Gogi uranium ore because any ground ore feed may contain particles with distributed properties like size, mineralogy, morphology, uranium content etc. as in any ore in general. The model was fitted according to the equation, $\boldsymbol{M(k,t) = \int_0^\infty M(k,0)e^{-kt}dk}$, where **M(t)** is the unleached uranium fraction in the solids at time t. The popular gamma distribution of the leaching rate constant was found to satisfactorily represent the function **M(k,0)**. The shape and scale parameters of gamma species distribution were obtained by least square regression fitting of above nonlinear equation to the experimental values of unleached fraction of uranium at different time periods, t in each kinetic experiment. The goodness of fit was found to be always ≥ 0.92. Effect of temperature, particle size, partial pressure of oxygen, stirring speed and the lixiviant concentration on the gamma distribution of weight fraction of ore material with respect to rate constant was found to be in good agreement with the theory of kinetics of leaching.

6.3. Comparison of uranium leaching from pure minerals vis-a-vis Indian ores

Plots of dissolution rates of uranium from Gogi ore, Tummalapalle ore and pure UO_2 at different temperatures and oxygen pressures are presented. Much higher dissolution rates (20 mg/l-min, at optimum conditions of leaching) of uranium from Gogi ore than pure UO_2 (13 mg/l-min, at optimum conditions of leaching) could be due to the presence of significant amount of U^{+6} in pitchblende (U_3O_8) occurring in Gogi ore [The uranyl (U^{+6}) form of uranium readily dissolves where as uranous (U^{+4}) form needs to be first oxidized before dissolution]. Whereas the lower rates of dissolution of uranium (7.3 mg/l-min, at optimum conditions of leaching) from Tummalapalle ore could be due to low grade, low permeability and pore diffusion controlling mechanism. The study indicates that the leaching models of pure UO_2 cannot be directly used for uranium ores.

If the competitor mineral pyrite, FeS_2, is present in significant quantities, more than a certain limit, in the ore, then it (1) limits the availability of oxygen and sodium carbonate for oxidation and dissolution of uranium mineral during leaching with carbonate solutions, and (2) excessive dissolution of pyrite lowers pH of the slurry that results in low dissolution rates of uranium. A low dissolution of uranium is observed for synthetic mixture of minerals containing >3% pyrite at 398 K and 7.5 pO_2. Low leaching of uranium was observed from Gogi ore (which contains about 5% pyrite) also, under the above high temperature and pressure conditions.

6.3.1. Role of oxygen in uranium leaching: The results of 22 leaching experiments conducted on both synthetic mixture and Indian uranium ores, using inert gases (Ar, N_2 and CO_2) at different temperatures and pressures, are described in this Section. Dissolution of both uranium and pyrite have been monitored.

Dissolution of uranium in absence of oxygen: The leaching of uranium from synthetic mixture of minerals (in which all the uranium is present in +4 oxidation state) using CO_2 and Ar in place of O_2 was found to be insignificant (<5%) in the range of temperature and pressure under which Indian uranium ores are to be leached. The phenomenon is in accordance with the theory that the first step in dissolution of uranium, oxidation of uranium from +4 state to +6 state, is not possible in the absence of O_2. Nevertheless, some amounts of uranium were found to be dissolved in the leaching of actual uranium ores in the absence of O_2.

Ideally, if any ore contains all of its uranium in uranous state as UO_2, no uranium should get dissolved into leach liquor without oxygen gas / a chemical oxidant. However, dissolution of some amount of uranium in an oxygen free environment (provided by inert gases, Ar and CO_2 in the present studies) could be due to presence of some amount of uranium in uranyl state as UO_3 in the mineral Uraninite in uranium ores. Dissolution of UO_3 takes place, if the solution contains ions such as SO_4^{2-} or CO_3^{2-} without the need for an oxidizing agent, oxygen gas. Hence, this study was aimed at clearly demarcating the two portions of uranium present in the ore, (1) the portion containing uranium (in +6 oxidation state) that is extracted without oxygen and (2) the portion containing uranium in +4 oxidation state, which requires oxygen for solubilization. About 9% of uranium in Tummalapalle ore was soluble in the absence of oxygen (pressurized by Ar gas). Higher amounts of uranium was found to be dissolving in oxygen free environment for Gogi uranium ore.

Dissolution of iron pyrite in absence of oxygen: No sodium sulphate was detected in the liquor (confirmed from the analysis of sulphur content in solids before and after leaching) obtained in the experiments conducted with Ar, CO_2 gases using three different feed materials (1) synthetic mixture of minerals (2) Tummalapalle uranium ore and (3) Gogi uranium ore. The absence of sulphate in leach solutions indicates pyrite does not react with inert gases; and oxygen is essential for its dissolution as can be seen in the reaction of gangue mineral, iron pyrite, in carbonate media (reaction 4 given in Section 2.3).

7. MODELING, SIMULATION AND EXPERIMENTAL VALIDATION OF CONTINUOUS LEACHING PROCESS

Commercial level operation of uranium leaching from the ores is carried out as a continuous process because of techno-economical benefits. In this chapter, a method is demonstrated to scale laboratory batch leaching process to commercial continuous operation for high pyrite containing uranium ores. Batch kinetic data (generated in a 5-litre autoclave) of leaching of uranium and iron pyrite from a lean ore (Tummalapalle ore), is scaled to multiple continuous stirred tank reactors using Residence Time Distribution (RTD) model according to the equation,

$M_t = \left[1 - \left[\sum_{N=1}^{N} \frac{1}{(N-1)!} \left(\frac{t}{t_{av}} \right)^{N-1} \right] e^{\frac{t}{t_{av}}} \right] \times 100$ where, t is time elapsed, M_t is reactor discharge in time t as a cumulative weight percentage of the original feed, N is number of reactors in series, t_{av} is average retention time per reactor and Nt_{av} being total retention time in N tanks [19]. A graphical approach reported in literature by other workers [24] earlier was improved for better predictions of the observed experimental results. Details of the implementation of the method are described in the Thesis. Scaling is used to predict the temperature rise in continuous reactor, which happens mostly due to conversion of pyrites present in the ore. The scaling obtained with the modified model was compared with measurements of uranium conversions and reactor temperatures in a pilot scale continuous reactor (850 L capacity) having three stirred tanks in series. A good comparison was obtained for several different operating conditions of the pilot and commercial scale reactors.

The recovery of uranium in laboratory batch leaching with Na_2CO_3 (50 g/l) and $NaHCO_3$ (70 g/l) at 398 K and 7.5 kg/cm^2 pressure in a 5 L capacity autoclave in 4 h residence time was 78%. About 77.7% of U_3O_8 values was leached in three continuous stirred tank reactors in 6.2 h residence time with a flow rate of 140 L/h. Under the same conditions, Residence Time Distribution (RTD) method adopted in the present study predicted a uranium recovery of 78.5%. The predictions are useful not only to design continuous leaching of uranium on a commercial scale but also to find the limit on pyrite content of the ore to operate commercial reactors below design temperature. It is predicted that if the Tummalapalle uranium ore enters the autoclave at 383 K, and the maximum design temperature of the reactor is 473 K (as in the case of pilot scale reactor), then care must be taken to have the pyrite content of the ore <3% in order to avoid shooting of temperature to>473 K.

8. CONCLUSIONS AND SCOPE FOR FUTURE STUDIES

8.1. Major outcomes of the study

A kinetic model that includes electrochemical mechanism was found to be applicable for leaching of pure UO_2. Michaelis Menton type of model equation was developed for dissolution of pure UO_2. Dissolution of pure pyrite followed chemical reaction controlled shrinking core model. The presence of pyrite up to 3 wt% was beneficial for uranium leaching, but beyond 3 wt%, it was detrimental to carbonate leaching of synthetic mixture of minerals at $T = 398$ K and $pO_2 = 5.2$ atm. The same effect of pyrite was observed in carbonate leaching of Gogi uranium ore, containing about 5 wt% pyrite, under high temperature and pressure conditions. Pyrites, if present in > 3 wt%, may be removed by flotation process before subjecting the uranium ore for hydrometallurgical extraction by alkaline leaching.

Pore diffusion controlled model incorporating particle size distribution was found to be the most applicable for leaching of uranium from Tummalapalle ore. Topochemical reaction controlled model coupled with particle size distribution best represents the leaching of uranium from Gogi uranium ore. The leaching models of pure UO_2 cannot be directly used for uranium ores. Oxygen is essential for dissolution of uranium. But ores may show some dissolution of uranium values in the absence of oxygen because of the UO_3 content of uranium minerals present in the ore. Leaching results were corroborated with in-depth optical and scanning electron microscopy images showing the morphological changes that occur during leaching of the pure minerals, uraninite and pyrite, vis-a-vis two Indian uranium ores.

Residence Time Distribution (RTD) model was proved to be a good tool for scale-up and design of commercial scale leaching of uranium from lean ores. This model was accurate in scaling-up from laboratory level to pilot level. The model predictions of extraction of uranium and temperature rise in the reactors on pilot scale operated with Tummalapalle uranium ore matched well with experiments on the same scale.

8.2. Scope for future studies

Scope exists to study the following aspects: (1) while the effect of particle size distribution exhaustively covered in the present work, the shape distribution of particles could be coupled with the rate equations for future work, (2) alkaline leaching models for most commonly found uranium mineral, Uraninite, were developed in the present study. As a follow up, other uranium minerals such as Coffinite, Brannerite etc. likely to occur in uranium ores, may also be studied to develop the corresponding leaching models and compare their rates of dissolution, (3) quantitative relation between the models of leaching of pure minerals and the leaching of uranium ores may be explored and thought may be given to obtain a unified model valid for uranium ore with any composition, (4) derive the final conversions of pyrite and UO_2 from the rate equations of individual reactions by numerical differentiation, and (5) Residence Time Distribution (RTD) scale up model for continuous leaching of Gogi uranium ore may be worked out following the same procedure as that adopted for the Tummalapalle ore in the present study.

REFERENCES

[1] http://www.world-nuclear.org (Accessed in February’2015).

[2] Cumming G.L., Krstic D, The age of unconformity-related uranium mineralization in the Athabasca basin, northern Saskatchewan, Canadian Journal of Earth Sciences 29, pp 1623-1639 (1992).

[3] Kotzer T.G., Kyser T.K., O, U, and Pb isotopic and chemical variation in uraninite: Implications for determining the temporal and fluid history of ancient terrains, American Mineralogist, 78, pp 1262-1274 (1993).

[4] Anon, Uranium 2014: resources, production and demand. A Joint Report by the Organization for Economic Co-operation and Development (OECD) Nuclear Energy Agency and the International Atomic Energy Agency, (OECD 2014 NEA No. 7209), p 18 (2014).

[5] Chaki A., Uranium Occurrences and Exploitation Experience in India. Proceedings of 3rd International Conference on Uranium, 40th Annual Hydrometallurgy Meeting, Uranium-2010 (CIM) held at Sasktoon, SK Canada during 15-18 August, 2010, Volume-I, pp 25-36 (2010).

[6] Merrit R.C., The Extractive Metallurgy of Uranium, Colorado School of Mines Research Institute, Colorado, USA, pp 27-38 (1971).

[7] Anon, Uranium Extraction Technology. Technical reports series no. 359, International Atomic Energy Agency, Vienna, p 36 (1993).

[8] Edwards C.R., Oliver A.J., Journal of Metals, Uranium Processing: a review of current methods and technology, J. Miner. Met. Mater. Soc. 52, pp 12-20 (2000).

[9] Peters E., Halpern J., Kinetics of the dissolution of pitchblende, Can. Min. Metall. Bull., 56, pp 350-354 (1953).

[10] Habhashi F., George Ann Thurston, Kinetics and mechanism of the dissolution of uranium dioxide, EnergiaNucleare, 14 (4), pp 238-245 (1967).

[11] Schortmann, W.E., Desesa, M.A., Kinetics of the dissolution of uranium dioxide in carbonate-bicarbonate solution. Proc. 2nd United Nations Int. Conf. on the Peaceful Uses Atomic Energy, Geneva 3, pp 333-341 (1958).

[12] Ciminelli V.S.T., Osseo-Asare K., Kinetics of Pyrite Oxidation in Sodium Carbonate Solutions”. Metallurgical and Materials Transactions B, 26B, pp 209-218 (1995).

[13] Joshi J.B., Shah Y.T., Albal R.S., Ind. Eng. Chem. Process Des. Dev., 21, pp 594-600 (1982).

[14] Hossain Mohammad Mohsin, Ella Ekeroth, Mats Jonsson, Effects of HCO_3 on the kinetics of UO_2 oxidation by H_2O_2, Journal of Nuclear Materials 358, pp 202-208 (2006).

[15] Christine Chin Choy, George P. Korfiatis, XiaoguangMeng, Removal of depleted uranium from contaminated soils, Journal of Hazardous Materials, 136, pp 53–60 (2006).

[16] Sunitha V., Muralidhara Reddy B., Ramakrishna Reddy M., Mineral Resources of Cuddapah Basin, Journal of Biological and Chemical Research, 31 (1), pp 226-235 (2014).

[17] Minati Roy, Dhana Raju, R., Mineragraphy and electron microprobe study of the u-phases and pyrite of the dolostone-hosted uranium deposit at tummalapalle, cuddapah district, Andhra Pradesh and its implication on genesis and exploitation, Journal of Applied Geochemsitry, Vol. 1 (No.2), pp 53-75 (1999).

[18] Srikantappa, C., Govindaiah, S., Nature and composition of basement and basinal fluids in the Proterozoic U-bearing sediments around Deshnur, Kaladgi Basin, Karnataka, The Indian Mineralogist, 44 (1), pp 1–7 (2010).

[19] Levenspiel, O., Chemical Reaction Engineering, John Wiley & Sons, New York (2001).

[20] Shaohua Ju, Tang Motang, Yang Shenghai, Li Yingnian, Dissolution kinetics of smithsonite ore in ammonium chloride solution, Hydrometallurgy, 80, p 69 (2005).

[21] Samuel A. Awe, Caisa Samuelsson, Ake Sandstrom, Dissolution kinetics of tetrahedrite mineral in alkaline sulphide media, Hydrometallurgy, 103, pp 167-172 (2010).

[22] Gbor, P.K., Jia, C.Q., Critical evaluation of coupling particle size distribution with the shrinking core model, Chem. Eng. Sci., 59, pp 1979–1987 (2004).

[23] Prosser, Alan P., Review of uncertainty in the collection and interpretation of leaching data, Hydrometallurgy, 41, pp 119–153 (1996).

[24] Sarkar, K.M., Selection of autoclaves in hydrometallurgical operations, Miner. Process. Ext. Metall., 94, pp C184 C194 (1985).

CONTENTS

PREFACE

This thesis on ‘**Carbonate Leaching of Uranium from Indian Alkaline host rocks using Oxygen: Mathematical Modeling and Experimental Validation’** is divided into five major parts. The first part consists of two chapters with introduction to the problem in Chapter 1 and review of literature in Chapter 2. The second part deals with characterization of materials used and products obtained in Chapter 3, description of equipment and experimental procedures in Chapter 4. Chapter 5 and 6 describe the third part. Chapter 5 includes basic studies which consist of development of batch kinetic models of leaching on (1) pure materials followed by (2) coexisting system i.e. synthetic mixture of these minerals. Separate studies on pure minerals include pure UO_2, metal of interest in the form of natural mineral uraninite, and pure pyrite (FeS_2), the reacting gangue mineral. The synthetic mixture is made of the above two minerals along with the two commonly occurring inert minerals in the ores, calcite ($CaCO_3$) and quartz (SiO_2). Chapter 6 includes the development of kinetic models on two Indian uranium ores namely the Tummalapalle uranium ore in Andhra Pradesh, and the Gogi uranium ore in Karnataka. This chapter also includes a Section relating the alkaline leaching of Indian uranium ores and their constituents. The fourth part is written as Chapter 7 which consists of modeling, simulation and experimental validation of continuous leaching process for the Tummalapalle uranium ore from Andhra Pradesh. Finally, Chapter 8, the fith part of the thesis, consists of major conclusions derived from the doctoral studies and the scope of future studies.

LIST OF FIGURES

LIST OF TABLES

LIST OF ABBREVIATIONS

ADU	Ammonium Diuranate
AHWR	Advanced Heavy Water Reactor
AMD	Atomic Minerals Directorate for Exploration and Research
ANOVA	Analysis of Variance
BET	Brunaer, Emmett and Teller
BRL	Bromoform Lights
CCD	Central Composite Design
CLR	Continuous Leach Reactor
EBC	Equivalent Boron Content
EDX	Energy Dispersive X-ray Spectroscopy
FBR	Fast Breeder Reactor
GGS	Gates Gaudin Schuhmann size distribution function
GSI	Geological Survey of India
IAEA	International Atomic Energy Agency
IR	Inferred Resources
LOI	Loss on Ignition
MDU	Magnesium Diuranate
MIH	Methylene Iodide Heavies
MIL	Methylene Iodide Lights
PHWR	Pressurized Heavy Water Reactor
RAR	Reasonably Assured Resources
RTD	Residence Time Distribution
ROM	Run-off-Mine
SDU	Sodium Diuranate
SEM	Scanning Electron Microscopy

LIST OF SYMBOLS

C_{UO2}	concentration of UO_2 in leach liquor at time t, g/L (or) mg/L
V, v	volume of leach liquor, L
$\frac{dC_{UO_2}}{dt}$	rate of dissolution of UO_2 , mg/L-min
t	reaction time, min (or) h
k_1, k_1, k_1	empirical constants of leaching rate equation
k_o, k_o', k_o''	overall rate constants of leaching rate equation
E_a	Arrhenius activation energy, kJ/mol
P_{O2}	partial pressure of oxygen, atm
P	total pressure, atm
D, d	particle diameter, µm
T	reaction temperature, K (or) °C
R	universal gas constant (8.3 J/g mol-K)
$[Na_2CO_3]$	concentration of Na_2CO_3 in leach liquor (mol/L), M
$[NaHCO_3]$	concentration of Na_2CO_3 in leach liquor (mol/L), M
$[Na_2SO_4]$	concentration of Na_2SO_4 in leach liquor (mol/L), M
$[U_3O_8]$	concentration of U_3O_8 in leach liquor, mg/L
X_{py}	fractional conversion of pyrite from solids, fraction
X_{UO2}	fractional conversion of UO_2 from solids, fraction
n, p, x, y	orders with respect to various reactants in a leaching rate equation
C_{py}	amount of pyrite leached per unit volume of leach liquor, mg/L

W_{py}	pyrite content of feed solids, percent
W, w	weight of feed solids to leaching, g
f	feed grade (%U_3O_8 wt/wt), percent
D_{eff}	effective diffusion coefficient for diffusion in a porous solid, cm^2/s
D_{AB}	ordinary diffusion coefficient for molecular diffusion in a fluid phase, cm^2/s
ε	porosity of the particle - volume fraction of pore space, fraction
K	integer index, integer
m	particle size parameter of the Gates Gaudin Schuhmann function
R_i	radius of i^{th} uranium ore particle, μm
R_{min}	radius of smallest uranium ore particle, μm
R_{max}	radius of largest uranium ore particle, μm
s	stirring speed, rpm
τ_D	tortousity factor for diffusion in pores (usually ≈ 2), ratio
$y(R_i)$	cumulative weight fraction of ore particles finer than radius R_i, fraction
$\Delta y(R_i)$	fraction of particles in size range between R_i and $R_i+\Delta R_i$, fraction
V	volume of leach liquor, L
$M(t)$	unleached mass fraction of uranium remaining in solids at time, t
a	shape parameter of a gamma distribution function
b	scale parameter of a gamma distribution function
D_t	size of particle below which particles are fully reacted at time t, μm
D_{max}	size of largest particle in the system, μm

k	overall rate constant of leaching, min^{-1}
k_n	leaching rate constant, µm/min
m	particle size parameter of the Gates Gaudin Schuhmann function
M_t	Continuous reactor discharge at time *t*, percent
N	Number of tanks in series in continuous reactor, number
t_{av}	Average retention time per tank in continuous reactor, h
Y_{batch}	Percent conversion of pitchblende in batch leaching, percent
Y_{UO2}	Percent conversion of pitchblende in continuous leaching, percent
Y_{UO3}	Percent conversion of UO_3 in continuous leaching, percent
Y_{FeS2}	Percent conversion of pyrite in continuous leaching, percent
Y_{NaHCO3}	Percent decomposition of $NaHCO_3$ in continuous leaching, percent
$\dot{M}_{solids}$	Mass flow rate of solids into / out of the continuous leach reactor, kg/h
$\dot{M}_{liquid}$	Mass flow rate of liquid into / out of the continuous leach reactor, kg/h
$\dot{m}_{UO_2}$	Mass flow rate of UO_2 into the continuous leach reactor, kg/h
$\dot{m}_{UO_3}$	Mass flow rate of UO_3 in the continuous leach reactor, kg/h
$\dot{m}_{FeS_2}$	Mass flow rate of FeS_2 into the continuous leach reactor, kg/h
$\dot{m}_{NaHCO_3}$	Mass flow rate of $NaHCO_3$ in the continuous leach reactor, kg/h
$C_{p,\ solids}$	Heat capacity of solids in continuous reactor, kJ/kg-°C
$C_{p,\ liquid}$	Heat capacity of liquid in continuous reactor, kJ/kg-°C

T_{in}	Temperature of inlet slurry to the continuous reactor, °C
T_{out}	Temperature of outlet slurry from the continuous reactor, °C
ΔT	Rise in temperature of slurry in the continuous reactor, °C
ΔH_{UO2}	Heat of reaction of oxidation of pitchblende /kg of pitchblende, kJ/kg
ΔH_{UO3}	Heat of reaction of dissolution of UO_3 /kg of UO_3, kJ/kg
ΔH_{FeS2}	Heat of reaction of oxidation of pyrite /kg of pyrite, kJ/kg
ΔH_{NaHCO3}	Heat of reaction of decomposition of $NaHCO_3$ /kg of $NaHCO_3$, kJ/kg

Greek Letters

α	fractional conversion of uranium at time t, fraction
$\alpha\ (t, R_i)$	fractional conversion of uranium ore particle of radius R_i at time t, fraction
α_{cal}	calculated value of fraction of uranium reacted, fraction
α_{exp}	experimental value of fraction of uranium reacted, fraction

CHAPTER 1

Introduction

Electricity is backbone of modern life. The per-capita electricity consumption is an indicator of human development index of a country [1]. Close to 67% of the world's electricity is generated from fossil fuels, which comes at a great cost of releasing 500 to 1069 tons of CO_2e/GWh into the atmosphere [2]. However, the emissions from common nuclear fuel, such as uranium is mere 28 tons of CO_2 e/ GWh [2]. Besides the low carbon foot print, the high reliability, high energy density for unit mass and low amounts of waste generated which can be safely stored and eventually disposed off, makes the nuclear fuel potentially an attractive source of energy. Thus, the production of electricity from nuclear fuel is one of the most eco-friendly and sustainable processes.

At present, nuclear fuel generates about 373 GWe of electricity which constitutes 11% of the world's total electricity production [2]. It is expected to grow to at least 511 GWe by 2030 according to conservative estimates, or may even touch 807 GWe as per estimates of the International Atomic Energy Agency (IAEA) [2]. It is unfortunate that the recent nuclear disaster at Fukushima Daiichi Nuclear Power Plant, Japan, in March 2011 damaged the public confidence in nuclear power and led to either instant closure or decision to phase-out the nuclear power reactors in Germany, Switzerland, Taiwan and Italy [3A]. But the nuclear setback of Fukushima has not deterred India from pursuing its atomic energy program. The likelihood of Fukushima-like accident is less in India because of adoption of passive cooling system during any incident in Indian reactors, higher safety measures and location of its nuclear reactors in lower seismic zone (III) reducing chance of simultaneous effect of an earthquake and tsunami [3B].

As of August 2015, India generates about 5.3 GWe through 21 nuclear reactors accounting for 3% of its total electricity production. It is projected that this number will grow to 63 GWe, which is 8% of the total power requirement projection by 2032 [4]. Further, India aims to produce 25% of electricity from nuclear power by 2050 [5].

India adopts its own prestigious three stage nuclear power program, envisioned by its nuclear program architect Dr. Homi Jehangir Bhabha, as the long term policy in view of limited uranium resources but availability of vast thorium resources. The three stage nuclear power program is briefly stated as: (1) building and operation of Pressurized Heavy Water Reactors (PHWRs) using natural indigenous uranium to produce electricity from fissile U^{235} (isotopic abundance in natural uranium is 0.7%) and plutonium (Pu^{239}) from the fertile isotope of uranium, U^{238} (isotopic abundance in natural uranium is 99.3%), (2) building and operation of Fast Breeder Reactors (FBRs) using Mixed Oxide (MOX) fuel and breed another fissile isotope of uranium, U^{233} from the fertile material (Th^{232}) which is used as blanket around the reactor core and (3) building and operation of Advanced Heavy Water Reactors (AHWRs) using U^{233} as fuel and breed more U^{233} from the Th^{232} blanket, thus utilizing the abundant thorium reserves of the country. Currently, India is implementing the first two stages and simultaneously pursuing R&D of the third stage. The success of India's nuclear power program depends on the adequate supply of natural uranium during implementation of the first stage. Unlike the nuclear power generation in rest of the world, where low enriched uranium (3- 5% content of U^{235}), India relies more on PHWR technology which uses natural uranium (0.7% content of U^{235}) as its fuel element [6].

The natural uranium is primarily extracted from its ores by the leaching process. Being cheaper, acidic leaching process is preferred over alkaline leaching process when ores contain siliceous minerals as main gangue. However, the latter is preferable when the ores contain high amounts (> 12 - 15%) of acid consuming gangue such as carbonate minerals [7, 8]. Since alkaline reagents are mild to react, the leaching technology usually requires drastic conditions like high temperature and pressure. This necessitates leaching to be carried out in autoclaves, which contribute up to 30% of capital cost of a hydrometallurgical plant [9]. Hence, efficient design and operation of autoclave leach reactors are essential. Better understanding of kinetics and mechanism of reactions involved will be of utmost use while setting up of new uranium mills. Mathematical models of leaching not only predict optimum conditions for maximum yield, but also aid in better understanding of the process and optimal design of commercial leach reactors. Besides, the mathematical models can easily predict the impact of the ore characteristics (mineralogical, physical and chemical) on leaching performance. It may be noted that the ore characteristics change either from one deposit to the other or from one place to the other within a particular deposit.

Recently, the techno-commercial importance of carbonate leaching of uraniferous ores in India has enhanced with the advent of two new carbonate hosted uranium deposits at Tummalapalle (in the state of Andhra Pradesh) and Gogi (in the state of Karnataka). Therefore, this thesis focuses on modeling and measuring the kinetics of alkaline leaching of uranium from lean tenor, high carbonate content synthetic mixture as well as Indian uranium ores from Tummalapalle, Andhra Pradesh and Gogi, Karnataka.

1.1 URANIUM RESOURCES, PRODUCTION AND DEMAND

Uranium is a widespread and ubiquitous element found on earth with an average crustal abundance of 2.8 ppm [10, 11]. It exists in nature as three radioactive isotopes: U^{238} (99.28%), U^{235} (0.72%) and U^{234} (0.0055%). Uranium was being used in pigmentation for coloring of glasses and ceramic glazes until the year 1939, when it was discovered that one of its isotope, U^{235}, was fissionable. The U^{235} isotope undergoes fission by the bombardment of thermal neutrons to release substantial energy and more neutrons. The isotope U^{238} is fertile and converts to another fissile isotope, Pu^{239}, upon absorption of thermal neutrons. The above nuclear reactions of the two isotopes make uranium valuable as a fuel or as an energy source in nuclear reactors for generation of electricity and for use in defense.

Uranium occurs in myriad of minerals due to its properties such as possession of multiple oxidation states, U(II), U(III), U(IV), U(V) and U(VI), variable cell units (permit substitution of similar ionic radii) and high solubility of its hexavalent form. U(IV) and U(VI) are stable in the earth's crust and rest are stable only under laboratory conditions. The geology, mineralogy and geochemistry of uranium deposits have been described in numerous papers and books [e.g., 12, 13, 14, 15].

Uranium occurs in over 200 minerals that can be grouped into chemical categories as oxides, salts, silicates, associations with hydrocarbons and the complex niobate-tantalate-titanate multiple oxides. These minerals are found in a wide variety of host rocks and can be broadly classified into primary and secondary minerals. The former are those formed in the earth's crust by direct precipitation from magmatic solutions and mostly have U^{+4} oxidation state. The latter are those formed by alteration of primary minerals by natural processes like surface weathering due to ground water, hydrothermal alteration and mostly have uranium in +6 oxidation state. A list of most common primary and secondary minerals found in workable deposits, grouped under different chemical categories, is given in Table 1.1. Uraninite, pitchblende and coffinite are the chief economic minerals of uranium [16, 17].

Uranium is produced from both conventional and unconventional resources. The conventional resources include: (1) primary sources - the ore deposits from which uranium is recoverable as a primary product, a co-product or an important by-product and (2) secondary sources – stocks held by government and private industry, spent nuclear fuel. Although the unconventional resources such as black shale, fly ash, and seawater, are huge, the uranium from them is recoverable only as a minor by-product. They do not currently contribute to world uranium supply [18], but have potential to become important source in future.

Table 1.1 The most common primary and secondary uranium minerals grouped under different chemical categories

Type → Chemical category ↓	Primary minerals		Secondary minerals	
	Name	Composition	Name	Composition
Oxides	Uraninite Pitchblende	$(U^{+4}_{1-x}, U^{+6}_{1-x})O_{2+x}$ Variety of Uraninite	Gummite	$Na(UO_2)(O,OH)$
Hydrated oxides	Becquerelite	$7UO_2.11\ H_2O$	-	-
Nb-Ta-Ti complex	Brannerite Davidite	$(U,Ca,Fe,Th,Y)_3Ti_5O_{16}$ $(Fe,Ce,U)(Ti,Fe,V,Cr)_3(O.OH)_2$	-	-
Silicates	Coffinite	$U(SiO4)_{1-x}(OH)_{4x}$	Uranophane Uranothorite	$Ca(UO_2)_2(SiO_3)_2(OH)_2.5\ H_2O$ Variety of thorite, $ThSiO_4$
Phosphates	-	-	Autunite Torbernite	$CaO.2UO_3.P_2O_5.8H_2O$ $Cu(UO_2)_2(PO_4)_2.12H_2O$
Vanadates	-	-	Carnotite Tyuyamunite	$K_2O.2UO_3.P_2O_5.8H_2O$ $Ca(UO_2)_2(VO_4)_2.5\text{-}8\ H_2O$
Hydrocarbons	-	-	Thucholite Asphaltite	

The uranium deposits occurring world-wide are classified on the basis of geological settings: age of uranium mineralization, mineralogy, host rock and morphology of the deposits. The classification scheme of uranium deposits is largely inspired by the pioneering work of F.J. Dahlkamp [13, 19]. The IAEA has classified uranium deposits occurring world-wide into 16 types (that include more than 40 subtypes) [20]. The distribution of various types of uranium deposits in India and elsewhere are listed in Table 1.2 (sources: [19, 21 – 23]). The 'carbonates' type of deposit has been added recently to the list, to accommodate the Indian uranium deposit at Tummalapalle in Andhra Pradesh owing to the extensive resources discovered in this area. Based on the uranium content, the ore deposits are classified into three categories: (1) low grade ores containing 0.05 – 0.1% U_3O_8 (2) medium grade ores containing 0.1 – 0.5% U_3O_8 and (3) high grade ores containing 1-20% U_3O_8 [21]. Based on the size, the uranium deposits are divided as (1) small (<5000 tons of U_3O_8), (2) medium (5000 – 20000 tons of U_3O_8) and (3) large (>20000 tons of U_3O_8).

Table 1.2 Classification of world uranium deposits by International Atomic Energy Agency (IAEA) along with share (reasonably assured resources and inferred) and examples of each type of deposit as of 1 January 2013 (sources: [19, 21 - 23])

No	Type of deposit	No. of deposits (World)	% U resources (World)	World Example	Indian Example	%U resources (India)
1	Proterozoic Unconformity related	86	10	Lake deposits, Canada; Aligator river, Australia	Lambapur (AP), Gogi (Karnataka)	9.95
2	Sandstone	652	31.3	Colorado Plateau, USA, Niger, Kazakhstan	Domiasiat (Meghalaya), Shiwalik belt	10.33
3	Paleo-Quartz-Pebble Conglomerate	70	5.2	Elliot lake, Canada, Witwatersrand, SA	Walkunji (Karnataka), Dhanjori basin	0.19
4	Vein deposits (Granite related deposits)	133	1.9	Massif Central, Fr, Bohemian, Massif, Schwartzwalder, USA	Singhbhum (Jharkhand), Aravallis (Rajasthan), Bodal-Jajawal (MP)	1.99
5	Polymetallic iron-oxide Breccia Complex	18	17.7	Olympic dam, Australia	Son valley (MP & UP)	0
6	Intrusive Deposits	87	8.5	Rossing, Namibia, Bancroft, Canada	-	0
7	Phosphate Deposits	59	1.7	USA, Brazil	Mussoorie, Maldeora	0
8	Collapse Breccia Pipe	17	0.2	Arizona, USA	-	0
9	Volcanic	128	3.8	Jiang Xi, China, Michelin, Canada	-	0
10	Surficial	66	3.5	Yeelirrie, AU, Langer, Heinrich, Namibia	-	0
11	Metasomatite	70	11.4	Zheltye Vody, Ukraine, Espinharas	Kerpura (Rajasthan)	3.74
12	Metamorphite	95	0.7	Brazil Forstau, Austria	Jaduguda, Bagjata, Bandhuhurang, Bhatin	31.55
13	Lignite	33	0.8	Czech Rep., Germany, Greece	-	0
14	Black Shale	48	0.0	Ranstad, Sweden Chattanooga, USA	-	0
15	Carbonates	7	0.6	Bentou-Sanbaqi, China	Tummalapalle (A.P.)	42.24
16	Unknown	2	2.6	Ulzitt, Mongolia	-	0
	Total	1571	100	-	-	100.00

1.1.1 World Scenario

The IAEA classifies uranium resources according to recoverable uranium, regardless of isotope, based on a set market price. As of 1st January 2013, the estimates of identified conventional resources of uranium recoverable at highest cost of < USD 260/kg U are 76,35,200 tons including reasonably assured resources (RAR) and inferred resources (IR) categories [21]. The global distribution of RAR plus IR in the top five countries and others is shown in Fig. 1.1. (source: [21]). Australia has the highest share of total identified resources with 22% and Kazakhstan stands in second place with 13%. About 97% of the world uranium resources is concentrated in 15 countries and the remaining 3% is distributed in 21 other countries [21].

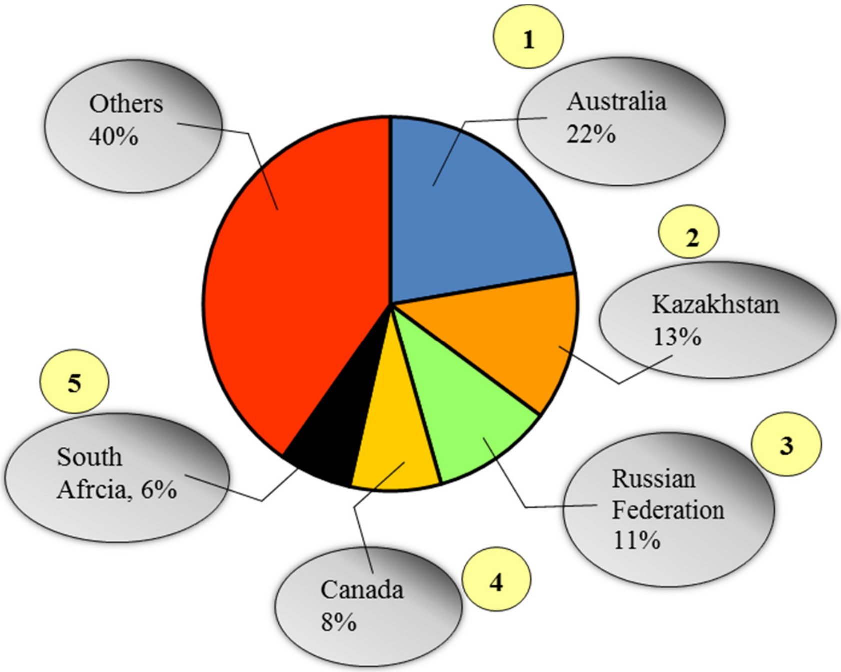

Fig. 1.1 Distribution of total uranium resources (Reasonably assured Resources plus Inferred resources) in the price category < USD 260/KgU as of 1st January 2013 (source: [21])

The world's highest grade uranium deposits occur in unconformity type of deposits that are located in the Athabaska Basin in Canada at Cigar lake with an average grade of 14% U (resources: 1,20,000 tU) and McArthur River with an average grade of 11.5% U (resources: 1,70,000 tU) [21]. The largest resource of low grade uranium is found in Breccia complex type deposit at Olympic dam in South Australia with 11,09,500 tU, as poly metallic ore (containing Cu, U, REE, Au, U3O8) and average uranium grade ranging from 0.035% to 0.07% U [21].

The current annual demand and supply of uranium across the world are 66,883 tons and 59,673 tons, respectively. Kazakhstan produces the largest share of 38% followed by Canada (16%) and Australia (11%) [24].

1.1.2 Indian Scenario

The total uranium resources in India are about 1,86,653 tons (2.4% of the world's total resources) as on October'2012, the state wise distribution of which is shown in Fig. 1.2 (source: [25]).

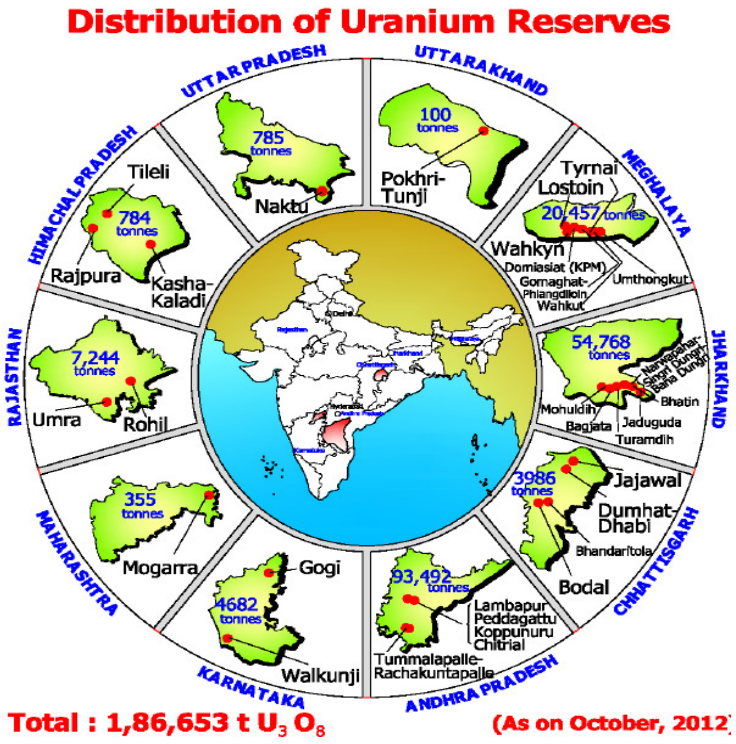

Fig. 1.2. Uranium reserves of India (source: [25])

Uranium ores in India are of low grade assaying in the range 400 - 1000 ppm U_3O_8. Principal uranium minerals of Indian uranium deposits are uraninite, pitchblende and coffinite, which are easily leachable when sufficiently liberated by grinding the ore rock pieces to required size. Two uranium mills are operating at Jaduguda and Turamdih in Singhbhum Thrust Belt (STB) in Jharkhand state. The Jaduguda mill is fed with uranium ore from Jaduguda, Bhatin, Narwapahar, and Bhagjata mines. While the Turamdih mill operates with ores from Turamdih, Banduhurang and Mohuldih mines. The U_3O_8 in the R.O.M. ore from these deposits ranges from 0.03 to 0.06% [21]. Since these ores contain mainly quartz and chlorite (up to 80% by wt) as gangue, acid leaching route has been adopted to extract uranium [26]. In addition, occurrence of large tonnage of uranium in Tummalapalle deposit, containing about 83% carbonates and 0.03 - 0.05% U_3O_8 [27, 28], has led to commissioning of the third mill in Tummalapalle area based on alkaline process route. Two more uranium mills are planned: one at Lambapur in Andhra Pradesh, with a medium tonnage deposit, containing 96% quartz and 0.05 – 0.06% U_3O_8 [29] and another at Kylleng–Pyndengsohiong–Mawthabah (KPM) in Meghalaya, with a medium deposit containing 90% quartz and 0.1% U_3O_8 [30]. A uranium plant is also now being designed for a low tonnage, medium grade (0.2% U_3O_8) deposit at Gogi, Karnataka [31].

Based on the 2013 uranium production statistics, about 400 tons of uranium were produced in India against the annual demand of ≈ 715 tons [21].

1.2 MOTIVATION

The supply-demand gap of uranium is speculated to increase all over the world in general and in India in particular. This gap drives the need for exploitation of lean tenor (<0.1% U_3O_8) ores or even those with characteristics that make their processing expensive like ores containing high carbonate content (> 12 - 15%), ores with refractory uranium minerals and high organic content [8, 32]. The importance of alkaline leaching of uraniferous ores in India has increased due to the discovery of two such uranium ore deposits of high carbonate content in Tummalapalle (Andhra Pradesh) and Gogi (Karnataka). The host rock of the former deposit is Phosphatic Silicious Calcitic Dolostone (PSCD) and that of the latter is brecciated limestone. The locations of the two deposits are shown in Fig. 1.3. The former two deposit contributes about 43% of India's uranium resources as on date, and the latter about 2.5%.

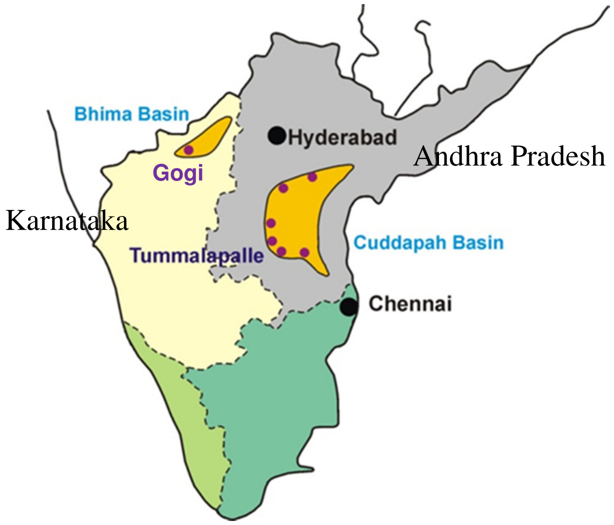

Fig. 1.3 Location of Tummalapalle and Gogi uranium deposits in South India

Utilization of the two important resources of uranium is essential for bridging the gap between demand and supply of uranium required for indigenous nuclear reactors. There is no reference to any previous work on modeling of leaching of the above mentioned two prominent Indian deposits: Tummalapalle and Gogi. The present research is aimed at thorough investigations of alkaline leaching of these uranium ores in southern India by experiments and mathematical modeling. The studies give an insight into the alkaline leaching process on uranium ores of the country and offer predictive models to know the leaching efficiency for the extraction of uranium and the dissolution / leaching of undesirable gangue minerals. The mathematical models will also help in predicting optimum values of operating variables required in alkaline leaching of uranium ores, given their mineralogical characteristics.

Most of the uranium leaching models reported in literature are developed for widely practiced insitu leaching, which accounted for 47% of the world's uranium production in the year 2013 [2]. These models are based on film diffusion (advective flow conditions) controlling mechanism as in situ leaching involves dissolving uranium by circulating the acidic/alkaline reagent in a porous ore body (forming a film over the solid phase), and pumping the pregnant solution to the surface [33]. The heap / insitu leaching models obviously cannot be applied to the uranium ores considered in the present study as these ores ought to be processed by agitation leaching in which the advective flow does not control the leaching. Besides, limited data is available in literature for extraction of uranium by agitation leaching, which is based on either simple homogeneous chemical rate equations for uranium ores or Michaelis–Menten type of kinetic models for pure uranium minerals [34-38]. In all of the above models the solid phase properties - particle size and its distribution, porosity, particle morphology, have not been considered. Hence, the present study is aimed at development of heterogeneous leaching models incorporating properties of solids taking the case studies of two Indian uranium ores from Tummalapalle and Gogi.

The ore mineralogy, morphological factors like grain size of uranium, gangue mineral pyrite, shape, and size distribution of the ore particles and association of uranium with pyrite have profound effect on the kinetics of leaching. Since no two ores have all the aforesaid properties same, each ore deposit requires to be studied separately for applicability of most appropriate leaching models. The variation in leaching conditions from one ore to the other, arising due to differences in ore characteristics, makes it difficult to draw analogies and direct comparisons with the already published data on other uranium ores. Hence, the present study has been taken up to develop leaching models, taking special note of incorporating properties of solid phase, for the two Indian uranium ores at Tummalapalle and Gogi.

After identifying the optimum leaching parameters in a batch reactor at laboratory scale, the commercial uranium mill needs to be designed for continuous process which offers superior operational convenience and savings on account of no shutdown time for loading and unloading of high throughputs (few thousand tons per day) of ore and reagent materials [39]. Hence, a Residence Time Distribution (RTD) model has been investigated for the scale up of batch leaching kinetic data of uranium to multiple continuous stirred tank reactors.

The carbonate leaching process becomes uneconomical for the ores containing >4% of pyrites (sulphides) because of the needless consumption of reagents [40]. Another problem associated with presence of large amounts of sufides is the heat generation due to chemical reaction of sulphides with carbonate medium. Detailed study on this aspect is not available in the literature till date. Hence, it is attempted to study the heat effects in carbonate leaching of uranium ores due to presence of pyrite. Neither reagent consumption nor the heat effects are crucial if the ores contain small quantities, < about 1%, of sulphides. If the ores contain >4% sulphides, the sulphides are removed by flotation or by roasting [40, 8] before the uranium is extracted. However, for ores containing intermediate quantities of pyrites that are recommended for direct alkaline leaching along with pyrites, as in the case of Tummalapalle uranium ore of India (contains about 1.5% FeS_2), the heat effects cannot be ignored. The present study includes a Section on predicting the leaching efficiency as a function of time, inlet slurry temperature and pyrite content of the ore. The simulation of residence time and heat of absorption/evolution for continuous leaching from the laboratory data is useful in operation of the recently commissioned alkaline leaching plant at Tummalapalle in India.

A brief description of the two Indian uranium ore deposits considered in the present thesis is given in the following Sections.

1.2.1 Tummalapalle uranium ore deposit

Uranium occurrence in dolostone near Tummalapalle was first discovered in 1986 during the investigation carried out by Geological Survey of India (GSI) for phosphates [23]. Subsequently, surface and sub-surface exploration by Atomic Minerals Directorate for Exploration and Research (AMD) in two phases i.e. from 1987 to 1993 and 2007 to date have proved significant resources of low grade large tonnage uranium deposit. Tummalapalle ore deposit is a unique type of uranium mineralization called strata-bound, which is not covered under the classification of world uranium deposits by IAEA till recently. The extensive uranium reserves in this deposit paved way for introducing a new type called ‘carbonates’ by IAEA in their list of classification of uranium ore deposits. Fig. 1.4 shows the geological map of Cuddapah basin including Tummalapalle ore deposit. It extends from Reddipalle in the northwest to Maddimadugu in the southeast over a belt of 160 km., with up to 800 m depth.

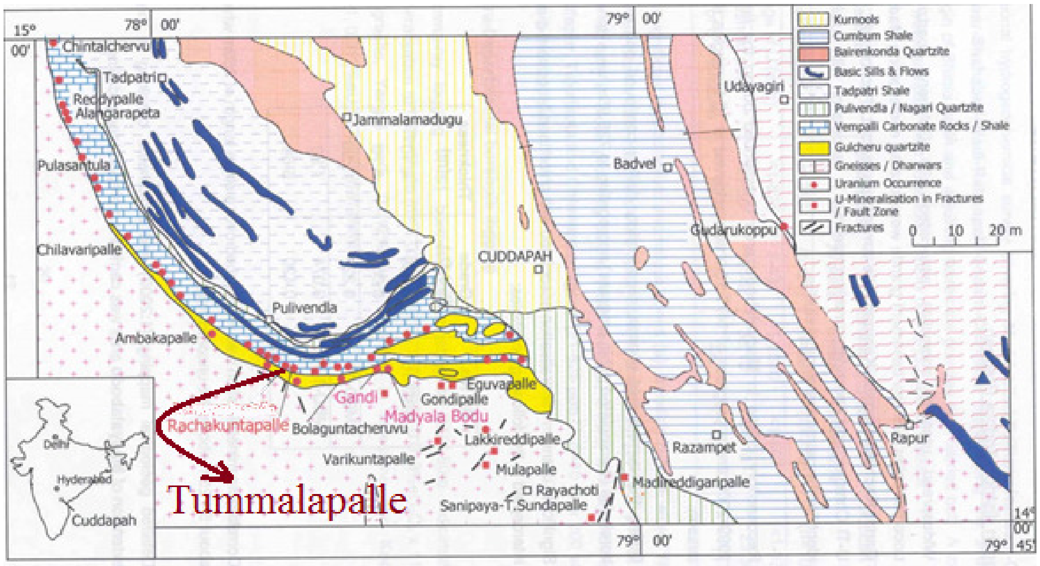

Fig. 1.4 Geological map of southern part of Cuddapah basin showing uranium occurrences including Tummalapalle uranium ore deposit (After: [20])

About 81,000 tonnes U_3O_8 have been established (average grade = 0.04% U_3O_8) in a strike length of 9.5 km up to a vertical depth of 500 m. It is likely that a reserve of 1,50,000 tonnes U_3O_8 will be established in 15 km sector up to a vertical depth of 800 m. It is the single largest deposit found in India so far and has the potential to become the world’s largest uranium deposit with probable estimates of 8,00,000 tons of uranium over a total strike length of 160 km [41]. A commercial mill with a throughput of 3000 tons of ore per day has been recently commissioned at Tummalapalle. A number of satellite deposits are envisaged in this belt of uranium resource, the characteristics of which may vary in mineralogy including tenor of the ore, pyrite content etc. from pocket to pocket. Hence, studies to understand the leaching behavior of Tummalapalle ore including the effects of the variations in ore characteristics will be of utmost use in maximizing the recovery of uranium in the existing / under expansion / new mills in and around this deposit.

1.2.2 Gogi Uranium ore deposit

The uranium deposit in the Bhima river basin at Gogi, Yadgir District of Karnataka has an average tenor in the range 0.15% U_3O_8, the country's highest grade so far reported. The deposit was discovered by AMD during 1994-96. Extensive exploration has so far proved nearly 4682 tonnes of U_3O_8 [25]. The deposit is classified under the category 'Protozoic unconfirmity' type among the 16 types of deposits listed in Table 1.2. The ore body is located in a marshy land near two natural lakes, 'Gogi Lake' and 'Rabanahalli Lake'. The mineralization is hosted by both basement granites and overlying Shahabad limestones, with nearly two thirds of the uranium values being distributed in limestone type and one third in granite. The studies presented in the thesis were carried out on the limestone sample. Fig. 1.5 shows the geological map of Bhima basin showing Gogi ore deposit (source: [23]).

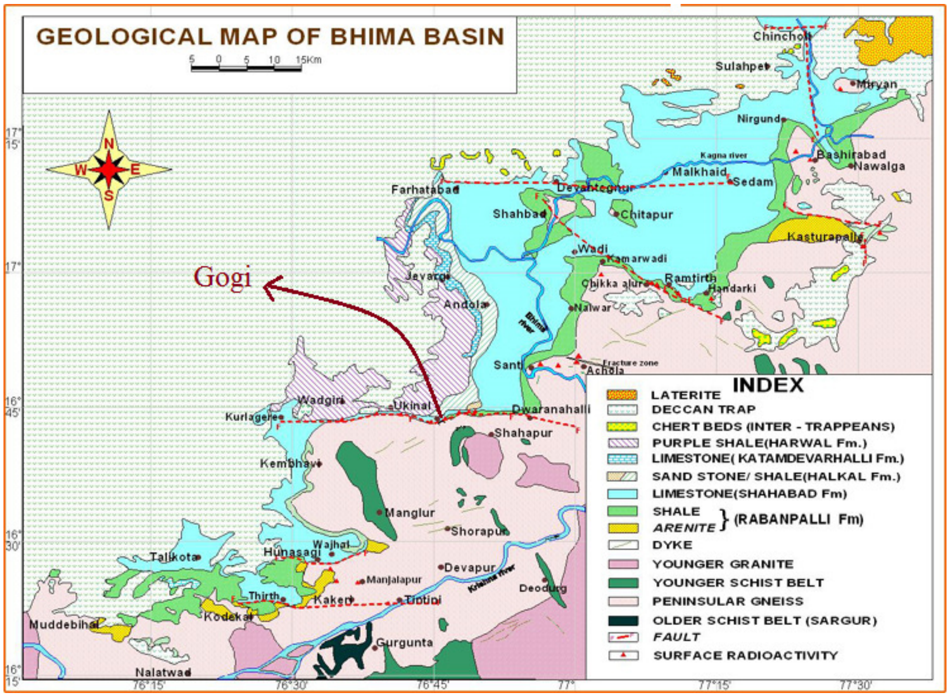

Fig. 1.5 Geological map of Bhima basin showing uranium occurrence at Gogi uranium ore deposit (source: [23])

In spite of being the highest grade ore deposit so far found in India, the Gogi deposit has not been considered seriously until a few years back, in view of the smaller tonnage of the deposit. However, the increasing demand of the uranium for the country's reactors, both operating and under construction, has created interest in this deposit.

1.3 OBJECTIVES AND SCOPE OF THE THESIS

Understanding the dissolution of pure uranium dioxide and iron pyrite minerals is important for the understanding of their leaching from complex natural ores. Hence, initial experiments were carried out on the leaching of pure materials both as individual and in the form of synthetic mixture followed by the experiments on actual low grade Indian uranium ores. Fig. 1.6 summarizes the components of the research work conducted.

The objectives of the thesis are: (1) to develop kinetic models of dissolution of uranium dioxide (UO_2), the chief uranium mineral of economic interest, and iron pyrite (FeS_2), the common reactive gangue mineral in uranium ores (under basic studies), (2) to develop kinetic models for leaching efficiencies of uranium in actual Indian ores, namely, Tummalapalle in Andhra Pradesh, and Gogi in Karnataka (under applied studies), (3) to determine the optimum values of leaching parameters such as reagent concentration, pressure, temperature, particle size, for mixtures of minerals, as well as for uranium ores, (4) to compare alkaline leaching behavior of synthetic mixture (ideal system) with actual uranium ores, (5) to elicit beneficial and deleterious effects of presence of the reactive gangue mineral, iron pyrite, on leaching of uranium, (6) to characterize the feed and leach residues and corroborate underlying microscopic phenomenon in alkaline leaching of pure minerals and low grade Indian alkaline host rock deposits, (7) to quantify the role of oxygen in alkaline leaching of uranium from Indian ores containing uraninite (U_3O_8) mineral, (8) to scale up the alkaline leaching process from batch level to continuous pilot level, using residence time distribution, and (9) to validate heat effects in the continuous leaching model on pilot scale for extrapolation to commercial alkaline leaching plant data of an Indian uranium ore.

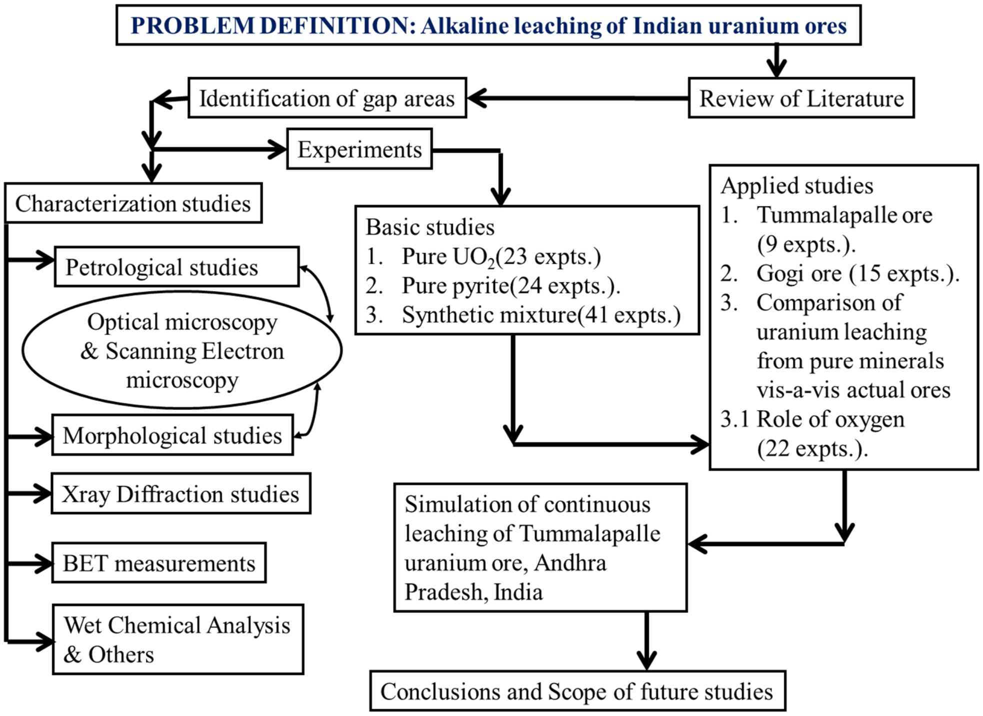

Fig. 1.6 The research layout

1.4 ORIGINAL CONTRIBUTIONS

- Development of a generalized topochemical reaction model to predict the leaching behaviour of Gogi uranium ore hosted in carbonate rocks of India.
- Development of a pore diffusion controlled model incorporating particle size distribution for leaching of uranium from Tummalapalle ore, Andhra Pradesh, India.
- Prediction of leaching efficiency and leach solution composition with the variation in the mineralogy of Indian ores from pocket to pocket during mining. This precludes the need of generating batch leaching kinetic data, whenever the ore characteristics change. The results of the present study serve as a reference for predicting the leaching efficiency as a function of time, inlet stream temperature and pyrite content of the ore in a commercial uranium leaching reactor.

- Scale-up of batch kinetic data to continuous pilot level operation by residence time distribution method. This scale-up is useful in operation of the recently commissioned alkaline leaching plant at Tummalapalle ore in India and design of uranium leaching plant at Gogi deposit (Karnataka), the committed and forthcoming commercial centre in our country.
- Quantification of the critical influence of iron pyrite (FeS_2), a gangue mineral commonly found in uranium ores on the dissolution of uranium dioxide under oxidative alkaline conditions. The rate of dissolution of UO_2 increases, at 125°C and 7.5 atm pressure using oxygen, with initial increase in FeS_2 content in the feed and decreases when the FeS_2 weight increases beyond 3% (by wt.).
- Corroboration of leaching results with in-depth optical and scanning electron microscopic studies including the morphological changes that occur during leaching of the pure minerals, uraninite and pyrite, vis-a-vis two Indian uranium ores.

CHAPTER 2

Literature Survey

The leaching behavior of an ore depends on its physical and chemical properties, composition and degree of liberation of each mineral present in the ore and the nature of leaching reagents. The siliceous uranium ores are processed by mild sulfuric acid leaching owing to the low cost of commercial acid. However, the uranium ores containing high carbonate (> 12-15% by wt) consume high amounts of acid and form gypsum that make the process uneconomical and impractical, if acid leaching process is adopted [7, 8]. Hence, these ores cannot be processed by acid leachant, but ought to be processed by alkaline leachants. The physical and chemical properties of the minerals commonly found in uranium ores conducive to alkaline leaching are shown in Table 2.1 [42 - 44]. Properties of leachants used in the present study are given in Table 2.2. Generic process flow sheet for the extraction of uranium from its ore to nuclear fuel and current status of uranium mills based on alkaline processing are reviewed in this Chapter. Various kinetic models propounded by different authors on alkaline leaching of uranium have been discussed. The Chapter is concluded by listing out the gap areas that need to be looked into in alkaline leaching of uranium. Some of the relevant aspects which could not be covered here, for want of continuity, are discussed in detail in the individual Chapters.

Table 2.1 Physical and chemical properties of the common minerals associated with uranium ores

Property	Uraninite	Iron Pyrite	Calcite	Dolomite	Quartz
Formula	$(UO_2)_x(UO3)_y$	FeS_2	$CaCO_3$	$CaMg(CO_3)_2$	SiO_2
Crystallography Lattice parameters					
$a(A^0)$	5.47	5.42	4.99	4.84	4.91
$Z(A^0)$	4	4	6	3	3
$b(A^0)$	-	-	-	-	-
$c(A^0)$	-	-	17.06	15.95	5.4
Crystal System	Isometric-Hexoctahedral	Isometric-Diploidal	Trigonal-Hexagonal Scalenohedral	Trigonal-Rhombohedral	Trigonal-Trapezohedrall
Cleavage	Indistinct	Poor	1,3 - rhombohdral	1,3 - rhombohdral	Indistinct
Specific Gravity	11	5	2.7	2.8-3	2.6
Hardness	5.5	6.5	3	3.5-4	7
Fracture	Conchoidal to uneven	Conchoidal	Conchoidal	Conchoidal	Conchoidal

Property	Uraninite	Iron Pyrite	Calcite	Dolomite	Quartz
Lustre	Sub metallic	Metallic	Vitreous	Vitreous, Pearly	Vitreous
Transparency	Opaque	Opaque	Transparent to Opaque	Transparent to Transluscent	Transparent
Colour	Brownish Black, Gray, Grayish Black, Black	Pale brass yellow	Colourless, white	Colourless, white	Brown, Colorless, Yellow
Streak	Brownish Black	Greenish black	White	White	White
Tenacity	Brittle	Brittle	Brittle	Brittle	Brittle
Magnetism	Paramagnetic	Paramagnetic	Non Magnetic	Non Magnetic	Non Magnetic
Occurrence	Crystalline	Druse, Stalactitic, Straited	Crystalline – Coarse, Stalactitic	Crystalline – Coarse	Crystalline – Coarse / Fine
Optical properties	Isotropic	Isotropic	Uniaxial (Anisotropic)	Uniaxial (Anisotropic)	Uniaxial (Anisotropic)
Melting point (°C)	2865	1177-1188	1339	≈2570-4660	1670
Solubility in water	Insoluble	Insoluble	Insoluble	Insoluble	Insoluble
Radioactivity	70 Bq/g to 150 kBq/g	Non-radioactive	Non-radioactive	Non-radioactive	Non-radioactive

The uraninite is only mildly radioactive. The radiation level at one metre from a drum of freshly-produced U_3O_8 is about half that - experienced from cosmic rays - on a commercial jet flight [2]. The uranium minerals contain a small amount of radium as a radioactive decay product of uranium. Uraninite also contains small amounts of the lead isotopes ^{206}Pb and ^{207}Pb, the end products of the decay series of the uranium isotopes ^{238}U and ^{235}U respectively [45].

Table 2.2 Physical and chemical properties of reagents used for alkaline leaching of uranium

Property	Na_2CO_3	$NaHCO_3$	O_2
Molar mass (g/mol)	106	84	32
Density (g/cc) @ NTP	2.54	2.2	1.331×10^{-3}
Melting point (°C)	851	50 (decomposes to Na_2CO_3)	-219
Solubility in water (g/L) @ 20°C and 101.3 kPa pressure	70	90	0.0076

2.1 EXTRACTION TECHNOLOGY OF URANIUM

Around 75% of the world's uranium supply is from the primary sources, the freshly dug uranium ores [18]. The rest is produced as a by-product from secondary sources such as recycled nuclear fuel, and from nuclear warheads that have been declared surplus. Uranium is extracted by hydrometallurgical process from both the primary and the secondary sources. Summary of the general extraction process is given in the following Section.

2.1.1 Generic process flow sheet – ore to nuclear fuel

The conventional production of nuclear grade uranium from its ores includes two steps: (1) Production of crude uranium concentrate, often termed as yellowcake, from the ore. The central process in this step is leaching, which is discussed in detail later in Section 2.1.3. (2) The yellowcake is then refined to nuclear grade uranium by adopting a series of solvent extraction steps and calcination stages. The generic flow sheet of extraction of uranium from ore to yellowcake, the intermediate concentrate (assays 50 - 70% U_3O_8, depending on the uranium compound produced) is shown in Fig. 2.1 (source: [46]).

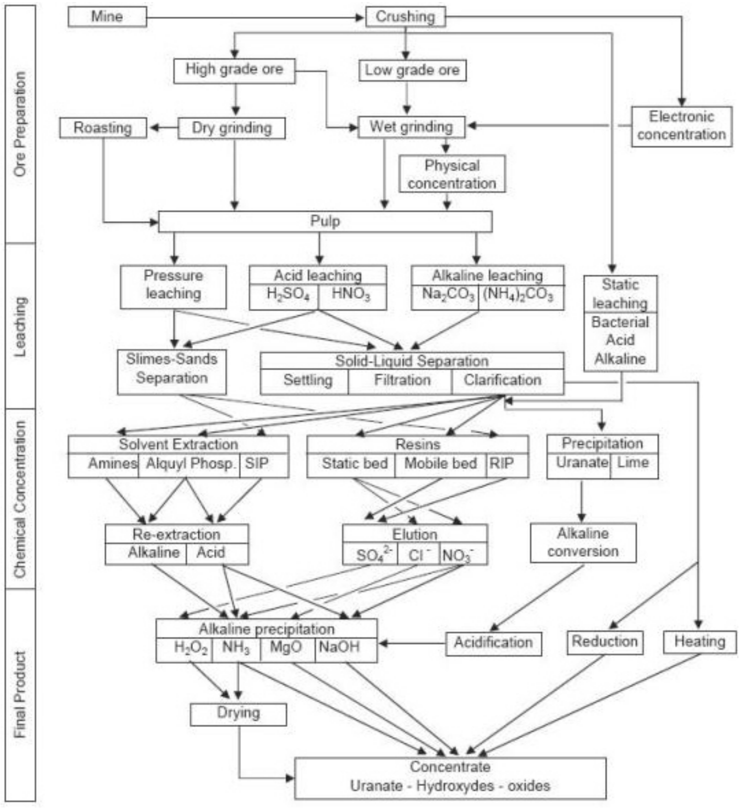

Fig. 2.1 Generic process flow sheet for recovery of uranium as intermediate concentrate (yellowcake) starting from the ore (source: [46])

Essentially, the uranium ores are crushed and ground to powder form using Gyratory and Jaw crushers followed by ball mills/rod mllls/autogenous mills. The ground ore is subjected to leaching directly in general. However, the ground ore sometimes is roasted before leaching either to improve the solubility of the valued constituents (like Vanadium) or to improve the physical characteristics of the ore (alteration of clay minerals to improve ore settling and filtering characteristics). Pretreatment of ore by roasting also helps in removal of organic carbon from carbonaceous type ores to prevent contamination of the leach solutions and interference with the solubilization of the uranium minerals [8]. The leaching of the uranium ore is carried out either by acid / alkaline reagents.

In the acid leaching, the leach liquor containing dissolved uranium is concentrated and purified by ion exchange / solvent extraction. In contrast to the acid leaching, the alkaline leaching, being selective yields relatively pure solution that does not require any pre-purification for precipitation of the uranium. The soluble uranium is precipitated as uranium compounds such as magnesium diuranate (MDU, MgU_2O_7), sodium diuranate (SDU, $Na_2U_2O_7$), ammonium diuranate (ADU, $(NH_4)U_2O_7$), uranium peroxide (UO_4). All of these precipitates often appear yellow and hence they are traditionally known as yellowcake. These are then further purified to nuclear grade by solvent extraction. The yellowcake is dissolved in nitric acid and the uranium is then selectively extracted from this acid by tributyl phosphate solvent-extraction process using kerosene as diluent. Uranium is stripped into acidified water to yield uranyl nitrate, $UO_2(NO_3)_2$, from which ammonium diuranate (ADU) is precipitated using aqueous ammonia. ADU is calcined to UO_3, which is then reduced to UO_2 with hydrogen. The UO_2 is used as ceramic nuclear fuel for the nuclear power reactors that run on natural uranium (in which the isotopic concentration of $U^{235} \approx 0.7\%$). A typical process flow sheet followed in India for the production of nuclear grade (>99% UO_2 with equivalent boron content

(EBC) < 4 µg/g on U weight basis) uranium oxide from the yellowcake, is shown in Fig. 2.2 (After: [47]). The flow sheet also gives an outline of the processes followed, in general, for any other ores elsewhere in the world. Minor variations are adopted depending on the differences between specific ores.

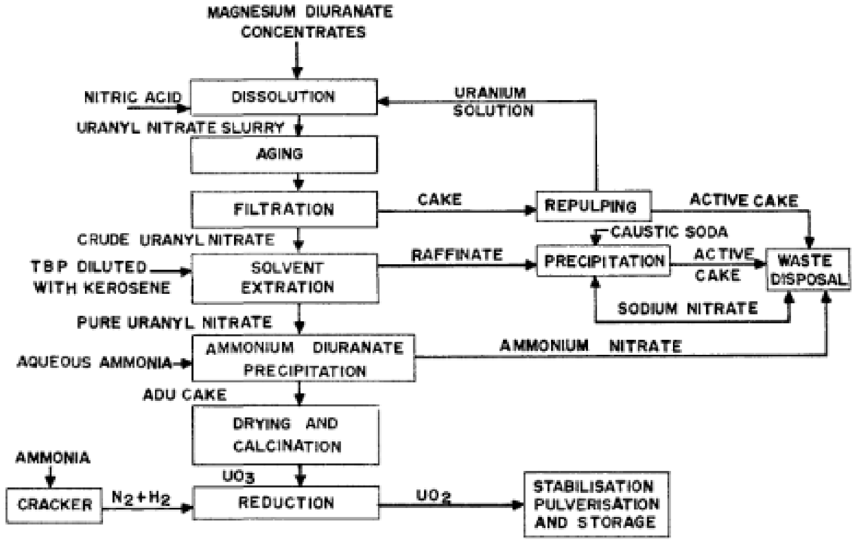

Fig. 2.2 Process flow sheet for producing nuclear grade uranium oxide starting from the intermediate concentrate (yellowcake) – After: [47]

Where the enriched uranium (contains 3-5 % U^{235} isotope) is required for producing nuclear power, the natural UO_2 is treated by gaseous HF at 550°C to produce gaseous UF_4. The UF_4 is fluorinated at 350°C with F_2 gas to volatile UF_6, which is then subjected to isotopic enrichment of U^{235}, the fissile atom by any of several methods – gaseous diffusion, gas centrifugation, liquid thermal diffusion. After enrichment, UF_6 is reacted with water vapor followed by hydrogen reduction to produce powdered UO_2 for use as ceramic fuel in nuclear power reactor. Where the final product required is uranium metal, UO_2 is converted to UF_4 by hydro fluorination and then converted to uranium metal ingots by calciothermy.

2.1.2 Uranium recovery from secondary and unconventional resources

The secondary and unconventional resources of uranium include: (1) phosphate rocks containing 50 to 200 ppm U, which are processed by the fertiliser industry, (2) monazite – a rare earth rich mineral containing traces of uranium, (3) depleted uranium – the recycled nuclear fuel, (4) uranium stockpiles in different countries, which are often not well quantified. Since most of the secondary resources of uranium reported to date in the Red book are associated with uranium in phosphate rocks [21], only the recovery of uranium from phosphates is discussed in brief in this thesis. The details of recovery of uranium from other secondary and unconventional resources can be found at [48, 49].

The potential uranium content of known phosphate rock around the world, mainly occurring in Morocco, United States, Mexico, Jordan and Kazakhstan, is about 14 million tonnes as of February 2015 [2]. The main mineral in phosphate rock is apatite, most commonly known as fluorapatite - $Ca_5(PO_4)_3F$, which contains rare earths, iron and uranium as impurities [50]. The fluorapatite is acidulated by H_2SO_4 to produce Wet Phosphoric Acid (WPA) containing uranium in soluble form predominantly in U(VI) valency. Before producing fertilizers from WPA, the uranium is generally extracted by three industrial solvent extraction processes [51]: (1) The di-octyl-pyro-phosphoric-acid (OPPA), (2) The di-(2-ethyl-hexyl-phosphoric)-acid tri-octyl-phosphine-oxide (DEHPA-TOPO), and (3) A mixture of mono-octyl-phenyl-phosphoric-acid and di-octyl-phenyl-phosphoric-acid (OPAP).

2.1.3 Leaching of uranium ores

Leaching forms central unit operation in the overall strategy for the extraction of uranium from its ores. It is carried out by either acidic or alkaline type reagents [8]. The choice of type of leaching is often determined by the chemical nature of gangue minerals rather than that of uranium minerals in the ore. Acidic reagents are used in majority of uranium mills, owing to their low cost and higher reactivity resulting in increased yields. The ores with quartz as the main gangue mineral are subjected to leaching with acidic type of reagents, usually dilute H_2SO_4. Some of the other common acidic reagents in practice are $Fe_2(SO_4)_3$ – H_2SO_4, HCl, $FeCl_3$ – HCl, HNO_3, Caro's acid [52]. The leaching reaction of acids is not only fast but also dissolves many impurities from the ore along with uranium. Hence the process flow sheets using acidic leachants employ purification steps, such as ion exchange / solvent extraction before precipitation of uranium.

However, acid leach technology is not techno-economically viable, when the ore contains high acid consuming gangue minerals like carbonates. Use of high acid in such cases is not only prohibitively costly but also forms gypsum ($CaSO_4$), which hinders slurry agitation and thereby diffusion of reactants to uranium mineral sites. Typically, ore containing >12-15% carbonates cannot be subjected to acid leaching [7, 8]. The alkaline reagents used for extraction of uranium are Na_2CO_3 – $NaHCO_3$, $(NH_4)_2CO_3$. They are very selective for uranium. Hence, the process flow sheets using alkaline leachants yield relatively pure uranium solutions and the requirement of conventional pre-purification operations like ion exchange are eliminated wherever possible. Since alkaline reagents are slow in reaction, extraction process using these reagents requires drastic process conditions like fine particle size, higher temperature and pressure to dissolve uranium from its ore. The alkaline leaching becomes costlier owing to the expensive nature of alkaline reagents and the above mentioned drastic conditions required for leaching.

Uranium occurs in +4 oxidation state in most of its minerals. Some of the uranium minerals include simple oxides such as Uraninite and Pitchblende, simple silicates such as Coffinite, Uranothorite, multiple oxides such as Microlite, Brannerite, Euxenite and Davidite and hydrated oxides and Uranyl salts such as Gummite, Autunite and Uranophane. Uranium minerals like Betafite, Brannerite and Davidite containing Ti are refractory in nature and hence difficult to leach. Minerals like lead uranate and Kasolite, $Pb(UO_2)SiO_3(OH)$ cannot be dissolved by alkaline leach reagents due to formation of insoluble layer of $PbCO_3$ on the mineral surface [53A]. Uranium in +4 oxidation state is not directly soluble in either alkaline or acidic leaching reagents. Hence, it inevitable to use an oxidant during both acid and alkaline leaching processes to convert U^{+4} to U^{+6}. Some of the oxidants used are $KMnO_4$, MnO_2, H_2SO_5 (Caros acid), SO_2-O_2, Cu-NH_3, $KClO_3$, $FeCl_3$, H_2O_2, NaOCl, O_2 at atmospheric pressure / under high pressure, air at atmospheric /under pressure [53B]. Some catalysts like $HgCl_2$ and Ag_2SO_4 have been found to be effective in increasing oxidation rate of uranium, but their use is prohibitively costly [8]. MnO_2 cannot be used in alkaline leaching as it does not reduce itself in higher pH conditions. Similarly, H_2SO_5, SO_2-O_2 also cannot be used in alkaline leaching due to their acidic nature. Once Uranium is converted to U^{+6}, it is highly soluble in any of the above mentioned lixiviants (acid/alkali). Owing to this high solubility, extent of leaching of uranium is not limited by chemical equilibrium. Hence, single stage of leaching is theoretically sufficient for highest extraction of uranium from the ore. The differences between acid and alkaline leaching processes is summarized in Table 2.3.

Table 2.3 Comparison of acid and alkaline leaching of uranium ores

Feature	Acid Leaching	Alkaline Leaching
Gangue minerals that dictate type of leaching	Silica-rich ores	Ores with >12-15% carbonates
Lixiviants	H_2SO_4, Fe_2SO_4-$H_2SO_{4,}$ HCl, $FeCl_3$-HCl$_,$ $HNO_{3,}$ H_2SO_5	Na_2CO_3 – $NaHCO_3$, $(NH_4)_2CO_3$
Reactivity	Vigorous	Mild
Conditions of leaching	Mild	Drastic – elevated T and P
Selectivity	Indiscriminate	Very selective
Oxidants	MnO_2, $KMnO_4$, H_2SO_5, HNO_3, Air, O_2	$KMnO_4$, $CuSO_4$-NH_4OH, $K_3Fe(CN)_6$, NaOCl, Air, $O_{2,}$ Pb_3O_4, PbO_2, $K_2S_2O_8$, H_2O_2
Ineffective oxidants	-	MnO_2, $NaBiO_3$, KNO_3, $NaNO_3$, $NaClO_3$, $KClO_3$, $K_2Cr_2O_7$, Ni_2O_3, $CuSO_4$
Catalytic oxidants*	$HgCl_2$, Ag_2SO_4	$CuSO_4.5H_2O$ - NH_4OH, $HgCl_2$, Hg_2Cl_2, Ag_2SO_4
Soluble complex	$UO_2(SO_4)_3^{-4}$, $UO_2(NO_3)_{2,}$ UO_2Cl_2	$UO_2(CO_3)_3^{-4}$

*Catalyst: oxidation-reduction couple with less negative potential than secondary oxidant , but more –ve than the couple UO_2 - $UO_2(CO_3)_3^{-4}$

<u>2.1.3.1 Basic chemistry of dissolution of uranium:</u> The acid and alkaline leachants have high solubility for anionic uranium complexes of U^{+6} ion only and not U^{+4}. Hence, invariably, the U^{+4} is oxidized first to U^{+6} and then solubilized by formation of complex anion either as uranyl sulfate ($UO_2(SO_4)_3^{-4}$) or as uranyl carbonate ($UO_2(CO_3)_3^{-4}$) using mild sulfuric acid or carbonate solution respectively. The Pourbaix diagram of U-O-H system given in Fig. 2.3 (source: [54]) illustrates the stability of UO_2^{+2} ion as the only important mobile form of uranium. $U(OH)_5^-$ is not considered as an important mobile form because it is difficult to attain the conditions (12<pH<14) under which it is stable according to Fig. 2.3.

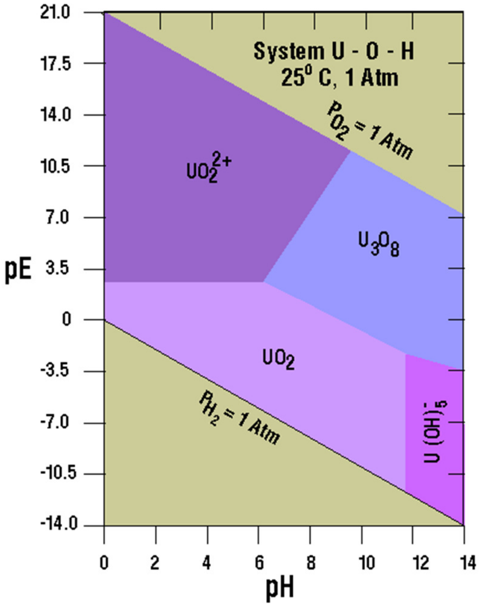

Eh =0.05917 pE

Fig. 2.3 Pourbaix diagram of U-O-H system (After: [54])

The basic chemical reactions that occur during acid and alkaline leaching of uranium ores are given below.

<u>Acid Leaching</u>

$$2Fe^{2+} + MnO_2 + 4H^+ \rightarrow 2Fe^{3+} + Mn^{2+} + 2H_2O \qquad [2.1]$$

$$UO_2 + 2Fe^{3+} \rightarrow UO_2^{2+} + 2Fe^{2+} \qquad [2.2]$$

$$UO_2^{2+} + 3SO_4^{2-} \rightarrow UO_2(SO_4)_3^{4-} \qquad [2.3]$$

In acid leaching, MnO_2 oxidizes Fe^{+2} to Fe^{+3}, which in turn oxidizes U^{+4} to U^{+6} as direct oxidation of uranium by MnO_2 is very slow [8, 55]. More details about acid leaching of uranium can be found in [8, 53A, 56].

Alkaline Leaching

$$2UO_2 + O_2 \leftrightarrow 2UO_3 \qquad [2.4]$$

$$UO_3 + Na_2CO_3 + 2NaHCO_3 \rightarrow Na_4UO_2(CO_3)_3 + H_2O \qquad [2.5]$$

$$UO_3 + 3\,Na_2CO_3 + \,H_2O \rightarrow Na_4UO_2(CO_3)_3 + \,2\,NaOH \qquad [2.5a]$$

$$NaOH + NaHCO_3 \rightarrow Na_2CO_3 + H_2O \qquad [2.5b]$$

$$2Na_4UO_2(CO_3)_3 + 6NaOH \rightarrow Na_2U_2O_7 + 6Na_2CO_3 + 3H_2O \qquad [2.6]$$

$$18(NH_4)_2CO_3 + 6UO_2 + 3O_2 + 6H_2O \rightarrow 6(NH_4)_4UO_2(CO_3)_3 + 12NH_4OH \qquad [2.7]$$

Oxidation of U^{+4} to U^{+6} shown in the reaction (2.4) could be achieved by any of the oxidants tabulated under the column captioned ‘alkaline leaching’ in Table 2.3. The oxidized uranium reacts with carbonate and bicarbonate of sodium to produce a soluble anion complex, sodium uranyl carbonate by reaction (2.5). In fact, this reaction is obtained by adding reactions (2.5a) and (2.5b). Though Na_2CO_3 alone can form soluble uranyl complex, $Na_4UO_2(CO_3)_3$, according to reaction (2.5a), it is necessary to use the combination of Na_2CO_3-$NaHCO_3$ leachants for neutralizing NaOH generated in reaction (2.5a) by $NaHCO_3$ according to reaction (2.5b). If not neutralized, the NaOH precipitates uranium as sodium diuranate, $Na_2U_2O_7$, by the reaction (2.6). Hence, sodium bicarbonate is also added to the leach solution as a buffer to control pH [52, 57, 58], which otherwise could be raised by hydroxyl ion. Alkaline leaching can also be carried out using ammonium carbonate alone as leachant according to the reaction (2.7). Addition of ammonium bicarbonate, unlike in case of sodium carbonate leaching, is not needed during leaching with ammonium carbonate leachant as the NH_4OH produced by reaction (2.7) cannot raise the slurry pH sufficiently high to precipitate ammonium diuranate[59]. In spite of the above advantage, ammonium carbonate is not a preferred alkaline leaching reagent due to its higher cost, higher toxicity and low reactivity.

If any pyrite (FeS_2) is present in the ore, reaction (2.8) also takes place during alkaline leaching with Na_2CO_3-$NaHCO_3$ leachants.

$$4FeS_2 + 15O_2 + 16Na_2CO_3 + 14H_2O \rightarrow 16NaHCO_3 + 4Fe(OH)_3 + 8Na_2SO_4 \qquad [2.8]$$

Reaction (2.8) generates $NaHCO_3$ which neutralizes NaOH which in turn avoids precipitation of uranium as sodium diuranate (SDU). The desirable limit of pyrite for dissolution of total uranium in a given ore can be calculated from the uranium content of the ore and the stoichiometry of reactions (2.5a) and (2.5b), considering that the OH^- ion produced in reaction (2.5a) is neutralized by $NaHCO_3$ produced in reaction (2.8). However, the oxidation of pyrite is highly exothermic [60] and the heat produced raises the temperature of reactor contents if the ore contains high pyrite. Excessive presence of pyrite in the ore also leads to needless consumption of reagent, Na_2CO_3, and oxidant, O_2, (the essential species required for solubilisation of UO_2). Besides, if the concentration of pyrite exceeds 2-4%, the risk of gypsum ($CaSO_4.2H_2O$) precipitation becomes very high [40]. This may cause irreversible plugging of the host rock, reducing the leachability of uranium from the ore. The critical influence of presence of pyrite has been undertaken as part of the present study, which is given in Section 5.3.2. If pyrite present in the ore is >4% by weight, it is removed by either flotation or roasting [40] before extraction of uranium from the non-pyrite portion. In the case of removal of pyrite by flotation, the pyrite rich concentrate and the tails are treated separately by acid and alkaline leaching, respectively, for recovery of uranium [62]. Extraction of uranium from Randfontein ore of South Africa uses a flotation step followed by roasting of flotation concentrate to remove the sulfur for reducing the carbonate reagent consumption by the chemical reaction of pyrite. The roasted concentrate was then subjected to pressure leaching with both sodium carbonate/bicarbonate and ammonium carbonate solutions [59].

Understanding the simultaneous dissolution of pyrite and uranium oxides is complex owing to the non-elementary nature of the parallel reactions (2.4) and (2.8) with respect to oxygen [52, 59]. Reaction (2.5b) forms Na_2CO_3 which in turn acts as reactant in reactions (2.5a) and (2.8). In parallel, $NaHCO_3$ decomposes to Na_2CO_3 according to reaction (2.9) at high temperatures.

$$2NaHCO_3 \rightarrow Na_2CO_3 + H_2O + CO_2 \qquad [2.9]$$

Unlike in the case of acidic leaching, alkaline leaching requires drastic conditions due to its mild reactivity of alkaline reagents compared to acidic leachants. In addition to the drastic conditions like fine grinding, alkaline leaching requires elevated temperature and pressure conditions in general. Depending on the uranium ore mineralogy, constituents of the ore other than uranium, if present, undergo the following reactions at elevated temperature and pressure during alkaline leaching.

If quartz is present in the ore, then reaction (2.10) takes place.

$$SiO_2 + H_2O + 2Na_2CO_3 \rightarrow Na_2SiO_3 + 2NaHCO_3 \qquad [2.10]$$

Alumina, if present in the ore, reacts according to reaction (2.11).

$$Al_2O_3.3H_2O + 2Na_2CO_3 \rightarrow 2NaAlO_2 + 2NaHCO_3 + 2H_2O \qquad [2.11]$$

Adding carbon to the U-O-H system changes its Pourbaix diagram (given in Fig. 2.3) significantly. The Pourbaix diagram of U-C-O-H is depicted in Fig. 2.4 (After: [54]). Uranium forms three carbonate complexes, two of which are soluble and occupy an area of the U-O-H Pourbaix diagram (Fig. 2.3) occupied by the insoluble U_3O_8.

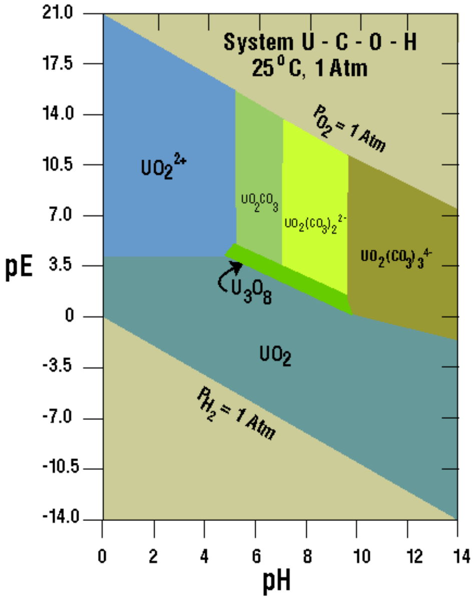

Eh =0.05917 pE

Fig. 2.4 Eh-pH diagram for uranium and carbonate system (After: [54])

Fig. 2.5 (After: [63]) shows the stability of different uranium complexes in carbonate solutions, from which it is evident that concentration of carbonate complex of uranium ($UO_2(CO_3)_3^{-4}$) is maximum at pH =10. It follows that the leaching of uranium is most favorable at pH = 10 using carbonate-bicarbonate leachants.

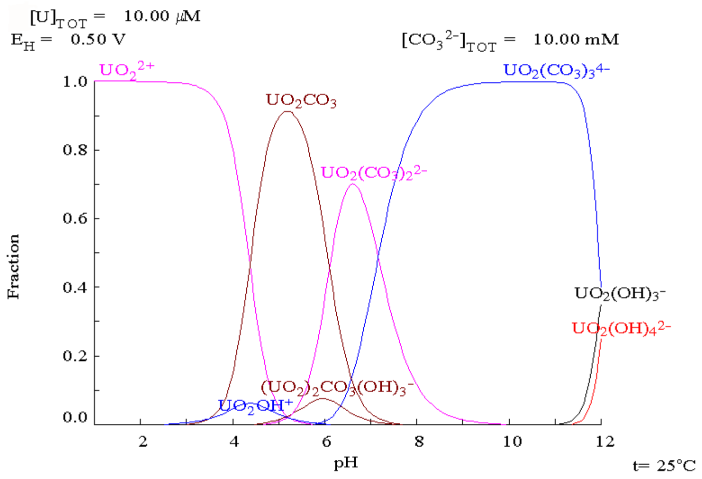

Fig. 2.5 Relative concentrations of the different chemical forms of uranium in an aqueous carbonate solution (After: [63])

Industrially, various types of leaching techniques namely, heap leaching, *In-situ* leaching, pug cure leaching, percolation leaching, conventional mechanical agitation leaching, air agitation leaching in pachucas (being one of the oldest methods in uranium industry) are in practice for uranium extraction from its ores [8, 53A]. Most of the uranium in the world is recovered by acid leaching and *in-situ* leaching technology [61]. While, the uranium ores containing refractory uranium minerals have to be leached in autoclaves at elevated temperature and pressure. Application of high pressures in leaching, not only keeps the lixiviant in liquid state but also increases solubility of gaseous oxidants like oxygen. Higher solubility of oxygen helps in increasing of rate of dissolution of uranium (reactions (2.4) and (2.5)). This thesis presents exhaustive studies on leaching of uranium using mechanical agitation at elevated pressures and temperatures.

2.2 OPERATING URANIUM MILLS BASED ON ALKALINE LEACHING TECHNOLOGY

Most of the uranium production world-wide is from the uranium mills based on acid leaching route. There are very few uranium mills operating at present based on alkaline leaching route, which are given in Table 2.4 [21]. The uranium deposit at Yeelirrie in central Western Australia contains uranium as carnotite ($K(UO_2)_2(VO_4)_2.3H_2O$) mineral, which occurs as coating in cavities and fractures or disseminated through the calcrete (hard material formed from calcium and magnesium carbonate minerals) and clay-quartz alluvium [64]. An in-situ alkaline leach process plant is planned in this deposit [65]. The process planned for Lake Way deposit consists of crushing and screening followed by alkaline heap leach and direct uranium precipitation [66]. The Rozna plant in Czech Republic is the longest operating uranium mill since 1957. The uranium mineralisation at Langer Heinrich occurs as carnotite associated with the calcretisation of valley-fill fluvial sediments in an extensive tertiary palaeodrainage system. The uranium values are recovered by atmospheric alkaline leaching, counter-current decantation, ion exchange separation and precipitation as sodium diuranate. The sodium diuranate product is re-dissolved using sulphuric acid before being re-precipitated with hydrogen peroxide which is dewatered, calcined and drummed as UO_4. Trekkopje uranium mine located in western Namibia in southern Africa, combines two deposits: the Trekkopje and the Klein Trekkopeje [67]. Minerals are largely found within calcium carbonate cemented conglomerates belonging to the Tertiary period. The ore is dug by open cast operation and the processing technology is alkaline heap leaching followed by ion exchange. The process is supported by a reverse osmosis desalination plant to remove chloride from sea water before using in ion exchange. The final product of this plant is sodium diuranate.

Table 2.4 Operating and planned uranium ore processing plants world-wide on alkaline leaching route (source: [21])

Country	**Deposit**	**Details**	
Czech Republic	Dolni Rozinka (Rozna)	Metamorphite Resource 25000 t U Grade 0.251 % U	Operating (1957)
Niger	Azelik – Teguidda Abokurum	Sandstone Resource 15900 t U Grade 0.2 % U	Operating (OP/UG) (2010)
Namibia	Langer Heinrich	Calcrete Resource 50590 t U Grade 0.045 % U	Operating (OP) (2006)
	Trekkopje, Klein Trekkopje	Calcrete Resource 28999 t U Grade 0.012 % U	Committed (OP)
India	Tummalapalle	Stratabound – Carbonate Resource 81000 t U Grade 0.04% U	Operating (2012) Pressurized alkaline leaching
	Gogi	Basement hosted-Proterozoic unconformity Resource 4000 t U Grade 0.2% U	Committed
Australia	Yeelirrie	Calcrete Resource 44500 t U Grade 0.13 % U	Planned
	Centipede, Lakeway	Calcrete Resource 6700 t U Grade 0.05 % U	Planned

2.3 OPERATING URANIUM MILLS IN INDIA

There are three uranium production centers in India at: (1) Jaduguda, (2) Turamdih, and (3) Tummalapalle. The run-off-mine ore (ROM) grades of all the three operating uranium mills is very low < 0.1% U_3O_8. A brief note about each of the uranium mills is described below.

Jaduguda uranium mill: The Jaduguda uranium deposit was first uranium mine in India operating since 1967 at Jaduguda, Jharkhand. The commercial production of magnesium diuranate (MDU) was commenced in 1968. Recently the flow sheet of Jaduguda process plant has been modified to produce a purer product, uranium peroxide ($UO_4.2H_2O$), in place of magnesium diuranate by the method published by [68]. One of the recently published original process flow sheet (source: [69]) of production of magnesium diuranate along with the modified technique for precipitation of uranium peroxide at Jaduguda mill is given in Fig. 2.6. The chlorite-biotite schist type of ore is crushed and ground in a rod and pebble mill to get a product of 60-65% passing through 75 µm size mesh. The ground ore slurry is dewatered using a high rate thickener followed by a disk filter. The filter cake is re-pulped to about 50% solids (by wt.) and then leached in the air agitated leaching tanks, known as Pachucas. Leaching is carried out using dilute sulphuric acid (at about pH 1.6 - 1.8) as leachant and pyrolusite as the oxidant. The leach slurry is filtered and clarified to get the uranium bearing mother liquor. This liquor is purified and concentrated by ion exchange using an anionic exchange resin. The uranium values from the resin are eluated by acidified brine solution, which is treated with lime to increase the pH to about 3.5. The excess iron and sulphate present in the system is removed as Iron-Gypsum Cake (IGC) and recycled back to re-pulping stage before leaching. The uranium is then precipitated as Magnesium Diuranate (MDU) using magnesia liquor at a pH of 6.5 to 7 as per the earlier practice. Currently, a new precipitation technique is adopted at Jaduguda mill which includes addition of H_2O_2 to the iron-free eluate after ion exchange to precipitate uranium peroxide. NH_3 is added to maintain the acidity (pH = 3.5). The leach residue and the barren liquor from ion exchange being devoid of uranium values form the waste streams. The waste streams are neutralized by limestone to precipitate radio-nuclides along with heavy metals like Mn, Fe, Cu etc. The waste slurry is then classified in a hydro cyclone. The cyclone underflow is sent back for mine-backfill and the overflow is sent to tailings pond. The tailings pond effluent is treated with barium chloride and lime to precipitate out radio-nuclides and sent back to tailings pond. The harmless liquid effluent is discharged into the environment.

Turamdih uranium mill: With the depletion of ore from Jaduguda mines, Uranium Corporation of India Limited opened up three more mines at Bhatin, Narwapahar and Turamdih located in the vicinity of Jaduguda. The second uranium mill was commissioned in 2007 which follows the process flow sheet similar to that of Jaduguda. However, the plant incorporates with latest technology in hydrometallurgy that includes apron feeders, particle size monitors, horizontal belt filters in place of drum filters (being used at Jaduguda mill) and high degree of instrumentation [70]. The leaching tanks have been changed from traditional Pachucas (air agitated tanks) to mechanically agitated tanks to have higher degree of mixing in order to keep coarser ore particles suspended in the leaching pulp.

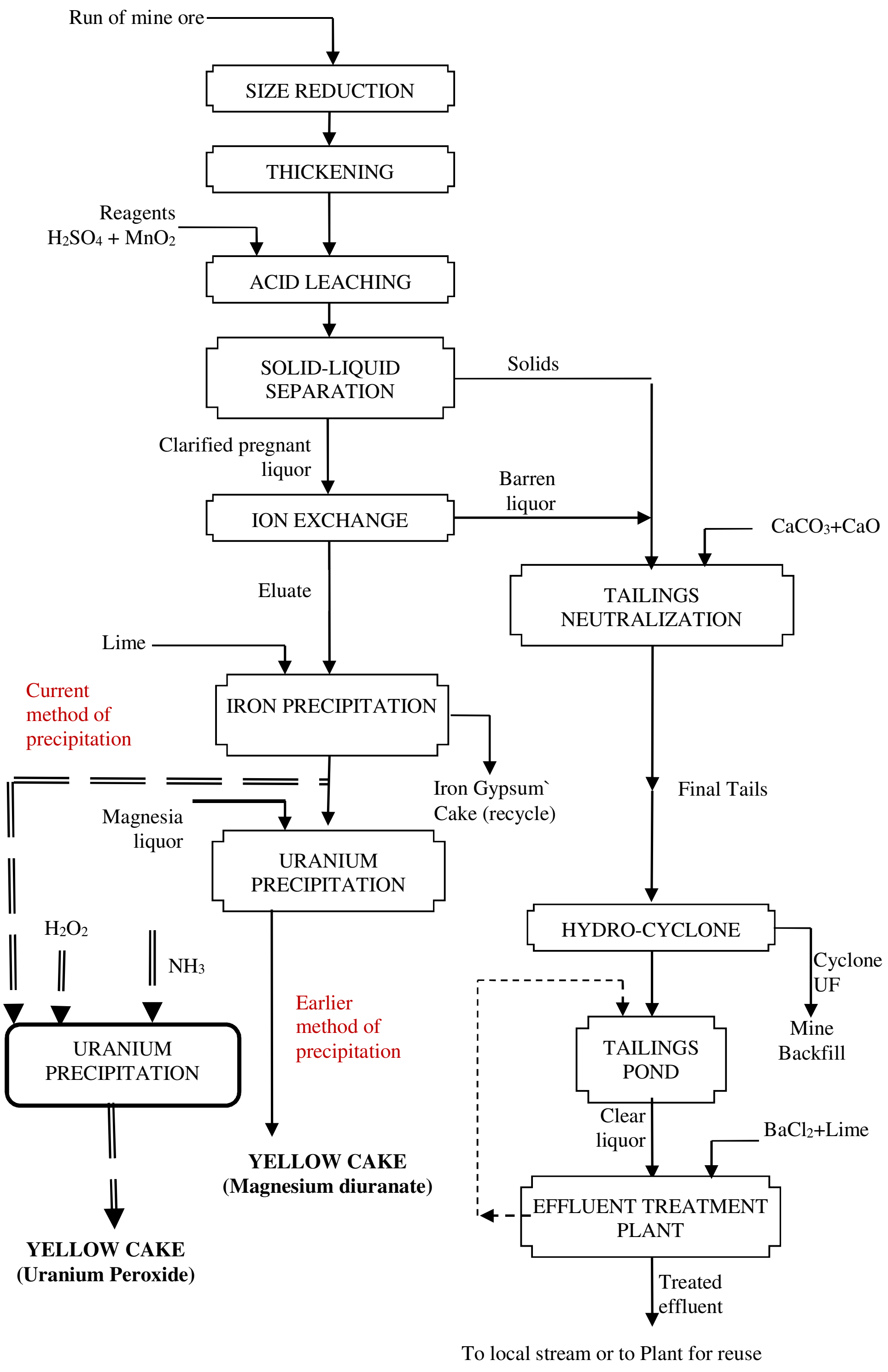

Fig. 2.6 Process flow sheet for the production of yellowcake at Jaduguda, India

Tummalpalle uranium mill: India's first ever uranium mill based on alkaline leaching has been set up by Uranium Corporation of India Limited at Tummalapalle in the year 2012. The process flow sheet is given in Fig. 2.7 (source: [69]), which comprises of alkaline pressure leaching – counter-current filtration – precipitation of sodium diuranate – with regeneration of reagents followed by their recycle. The ROM ore analyses 0.035 % U_3O_8 and 1.6-1.8 % FeS_2. The carbonate ore is crushed and ground to 80-85% passing 75 μm size. The ground ore is subjected to high temperature leaching in an autoclave at 125°C and 7.5 atm pressure using Na_2CO_3– $NaHCO_3$ as leachants and oxygen as oxidant. The plant utilizes two autoclave reactors of 680m^3 volume each with Inconel 600 as material of construction of wetted parts. The hot leach slurry is cooled in a spiral heat exchanger by the counter current flow of incoming feed slurry to the autoclave. The leached slurry is then depressurized into a flash tank. The Tummalapalle plant is one of few plants in the world using spiral heat exchanger for heat recovery from the leach slurry. The leached slurry is filtered using 8 horizontal belt filters of 110m^2 area each with four stage counter-current washing of the filter cake at about 40°C. Part of the leach liquor is bled out, while the rest is recycled to the leaching circuit for increasing the concentration of uranium values in the leach liquor. A bleed-out of 0.28 fraction (by volume) of leach liquor is fixed in order to get the threshold concentration levels of uranium in leach liquor for effective direct precipitation of dissolved uranium as sodium diuranate using NaOH. Close control of solution balance across various stages in the process circuit is imperative in re-cycle mode leaching circuits. The U_3O_8 content of sodium diuranate (SDU) product is about 80% and the equivalent boron content (EBC) is 26 μg/g on uranium metal basis. The caustic values present in the barren solution obtained after SDU precipitation are recycled back through the grinding circuit after causticization and carbonation. The sulfate values present due to oxidative leaching of pyrite are separated out as Glaubers Salt ($Na_2SO_4.7H_2O$) by freeze crystallization. The sodium sulfate byproduct has only 1Bq/g of radioactivity. The treatment of waste streams is similar to that followed in Jaduguda sans neutralization stages.

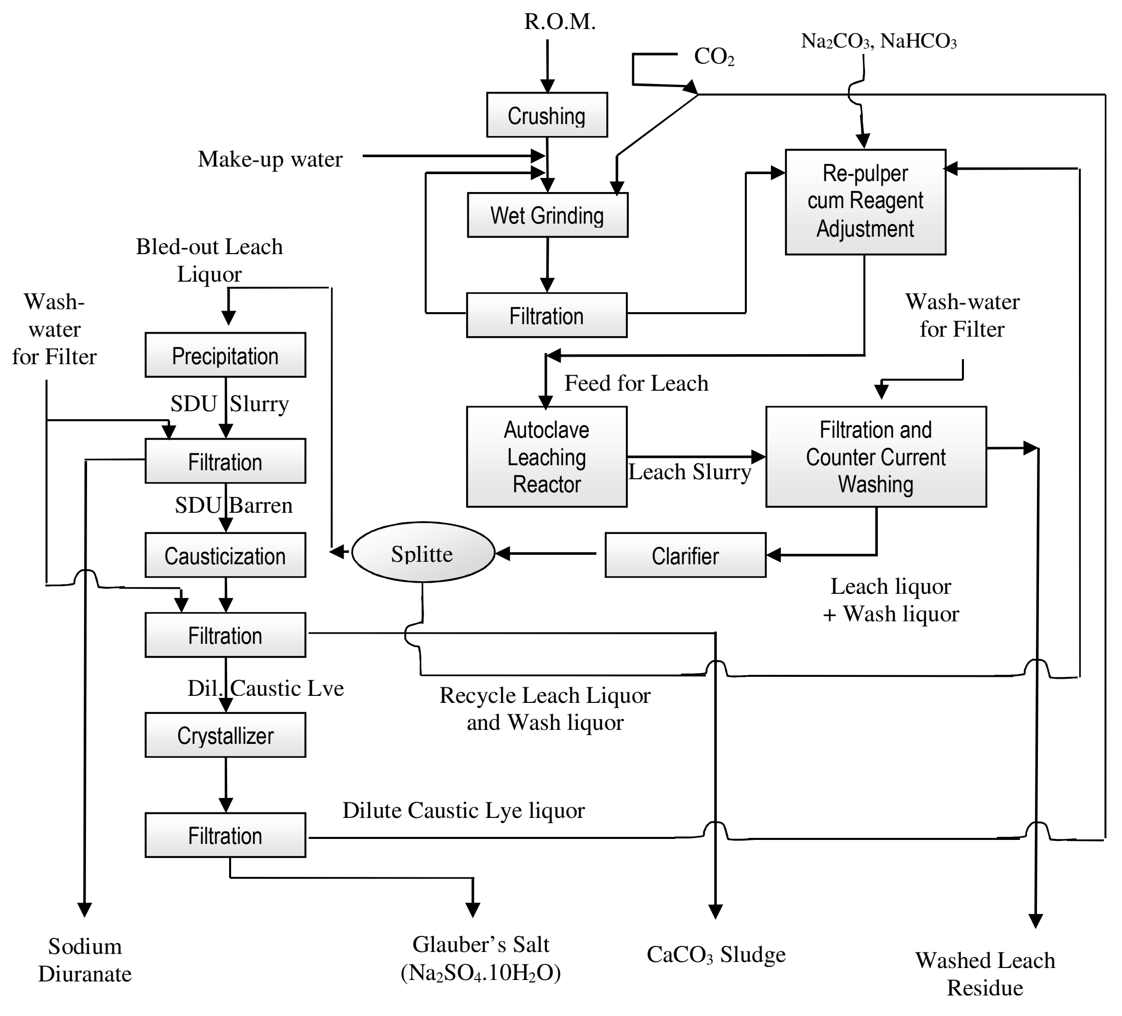

Fig. 2.7 Process flow sheet for the recovery of uranium values from low-grade dolostone type uranium ore at Tummalapalle, India (source: [69])

The Tummalapalle uranium deposit became techno-economically viable because of the process features like: fewer number of processing stages, regeneration and recycle of cost-intensive reagents, purer yellowcake, environmentally safe technology with respect to tailings disposal, a technology which has relatively low equipment corrosion in comparison to conventional sulfuric acid leaching route, minimum process water inventory, zero liquid waste generation and production of by-products like sodium sulfate and high purity calcium carbonate.

2.4 MODELING OF LEACHING PROCESSES

The chemical reactions during extraction of uranium into the liquid phase from the ground ore are controlled by various factors, of which, the main ones are: (1) degree of liberation of uranium mineral in the ore, (2) grain size of uranium mineral, (3) porosity of host rock including gangue as well as uranium minerals, (4) type of leachant, (5) type of oxidant, and (6) system properties like temperature, pressure, stirring speed and type of stirrer. Various mathematical models available in literature for fitting the experimental kinetic data of leaching are summarized in Fig. 2.8.

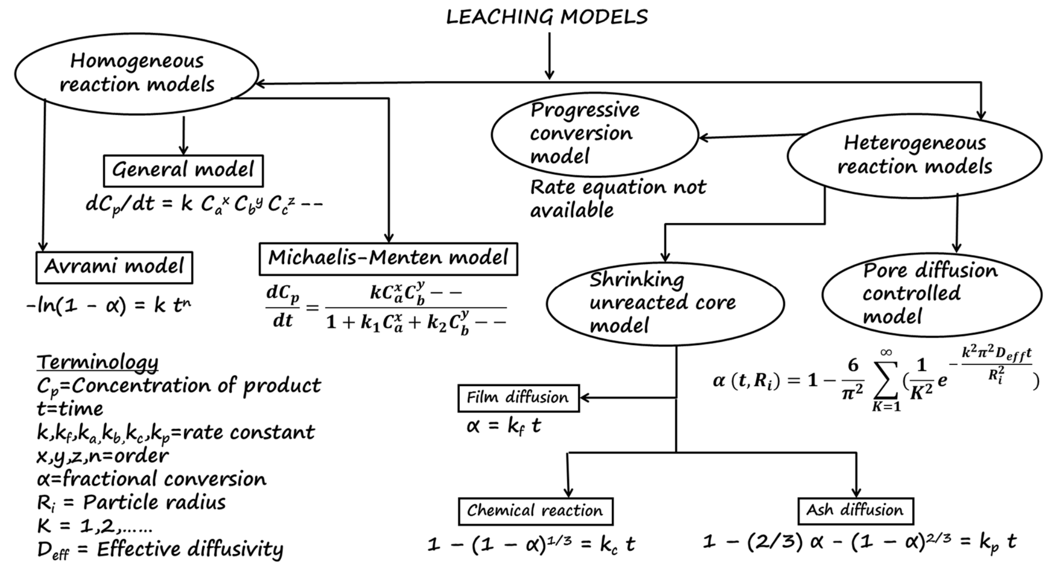

Fig. 2.8 Various leaching models available for fitting experimental kinetic data and their governing rate equations

Even though leaching is a heterogeneous reaction, it is sometimes modeled by homogeneous reaction rate equations [39, 71]. These rate equations obviously do not take into account the specific properties of solid phase such as particle size, specific surface area, porosity. They are applied to leaching based on an assumption that the particle size of solids is so small that the percentage of molecules physically free to react is high enough and the behavior of a solid becomes more nearly like the behavior of a dissolved reactant [37]. Under the general homogeneous models, the first order homogeneous rate equation can be explained by law of mass action: the reaction proceeds faster when the concentration of reactants are increased due to an increase in number of molecules for reaction. Nevertheless, many times the experimental data does not adequately fit the first order rate equation, but fit the rate equations of higher order. There is no strong phenomenological evidence for higher orders in the rate equations other than an analogy with that of first order rate equation [72]. Thus, the orders with respect to each reactant merely serve as empirical constants. Avrami model is another homogeneous model used extensively for rate of crystallization, but also rarely for leaching [73]. This rate function is sigmoidal, with an initial lag-period, where reaction occurs very slowly, followed by a rapid increase and eventually reaching a plateau towards end of the reaction. The Michaelis–Menten kinetics is one of the best known models for enzyme kinetics. However, this form of rate equation is also frequently used for leaching reactions of uranium, pyrites etc. which are driven by electrochemical mechanism [74 - 76]. At lower concentrations of reactants, the Michaelis–Menten rate equation reduces to general homogeneous model equation. And at higher reactant concentrations the leaching progresses as zero order reaction, i.e., at a constant rate independent of reactant concentrations. The heterogeneous rate equations are based on phenomena taking into consideration the solid phase participating in leaching reaction. Fundamentals of kinetics of heterogeneous reaction systems in hydrometallurgy have been dealt with extensively by Sohn and Wadsworth [77]. The progressive conversion model is not generally considered as it does not represent reality of the physical systems [39]. The shrinking core model is most widely applied for leaching reactions taking into account the solid phase. It is also known as topochemical model according to which the rate of leaching is given by product of thermal function, chemical function encompassing concentration of reagents and the topological function representing changing solid grain topology [78]. This model is found to be applicable for some of the experimental data generated in the present study. The application and detailed discussion of this model is given in Sections 6.1.3.1 and 6.2.3.2. The penetration of dissolved reactants and products through pores of the ore particles is aptly represented by pore diffusion controlled model, which is found to be applicable for Tummalapalle uranium ore in the present study. Detailed discussion of this model is given in Section 6.1.3.2.

2.4.1 Models for alkaline leaching of pure uranium dioxide

Several authors have published experimental data and proposed models delineating the influence of reagent concentrations, various oxidants and their concentration, temperature on the kinetics of dissolution of UO_2. Forward et al. [79] and Peters and Halpern [80] suggested that dissolution of UO_2 takes place in two consecutive steps: (1) oxidation of UO_2 to UO_3 followed by (2) dissolution of UO_3 by complexing with CO_3^{-2} ions, in case of alkaline leaching, SO_4^{-2} ions in acid leaching. Habashi and Thurston [36] first proposed that the dissolution of UO_2 was driven by electrochemical mechanism similar to the corrosion of metals. The schematic representation of the electrochemical reaction during leaching of UO_2 proposed by them is shown in Fig. 2.9 (source: [36]).

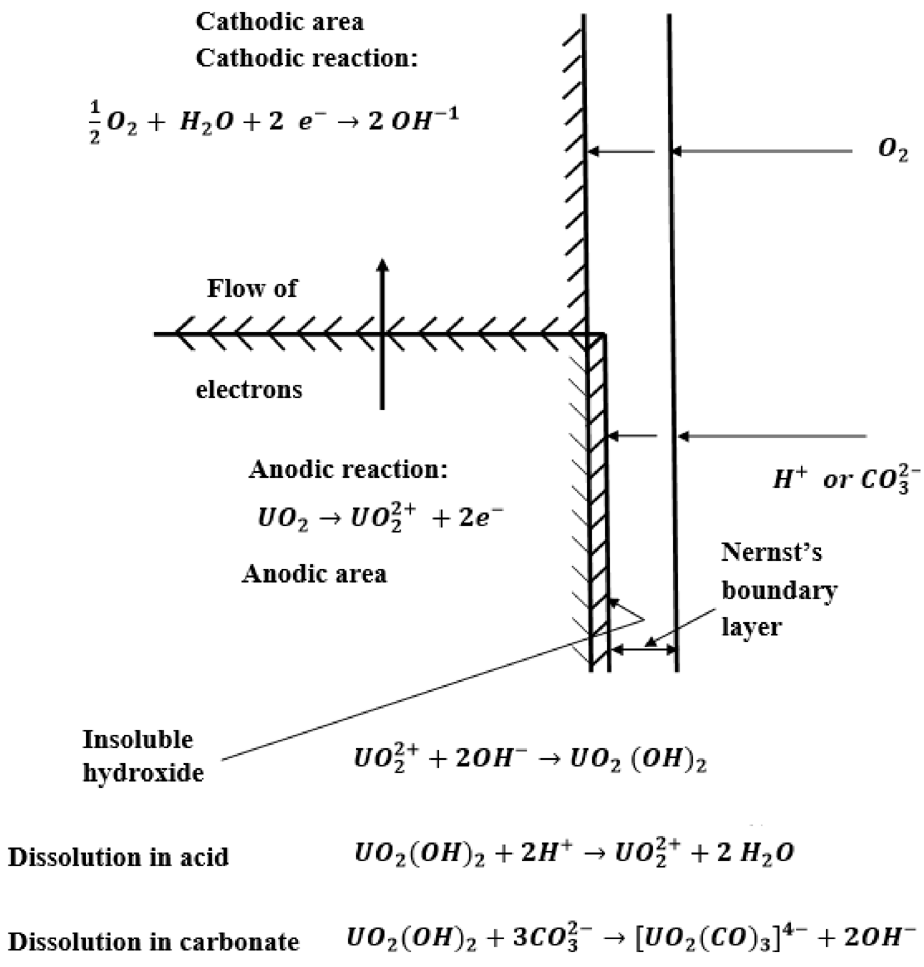

Fig. 2.9 Schematic representation of the electrochemical reactions during leaching of uranium dioxide (source: [36])

Needes et al. [81] could overcome some of the difficulties of previous kinetic models. Activation energy of dissolution of pure UO_2 in carbonate-bicarbonate medium, with sodium hypochlorite as oxidant, was observed to be 57.5 kJ/mol by Sharma et al. [38] indicating the dissolution is surface chemical reaction controlled.

Shane et al. [82] have found that H_2O_2, at 0.1 M concentration is the most efficient oxidant for dissolving UO_2. They have also demonstrated that highest rate of dissolution that could be obtained is 1038 mg/L/min using H_2O_2 as an oxidant at 0.5 M Na_2CO_3 concentration. Increased H_2O_2 concentration leads to decreasing rate of dissolution possibly due to either the effect of increased ionic strength or an increased rate of H_2O_2 degradation. Kweto et al. [83]

determined the kinetics of dissolution of uranium dioxide in ammonium carbonate media using H_2O_2 as an oxidant. They found the order of reaction to be 1 and Arrhenius Activation energy to be 40.2 kJ/mol. The order with respect to concentration of H_2O_2 reported by different authors varied significantly. Smith et al. [84] reported that the order of dissolution of uranium with respect to H_2O_2 concentration is 2.41 with 1 M ammonium carbonate for peroxide concentration between 0.05 and 2 M. Hiskey [85] reported that the order with respect to H_2O_2 is dependent on pH at constant total carbonate concentration (0.5 M ammonical carbonate). At low hydroxide concentrations ($pH < 9.8$), the reaction order was 0.28 and -0.48 at higher hydroxide concentrations. He also reported that the order of the dissolution of uranium dioxide with respect to concentration of total carbonate is 0.5. The leaching rate with H_2O_2 is found to be approximately two orders of magntitude greater than that with O_2 by Hiskey [86] using 0.5 M $(NH_4)_2CO_3$ as leachant. Clarens et al. [87] observed that the dissolution rate of uranium dioxide increased with increasing hydrogen peroxide concentration in carbonate medium.

Some of the kinetic models for leaching of UO_2 proposed by various authors are given in Table 2.5. Shortmann and Desesa [37] deduced a Michaelis–Menten type kinetic rate equation using an electrochemical mechanism which was validated with exhaustive kinetic data on leaching of UO_2 using concentrations of Na_2CO_3 and $NaHCO_3$ in the range 0 to 0.2 M, temperature in the range 60 to 100°C and partial pressure of oxygen from 0.5 to 13.5 atm. The particle size (d_{55}) of the feed solids used is about 45μm. The maximum rate of leaching obtained is 15 mg/L/min. at 93°C, 7 atm. P_{O2} and high reagent concentrations (≈ 0.5 M each of carbonate and bicarbonate). The rate was found directly proportional to the surface area per unit volume. Pearson and Wadsworth [88] found that oxidation of uranium dioxide is directly proportional to the square root of the oxygen partial pressure. Habashi and Thurston [36] have confirmed the necessity of oxygen in oxidizing the UO_2 during its leaching and established an electrochemical mechanism for dissolution of uranium. They have found that the orders of rate of leaching with respect to P_{O2} and $[CO_3^{-2}]$ to be 0.5 and 1 respectively. They reported maximum rate of leaching to be 12 mg/L/min. at 100°C and $P_{O2} = 1.7$ atm. Sharma et al. [38] and Du Preez [58] have found Arrhenius activation energy to be 57 and 51.1 kJ/mol, respectively using sodium hypochlorite as oxidant and 0.5 M total carbonate - bicarbonate conccentration. De Pablo et al. [34] suggested an order of 1 with respect to both dissolved oxygen and $NaHCO_3$, in the absence of H_2O_2. Hossain et al. [71] found that the second order rate constant of kinetics of the leaching of UO_2 incrases linearly with increase of HCO_3^- concentration, below 0.1 M of $[HCO_3^-]$. Above 0.1 M $[HCO_3^-]$, the leaching rate of dissolution was found to be independent of concentration of bircarbonate ion. It follows that the rate of reaction depends on both oxidation and dissolution below 0.1 M $[HCO_3^{-1}]$, while at higher concentrations it is solely governed by oxidation.

The Arrhenius activation energy of the uranium dissolution indicates the temperature dependence of the reaction. The vast range (42 – 59 kJ/mol) of Arrhenius activation energies reported in Table 2.5, shows the varying nature of the dissolution of uranium dioxide in carbonate and peroxide solutions. Casas et al. [90] reported the activation energy of uranium dioxide dissolution in sodium carbonate and hydrogen peroxide as 40 kJ/mol in the temperature range from 20 to 50°C. Hiskey [85] also reported activation energies of 42.9 and 46.5 kJ/mol in ammonium carbonate at 1 and 7.9 atm of oxygen pressure respectively, in the same temperature range. Magno and Desesa [91A] studied the effect of all possible oxidants on leaching rate of UO_2 using Na_2CO_3-$NaHCO_3$ (0.5 M each) along with their cost implication.

Table 2.5 Rate equations of dissolution of pure UO_2 in carbonate medium proposed by various authors

Leching reagents+Oxidant	Rate equation	E_a (kJ /mol)	Source
Na_2CO_3 $+NaHCO_3$ $+ O_2$	$-\frac{dc}{dt}=\frac{k(\frac{S}{L})(p_{O_2})^{\frac{1}{2}}C_r{}^2e^{-\frac{E_a}{RT}}}{K_2+C_r{}^2}$	56	(Schortmann etal, [37])
Na_2CO_3 $+NaHCO_3$ $+ O_2$	$-\frac{d[U_3O_8]}{dt}=k.S.(p_{O_2})^{\frac{1}{2}}e^{-\frac{E_a}{RT}}$	51.4	(Peters etal. [80])
Na_2CO_3 $+NaHCO_3$ $+ NaOCl$	$-\frac{dc}{dt}=k(C_{NaOCl})^{0.98}e^{-\frac{E_a}{RT}}$	57.3	(Sharma et al. [38])
$(NH_4)_2CO_3 + O_2$	$-\frac{dc}{dt}=k(p_{O_2})^{0.6}(C_{[CO_3{}^{2-}]_t})^{0.53}C^a[OH^-]e^{-\frac{E_a}{RT}}$ where a = 0.3 for pH ~<9.8 = -0.48 for pH ~>9.8	42.6 - 46	(Hiskey, [85])
$(NH_4)_2CO_3 + O_2$	$-\frac{dc}{dt}=k(C_{[CO_3{}^{2-}]_t})^{0.57}$	-	(Needes etal. [81])
water	$-\frac{dU}{dt}(gm/cm^2-day)=10^{20.25}(SS)(RF)^{-1}10^{(-3.38-10.8NOC)}(DO)a_{\sum CO_2}a_{\sum H^+}e^{-\frac{E_a}{RT}}$		
		58.5	[Grandstaff [91B])
40 gpl Na2CO3 + 15 gpl NaHCO3 and 0.25 gpl KCN, O2 as oxidant (30°C to 80°C)	$1-(1-X)^{\frac{1}{3}}=k\ t$	51	(Du preez et al. [58])

2.4.2 Models for alkaline leaching of pyrite

Several authors have studied the dissolution of pyrite in alkaline media from coal and systems other than uranium ores [92, 93]. It is reported that dissolution of pyrite in basic media is greater than in acidic media [94]. The main difference between pyrite oxidation under acidic and alkaline conditions is the hydrolysis and precipitation of ferrous/ferric ions as pH increases. The increase in rate of pyrite oxidation with increase in pH and temperature is well established by Nicholson et al. [95]. One hypothesis to explain the carbonate effect is the possible formation of soluble iron carbonate complexes in neutral and alkaline solutions. Hood [96] attempted to identify iron-carbonate complexes in the products of pyrite aqueous oxidation by

FTIR but no evidence of the characteristic bands related to the carbonate species was presented. Evangelou et al. [97] and Evangelou and Huang [98] identified Fe(II) CO_3 complexes and carboxylic groups only when pyrite samples were exposed to atmospheric oxidation; the complexes were ascribed to the presence of carbon dioxide at pyrite surface. With the aid of FTIR analyses, Descostes et al. [99] suggested the formation of siderite ($FeCO_3$), but only in very concentrated carbonate/bicarbonate solutions (1 mol/L).

Pyrite is a semiconductor and the dissolution kinetics is usually described in terms of an electrochemical mechanism. The anodic reaction produces ferrous and sulfate ions [100, 101]. Mishra and Osseo-Asare [102] and Wei and OsseoAsare [101] have pointed the important role played by holes in the anodic dissolution of pyrite and offered an explanation for the pathways involved in sulfur oxidation.

2.4.3 Models for alkaline leaching of uranium from natural systems

The literature on kinetic models for extraction of uranium from the ores is scanty. Most of the kinetic models available in literature are for heap / insitu leaching of uranium from the ores using acidic leachants, which are based on film diffusion controlling mechanism [33, 103 - 105]. These models obviously cannot be applied to the uranium ores considered in the present study as these ores ought to be processed by agitation leaching in which the advective flow does not control the leaching. Ping Zhou and Baohua Gu [106] generated kinetic data for dissolution of uranium and showed that at least three different forms of uranium existed in the contaminated soil, U(IV), U(VI), and U(VI) complexed with soil organic matter. Trygve et al. [107] critically reviewed the modeling approaches developed for dissolution of UO_2, based on the large body of chemical and electrochemical experimental data. For a low grade uranium ore, containing 0.07% U_3O_8, from New Mexico, the activation energy was found to be 4.5 kcal/mol (18.8 kJ/mol) indicating a diffusion-controlled mechanism of dissolution of uranium using sodium carbonate-bicarbonate as lixiviant and oxygen as oxidant [108].

High rock permeability and liberation of uranium minerals in coarse sizes render leaching kinetics of medium to high grade (>0.1% U_3O_8) uranium ores to be best described by either homogeneous or shrinking unreacted core reaction models. However, in case of uranium ores with low grade and very fine dissemination of uranium minerals, diffusion of dissolved ions in liquid within pores of rock particles is likely to be rate controlling step. Fig. 2.10 depicts the various aspects of ore characterstics that come into play during leaching of uranium ores and the possible kinetic models.

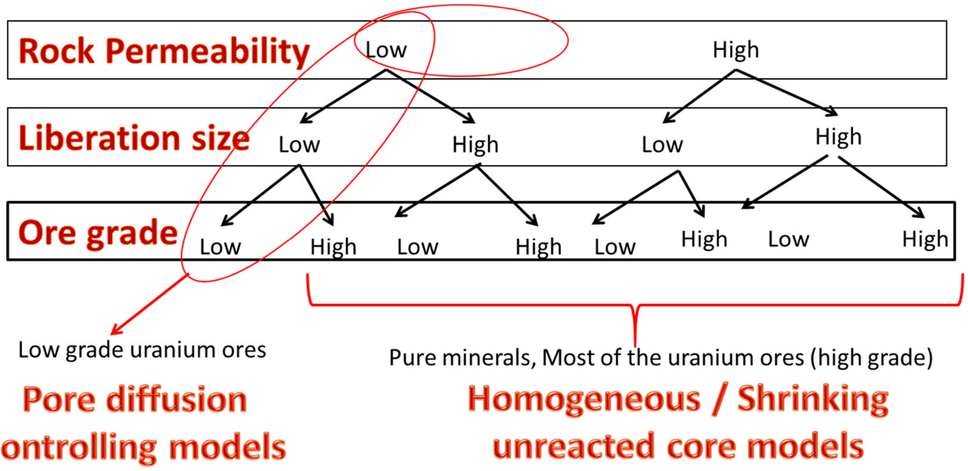

Fig. 2.10 Ore characteristics and possible leaching models

2.4.4 Modeling of continuous leaching of uranium ores

Commercial exploitation of a uranium resource is primarily assessed on the basis of maximum extractable uranium from it by leaching on a laboratory scale. After identifying optimum leaching parameters at laboratory scale, they are scaled up to a pilot level and then to a commercial level. There are several theoretical scale up methods for designing continuous leaching process from laboratory batch kinetic tests.

Nikkhah Khosrow [9] outlined methods for homogeneous or heterogeneous leaching systems. He assumed the reaction rate in continuous reactor to be equal to the minimum that prevails at the end of a corresponding batch leaching cycle in the case of homogeneous systems.

The heterogeneous method is based on shrinking core model described by [39]. Henein and Beigler [109] reported the design equations for scale up of heterogeneous systems to predict residence time in continuous leaching using a dimensionless residence time, Damkohler number. They provided fairly accurate assessment of scale-up factor required for sizing a continuous leach reactor for same feed size distribution for batch and continuous cases. Pritzker [110] extended steady-state design equations for continuous leaching in plug-flow and continuous stirred-tank reactors taking into account the simultaneous depletion of solid and aqueous reactants. Peters [111] presented a micro-model by writing general mathematical equation for single particle leaching and then integrated over all initial particle sizes and residence time distribution applicable to leaching system. Similar approach has been presented for chemical reaction controlled micro-model (segregated-flow model) by Dixon [112]. A comparison of segregated-flow model and population-balance model is well described by Crundwell et al. [113, 114]. Crundwell et al. [115] showed the population balance approach, incorporating particle size distribution, on performance of continuous reactors with the help of leaching number, defined as linear rate of shrinkage times residence time divided by mean particle size, assuming unreacted shrinking-core model. Rubisov and Papengelakis [116] developed a mathematical model to analyze the performance of continuous hydrometallurgical reactors when process upsets occur due to the sudden changes in oxygen mass transfer, oxygen feed rate, solids feed rate, cooling water injection, etc. Sarkar [117] developed a graphical method, based on residence time distribution in a continuous reactor, for scale-up without assuming a rate equation for batch leaching.

The following gap areas have been identified in alkaline leaching of uranium. Though leaching is a heterogeneous process, the kinetic models reported in literature on leaching of various minerals and ores are derived from the rate equations of both homogeneous and heterogeneous processes. Leaching of eulexite mineral in perchloric acid [73] was found to follow Avrami equation, a homogeneous kinetic model. Leaching models are reported for ore particles with valuable minerals in pores of the ore rocks using heterogeneous reactions [118]. Bartlett [119] coupled the pore diffusion limited model with particle size distribution. Most leaching models are governed by shrinking core model equations assuming uniform particle size and spherical shape of the reacting solids [120 - 122]. However, the models with particular reference to leaching of uranium are at large based on either general or Michaelis–Menten type (Fig. 2.8) of homogeneous chemical rate equations [34 - 38].

De-Xin Ding [33] developed a model incorporating particle size distribution for heap leaching, characterized by advective flow conditions, of uranium using aqueous acid solution. Similarly, a number of publications are available on alkaline leaching of uranium dioxide from ores that do not contain significant pyrite content [71, 123]. But, no focussed study on combined agitation leaching of uranium dioxide and pyrite is available in the literature. Hence, the present study aims to address the leaching aspects of uranium ores with significant pyrite content. However, the ores considered in the present study contain pyrite in the intermediate range of concentration (1 to 4%).

In most of the leaching models cited in the literature, particle size distribution of the solid material was disregarded. Nunez and Espiell [124] have purported that particles possess not only a distribution of size but also shape. However, Dixon [112] presented the doubly integrated micro model for batch leaching for distribution of particle size. Suni et al. [125] illustrated experimental evidence that leaching models without consideration of the variation of particle size are prone to erroneous conclusions. Gbor and Jia [126] have found that neglecting particle size distribution results in substantial errors in predicting the leaching efficiency. Amongst other parameters, the effect of particle size distribution has been particularly incorporated in the leaching models developed in the present study for two Indian uranium ores. Grenman et al. [127] discussed methods for avoiding common potholes in modeling the solid-liquid reactions.

Very few studies are published on morphological changes that occur during leaching of uranium ores. It is reported in literature that SEM images with EDX on low grade uranium ore (0.07% U_3O_8) and its leach residue have indicated dissolution, characteristic thinning of clay plates, amorphous mass containing voids where material may have been removed by leaching or agitation [52]. In the present study, a special effort was made to study the changes in morphology during leaching of the two Indian uranium ores.

There is only a little overlap in the experimental conditions (temperature, pressure, reagent concentrations, particle size, and particle size distribution) of leaching of Indian uranium ores and previous reported studies on leaching of uranium minerals or other ores elsewhere in the world. Scale up from batch leaching reaction model to continuous industrial scale autoclave for alkaline leaching of Indian uranium ores is not available.

CHAPTER 3

Materials and Characterization

Alkaline leaching experiments were conducted on (1) pure materials, and (2) Indian uranium ores from alkaline host rocks. The materials used for leaching under the basic studies (presented in Chapter 5) include following pure materials / minerals which represent either important or bulk constituents of alkaline rock hosted uranium ores of Indian origin.

1. Uranium Dioxide (UO_2) – synthesized compound.
2. Iron Pyrite (FeS_2) – pure mineral.
3. Calcite ($CaCO_3$) – pure mineral.
4. Silica (SiO_2) – pure mineral.

Sintered natural ('natural' here refers to concentration of U^{235} isotope $\approx 0.7\%$) uranium dioxide fuel pellets (99.8% pure) were brought from Nuclear Fuel Complex, Hyderabad, India and ground to powder form using a laboratory ball mill. Hence, it is to be noted that the uranium dioxide powder used in the present study is a synthetic compound and not a naturally occurring mineral. The pure iron pyrite sample was purchased from M/s Jainson Labs, Meerut, U.P., India. The pure calcite and silica samples were purchased from M/s The Misra Mineral Industry, Hyderabad, India. All the four powder samples were separated into desired close size ranged fractions: -65+100#[-212+150μm], -100+150#[-150+100μm], -150+200#[-100+75μm], -200+270#[-75+53μm], -270+400#[-53+37μm] and -400#[-37μm] by wet sieving. The fractions were dried and stocked for use in leaching experiments. Wet sieving was preferred, over dry sieving, as it removes finer fractions that adhere to larger ones [126].

The uranium ore samples used for leaching under the applied studies (presented in Chapter 6) are from the following two alkaline rock hosted deposits of southern India.

1. Tummalapalle in Cuddapah Basin (Andhra Pradesh).
2. Gogi in Bhima Basin (Karnataka).

Representative samples were drawn for leaching studies from the exploratory mine samples produced by M/s Uranium Corporation of India Limited, Jharkhand, India. The ore samples were crushed in jaw crusher, roll crusher and then ground in wet ball mill for suitable time period to get the required size for leaching studies.

Na_2CO_3 and $NaHCO_3$ of L.R. grade (99.5% pure) were used as leachants in required concentrations in various experiments. Distilled water was used for leaching of pure mineral samples while normal tap water was used for leaching of actual uranium ores. Industrial oxygen, nitrogen and argon gases of commercial grade (99.6% pure) from cylinders were used to maintain the required partial pressures in the autoclave.

The various samples used in the present studies were characterized by measurement of specific surface area and specific gravity, porosimetry, X-ray diffraction, chemical analyses, optical microscopy and scanning electron microscopy. The ore samples were characterized by additional techniques such as spectrograph analyses, whole rock analyses and petrographic studies using optical microscope. The details and results of all of these investigations are described in the following Sections.

3.1 PHYSICAL PROPERTIES

The photo pictures and the specific gravities (determined by standard method using specific gravity bottle) of the powdered samples used are given in Fig. 3.1 and Table 3.1, respectively.

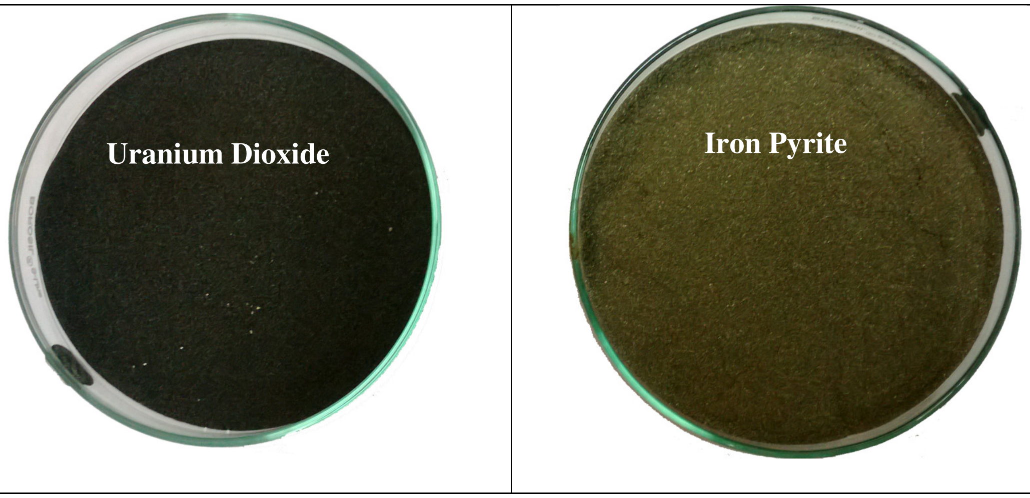

Fig. 3.1 Feed materials used in the leaching studies

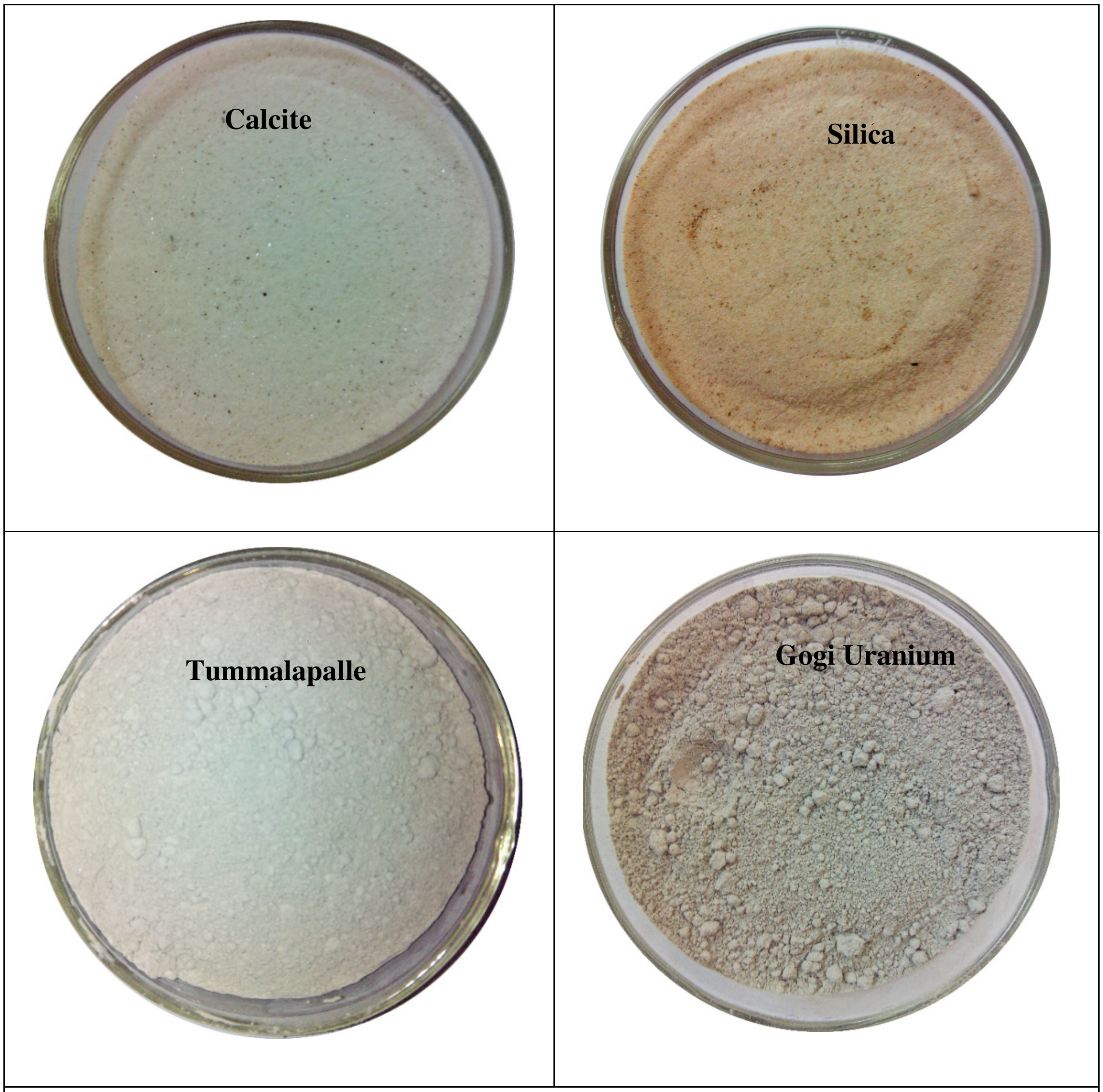

Fig. 3.1 Feed materials used in the leaching studies

The powders of uranium dioxide, iron pyrite, calcite and silica appear black, golden yellow, white and light brown respectively. The ground Tummalapalle and Gogi uranium ores look alike, light gray in color.

Table 3.1 Measured specific gravities of feed materials used in leaching studies

Sl. No.	Name of the sample	Specific gravity (g/cc)
1	Uranium dioxide	9.62
2	Iron pyrite	4.98
3	Calcite	2.71
4	Silica	2.40
5	Tummalapalle uranium ore	2.79
6	Gogi uranium ore	2.75

The specific surface area of different size fractions of feed materials given in Table 3.2 was measured by Brunauer, Emmett and Teller (BET) single point method using nitrogen adsorption by surface area analyser (model SAA-2000) of M/s S.P. Consultants, Mumbai in India. The samples were degassed at 125°C for 3 h prior to analysis. The specific surface area of the samples will be useful in estimating the leaching rates per unit surface area from the experimental conversions of either uranium dioxide or iron pyrite under different leaching conditions (The leaching rate per unit surface area can be readily compared with those cited in literature by other authors).

Table 3.2 Specific surface area (m^2/g) of samples used in leaching studies

Size Sample	-65#+100# [-212+150µm]	-100#+150# [-150+100µm]	-150#+200# [-100 + 75µm]	-200+400# [-75+53µm]	-400# [-37µm]
UO_2	0.004	0.005	0.01	0.325	0.339
Pyrite	0.041	0.048	0.077	0.148	0.41
Calcite	0.107	0.15	0.2	0.259	0.3
Silica	0.08	0.13	0.296	2.645	ND
Tummalapalle ore	0.701	0.833	1.2	2.5	ND
Gogi ore	1.657	1.965	2.1	2.8	ND
ND = Not Determined					

It may be observed that the specific surface area of ore samples is higher than that of pure UO_2 and pure minerals for the same size of particles in general, which could be due to higher porosity in the natural ores that might have resulted during rock formation of multi minerals. As expected the specific surface area is high for fine sized particles.

The properties of Tummalapalle and Gogi ore rock pieces (- ¼” size) measured by Mercury Intrusion Porosimeter (Model: Pascal 440 series, Thermo Electron Corporation, USA) are given in Table 3.3. The porosity of Gogi ore is higher compared to that of Tummalapalle ore.

Table 3.3 Properties of ore samples measured by Mercury porosimeter

Sample Property	Gogi ore	Tummalaplle ore
Specific surface area (m^2/g)	0.91	0.42
Average pore diameter (nm)	4.3	30
Total porosity (%)	7.19	2.39
Pore volume (cm^3/g)	0.14	0.02

3.2 SPECTROGRAPH ANALYSES

Tables 3.4 and 3.5 present the spectrograph analyses of Tummalapalle and Gogi ore samples respectively, which were carried out using a Wavelength Dispersive X-ray Fluorescence Spectrometer (WDXRFS), Model: PANalytical (PW-2440) MagiX-PRO, Netherlands.

Table 3.4 Spectrographic data of Tummalapalle ore sample

Major (>1% by wt.)	Minor (<1% but >0.1% by wt.)	Traces (<0.1% by wt.)
Ca*, Mg*, Si, Al, P	Fe*, Mn	Cu, Mo*, Pb, U, Ni, Ti, V, Cr, Na, Zr
* *in good concentration;* Y, Bi, Co, B, Nb, Ag are below detection limit.		

Table 3.5 Spectrographic data of the Gogi ore sample

Major (>1% by wt.)	Minor (<1% but >0.1% by wt.)	Traces (<0.1% by wt.)
Si, Al, Fe, Mg, Ca	Na, Ti, Mn	Be, V, Cr, Co, Ni, Cu, Ga, Y, Zr, Mo, Pb, U
Below detection limit (BDL): Ag, Ta, Sn, La.		

Both the ore samples contain high amounts of Ca, Mg, Si which form the host rock. It is interesting to note that the Gogi ore sample has rare-earth (REE) elements like Ga, Y and Zr in the trace element category. Flow path of these elements or their compounds needs to be monitored during various processing stages as the permissible limit for REE content in the intermediate uranium concentrate (yellowcake) is rather low.

3.3 CHEMICAL ANALYSES

The purity of calcite, pyrite and UO_2 powders was found to be >99% from the analysis carried out by Inductively Coupled Plasma-Optical Emission Spectrometer (ICP-OES) of M/s Horiba Jobin Yvon (type: ULTIMA 2), France. The uranium content of UO_2 powders was determined by Davies and Grey titration method [128]. The complete chemical analysis of the UO_2 and SiO_2 powders are given in Tables 3.6 and 3.7 respectively.

Table 3.6 Complete chemical analysis of the uranium dioxide powder used for leaching studies (contents are in ppm unless stated otherwise)

Element	Ag	Al	B	Ca	Cd	Ce	Co	Cr	Cu	Dy	EBC *	Er
Content in ppm	<1	<25	0.19	19	<0.1	<0.5	<0.2	10	<6	<0.1	~0.58	<0.1
Element	Eu	Fe	Gd	Mg	Mn	Mo	Na	Ni	Si	Sm	U	Zn
Content in ppm	0.1	20	~0.04	9	1	5	13	<1.0	<30	<0.1	87.96%	<1.0
* Equivalent Boron Content												

Table 3.7 Complete chemical analysis of the silica powder used for leaching studies

Analyte	SiO_2	Al_2O_3	Fe_2O_3	CaO & MgO	Alkalies (Na_2O, K_2O)	LOI*
Content (% wt)	99.6	0.15	0.05	0.01	0.1	0.1
* Loss on Ignition						

The uranium content of 87.96% in Table 3.6 corresponds to 99.78% as UO_2. The purity of silica was found to be 99.6% by molybdenum blue method using UV/Visible spectrophotometer at wavelength of absorption = 660 nm (model: UV3000+, M/s Lab India Analytical, India).

The whole rock chemical analysis of the Tummalapalle and Gogi uranium ores is (analysed by ICP-OES, Atomic Absorption Spectroscopy, Spectrophotometry) given in Table 3.8.

Table 3.8 The whole rock analyses of Tummalapalle and Gogi uranium ores (in %wt)

Analyte	Tummalapalle ore	Gogi ore
U_3O_8	0.048	0.193
SiO_2	19.38	24.52
CaO	24.66	32.3
MgO	13.72	Traces
LOI*	31.76	23.06
S(Total)	0.8	2.23
Fe(Total)	-	3.38
Fe_2O_3	1.23	-
FeO	0.65	-
Ni	Traces	0.011
P_2O_5	2.76	Traces
MnO	0.17	0.20
Mo		<0.01
Na_2O	0.18	1.35
K_2O	1.78	0.14
TiO_2	0.11	0.32
Al_2O_3	2.17	3.98
* Loss on Ignition		

The U_3O_8 assays of Tummalapalle and Gogi ore samples was 0.048% and 0.193% respectively. Analyses indicate that Tummalapalle ore has dolomite and calcite along with silica as main gangue and Gogi ore has mainly calcite and silica as gangue. The total sulfur (S) in Gogi ore was found to be 2.23% which indicates presence of high pyrite.

3.4 X-RAY DIFFRACTION ANALYSES

The mineral phases in pure materials and in the two ore samples were ascertained by their unit cell parameters and the characteristic peaks identified in the corresponding X-ray diffractograms obtained using GE XRD-3003TT machine (Germany) at operating voltage, 40 kV, and current, 30 mA. The characteristic radiation of CuK_α (λ = 1.5418 A°) with graphite crystal monochromator was used for diffraction studies. The samples were scanned in the angular range (2Θ) of 4° and 134°, with a detector EHT = 1000 volts, Gain = 200%, time constant of 1 s and dead time of 0 μs. The observed ‘d’ spacings and the integrated intensities of the mineral sample was compared with the published data of International Committee for Diffraction Data (ICDD). The X-ray diffractograms of pure materials are given in Figs. 3.2[A] to 3.2[D].

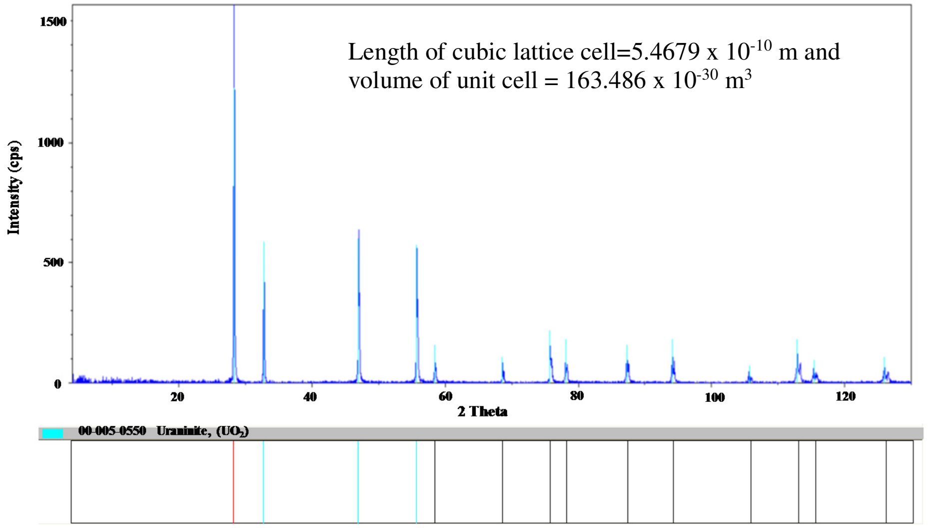

Fig. 3.2 [A] X-ray diffractogram of pure UO_2

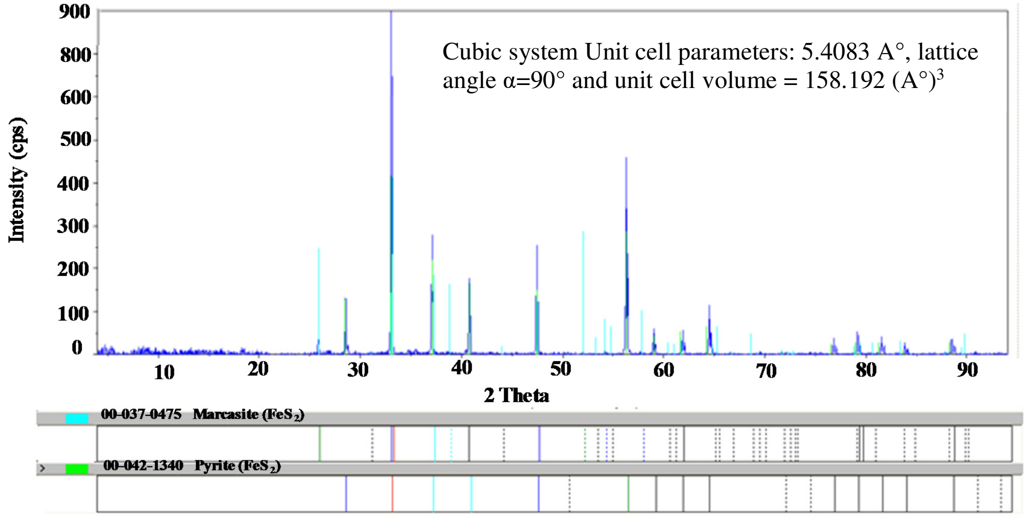

Cubic system Unit cell parameters: 5.4083 A°, lattice angle α=90° and unit cell volume = 158.192 $(A°)^3$

Fig. 3.2 [B] X-ray diffractogram of pure Pyrite

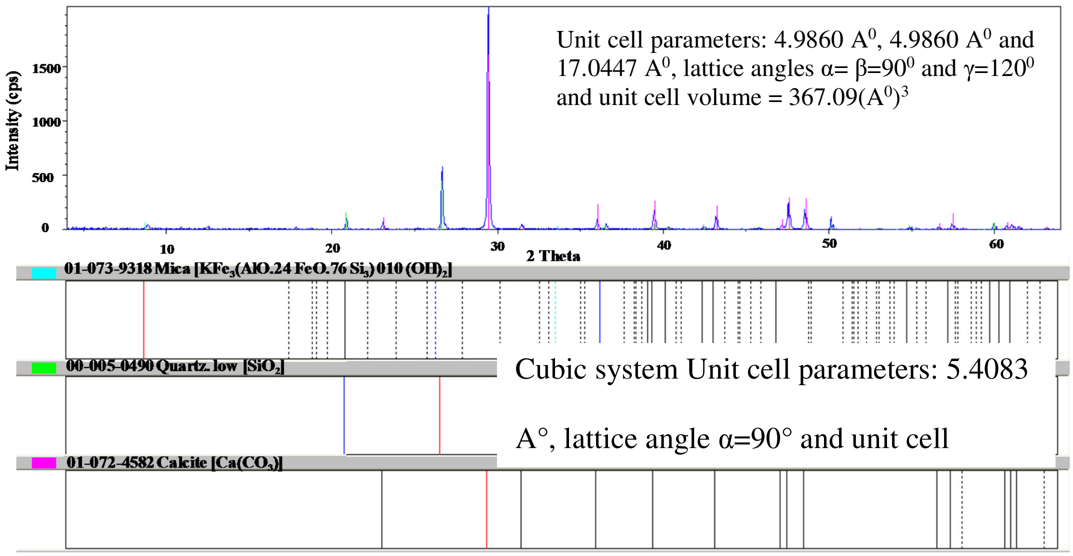

Unit cell parameters: 4.9860 A^0, 4.9860 A^0 and 17.0447 A^0, lattice angles α= β=90^0 and γ=120^0 and unit cell volume = 367.09$(A^0)^3$

Cubic system Unit cell parameters: 5.4083

A°, lattice angle α=90° and unit cell

Fig. 3.2 [C] X-ray diffractogram of pure Calcite

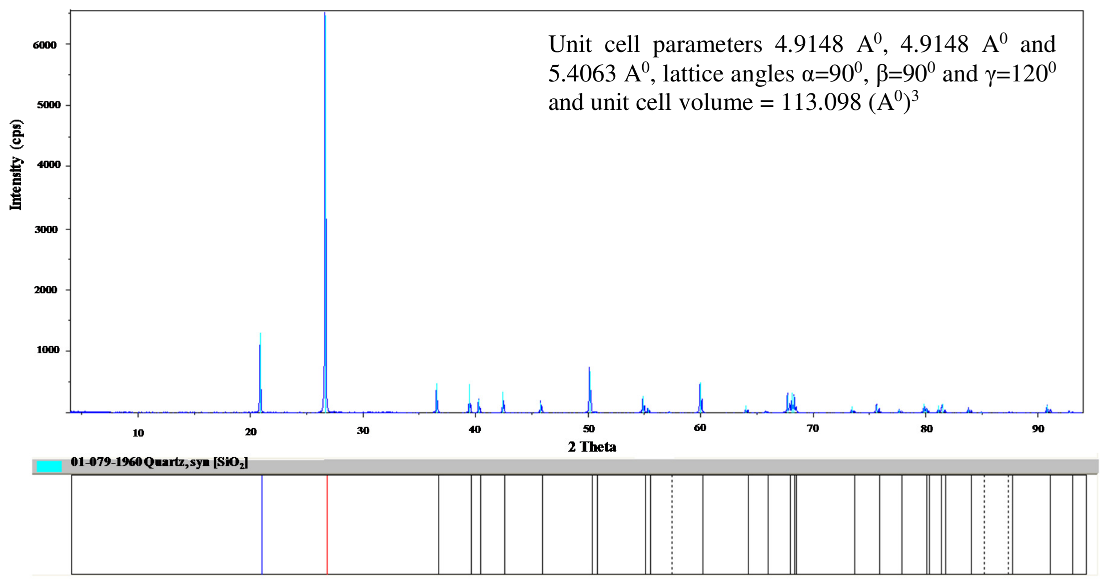

Unit cell parameters 4.9148 A^0, 4.9148 A^0 and 5.4063 A^0, lattice angles $\alpha=90^0$, $\beta=90^0$ and $\gamma=120^0$ and unit cell volume = 113.098 $(A^0)^3$

Fig. 3.2 [D] X-ray diffractogram of pure Silica

Figs. 3.3[A] to 3.3[D] shows X-ray diffractograms of various materials concentrated by physical methods (heavy media and magnetic separation of different sieve fractions shown in Fig. 3.4) from the two ore samples.

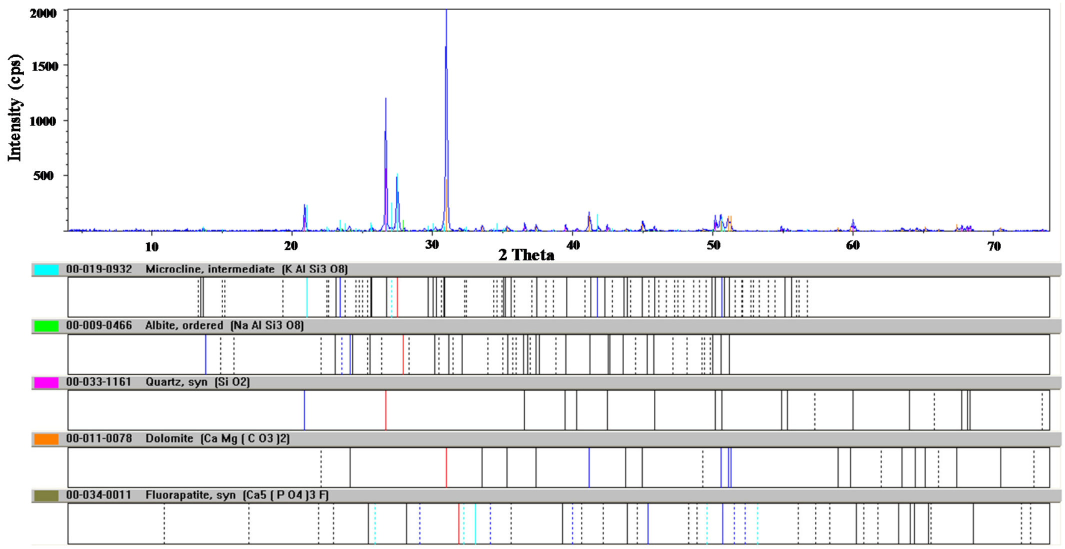

Fig. 3.3[A] X-ray diffractogram of Bromoform lights fraction of Tummalapalle uranium ore

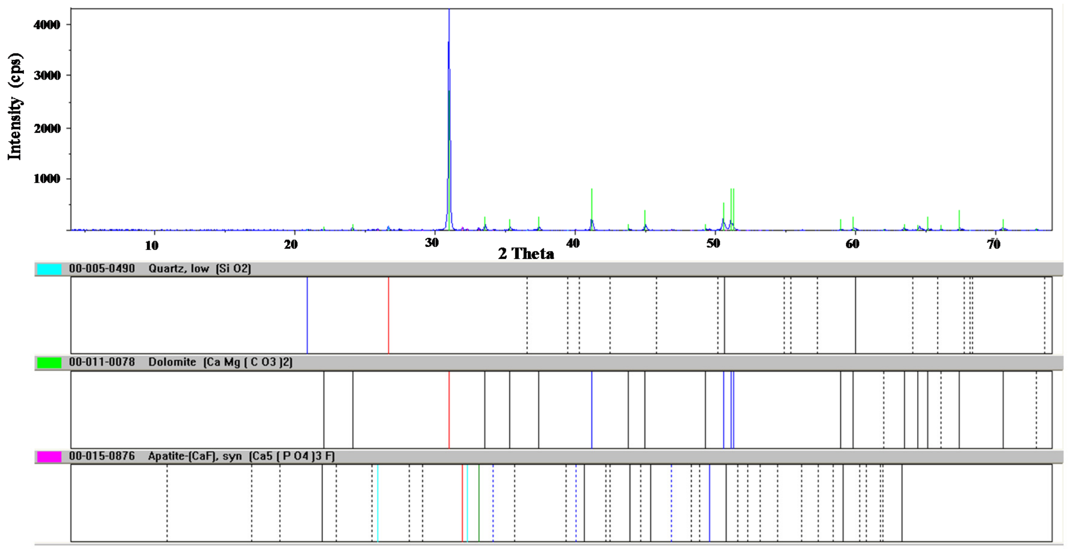

Fig. 3.3[B] X-ray diffractogram of Methylene Iodide lights fraction of Tummalapalle uranium ore

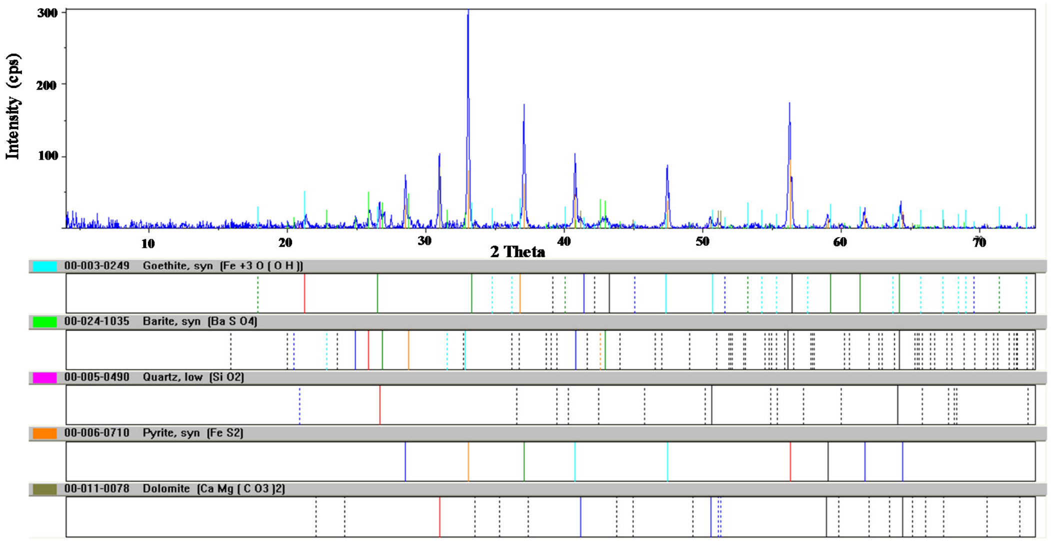

Fig. 3.3[C] X-ray diffractogram of Methylene Iodide heavies fraction of Tummalapalle uranium ore

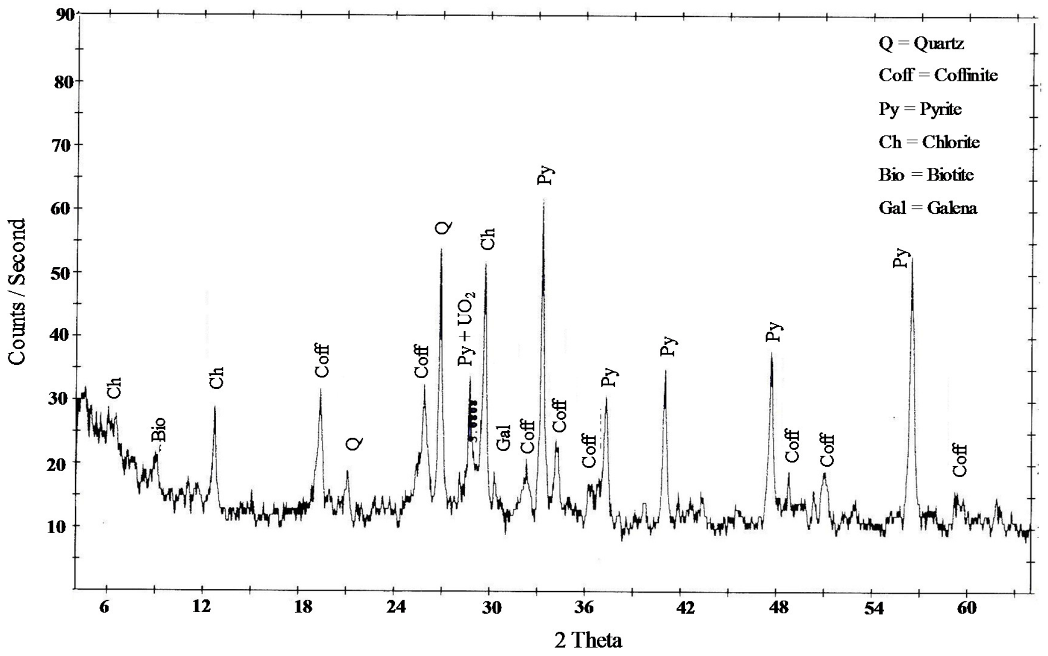

Fig. 3.3[D] X-ray diffractogram of Methylene Iodide Heavies and Magnetic fraction of Gogi uranium ore

Uranium dioxide powder has shown the stoichiometry of $UO_{2.02}$ by X-ray diffraction. Iron pyrite sample contains traces of marcasite. No uranium minerals could be traced in the present sample of Tummalapalle ore analyzed by X-ray diffraction. The reason could be the low concentration and ultrafine disseminations of uranium minerals present in this ore as reported in the literature [129, 130]. Minati Roy and Dhanaraju [130] could identify pitchblende, coffinite, U-Si-Ti complex, uranophane and adsorbed uranium phase in their electron microprobe (EPM) studies. In the present study, the uranium content of the Tummalapalle ore sample could be confirmed by chemical (Section 3.3) and mineralogical (Section 3.5.2.1) analysis. The other minerals identified in Tummalapalle ore are dolomite, pyrite, quartz, traces of albite, barite, fluorapatite, goethite and microcline (Figs. 3.3[A] through 3.3[C]). Coffinite is the uranium mineral identified in Gogi ore (Fig. 3.3[D]). Other minerals identified in Gogi ore sample are calcite, chlorite, magnetite, pyrite, quartz and traces of hornblende, mica and siderite.

3.5 MORPHOLOGICAL AND PETROGRAPHIC STUDIES

The change in morphology of solids at microscopic scale on leaching will directly reveal what has occurred during leaching. Therefore, it was attempted to study the morphological behavior of the pure materials as well as two Indian uranium ores during leaching. The pure materials used as feed to leaching were directly observed under the microscope. However, the valuable (uranium) minerals in the ores are too low in concentrations and finely disseminated to examine under microscope. Hence, each of Tummalapalle and Gogi uranium ores were concentrated by different heavy media methods to obtain separate fractions rich in individual minerals as per the following procedure pictorially depicted in Fig. 3.4.

About 10 kg of each of the ore samples was crushed and subjected to wet grinding in a ball mill for liberation of ore minerals. Wet sieving of the ground product using test sieves 65# (212μm), 100# (150μm), 140# (106 μm) and 325# (45 μm) was carried out to facilitate proper washing of the ultrafine material that tend to adhere to coarse particles due to surface forces. Different size fractions were dried and the magnetite in them was removed by hand magnet before subjecting to heavy media separation according to standard procedures using separating funnels, methyl alcohol/acetone for washing and NaOH for regeneration of heavy liquids, for concentration of heavy minerals. First stage of heavy media separation was carried out using bromoform (sp.gr. = 2.8). Bromoform lights are expected to be concentrated in Calcite and Silica. The bromoform heavies were then subjected to separation by methylene iodide (sp.gr. = 3.3). The Methylene iodide heavies were separated by magnetic separation using a Frantz isodynamic separator (model L-1, serial no. 1926) setting the current at 1 Ampere, for which all the paramagnetic minerals with mass magnetic susceptibility $< 3.4\text{x}10^{-9}$ m^3/kg would be collected into magnetic fraction [131A]. The mass susceptibility of uraninite is reported to be $2.8\text{x}10^{-9}$ m^3/kg in literature [131B]. A small sample (< 0.5 g) was drawn from the magnetic fraction which is expected to be enriched in uranium minerals (uraninite, pitchblende, coffinite in the present case).

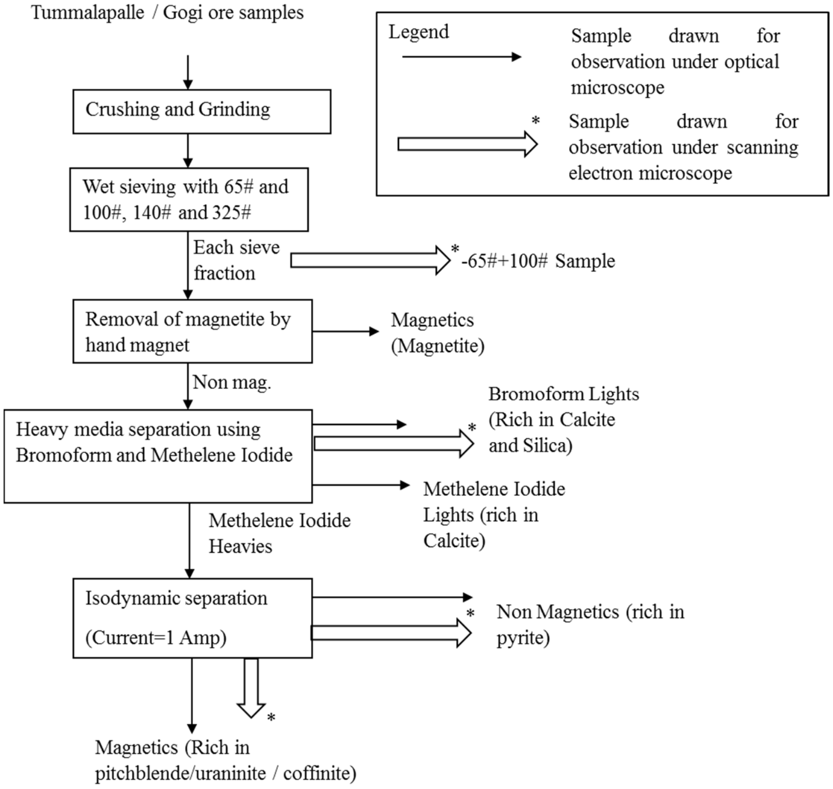

Fig. 3.4 Schematic flow sheet followed for preparation of ore samples for observation under Optical Microscope (single arrow mark) and Scanning Electron Microscope (SEM) marked with double arrow

Grains of powdered samples of pure uranium dioxide, iron pyrite, calcite and silica and the concentrated fractions of specific ore samples (prepared by the procedure described in Fig. 3.4) were sprinkled, minimizing overlapping of grains, on a glass slide pasted with epoxy resin mixed with hardener. After slides were dried, they were ground with the help of 400#, 600# and 800# carborundum powder, polished and observed under optical microscope (Model: Nikon Eclipse, E600 POL, with NIS-Elements BR Image analysis software, Japan). Reflected light (RL) was used for identifying opaque (ore / metallic) minerals and Transmitted light (TL) for identifying gangue (nonmetallic) minerals using the optical microscope.

The optical microscope, mentioned above, has a resolution of about 50µ (about 10 to 600x magnification) and the images have been obtained on polished sections which may not give the true morphology of the particles. In order to get more insight of the morphology, the pure materials and the concentrated fractions of ore samples (generated by the procedure described in Fig. 3.4) were sprinkled on a double sided carbon tape pasted to a brass disk (1" diameter x 1" height) and examined under Scanning Electron Microscope (SEM) attached with Energy Dispersive X-ray spectroscope (EDX) model CAMSCAN MB 2300 CT/100 (United Kingdom make) which has a resolution of about 5 nm and magnification in the range 10 to 5,00,000 times.

3.5.1 Pure materials

The optical images (of the grain mounts) and the scanning electron micrographs (of the brass disk mounted samples) of pure materials used in leaching studies are shown in Figs. 3.5[A] through 3.5[H].

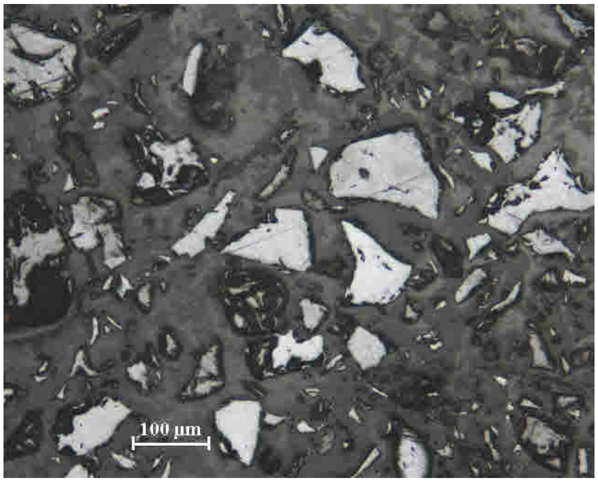

Fig. 3.5[A] Optical micrograph of UO_2 (10X, 1 Nicol, Reflected Light)

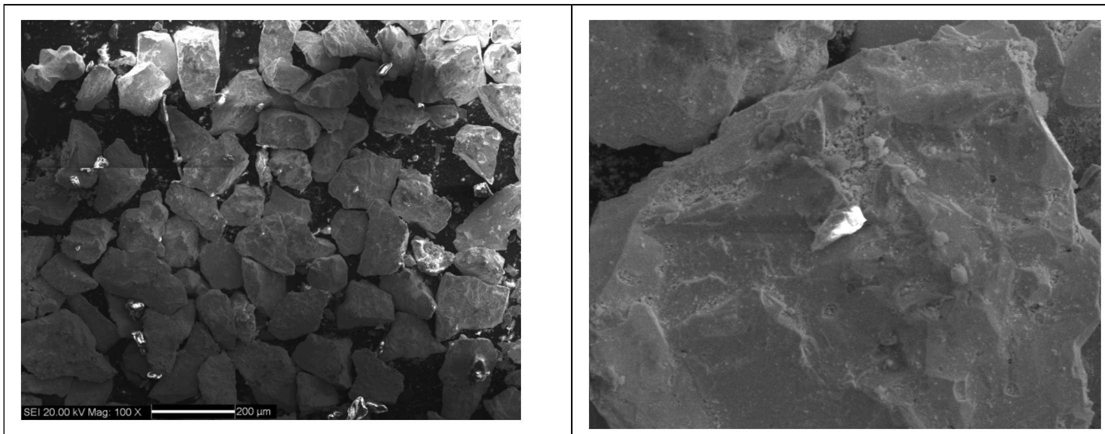

Fig. 3.5[B] Scanning Electron Micrographs of Pure UO_2

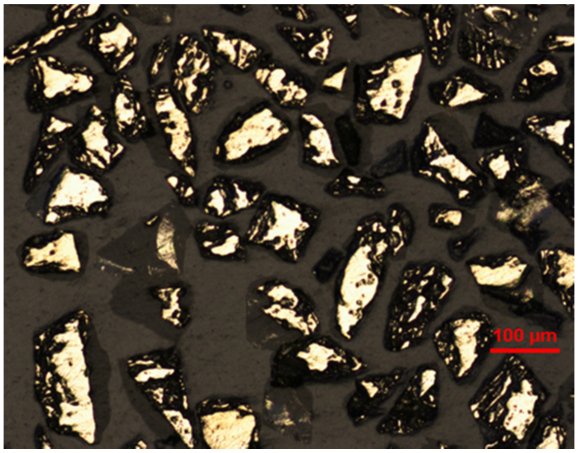

Fig. 3.5[C] Optical micrograph of Iron Pyrite (10X, 2 Nicol, Reflected Light)

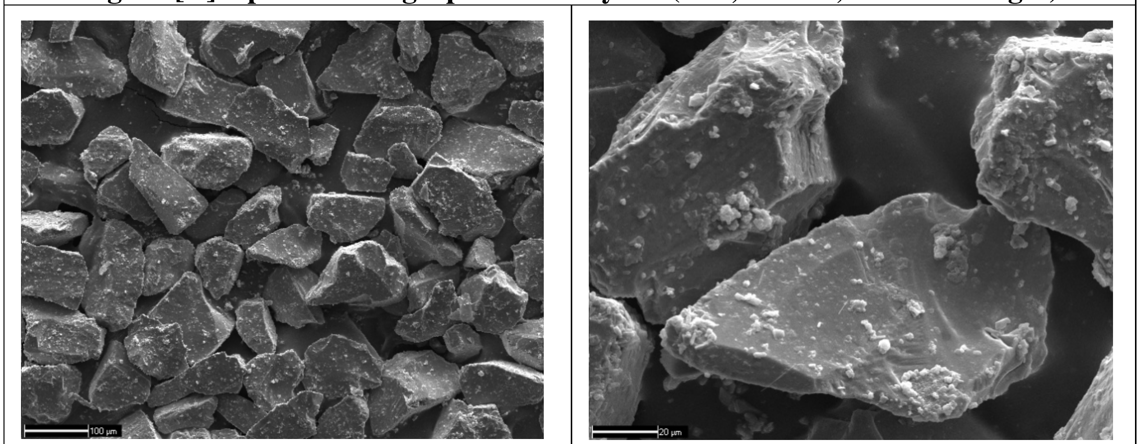

Fig. 3.5[D] Scanning Electron Micrographs of Iron pyrite

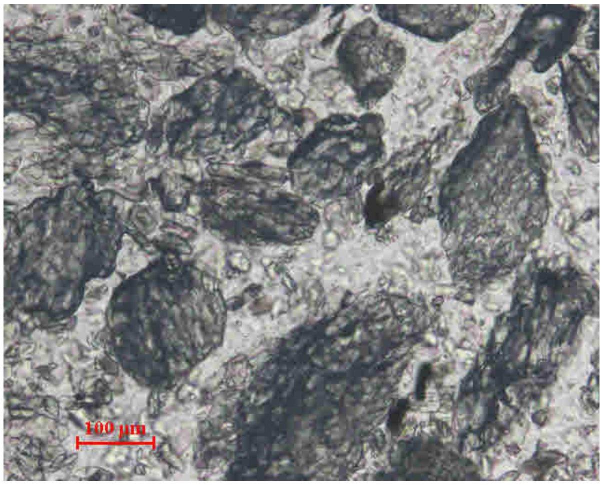

Fig. 3.5[E] Optical micrograph of Calcite (10X, 1 Nicol, Transmitted Light)

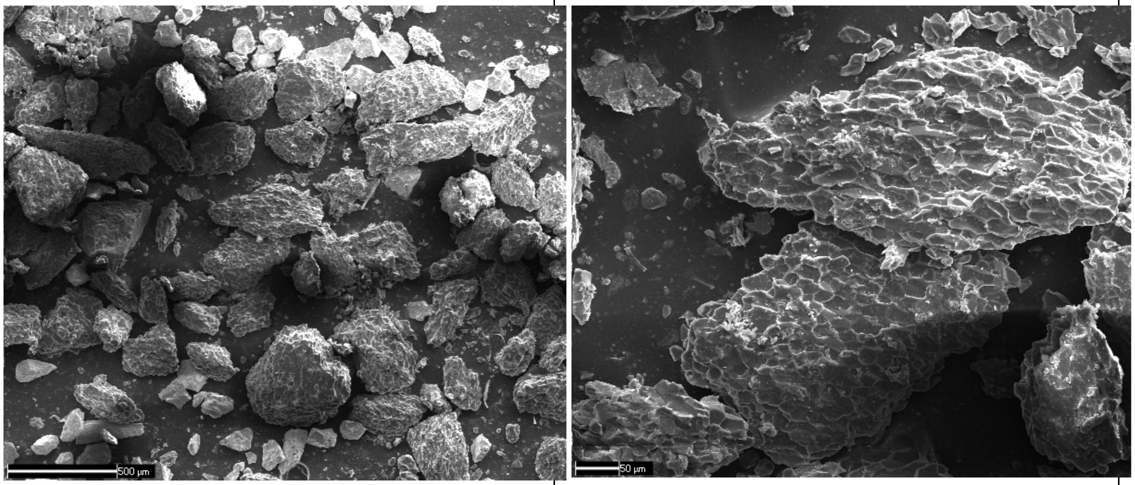

Fig. 3.5[F] Scanning Electron Micrographs of Calcite

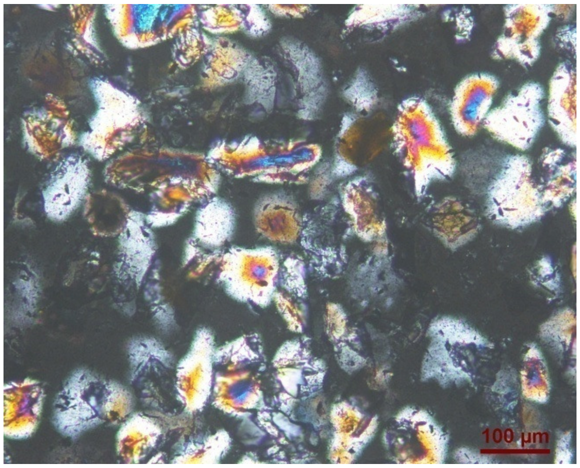

Fig. 3.5[G] Optical micrograph of Silica (10X, 2 Nicol, Transmitted Light)

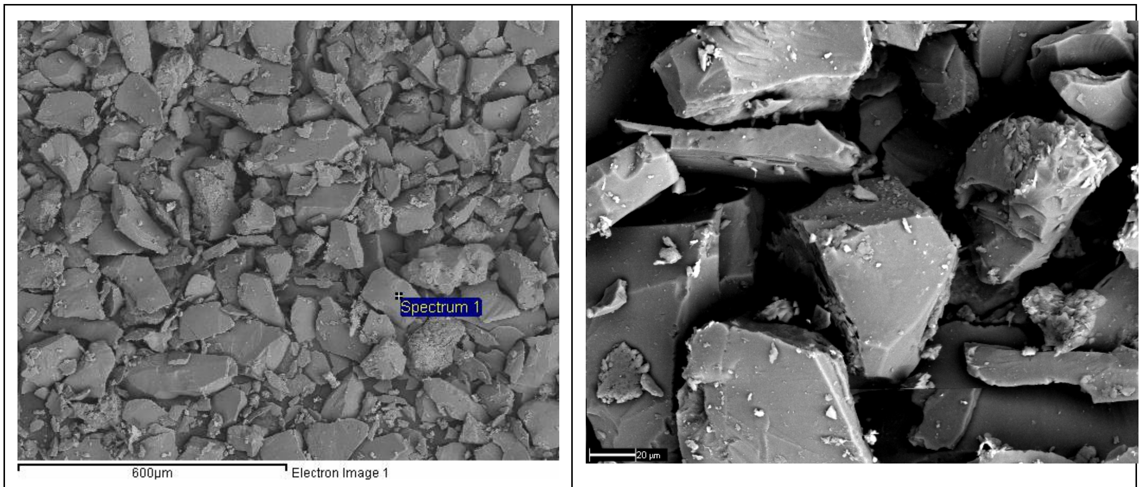

Fig. 3.5[H] Scanning Electron Micrographs of Silica

Following observations can be made from optical and scanning electron micrographs shown in Figs. 3.5[A] through 3.5[H]: The UO_2 grains are angular and anhedral in shape and display gray color and isotropism under reflected light. The reflectance is low (about 15%). The pyrite grains are yellowish white in color with high reflectance (45-50%) and display isotropism. No cleavages or fractures are seen on the surfaces of both UO_2 and iron pyrite mineral grains. Calcite grains observed under transmitted light are colorless, showing change of relief on rotation with rhombohedral cleavage. They appear to be mechanically interlocked. Quartz grains are anhedral granular, colorless and display no variation in indices of refraction on rotation under the transmitted light of the optical microscope. They have faceted microstructure.

3.5.2 Petrographic studies of the ore samples

3.5.2.1. Tummalapalle Uranium ore: The mineralogical composition of Tummalapalle ore sample computed by grain counting method by observing the samples (generated according to the procedure shown in Fig. 3.4) under optical microscope is given in Table 3.9.

Table 3.9 Mineralogical composition of Tummalapalle* uranium ore

Mineral	%weight
Carbonates	79.80 [mainly dolomite ($MgCO_3$)]
Quartz and feldspar clasts	12.15
Collophane	3.90
Micaceous minerals	1.20 [chlorite]
Chert	0.82
Sulfides	1.24 [pyrite]
Chalcopyrite & Galena	0.06
Oxides	0.18 [magnetite]
Ilmenite inclusive of leucoxene	0.23
Iron hydroxides	0.41[goethite]
Radioactive minerals	0.01[pitchblend in intimate association with pyrite]
* A small town in the district of Cuddapah located in the state of Andhra Pradesh, India.	

The host rock of Tummalapalle ore deposit is phosphatic siliceous calcitic dolostone (PSCD). Carbonates form the bulk of the Tummalapalle ore constituting 79.80 wt%. The quartz-feldspar assemblage and collophane constitutes significant proportion of the ore amounting to 16.05 wt%. Pyrite is the common sulphide ore mineral occurring mainly as swarms of minute pellets in dolomicrite, isolated clusters of coalesced pellets and idioblasts. Chalcopyrite is seen as distinct grains of varying size. Magnetite and Ilmenite are the oxide ore minerals. Goethite is the significant ore mineral and is derived from the alteration of pyrite.

The distribution of radioactive phases in the fractions generated from physical methods (depicted in Fig. 3.4) was estimated by auto-radiography using Solid State Nuclear Tract Detection (SSNTD) technique, in which the grain mounts were exposed to alpha sensitive, transparent flexible sheet of 85 μm thick Cellulose Nitrate - 85 (CN-85 film) for 72 hours. The CN-85 film was then etched overnight with 10% NaOH solution. Radioactive mineral was identified by the alpha tracks appeared on CN-85 film. The results of measured radioactivity of different density fractions of each size generated by heavy media separation are given in Table 3.10.

Table 3.10 Distribution of uranium values in different density and size fractions of Tummalapalle uranium ore

	-60 +140#			-140 +325#			-325#			Total		
Density	Mass%	U_3O_8 Assay%	Dist%	Mass%	U_3O_8 Assay%	Dist%	Mass%	U_3O_8 Assay%	Dist%	Mass%	U_3O_8 Assay%	Dist%
BRL	36	0.041	31.6	12.52	0.04	10.73	33.88	0.041	29.77	82.4	0.041	72.15
MIL	8.12	0.072	12.5	3.06	0.062	4.07	5.87	0.05	6.29	17.05	0.063	22.89
MIH	0.28	0.595	3.6	0.11	0.284	0.67	0.16	0.210	0.72	0.55	0.421	4.97
Total	44.4	0.050	47.7	15.69	0.046	15.47	39.91	0.043	36.79	100	0.047	100.00

BRL – Bromoform Lights MIL – Methylene Iodide Lights MIH – Methylene Iodie Heavies

It may be concluded from Table 3.10 that (i) the uranium assay does not increase with decrease in size, thereby indicating no progressive liberation with decrease in size, (ii) distribution of uranium in various size fractions and their weight percentages are more or less same suggesting uniform distribution of uranium, and, (iii) About 95% uranium values are associated with gangue constituents present in Bromoform Lights (BRL) and Methylene Iodide Lights (MIL) fractions and the balance of about 5% is accounted by observable discrete pitchblende, which is mostly associated with pyrite in the Methylene Iodide Heavies (MIH) fractions and collophane. Distribution of 95% of U_3O_8 values in BRL and MIL indicate ultra-fine dissemination of uranium in lighter minerals which calls for extremely fine size grinding for adequate exposure to the lixiviant during leaching for obtaining near complete recovery. The images of different minerals present in Tummalapalle ore obtained with the optical microscope are given in Fig. 3.6.

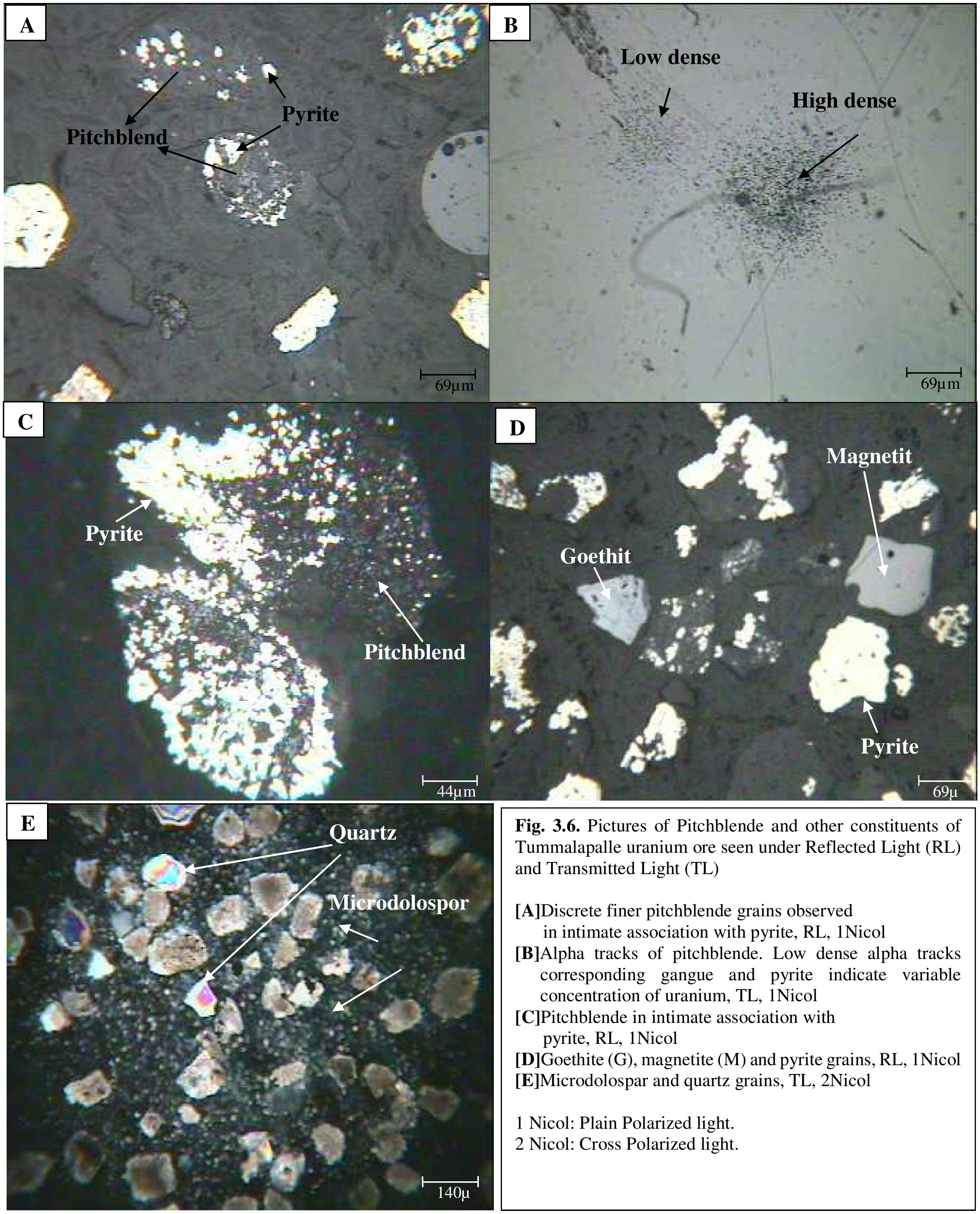

Fig. 3.6. Pictures of Pitchblende and other constituents of Tummalapalle uranium ore seen under Reflected Light (RL) and Transmitted Light (TL)

[A]Discrete finer pitchblende grains observed in intimate association with pyrite, RL, 1Nicol

[B]Alpha tracks of pitchblende. Low dense alpha tracks corresponding gangue and pyrite indicate variable concentration of uranium, TL, 1Nicol

[C]Pitchblende in intimate association with pyrite, RL, 1Nicol

[D]Goethite (G), magnetite (M) and pyrite grains, RL, 1Nicol

[E]Microdolospar and quartz grains, TL, 2Nicol

1 Nicol: Plain Polarized light.
2 Nicol: Cross Polarized light.

A few discrete grains of pitchblende could be observed in intimate association with pyrite segregations (Figs. 3.6[A] & 3.6[C]) in dolomicrite. The alpha particle radiography of polished grain mounts (Fig. 3.6[B]) of different density fractions of coarser size [-60 + 140 mesh] has revealed that apart from discrete pitchblende, uranium in variable concentration is associated with dolomicrite, ferruginous or pigmented carbonates, microstylolite prisms, and collophane. It is rather difficult to identify uranium phases in finer size fractions. Several other authors have also reported uranium minerals in Tummalapalle ore. Sunitha et al. [129] reported that uranium minerals such as coffinite and uraninite / pitchblende and brannerite occur as fracture filling and ultrafine disseminations with association of sulphide minerals like chalcopyrite, arsenopyrite and bornite. Minati Roy and Dhanaraju [130] could identify pitchblende, coffinite, U-Si-Ti complex, uranophane and adsorbed uranium phase in their electron microprobe (EMP) studies.

The other minerals present in Tummalapalle ore are dolomite, pyrite, quartz, traces of albite, barite, fluorapatite, goethite and microcline (as shown in Figs. 3.6[D] & 3.6[E]). The overburden of the Tummalapalle ore is made of cherty limestone. Thin section of a typical rock piece from the overburden material of Tummalapalle ore was made using cutting and polishing machine for observation under optical microscope. The optical images are shown in Figs. 3.7 and 3.8.

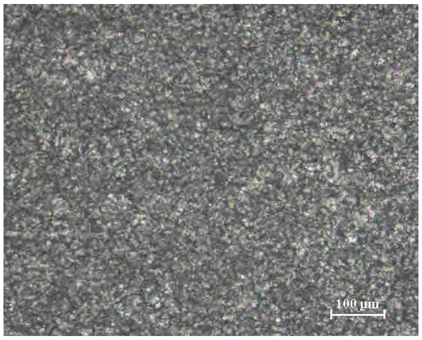

Fig. 3.7. Cherty lime stone in Tummalapalle ore overburden (10X, 2Nicol, Transmitted Light)

Fig. 3.8. Cherty lime stone with quartz-calcite vein in Tummalapalle ore overburden (2X, 2Nicol, Transmitted Light)

3.5.2.2 Gogi uranium ore: The mineralogical composition of Gogi ore sample computed by grain counting method by observing the samples (generated according to the procedure shown in Fig. 3.4) under optical microscope is given in Table 3.11.

Table 3.11 Mineralogical composition of Gogi uranium ore

Mineral	%weight
Calcite	61.57
Quartz+chert	13.10
Feldspar clasts	1.59
Micaceous minerals	5.89 [chlorite+biotite+clay]
Ferromagnesian minerals	0.37 [hornblende with minor epidote]
Barite	0.64
Zircon	0.076
Sulfides	6.13 [pyrite+marcasite+chalcopyrite]
Oxides	0.45 [magnetite+hematite+goethite]
Radioactive minerals	0.886 [coffinite+pichblend+adsorbed uranium in association with carbonaceous matter and goethite]
Others	9.3

The feed-rock is formed by fractured lime stones composed of micrite and sparite in varying proportions with minor quartz and dolomite. The mineralogical composition of the Gogi ore sample indicates presence of radioactive ore minerals (0.886%), non-radioactive ore minerals (6.58%) and gangue minerals (92.539%). The radioactive ore minerals are coffinite, the predominant uranium phase, followed by pitchblende, urano-organic complex and some labile uranium that occurs in association with hydrous iron oxides, clay segregations with carbonate mud. Among non-radioactive ore minerals sulphides are predominant over oxides. Pyrite is by far the most abundant mineral followed by chalcopyrite and galena. Oxides are represented mainly by goethite with traces of magnetite and hematite. Calcite (61.57%) and quartz+chert (13.10%) are major gangue minerals associated with subordinate amounts of feldspar (1.59%), biotite + chlorite + clay (5.89%). Dolomite, hornblende, epidote, zircon and barite form the minor component of the gangue. The measured radioactivity of different density fractions of each size generated by heavy media separation (depicted in Fig. 3.4) was analysed by SSNTD technique (described in Section 3.5.2.1) the results of which are given in Table 3.12.

Table 3.12 Distribution of uranium values in different density and size fractions of Gogi uranium ore

Density	-60#+100#			-100 +150#			-150#+325#			-325#			Total		
	Mass%	U_3O_8 Assay%	Dist%	Mass%	U_3O_8 Assay%	Dist%	Mass%	U_3O_8 Assay%	Dist%	Mass%	U_3O_8 Assay%	Dist%	Mass%	U_3O_8 Assay%	Dist%
BRL	35.3	0.07	9.48	9.12	0.07	2.448	12.1	0.14	6.50	33.1	0.14	17.77	89.62	0.105	36.19
MIL	0.59	4.4	9.96	0.15	3.71	2.134	0.28	0.19	0.20	0.02	76.5	5.87	1.04	4.554	18.16
MIH	4.73	1.2	21.77	1.37	1.28	6.725	2.06	1.45	11.45	1.18	1.26	5.70	9.34	1.274	45.65
Total	40.62	0.264	41.20	10.64	0.277	11.307	14.44	0.328	18.16	34.3	0.223	29.34	100	0.261	100.00

It may be observed from Table 3.12 that uranium assay does not uniformly increase with decreasing size due to the distribution of uranium both as discrete uranium minerals and its association with sulphides and hydrous iron oxides. About 50% of uranium values are associated with Methylene Iodide heavies (MIH) fraction (sp.gr. > 3.3), where discrete uranium phases are predominant and balance is accounted by dispersed uranium with fine-grained pyrite and iron pigmented gangue mineral segregations. Both discrete and dispersed uranium phases are noticed in MIL fractions where compound grains are predominant. The images of ore and gangue minerals in Gogi ore are shown in Fig. 3.9.

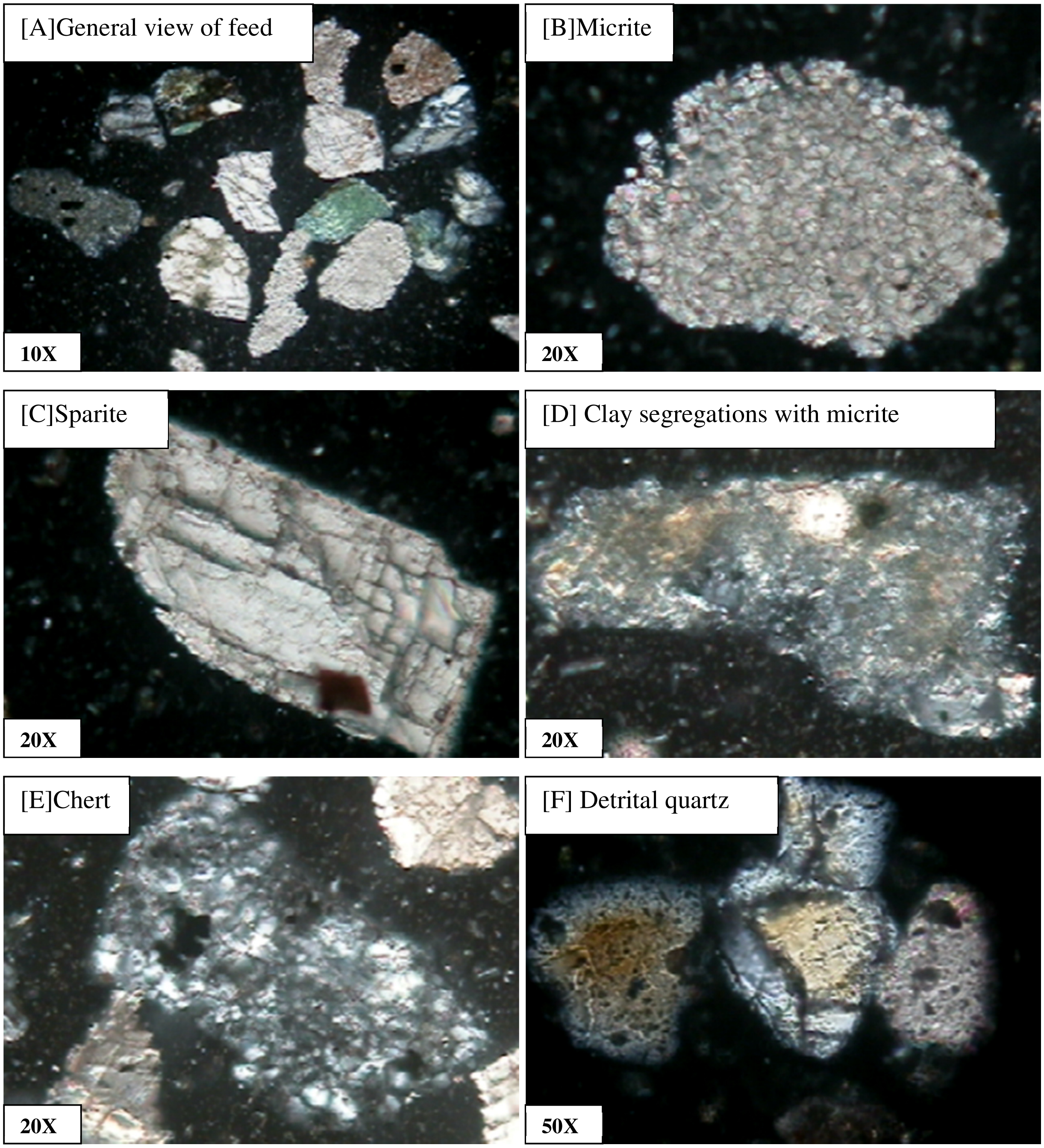

Fig. 3.9 Pictures of gangue minerals resulted due to limestone components of Gogi uranium ore seen under Transmitted Light (TL) of the optical microscope (2 Nicol)

The gangue mineralogy due to limestone is represented by micrite in Fig. 3.9[B]. The calcite is mostly impure with the presence of syndepositional clay (Fig. 3.9[D]) and chemically precipitated chert (Fig. 3.9[E]) occurring in intimate association, in addition it also contains fine clasts of detrital quartz as impurity (Fig. 3.9[F]). The non-radioactive ore minerals in Gogi uranium ore are mainly represented by sulphides with minor oxides and carbonaceous matter as shown in Fig. 3.10.

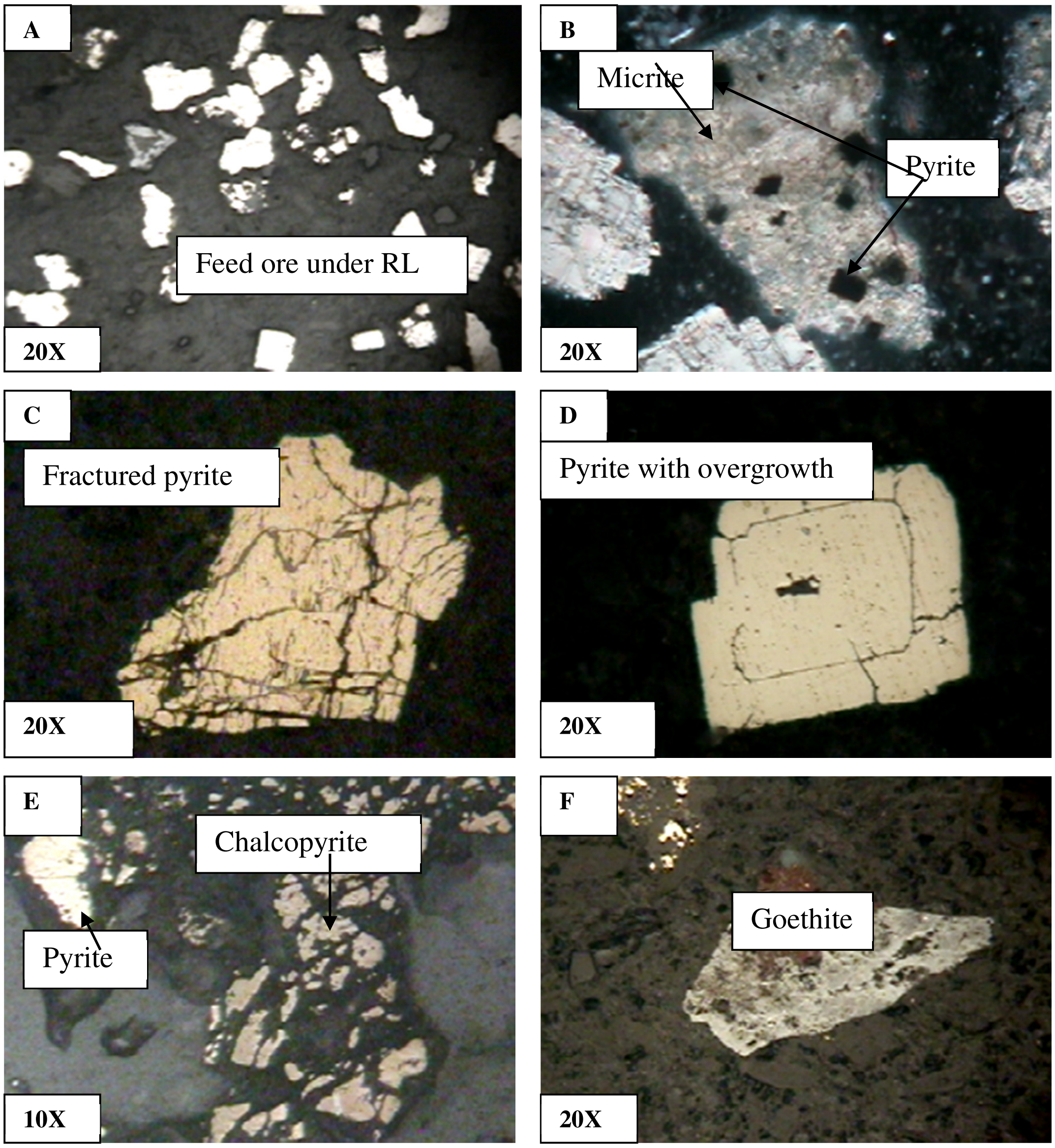

Fig. 3.10 Pictures of non-radioactive ore minerals of Gogi uranium ore seen under Reflected Light (RL) of the optical microscope (1 Nicol)

Pyrite constitutes the major sulphide phase with minor marcasite, traces of chalcopyrite and galena. Pyrite of different generations occurs as grains of different sizes and shapes. The minute segregated inclusions in micrite (Fig. 3.10[B]) and the euhedral pyrite with overgrowths (Fig. 3.10[D]) indicate syngenetic origin, whereas fractured (Fig. 3.10[C]) and brecciated pyrite represent pre-deformational hydrothermal phase. Traces of chalcopyrite and galena are the other sulphides observed (Fig. 3.10[E]). Goethite (Fig. 3.10[F]) is the major oxide mineral associated with traces of magnetite and hematite.

Uranium occurs both as discrete grains with coffinite ($U(SiO_4)_{1-x}(OH)_{4x}$) and pitchblende (U_3O_8), as well as in association with sulphides, hydrous iron oxides and clay segregated with carbonate mud as shown in Fig. 3.11. 72 hours of exposure to CN-film has yielded high density alpha tracks corresponding to coffinite (Figs. 3.11[B], 3.11[E] & 3.11[F]). Coffinite occurs as independent grains (Fig. 3.11[B]) and also in intimate association with pitchblende (Fig. 3.11[C]) and pyrite Fig. 3.11[D] & Fig. 3.11[E]. Carbonaceous matter forms minor opaque phase in the feed Fig. 3.11[A]. Pitchblende mostly shows coffinitisation indicating that it has formed early in the paragenetic sequence. Some grains of carbonaceous matter and goethite are radioactive due to presence of adsorbed uranium. Besides dispersed uranium is observed in association with clay segregations occurring in association with micrite-pyrite Fig. 3.11[F].

Srikantappa and Govindaiah [132] too have reported close association of pitchblende and coffinite with pyrite, chalcopyrite, galena and sphalerite in Gogi uranium ore deposit in their microscopic and fluid inclusion studies.

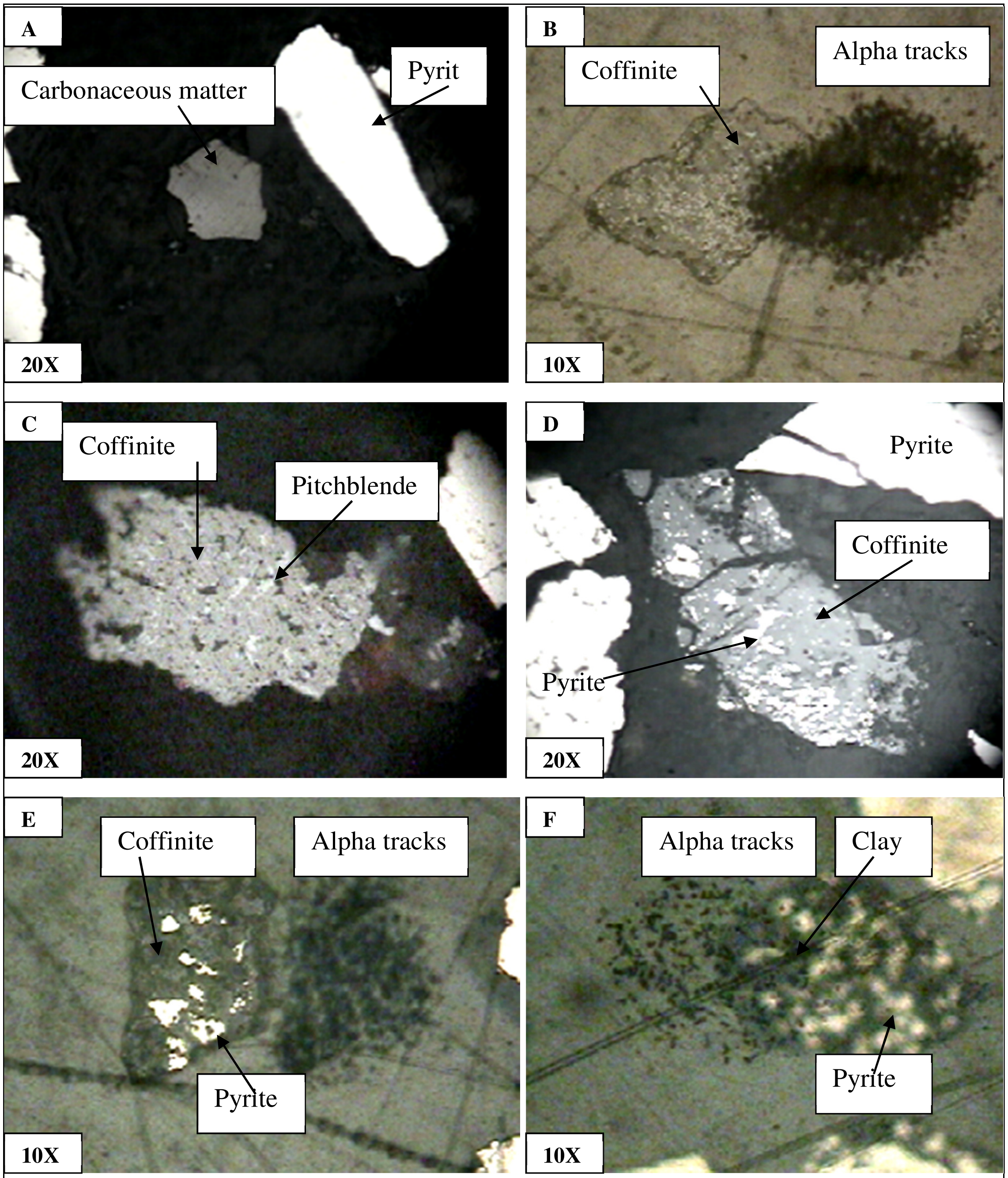

Fig. 3.11 Images of carbonaceous matter, pyrite and radioactive minerals observed under Reflected Light (RL) of the optical microscope (1 Nicol)

3.5.3 Scanning Electron microscopic studies of ore samples

The ore samples of separated fractions generated by heavy media separation (depicted in Fig. 3.4) were mounted on carbon taped brass disks (procedure described in the beginning of the Section 3.5) for examining under scanning electron microscope to study surface characteristics. The Scanning Electron Micrographs of ore sample, Ca-Mg rich, Fe rich and Ti rich particles of Tummalapalle ore along with EDX analyses are given in Figs. 3.12[A] through 3.12[D].

Uranium could not be spotted in any of the Energy dispersive X-ray spectrographs of Scanning Electron Micrographs of Tummalapalle ore samples given in Figs. 3.12[A] through 3.12[D]. It could be due to low grade, low liberation size and fine dissemination of uranium in Tummalapalle ore. The liberation size of uranium must be much lower than the average size, 150 μm, of the ore sample seen under microscope in the present study. The observation is in agreement with the low liberation size, 20-60 μm, of uranium in Tummalapalle ore reported by Minati Roy and Dhanaraju [130].

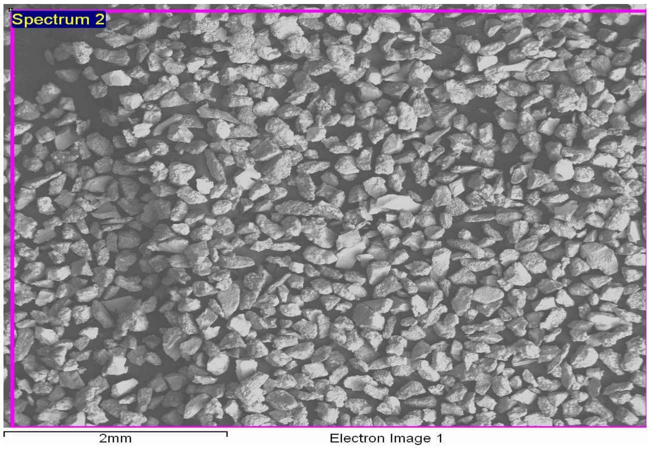

Element	%Wt.
O	52.05
Mg	4.64
Si	5.57
S	8.65
Ca	8.13
Fe	20.37
Total	100.0

Fig. 3.12 [A] Scanning Electron Micrograph of Tummalapalle ore sample

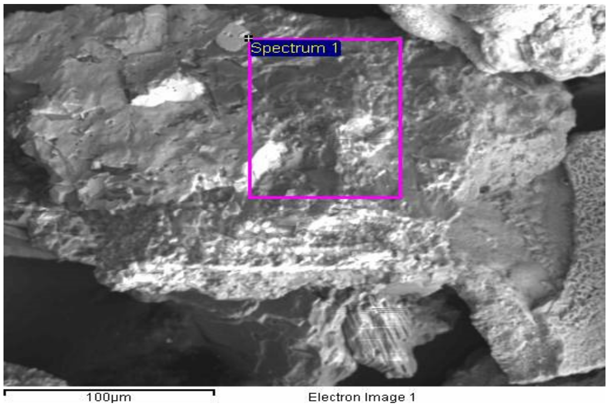

Element	%Wt.
O	60.2
Mg	7.46
Al	1.75
Si	4.51
P	2.36
S	5.86
K	1.2
Ca	10.88
Mn	0.14
Fe	5.62
Total	100.0

Fig.3.12 [B] Scanning Electron Micrograph of Ca-Mg rich particle of Tummalapalle ore

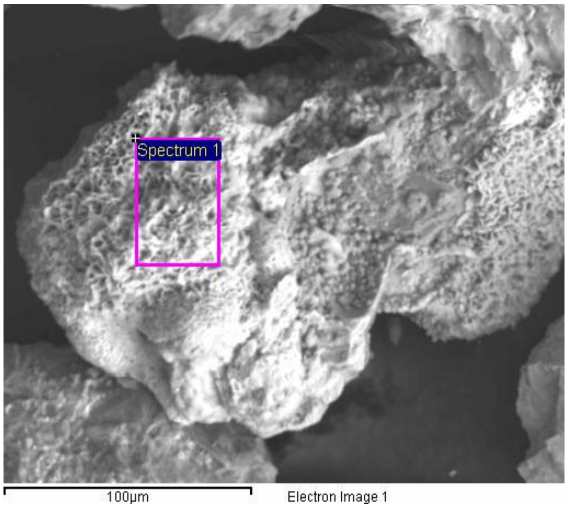

Element	%Wt.
O	2.84
Mg	0.28
Al	0.18
Si	0.36
P	0.14
S	0.74
Ca	0.98
Fe	93.38
I	1.09
Total	100.0

Fig. 3.12 [C] Scanning Electron Micrograph of Fe rich particle of Tummalapalle ore

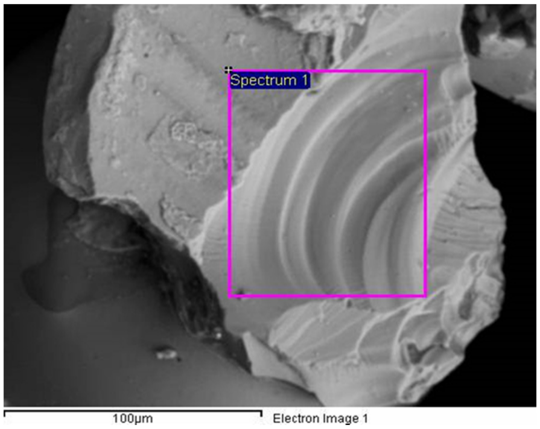

Element	%Wt.
Al	5.07
Si	16.71
K	3.62
Ca	4.42
Ti	27.41
Mn	11.75
Fe	31.02
Total	100.0

Fig. 3.12 [D] Scanning Electron Micrograph of Ti rich particle of Tummalapalle ore

Images in Fig. 3.12[B] indicate that the grains with high Ca-Mg contain high sulfur evidencing association of dolomite with pyrite mineral. The Fe rich particle shown in Fig. 3.12[C] contains sulfur indicating presence of pyrite and it appears to be very porous, which could be due to surface oxidation of pyrite (which easily undergoes oxidation) due to weathering. The Ti rich particle Fig. 3.12[D] has smooth surface and is not porous. This indicates the non-reactive nature of the Ti containing particle. The U-Ti complexes are refractory in nature.

Scanning Electron Micrograph of Gogi ore given in Fig. 3.13[A] indicates that feed to leaching has about 150 to 200 μ size particles which are in confirmation to the sieves used while generating the samples for leaching. The particles are very irregular in shape. The average elemental analysis by EDX (Fig. 3.13[A]) shows presence of 5.62% U_3O_8 in the total sample (Magnetic fraction of Methylene Iodide heavies generated by heavy media separation depicted in Fig. 3.4) mounted on the brass disk. The ore appears to be more porous than Tummalapalle uranium ore, which is in agreement with the porosity measurements presented in Table 3.3 in Section 3.1.

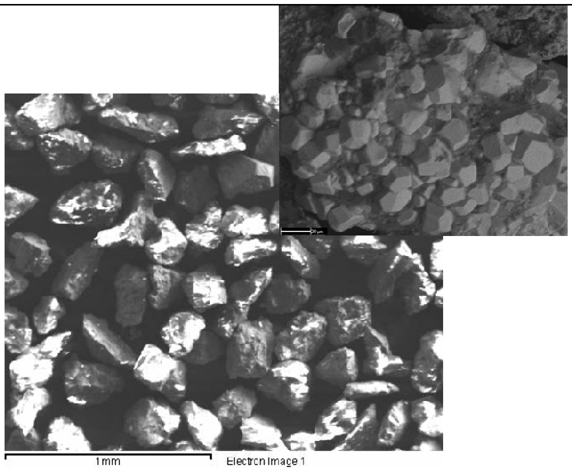

Element	%wt.
O	52.43
Mg	0.76
Al	3.13
Si	9.66
P	0.28
S	9.58
K	0.85
Ca	6.29
Ti	0.23
Fe	11.18
U	5.62
Total	100

Fig. 3.13 [A] Scanning Electron Micrograph of magnetic fraction of Methylene Iodide Heavies of Gogi ore concentrated by physical methods described in Fig. 3.4

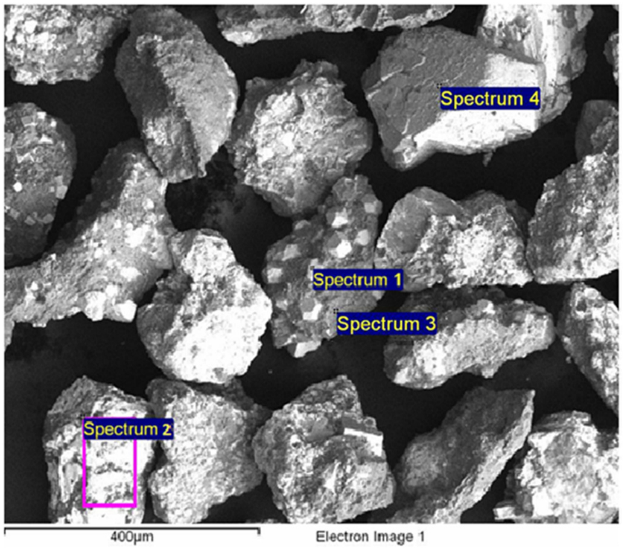

Element	Wt.%
Spectrum 1	
S Fe	71.82 28.18
Total	100.00
Spectrum 2	
O Mg Si S Ca Fe U	43.83 0.73 4.64 1.36 7.42 2.91 39.11
Total	100.00

Spectrum 3	
Element	**Weight%**
O **Mg** **Si** **S** **Ca** **Fe**	**62.48** **5.79** **13.09** **1.18** **1.4** **16.05**
Total	**100.00**

Spectrum 4	
Element	**Weight%**
O **Si** **S** **Ca** **Fe**	**22.76** **1.02** **40.25** **0.52** **35.46**
Total	**100.00**

Fig. 3.13 [B] Scanning Electron Micrograph of Methylene iodide heavies - nonmagnetic fraction of Gogi ore concentrated according to procedure described in Fig. 3.4

The Scanning Electron Micrograph of the Mehtylene Iodide-non magnetic fraction of Gogi ore, captured at a higher magnification, is given in Fig. 3.13 [B] along with Energy Dispersive X-ray spectrographs of different mineral particles. Spectrum 1 is pertinent to a prominent face of pyrite (cubic system) having a crystalline outline within the gangue minerals: calcite and dolomite. Many such occurrences of pyrite are conspicuous. While vein type pyrite is free and liberated (spectrum 4). Spectrum 2 shows that a particular portion of a particle contains as much as 39% U indicating that it is not liberated completely with respect to uranium. The liberation size for uranium is less than 150 µm. Spectrum 3 portion of particle seems to consist of dolomite, silica and pyrite from EDX.

CHAPTER 4

Equipment and Experimental Methods

4.1 LEACHING EXPERIMENTS

A number of batch leaching experiments have been carried out on pure minerals as part of basic studies using one-liter autoclave. For applied studies on the actual uranium ores of Indian origin from Tummalapalle (Andhra Pradesh) and Gogi in Karnataka, a five-liter autoclave was used. Experiments were conducted on a pilot scale 850 liters continuous autoclave to validate the scaling up of batch leaching to continuous leaching based on Residence Time Distribution (RTD) model. The description of the three autoclaves of different capacities used, leaching methods, procedures for analyzing the feed solids, leach residues and leach liquors for uranium and sulfur, are given in this Chapter.

4.1.1 Experimental set up for batch leaching tests

The one-liter and five-liter autoclaves were conceptualized and procured from M/s Amar Equipments Pvt. Ltd., Mumbai, India. The former was used for leaching studies on pure minerals taken in small quantities, 7 to 35 g. The later autoclave was used for conducting experiments with large quantities of solids, up to 1 kg, for actual uranium ores. Both the autoclaves are provided with similar paraphernalia whose schematic diagram is shown in Fig. 4.1.

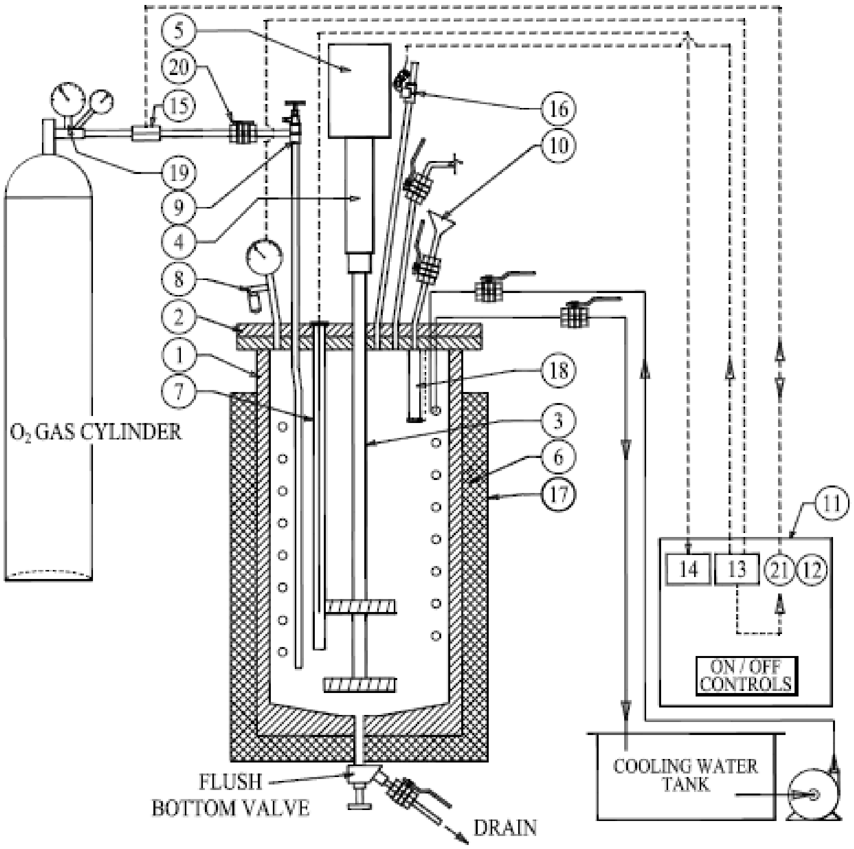

LEGEND :

1. SS BODY.
2. HEAD.
3. STIRRER.
4. MAGNETIC DRIVE COUPLING.
5. MOTOR.
6. HEATER.
7. THERMOWELL FOR THERMOCOUPLE.
8. RUPTURE DISC.
9. ANGULAR NEEDLE VALVE.
10. FUNNEL FOR POWDER INLET.
11. ELECTRICAL CONTROL PANEL.
12. VFD DRIVE FOR MOTOR REGULATION (STIRRING SPEED).
13. PRESSURE INDICATOR.
14. TEMPERATURE INDICATOR AND CONTROLLER.
15. OXYGEN GAS MASS FLOW CONTROLLER
16. SOLENOID VALVE.
17. INSULATION.
18. REAGENT ADDITION DEVICE.
19. PRESSURE REGULATOR.
20. NON RETURN VALVE.
21. OXYGEN GAS FLOW INDICATOR AND CONTROLLER.

Fig. 4.1 Schematic diagram of laboratory batch autoclaves

Experimental set up for one-liter capacity laboratory autoclave consisted of two separate interchangeable cylindrical vessels of same size (0.1 m inside diameter, 0.16 m height), one made of glass and the other made of stainless steel. The borosilicate glass vessel can be used for temperature and pressures below 150°C and 6 atm, whereas stainless steel vessel can be used up to 200°C and 50 atm pressure. Both vessels have a common top lid made of stainless steel coupled to motor drive with a magnetic seal. It is equipped with two stage gas induction pitched blade turbine type impeller of 0.04 m diameter (height from bottom = 0.005 m), thermo well for thermocouple, oxygen inlet pipe, sample addition devise to add samples under high temperature and pressure, cooling water coil, pressure sensor, rupture disk and solenoid valve to release pressure in the reactor if it exceeds the set point. The oxygen inlet pipe is connected to an oxygen cylinder through a mass flow controller that opens whenever there is a drop in the pressure inside the reactor. Electrical heater was wrapped outside the stainless steel vessel and covered with insulation. The heater was provided at the bottom for the glass vessel. Heaters of both the vessels are connected to a common temperature indicator and controller to maintain constant temperature in the vessels. When the temperature rises (which could be due to exothermic reactions) above the set point, water is pumped from a cooling tank into the cooling coil provided inside the vessel. The photo picture of one-liter autoclave used for the experiments in the present studies is given in Fig. 4.2.

The five-liter autoclave used for leaching of uranium ore samples is identical to one-liter autoclave described above, except that it has a single stainless steel cylindrical vessel of height = 0.32 m, inside diameter = 0.15 m and impeller diameter = 0.05 m. Both one-liter and five-liter autoclaves are provided with fully automated PC to continuously monitor, control and record temperature, pressure, impeller speed, gas flow.

Fig. 4.2 Photo picture of one liter batch autoclave

4.1.2 Experimental set up for continuous leaching tests

Continuous mode pressure leaching tests were carried out on pilot scale in a 850 L capacity horizontal Continuous Autoclave Leaching Reactor (CLR) with length = 2.1 m and internal diameter = 0.7 m. Fig. 4.3 shows CLR, divided into three stirred tanks by weir plates; the effective volumes of the tanks holding the leach slurry are 267, 170 and 113 liters respectively, from left to right. The reactor is jacketed for external heating and cooling as per the need. Pitched blade turbine type impellers (0.28 m diameter), operated through a variable frequency drive (VFD), agitate the contents of the three compartments at the desirable speed. Double mechanical seals are provided for shaft seal. The reactor and the steam jackets are provided with pressure relief valves set to discharge at 10% above the operating pressure of autoclave. Manual vent valve is provided for de-pressurizing / shut-down operations during an emergency. The photo picture of continuous leach reactor is shown in Fig. 4.4.

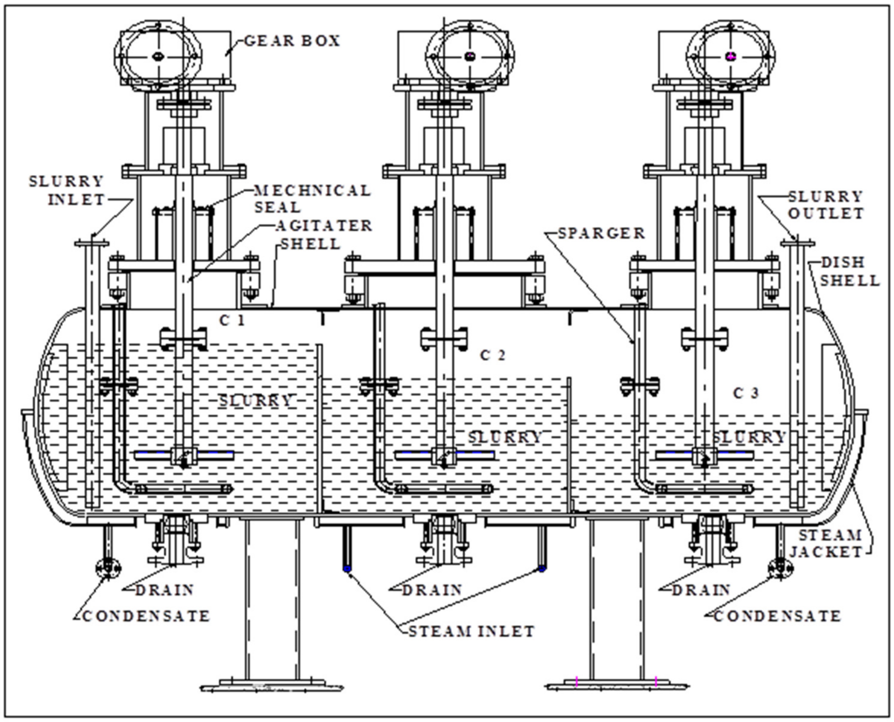

Fig. 4.3 Pilot scale 850 L continuous leach reactor with three stirred compartments (C1, C2 and C3) in series

Fig. 4.4 Photo picture of 850 L capacity pilot scale continuous leach reactor

4.1.3 Batch leaching procedure

The pulp density in each experiment was maintained low at arbitrarily chosen values of either 1% or 5% solids (by weight) in order to minimize the effect of change in pulp density when liquor samples are withdrawn periodically during experiment. In each leaching experiment conducted with synthetic materials, predetermined amounts of the reacting materials (UO_2 and / or FeS_2) were filled in the sample addition device of autoclave and the cap of sample addition device was plugged. Required amounts of sodium carbonate and sodium bicarbonate, dissolved in 700 ml water, silica and calcite powders were loaded into the autoclave. Autoclave lid was then closed and the agitator was started at a low speed. The autoclave was heated up to 70°C during which period the vent valve was kept open to expel the atmospheric gases like N_2 out of the autoclave and fill the autoclave with water vapor. The vent valve was then closed and heating continued. When the autoclave attained the desired temperature, the tube connected to the sample addition device was pressurized with a gas (O_2 / Ar / N_2, as the case may be) from a pressurized cylinder so that the cap of sample addition device opens and the feed solids contained are dropped into the autoclave. The pressure of the reactor was increased to the desired total pressure using the same gas. The agitator motor was set to the desired stirring speed. The time course of the experiment began at this point.

Leaching continued in most of the experiments for 6 h or as stated otherwise. Small samples of leach liquor were drawn at time intervals of 0.166, 0.333, 0.5, 0.666, 1, 1.5, 2, 2.5, 3, 4, 5 and 6 h through dip tube and analyzed for their U_3O_8 and sulfate content by Spectrophotometry and Gravimetry (precipitation with $BaCl_2$) respectively. Further, these leach liquor samples were also analysed for their Na_2CO_3 and $NaHCO_3$ contents by Volumetry. The U_3O_8 and S contents of leach residue sample obtained at the end (6 h) of each experiment were also determined by Pellet Fluorimetry and Gravimetric techniques respectively. The detailed procedures followed for all the above mentioned chemical analyses are given in

Section 4.2. The back calculated feed values of both pyrite and UO_2 from the assays of leach liquor and residue were confirmed with the original quantities of UO_2 and pyrite used in each experiment. The input sodium (calculated from the sodium carbonate and sodium bicarbonate contents added initially) was checked to be equal with that of output sodium (calculated from the sodium carbonate, sodium bicarbonate and sodium sulfate, which would have formed from reaction of pyrite) in each sample of leach liquor drawn at different time intervals.

Similar procedure was also followed for leaching of two actual uranium ore samples from Tummalapalle (Andhra Pradesh) and Gogi (Karataka) except the percent solids and volume of the leach reactor. The percent solids (wt / wt) was 50 in all these experiments and the volume of leach reactor was 5 L.

4.1.4 Continuous leaching procedure

Tummalapalle uranium ore sample was used for the pilot scale continuous leaching studies. The ore analyzed 0.05% U_3O_8 and 1.5% FeS_2. In each test, the slurry was fed in the first compartment; the reactor contents overflow from this compartment to the next and from there to the third. The slurry discharge from the third compartment is through a dip tube. Steady state samples were withdrawn through sampling outlets. During steady state sample collection, the reactor contents were first allowed to into sampling port through a ball valve, which was isolated after required slurry volume was collected. This valve was then closed and the entrapped sample was cooled to about 40°C and then discharge valve was opened for collection of sample for analyses.

The feed and discharge outlets of the slurry from the Continuous Leach Reactor (CLR) were controlled by two separate interlocks. The solenoid valve in the feed-line opens only if the pressure of input slurry exceeds the reactor pressure. The slurry is discharged through a dip tube in line with a pneumatically operated control valve. The opening of the control valve is interlocked with the level in the third compartment. The level in the third compartment is monitored with a differential pressure transmitter (DP), which sends signals to the control valve. CLR was fed continuously with feed slurry of 50% solids (w/w) and 50 g/L Na_2CO_3 and 70 g/L $NaHCO_3$ reagent concentrations at pre-set feed flow rate and inlet temperature with the aid of a screw-pump. The reactor contents were maintained at 125 – 130°C under 7.2 – 7.5 atm over-pressure.

4.2 CHEMICAL ANALYSIS PROCEDURES

The methods of analysis followed are the standard procedures from the prescribed text books [133 - 135].

4.2.1 Estimation of uranium

4.2.1.1 Solids (Pellet fluorimetry): About 0.1 - 1 g of the sample was accurately weighed in a platinum dish. About 10 ml of HF and 5 ml of concentrated HNO_3 were added to the sample in the dish. HF converts silica to its fluoride complex and HNO_3 converts uranium to +6 oxidation state. The mixture was slowly heated in a boiling water bath and evaporated to dryness to expel silicon fluoride complexes. The HF-HNO_3 treatment was repeated once again. After the second evaporation, 10 ml of concentrated HNO_3 was added and evaporated to dryness twice. Finally, 10 ml of concentrated HNO_3 was added, the sides of the dish washed with a jet of distilled water and warmed in a water bath. The contents were cooled and filtered through Whatman No. 540 filter paper. The residue in the filter paper was washed with hot water till free of acid. The washings were added to the filtrate and made up to 100 ml with distilled water.

A 3 ml aliquot of the solution was transferred to a separating funnel and 10 ml of saturated Aluminium nitrate solution was added. Then 5 ml of ethyl acetate was added to the separating funnel and shaken for 2 minutes. The uranium gets extracted in the organic layer leaving behind the interfering matrix in the aqueous phase. After the two layers separate clearly, the aqueous layer was drained out and the organic layer was collected. Three standard uranium solutions containing 2, 5 and 10 mg/L uranium and a blank solution were also treated in the same way.

With a micropipette 0.1 ml each of the organic layer of samples and standards were transferred into a platinum planchet and 0.1 ml of distilled water was also added to each of the planchets. They were placed under an infra-red lamp and solution was evaporated to complete dryness. The planchets were cooled and 0.3 g of Na_2CO_3-NaF (3:2) flux was added to each planchet. The planchets were kept in a muffle furnace and the flux was melted at 900°C for 3 min. The planchets were taken out and cooled. The fluorescence intensity was of the solidified flux in the planchet was read in the Fluorimeter. (ECIL make, model No.FL-6224A). The instrument was calibrated with standards taken. The Excitation radiation wave length was set to 365nm and Emission intensity was measured at 555nm. The spectral bandwidth for both excitation and emission was set to 10nm and photomultiplier EHT was set to 500 V. A calibration graph was constructed from the measured emission intensities of the standards. The U_3O_8 concentration in the sample was calculated from the calibration graph.

<u>4.2.1.2 Liquids (Spectrophotometry):</u> 5 ml aliquot of the sample solution, 2 ml of 25% (w/v) NaOH solution and 1 ml of 30% (w/w) Hydrogen Peroxide (GR grade of Merck) were taken in a 25 ml standard flask and the volume was made up to the mark with distilled water. The solution was mixed well and allowed to stand for about 15 minutes. A set of standard solutions containing known quantities of uranium were also processed in the same way. A blank was prepared using only NaOH and H_2O_2. The absorbance of the samples and standards was measured with a UV/Visible spectrophotometer (model: UV3000$^+$, supplied by M/s Lab India Analytical, India) using Beer-Lambert law. The blank was used to adjust zero every time before measuring the absorbance (log $[I_0/I_t]$) of samples. I_0 = Intensity of incident light and I_t = Intensity of transmitted light. A calibration graph was constructed from the measured absorbances of the standard solutions. The concentration of U_3O_8 in unknown solutions was determined using calibration graph (Fig. 4.5).

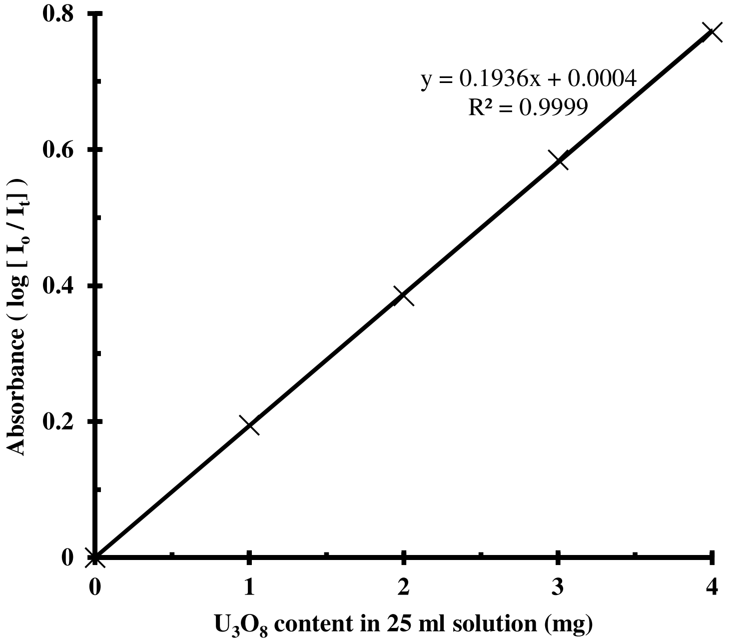

Fig. 4.5 Calibration curve for measurement of U_3O_8 concentration in Spectrophotometer

4.2.2 Estimation of sulfur (Gravimetry)

4.2.2.1 Solids: One gram of sample was accurately weighted into a 250 ml beaker and 20 ml concentric nitric acid was added and heated slowly on a hot plate and evaporated to almost dryness. The step was repeated once. This oxidizes all the sulphur to sulphate form. To the mass in the beaker 10 ml of concentrated HCl and 50 ml of distilled water were added. The contents were boiled well, cooled, filtered through Whatman filter paper 540 and washed well till free of acid (detected by dipping the pH paper in the filtrate). The filtrate and washings were collected together.

To the combined filtrate and washings about 50 ml distilled water was added and heated to boiling on the hot plate. To the boiling solution 10 ml of 10% (w/v) barium chloride solution was added drop wise, stirred, boiled well and kept overnight for cooling. The contents were filtered through Whatman filter paper no. 542 and washed with cold 2% ammonium nitrate solution till the precipitate was free of chloride. The precipitate along with the filter paper was transferred to a silica crucible (already heated, cooled and weighed) and ignited in a muffle furnace by initially maintaining the temperature at 375°C for 45 minutes and thereafter at 900°C for 45 minutes. The crucible was taken out and cooled in a desiccator. The crucible was weighed. The difference between the final weight and initial weight is the amount of barium sulphate obtained from which the amount of sulphur was calculated.

4.2.2.2 Liquids: Suitable volume of aliquot of the solution, 10 ml of concentrated HCl and 100 ml of distilled water were taken in a 250 ml beaker and heated to boiling on a hot plate. Sulphate in the solution was precipitated as barium sulphate by adding about 10 ml (excess of stoichiometric requirement) of 10% (w/v) $BaCl_2$ solution and sulphate was estimated by following the same procedure described in Section 4.2.2.1.

4.2.3 Estimation of sodium carbonate and sodium bicarbonate in liquids (Volumetry)

A 1% solution of HCl was prepared by diluting 1 ml of concentrated HCl with 100 ml of distilled water. This gives a concentration of approximately 0.1 N HCl. This solution was standardized as follows:

A standard Na_2CO_3 solution of 0.1 N concentration was prepared. 10 ml of this solution is titrated against the prepared HCl solution using methyl orange indicator. The end point was detected when the color of sample changed from yellow to light orange. The volume of acid required for neutralization was noted down. The normality of acid was measured by using the Eq. 4.1.

$$N_1V_1 = N_2V_2 \qquad [4.1]$$

Where, N_1 = Normality of HCl, V_1 = Titration volume of HCl, N_2 = Normality of Na_2CO_3 solution = 5N and V_2 = Volume of Na_2CO_3 solution = 10 ml.

For estimation of carbonate in the samples, suitable aliquot of sample (y ml) was pipetted out in a conical flask and 30 - 40 ml of distilled water was added. Two drops of phenolphthalein indicator were added. This solution was titrated against HCl of known normality. Titration continued until the pink colored solution turns colorless. At this stage Na_2CO_3 is converted to $NaHCO_3$. The volume of HCl required for neutralization was noted down as V_2. The concentration of sodium carbonate was calculated using Eq. 2.

$$\text{Normality of Na}_2CO_3 = \frac{N_1(2V_1)}{y} \qquad [4.2]$$

Where, N_1=normality of HCl, V_1= titre value (ml), y = Volume of unknown sample (ml).

For estimation of bicarbonate in the sample an aliquot of the sample solution (y ml) was taken into another conical flask, diluted with about 50 ml of water, two drops of methyl orange were added and titrated against standard HCl till the solution in the conical flask turned orange. At this stage all the Na_2CO_3 and $NaHCO_3$ in the solution is converted NaCl. The titre value was noted as V_2. The concentration of sodium bicarbonate (as normality) in the solution was calculated from the Eq. 4.3.

$$\text{Normality of NaH}CO_3 = \frac{N_1(V_2 - 2V_1)}{y} \qquad [4.3]$$

Where, N_1=normality of HCl, V_1= titre value (ml) in first titration, V_2 = titre value (ml) in second titration, y = Volume of sample (ml).

CHAPTER 5

Modeling Leaching Kinetics of Single and Binary Mixtures of Uranium Dioxide and Pyrite (Basic Studies)

Leaching studies carried out separately on pure uranium dioxide (the target mineral) and iron pyrite (the undesired reactive gangue mineral) are presented in this Chapter. Understanding the simultaneous leaching of uranium oxide and pyrite in co-existing systems is complex owing to the non-elementary nature of the parallel reactions of these two compounds [52 – 59]. Hence, further leaching studies were under taken on synthetic mixture consisting of both uranium dioxide and iron pyrite. The effects of leaching parameters (temperature, pressure, concentration of leachants Na_2CO_3 & $NaHCO_3$, and particle size) are determined, and the kinetic models developed for each of uranium oxide and pyrite, in isolation, as well as when present as mixture. Additionally, a study on morphological changes during leaching of pure materials formed part of this Chapter.

Numerous examples cited in the literature provide evidence of the complexity involved in the development of phenomenological models for leaching of ores, particularly for alkaline leaching of uranium ores [106 - 108, 136]. The leaching of uranium from natural ores varies significantly due to the differences in composition of individual uranium minerals, their proportion, gangue mineralogy and degree of liberation. For better understanding of the leaching process, the studies were undertaken on pure constituents present in uranium ores conducive for alkaline leaching. These constituents were: uranium dioxide (UO_2), iron Pyrite (FeS_2), silica (SiO_2), and calcite ($CaCO_3$).

The simple oxide species, uraninite (nominally UO_{2+x}), is the most common uranium ore mineral of economic interest. Pyrite is a common mineral, found in a wide variety of geological formations from sedimentary deposits to hydrothermal veins and as a constituent of metamorphic rocks. In alkaline leaching of carbonate type of uranium ores containing pyrite, both the target mineral (uranium bearing mineral) and reactive gangue mineral (pyrite) consume oxidant as well as the leachants according to the reactions (2.4), (2.5) and (2.8) given in Section 2.1.3.1. If the competitor mineral pyrite, FeS_2, is present in significant quantities in the ore then FeS_2 limits the availability of oxygen and sodium carbonate (according to above reactions) for oxidation and dissolution of uranium mineral during leaching with carbonate solutions. The attack on pyrite by carbonate leach solutions may become serious [53A]. Thus, it is important to study the kinetics of leaching of pure pyrite mineral separately; these kinetics can be extended to leaching of multi mineral systems, i.e., the uranium ores containing pyrite in the present case. Literature is available on reaction kinetics of pyrite in acidic systems while limited information is available on pyrite reaction in alkaline solutions [92].

As a rule of thumb, the uranium ores containing carbonate gangue minerals >12-15% cannot be treated by conventional acid leaching due to consumption of large acid [7, 8]. Calcite and dolomite are the two carbonate minerals found in such ores, which ought to be treated by alkaline leaching. Since both of them have similar chemical nature, only calcite was added to the leaching solids in the present study, and it was assumed that dolomite will have similar behaviour during alkaline leaching. Silica is the most ubiquitous gangue mineral that occurs in ores of any metal. Hence, calcite and silica are chosen to represent the inert minerals likely to be present in naturally occurring uranium ores.

5.1 LEACHING STUDIES ON PURE URANIUM DIOXIDE

5.1.1 Materials and Methods

The kinetics of dissolution of pure UO_2 in carbonate solution was investigated using a one-liter autoclave described in Section 4.1.1. The scheme of experiments carried out is given in Table 5.1 including the feed used and conditions of leaching. In Expt. No. PUL/1, the base levels of concentration of Na_2CO_3 ($[Na_2CO_3]$), concentration of $NaHCO_3$ ($[NaHCO_3]$), particle size (d), and partial pressure of oxygen (P_{O2}) were fixed based on few screening experiments and on the data available in literature on alkaline leaching of uranium [37, 83]. The actual particle size ranges (sieve fractions of pure minerals UO_2 and calcite) used in experiments were −72+100#[−210+150μm], −100#+150#[−150+100μm], −150+200#[−100+75μm], and

−325+400#[-44+37µm]. Geometric average values of these particle size range classes are given in Table 5.1, which are considered for modeling purpose.

Table 5.1 Details of feed and experimental scheme of leaching of pure UO_2

Distilled water=	700 ml		Wt. of pure UO_2 in each experiment =			7 g	
Speed of rotation =	1000 rpm		Wt. of pure Calcite in each experiment=			28 g	
Time of reaction = 6 h (Liquid samples drawn at intervals of 0.33, 0.66, 1, 1.5, 2, 3, 4, 5, 6 h for analysis of U_3O_8 by spectrophotometry)							
Exp. No.	Variable parameters						
PUL /	Concentration of Na_2CO_3 (M)	Concentration of $NaHCO_3$ (M)	Temperature (K)	P_{O2} (atm)	Size (µm)	P_{H2O} (atm)	$P_{(total)}$ (atm)
1*	0.5	0.5	353	10	87	0.5	10.5
Effect of Na_2CO_3 Concentration							
2	0.05	0.5	353	10	87	0.5	10.5
3	0.1	0.5	353	10	87	0.5	10.5
4	0.2	0.5	353	10	87	0.5	10.5
5	0.3	0.5	353	10	87	0.5	10.5
6	0.4	0.5	353	10	87	0.5	10.5
7	0.6	0.5	353	10	87	0.5	10.5
8	0.7	0.5	353	10	87	0.5	10.5
Effect of $NaHCO_3$ Concentration							
9	0.5	0.1	353	10	87	0.5	10.5
10	0.5	0.3	353	10	87	0.5	10.5
11	0.5	0.4	353	10	87	0.5	10.5
12	0.5	0.6	353	10	87	0.5	10.5
13	0.5	0.7	353	10	87	0.5	10.5
Effect of Temperature							
14	0.5	0.5	373	10	87	1	11
15	0.5	0.5	393	10	87	2	12
16	0.5	0.5	213	10	87	3.6	13.6
Effect of Po_2							
17	0.5	0.5	353	0	87	0.5	0.5
18	0.5	0.5	353	3	87	0.5	3.5
19	0.5	0.5	353	5	87	0.5	5.5
20	0.5	0.5	353	7	87	0.5	7.5
Effect of Size							
21	0.5	0.5	353	10	40	0.5	10.5
22	0.5	0.5	353	10	125	0.5	10.5
23	0.5	0.5	353	10	177	0.5	10.5
* Base experiment – conducted with constant values of the levels of variables while each variable was varied							

The leach liquor samples drawn at different time intervals in each experiment were analyzed for [U_3O_8], [Na_2CO_3] and [$NaHCO_3$], according to the procedures described in Section 4.2. The leach residue in each experiment was also analyzed for U_3O_8. The uranium balance was checked in each experiment by confirming that the back calculated feed value of UO_2 from the assay of leach liquor and leach residue obtained at the end of each experiment, after 6 h, was equal to the original quantity of UO_2 (7 g) used as feed. Similarly, the sodium balance was also checked in each experiment. The input sodium (calculated from the sodium carbonate and sodium bicarbonate contents added initially) to the leaching, was checked to be equal to that of output sodium (calculated from the sodium carbonate, sodium bicarbonate and sodium sulfate values obtained from analyses of leach liquors) in each sample of leach liquor drawn at different time intervals.

5.1.2 Results and Discussion

The results of leaching experiments conducted on pure UO_2 are modeled for effects of each of the leaching parameters.

Effect of concentrations of Na_2CO_3, $NaHCO_3$ and partial pressure of O_2 on leaching of pure UO_2: Figs. 5.1, 5.2 and 5.3, respectively, show the variation of concentration of uranium, expressed as UO_2, in the leach liquor with time for different concentrations of carbonate, bicarbonate and partial pressure of oxygen. The data from some of the experiments are not included in these figures, to provide a clearer view in the plots.

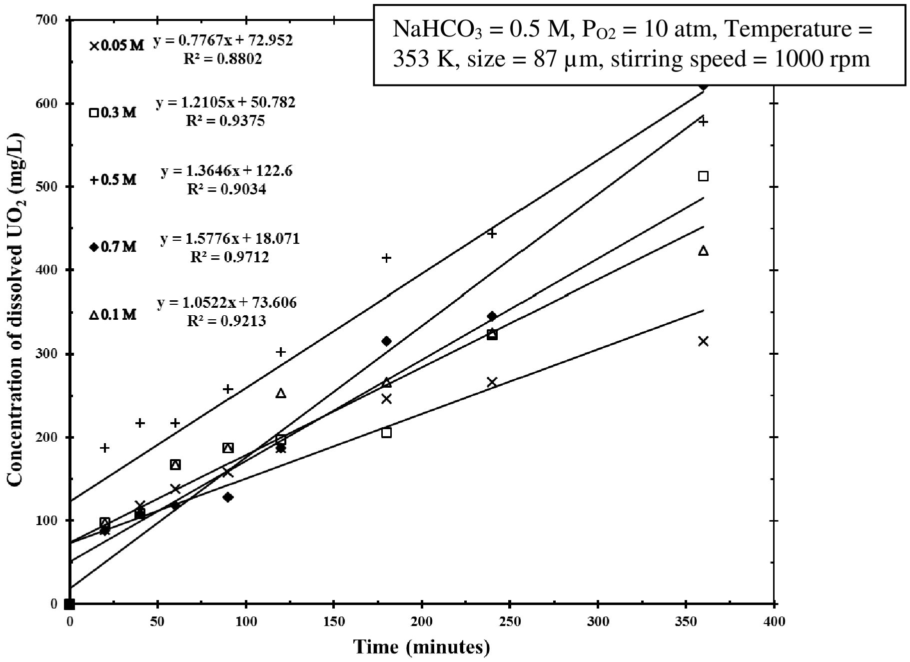

$NaHCO_3$ = 0.5 M, P_{O2} = 10 atm, Temperature = 353 K, size = 87 μm, stirring speed = 1000 rpm

Fig. 5.1. Rate of dissolution of UO_2 as a function of Na_2CO_3 concentration

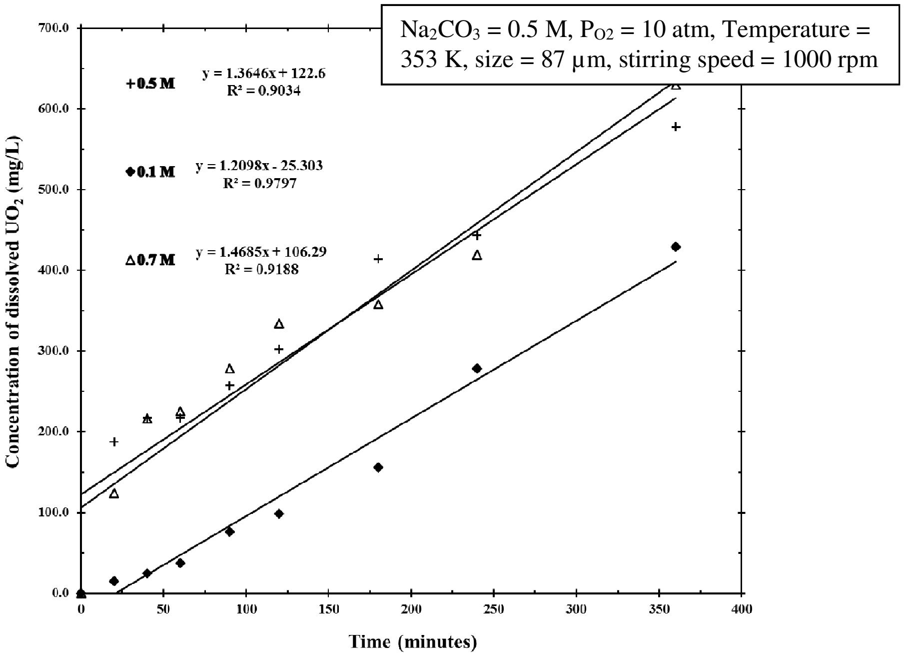

Na_2CO_3 = 0.5 M, P_{O2} = 10 atm, Temperature = 353 K, size = 87 µm, stirring speed = 1000 rpm

Fig. 5.2. Rate of dissolution of UO_2 as a function of $NaHCO_3$ concentration

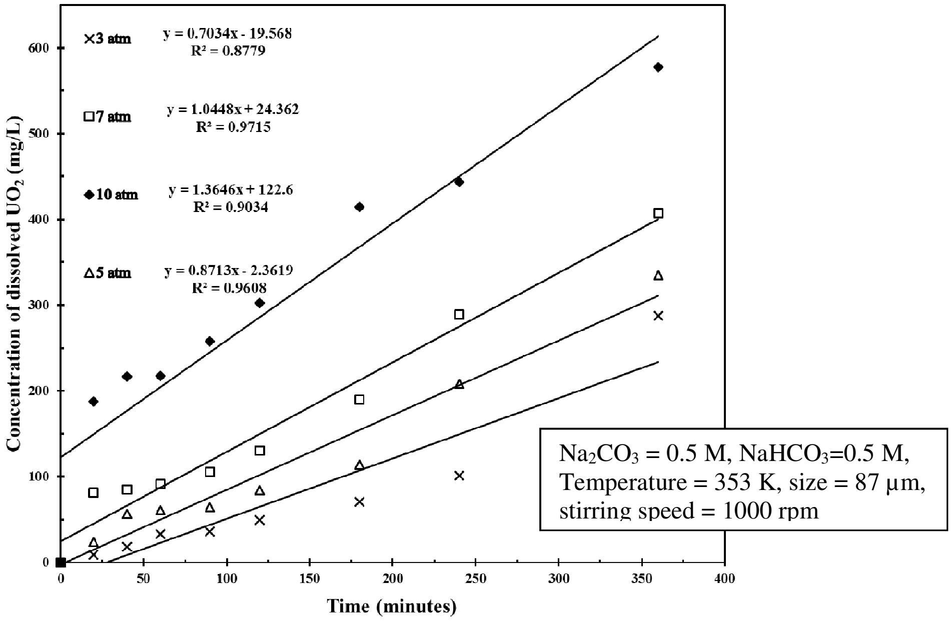

Na_2CO_3 = 0.5 M, $NaHCO_3$=0.5 M, Temperature = 353 K, size = 87 µm, stirring speed = 1000 rpm

Fig. 5.3. Rate of dissolution of UO_2 as a function of partial pressure of oxygen

The data plotted in Figs. 5.1 through 5.3 are tested for linear relation using Microsoft Excel (MSExcel®) regression plots. R^2 (coefficient of determination) ≥ 0.9 indicates that the relation is good. The slopes of fitted straight lines in these figures represent the rates of dissolution of UO_2 as mg/L-min, which are shown in Table 5.2.

Table 5.2 Rate of dissolution of UO_2 under different concentrations of sodium carbonate, bicarbonate and partial pressures of oxygen

Expt. No. PUL/	Concentration of Na_2CO_3 (M)	Rate of dissolution of UO_2 (mg / L-min)
2	0.05	0.7767
3	0.1	1.0522
4	0.2	1.1400
5	0.3	1.2105
6	0.4	1.3000
1	0.5*	1.3646
7	0.6	1.5000
8	0.7	1.5776
Expt. No.	Concentration of $NaHCO_3$ (M)	Rate of dissolution of UO_2 (mg / L-min)
9	0.1	1.2098
10	0.3	1.3212
11	0.4	1.3431
1	0.5*	1.3646
12	0.6	1.41655
13	0.7	1.4685
Expt. No.	Partial pressure of Oxygen (atm)	Rate of dissolution of UO_2 (mg / L-min)
17	0	0
18	3	0.7033
19	5	0.8713
20	7	1.0448
1	10*	1.3646
* constant while other parameters are varied.		

Several authors have reported that the dissolution of pure UO_2 follows the Michaelis–Menten type of equation for homogeneous reactions, based on electrochemical mechanism [34, 36, 37, 85, 137]. In the present study too, the reaction orders with respect to concentration of sodium carbonate, bicarbonate and partial pressure are estimated by Michaelis–Menten type of equation given by Eq.5.1.; Representing UO_2 dissolution rate, $\frac{dC_{UO_2}}{\mathrm{dt}}$ (in mg/L-min), and concentration of Na_2CO_3 / $NaHCO_3$ / partial pressure of oxygen as ‘x’.

$$\frac{dC_{UO_2}}{\mathrm{dt}} = \frac{\mathrm{k_1 \times x^n}}{\mathrm{k_2 + k_3 \times x^n}} \qquad [5.1]$$

The empirical constants (k_1, k_2, k_3 and n) are determined separately for each of the three variables (concentration of sodium carbonate, bicarbonate and partial pressure) according to

Eq. 5.1; using a curve fitting tool for nonlinear equations available in MATLAB® software. The estimated parameters for the three leaching variables, including calculated and experimental rates of dissolution of UO_2, are shown in Table 5.3.

Table 5.3 Estimated empirical constants of Eq. 5.1* (given in footnote) for three parameters of uranium leaching along with experimental and calculated rates of dissolution

Leaching parameter (x)	k_1	k_2	k_3	n	Experimental rate of dissolution (mg/L-min)	Calculated rate of dissolution (mg/L-min)	% error in calculated value
Concentration of Na_2CO_3 (M)							
0.05	2	1.201	$3x10^{-7}$	0.24	0.78	0.82	5.1
0.1					1.05	0.96	-8.5
0.2					1.14	1.14	-0.4
0.3					1.21	1.25	3.3
0.4					1.30	1.34	3.0
0.5					1.36	1.41	3.5
0.6					1.50	1.47	-1.7
0.7					1.58	1.53	-3.0
Concentration of $NaHCO_3$ (M)							
0.1	1.95	1.312	$1.5x10^{-4}$	0.09	1.21	1.20	-1.1
0.3					1.32	1.33	0.4
0.4					1.34	1.36	1.4
0.5					1.36	1.39	1.9
0.6					1.42	1.41	-0.1
0.7					1.47	1.44	-2.3
Partial pressure of O_2 (atm.)							
0	1.47	4.16	$1.9x10^{-5}$	0.58	0.00	0.00	0
3					0.70	0.67	-5.4
5					0.87	0.89	2.6
7					1.04	1.09	3.9
10					1.36	1.33	-2.2
*Eq.5.1.	$\frac{dC_{UO_2}}{\mathrm{dt}} = \frac{k_1 \times x^n}{k_2 + k_3 \times x^n}$ in mg/L-min						

An overall model equation (Eq.5.2) is formed combining the above empirical constants, given in Table 5.3, determined for the effects of $[Na_2CO_3]$, $[NaHCO_3]$ and PO_2.

$$\frac{dC_{UO_2}}{\mathrm{dt}} = \frac{k_0^{11} \times [Na^2CO^3]^{0.24} \times [NaHCO^3]^{0.09} \times Po_2{}^{0.58}}{(3 \text{ x } 10^{-7} \times [Na^2CO^3]^{0.24}) + (1.5x10^{-4} \times [NaHCO^3]^{0.09}) + (1.9x10^{-5} \times Po_2{}^{0.58})} \qquad [5.2]$$

The empirical constant, k_0^{11}, is in turn determined from the slope of regression straight line fitted for the product term $\frac{[Na^2CO^3]^{0.24}\times[NaHCO^3]^{0.09}\times Po_2{}^{0.58}}{(3\text{ x }10^{-7}\times[Na^2CO^3]^{0.24})+(1.5\text{x}10^{-4}\times[NaHCO_3]^{0.09})+(1.9\text{x}10^{-5}\times Po_2{}^{0.58})}$ and experimental rate of dissolution, $(\frac{dC_{UO_2}}{dt})_{expt}$, using the data in Table 5.3 as shown in Fig. 5.4. The value of k_0^{11} is found to be $1\text{x}10^{-4}$ from Fig. 5.4. This value of k_0^{11} is found as a function of particle size and temperature in the following two Sections.

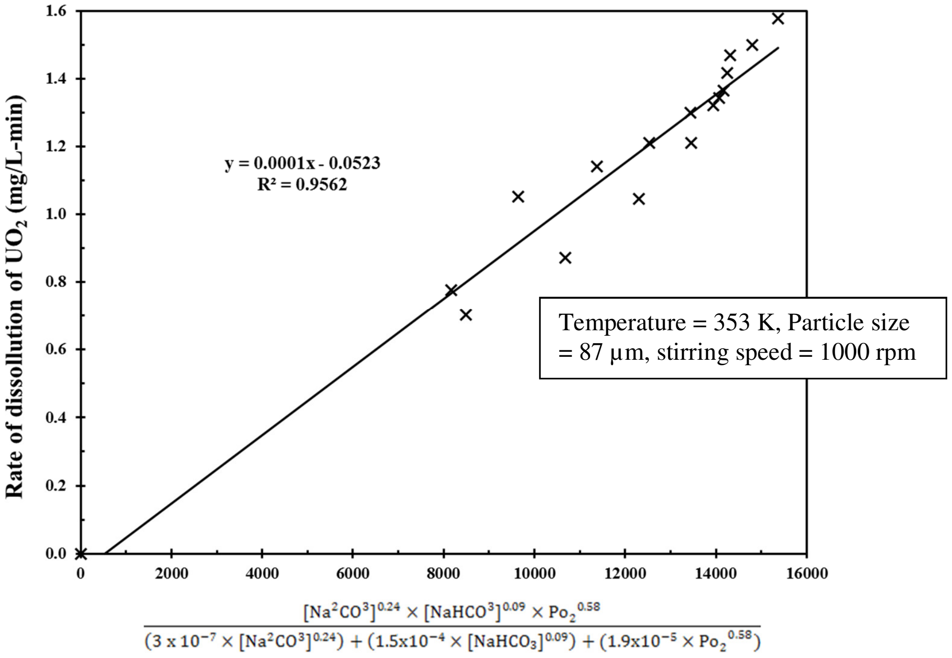

Fig. 5.4 Rate of dissolution of UO_2 Vs Product term

<u>Effect of particle size on leaching of pure UO_2:</u> Experimental results of dissolution of UO_2 with time for the range of particle sizes 41 to 177 µm are plotted in Fig. 5.5. The rates of dissolution for different particle sizes obtained from the slopes of the corresponding fitted straight lines are plotted in Fig. 5.6 to find the order with respect to particle size according to Eq. 5.3.

$$\frac{dC_{UO_2}}{dt} = k_0^1\, d^n \qquad [5.3]$$

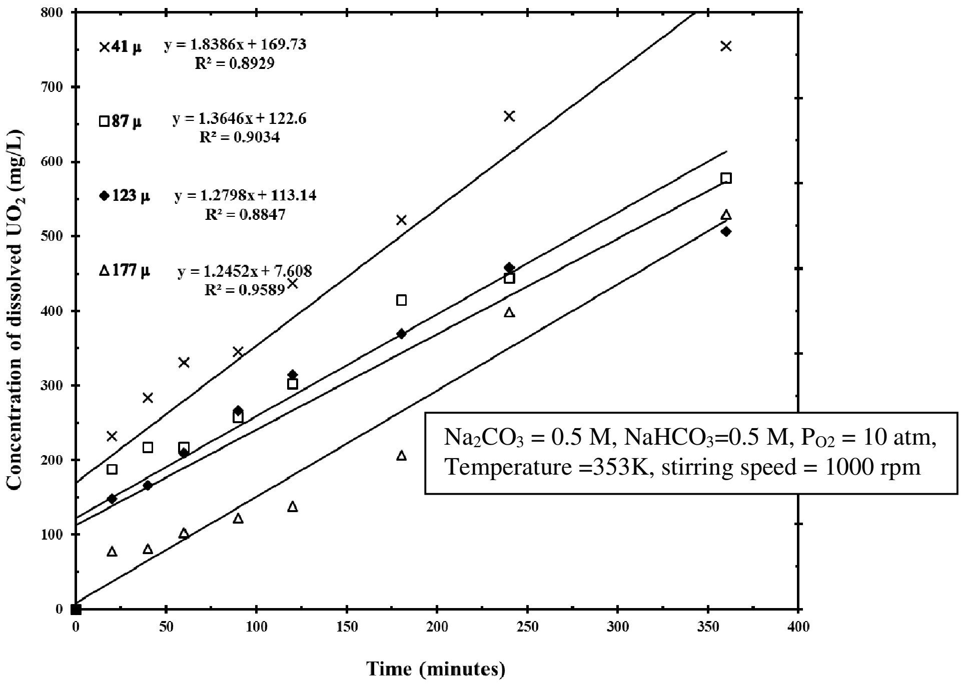

Fig. 5.5. Effect of particle size on dissolution of UO_2

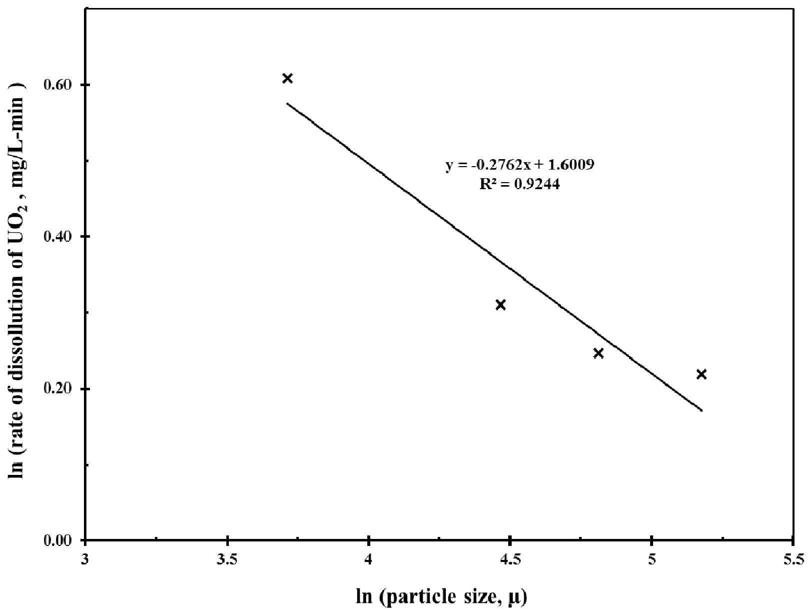

Fig. 5.6. Plot of order for dissolution of UO_2 with respect to particle size

The order of rate of dissolution with respect to particle size is found to be -0.28 from Fig. 5.6. The negative value of the order indicates decreasing trend of rate with increase in particle size, which could be due to lower specific surface area for larger particles.

Effect of temperature on leaching of pure UO_2: The concentration of UO_2 at different temperatures is plotted in Fig. 5.7. Arrhenius plot is constructed from the slopes of the straight lines (rates of dissolution of UO_2) at different temperatures in Fig. 5.8. The activation energy is determined to be 36.8 kJ/mol from the plot.

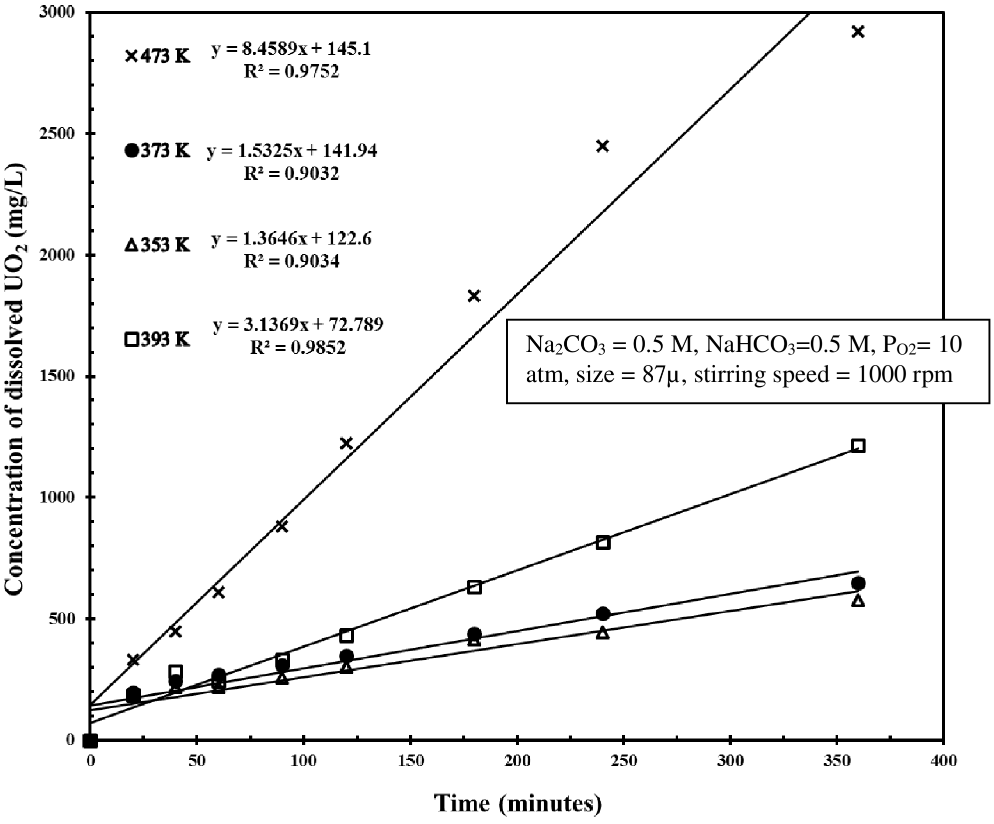

Fig. 5.7. Effect of temperature on dissolution of UO_2

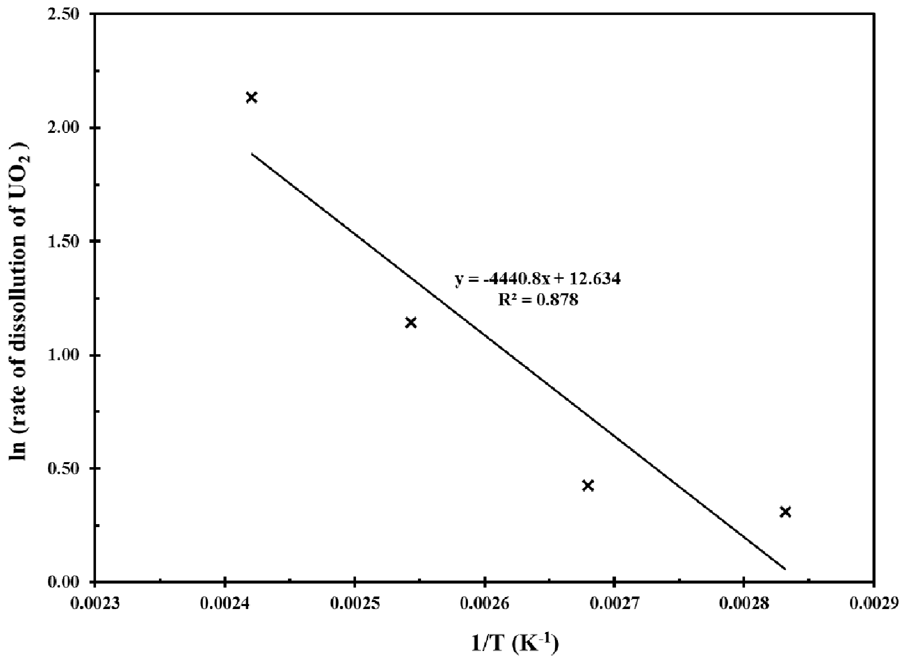

Fig. 5.8 Arrhenius plot of dissolution of UO_2

Determination of apparent rate constant (k_o): As mentioned before, the empirical constant, k_0^{11}, in Eq.5.2 is assumed to be a function of particle size, d and temperature, T, using the order of particle size and Arrhenius activation energy determined in previous Sections. The relation is given by Eq.5.4.

$$k_0^{11} = k_0 d^n \, e^{-\frac{E_a}{RT}} \qquad [5.4]$$

The apparent rate constant, k_0, can be determined by substituting the value of k_0^{11} ($1\text{x}10^{-4}$) found for the base values of particle size, d (= 87 µm) and temperature, T (= 353 K), along with the order with respect to particle size, n (= -0.2762) and the Arrhenius activation energy term, E_a/R (= 4440.8) from Figs. 5.6 and 5.8. The value of k_0 is found to be 99.1. The overall equation developed for dissolution rate of UO_2 (as mg/L-min) in the range of variables studied is given by Eq. 5.5.

$$\frac{dC_{UO_2}}{dt} = \frac{99.1 \times [Na^2CO^3]^{0.24} \times [NaHCO^3]^{0.09} \times {Po_2}^{0.58} \times d^{-0.2762} \times e^{-\frac{4440.8}{T}}}{(3 \text{ x } 10^{-7} \times [Na^2CO^3]^{0.24}) + (1.5\text{x}10^{-4} \times [NaHCO^3]^{0.09}) + (1.9\text{x}10^{-5} \times {Po_2}^{0.58})} \qquad [5.5]$$

__Comparison of calculated and experimental rate of dissolution:__ The calculated values according to Eq. 5.5 and experimental values of rates of dissolution of UO_2 for each set of experiments (experiments that include variation of one parameter) are plotted as parity plot in Fig. 5.9. The predicted rates agree reasonably well with the experimental data.

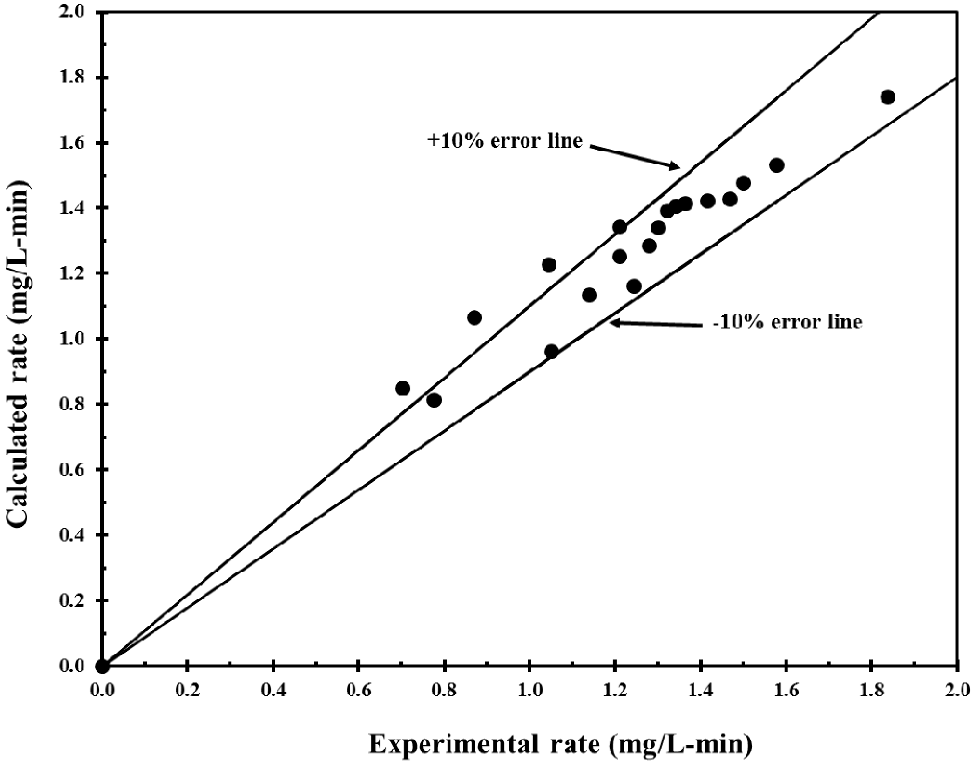

Fig. 5.9 Parity plot comparing calculated and experimental rates

__Comparison of leaching rate of UO_2 reported in literature with that predicted by the model developed in the present study:__ The kinetic models proposed by various workers have already been presented in Section 2.3.1. Among these models, the one published by Schortmann and DeSesa [37] is a milestone work encompassing important variables of alkaline leaching of uranium, and is closer to the present study. Hence, leaching rate of UO_2 is calculated using the model developed in the present study (Eq. 5.5) for the leaching conditions reported by Schortmann and DeSesa [37]. The commonalities and differences in the leaching of UO_2

undertaken in the present study and that reported by Schortmann and DeSesa [37] is given in Table 5.4. The Table also includes predicted and reported leaching rates along with the model equations.

Table 5.4 The commonalities and differences in the leaching of UO_2 undertaken in the present study and that reported by Schortmann and Desesa [37] along with the predicted and reported leaching rates including the model equations

Leaching condition	Present study	Reported by Shortmann and Desesa [37]
Temperature (°C)	80	80
Partial pressure of O_2 (atm)	3.5	3.5
Particle size (µm)	close size range (-100 + 74 µm)	wide size range (all passing 297 µm) with most material in fine sizes, 55% (by wt) passing 45 µm
Na_2CO_3 (M)	0.5	0.5
$NaHCO_3$ (M)	0.5	0.5
Specific surface area of UO_2 (m^2/g)	0.01 (given in Table 3.2), The material used in the present study is obtained from grinding the sintered UO_2 pellets.	Specific surface area and origin of UO_2 sample used are not available.
Initial UO_2 solids concentration (weight of UO_2 in g / volume of leachants in L)	10	1
Rate of leaching of UO_2 (mg/L/min)	0.91	2
Leaching model	$\frac{\mathrm{dC}}{\mathrm{dt}} = \frac{99.1 \times \mathrm{Na_2CO_3}^{0.24} \times \mathrm{NaHCO_3}^{0.09} \times \mathrm{Po_2}^{0.58} \times d^{-0.2762} \times e^{-\frac{4440.8}{T}}}{(3 \text{ x } 10^{-7} \times \mathrm{Na_2CO_3}^{0.24}) + (1.5\text{x}10^{-4} \times \mathrm{NaHCO_3}^{0.09}) + (1.9\text{x}10^{-5} \times \mathrm{Po_2}^{0.58})}$	
		$-\frac{dc}{dt} = \frac{k(\frac{S}{L})(p_{O_2})^{\frac{1}{2}} C_r^{2} e^{-\frac{E_a}{RT}}}{K_2 + C_r^{2}}$
Arrhenius activation energy (kJ/mol)	36.8	56

The lower rate of dissolution of UO_2 observed in the present study could be due to the difference between the origins of pure uranium oxide (UO_2) used in the present study and that used by Schortmann and DeSesa [37]. The synthetic UO_2 used in the present study is obtained by crushing and grinding of a sintered material (as mentioned in Chapter 3). Sintered materials may have low specific surface area leading to lower dissolution rates [138]. The measured specific surface area of UO_2 powder used in the present study is 0.01 m^2/g (Table 3.2). Mahabub et al. [139] also reported that the apparent density of the sintered sample increases with the increase in sintering temperature and consequently porosity decreases which would lower the dissolution rates. Further, the particle size used in the present study is 87 μm (average) and that of material reported in literature [37] has < 45 μm size. The rate of dissolution is lower for higher particle size (used in present study) due to lower specific surface area. The other differences between the reported and present study are: (1) The fitted model in the present study is for range of temperatures from 80°C to 140°C in which Arrhenius energy is found to be 36.8 kJ/mol, which is less than the value (56 kJ/mol) reported by Schortmann and DeSesa [37]. (2) The leaching rate reported is with 1 g/L initial solids concentration and the concentration used in present study is 10 g/L. The predicted rate will be lesser at the solids concentration reported (1 g/L) due to lesser surface area available.

5.2 LEACHING STUDIES ON PURE PYRITE MINERAL

5.2.1 Materials and Methods

Each batch leaching experiment was conducted in a one-liter capacity stainless steel autoclave (mentioned in Section 4.1.1) according to the procedure described in Section 4.1.3., using 7 g of pure pyrite powder and 700 ml of solution of sodium carbonate & bicarbonate. The solids concentration in each experiment was maintained low at arbitrarily chosen value of 1% solids in order to minimize the effect of change in pulp density when liquor samples are withdrawn periodically during experiment. The ranges of leaching parameters studied are given in Table 5.5.

Table 5.5 Range of parameters used for design of leaching experiments with pure pyrite

Parameter	Levels of parameters	Base level*
Concentration of Na_2CO_3, M	0, 0.1, 0.3, 0.5, 0.7, 1	0.5
Concentration of $NaHCO_3$, M	0, 0.1, 0.3, 0.5, 0.7, 1	0.5
Particle size, µm	6, 44, 58, 87, 123, 253	87
Temperature,°C	70, 80, 90, 100, 110, 120	90
Oxygen partial pressure, atm	0.5, 1, 2, 3	0.5
* Constant value while other parameters are varied		

5.2.2 Results and Discussion

It is attempted to fit the experimental data to the popular and well proven shrinking core model [39]. Since experiments in the present study were conducted in an autoclave with continuous agitation, film diffusion does not control the leaching reaction as the film layer on the particles is continuously replaced due to agitation leading to fast diffusion of solutes in the film. The leaching rate is investigated with the shrinking core model controlled by chemical reaction at the unreacted particle surface, which is given by Eq. 5.6.

$$1-(1-X_{py})^{\frac{1}{3}} = \; k\,t \qquad [5.6]$$

where X_{py} is the fractional conversion of pyrite at time t. The overall rate constant, k, is described by the general form according to Eq. 5.7.

$$k = k_0 P_{O_2}^{n}\, d^{p}\, [Na_2CO_3]^{x}\, [NaHCO_3]^{y}\, e^{-\frac{E_a}{RT}} \qquad [5.7]$$

In the present study, the overall rate constant, k, is evaluated in each kinetic experiment according to Eq. 5.6 and the orders of the reaction with respect to each variable parameter, n, p, x, y and Arrhenius activation energy, E_a are calculated using Eq. 5.7.

The fractional conversion of pyrite (X_{py}) with time in each leaching experiment is calculated from the analysis of sulfate in the leach liquor at time t using the following Eq. 5.8.

$$X_{py} = \frac{Amount\ of\ sodium\ sulfate\ formed\ in\ leach\ liquor\ at\ time\ t}{Total\ amount\ of\ sodium\ sulfate\ that\ would\ have\ formed, if\ all\ the\ pyrite\ is\ leached} \qquad [5.8]$$

<u>Effect of concentration of sodium carbonate:</u> Experimental data of pyrite oxidation in carbonate solution was plotted according to topochemical model for the range of concentrations of sodium carbonate from 0 to 1 M as shown in Fig. 5.10. It is observed that the rate constants of pyrite oxidation increases for the range of concentration of sodium carbonate from 0 to 0.7 M and decreases in the range from 0.7 to 1 M. The reaction order with respect to concentration of sodium carbonate, estimated from the slope of ln (k) Vs ln ([Na_2CO_3]) plot, is 0.8 for concentration of Na_2CO_3 from 0 to 0.7 M, and -2.9 for the range 0.7 to 1 M as shown in Fig. 5.11. The negative order at higher concentration (> 0.7 M) of Na_2CO_3 could be due to shrouding of the pyrite mineral surface by excessive carbonate ions that may hinder the diffusion of oxygen gas to the reaction sites. An analogy is available in literature in the case of leaching of gold ores that the rate of reaction decreases when the concentrations of competing reactants increases beyond certain limit [140, 141].

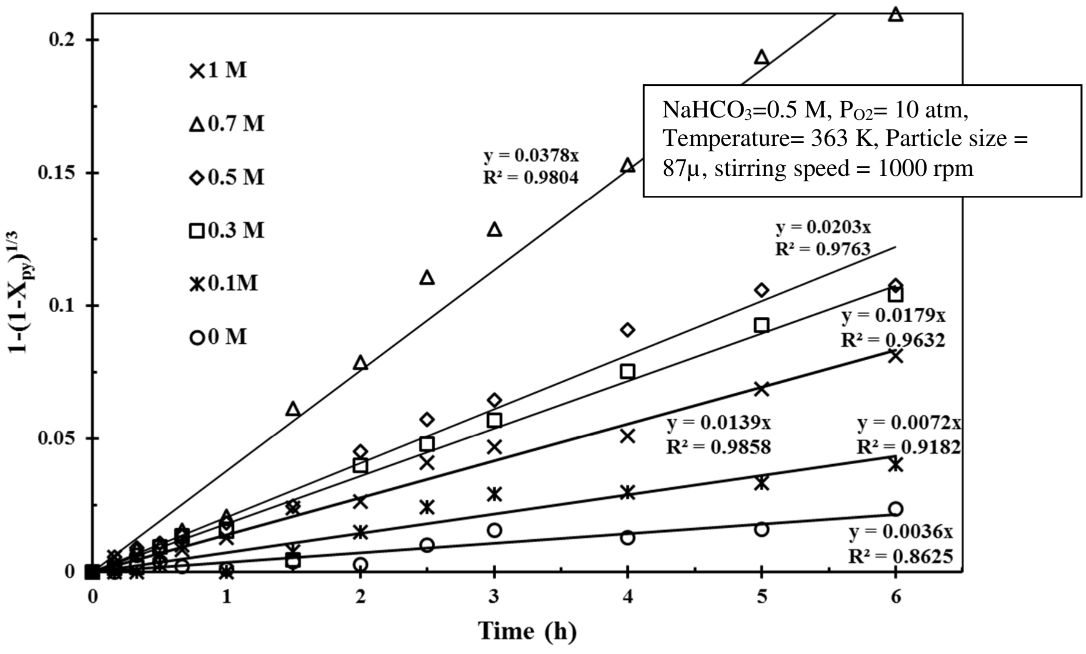

Fig. 5.10 Effect of sodium carbonate concentration on pyrite oxidation, plotted according to topochemical model

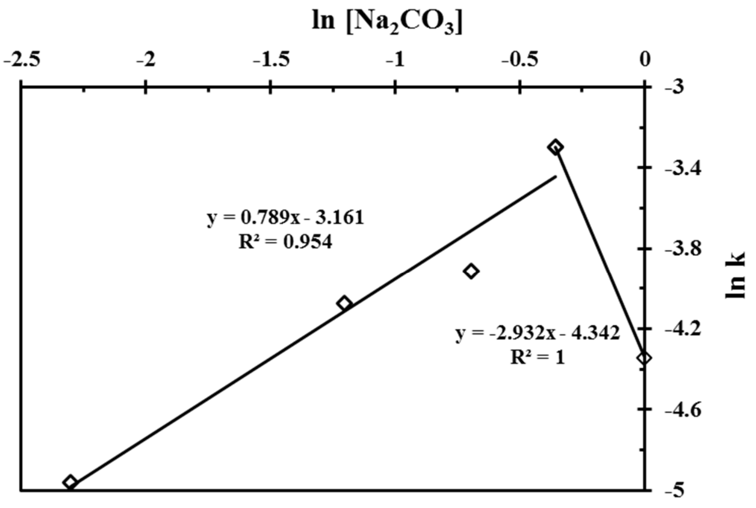

Fig. 5.11 Plot of ln (k) Vs ln ($[Na_2CO_3]$) of pyrite leaching

Effect of concentration of sodium bicarbonate: Plots of conversion of pyrite with time according to topochemical model are shown in Fig. 5.12. The rate constants of pyrite oxidation increases as the concentration of sodium carbonate increased from 0 to 0.7 M and decreases as the concentration is further increased from 0.7 to 1 M. The reaction order with respect to concentration of sodium bicarbonate is estimated from the slope of ln (k) Vs ln ($[NaHCO_3]$) plot as 0.2 for concentration of $NaHCO_3$ from 0 to 0.7 M and -2.1 for the range 0.7 to 1 M as shown in Fig. 5.13. The same reason cited in the case of effect of Na_2CO_3 concentration on leaching of pyrite, is applicable for decrease of leaching rate of pyrite at higher concentration (> 0.7 M) of $NaHCO_3$.

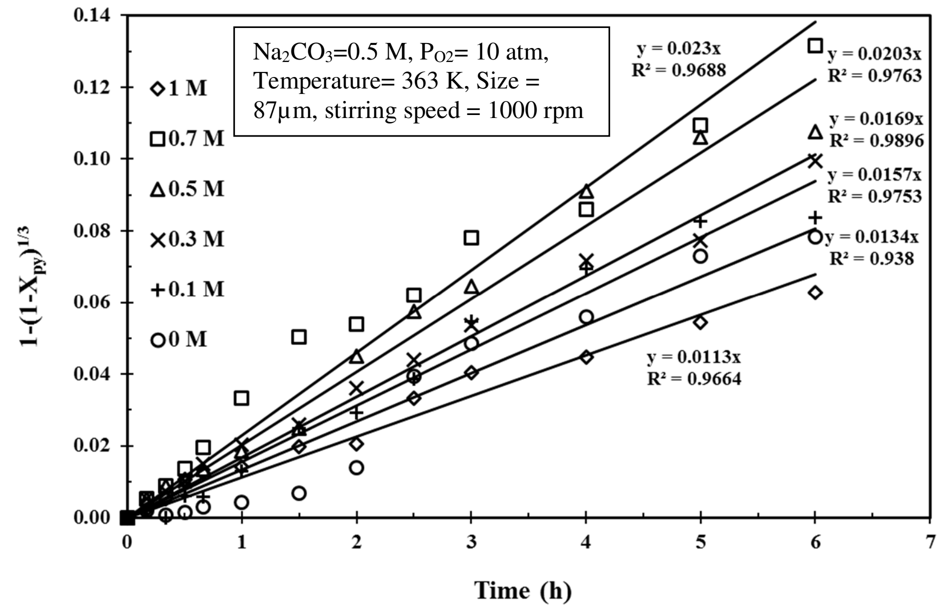

Fig. 5.12 Effect of sodium bicarbonate concentration on pyrite oxidation, plotted according to topochemical model

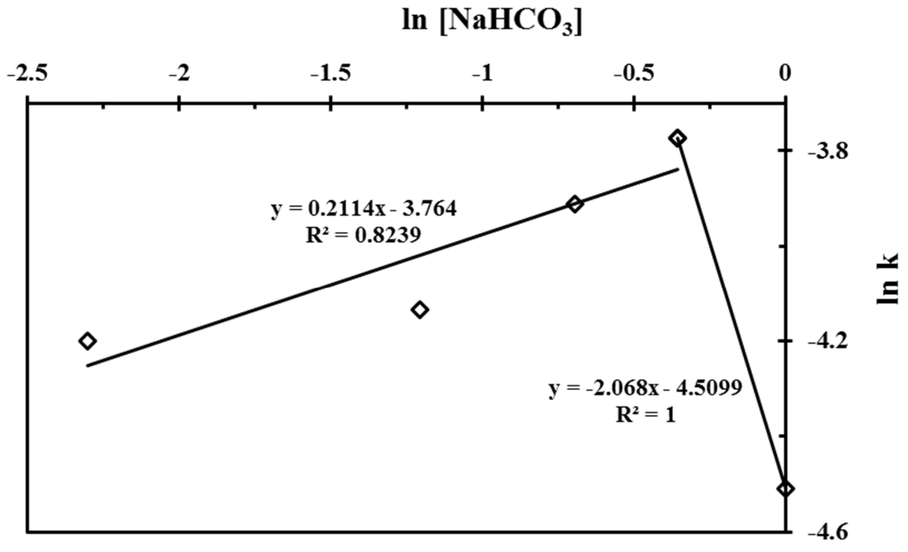

Fig. 5.13 Plot of ln (k) Vs ln ([NaHCO$_3$]) of pyrite leaching

Effect of particle size: Experimental data of pyrite oxidation in carbonate solution is plotted according to topochemical model for the range of average particle sizes from 6 to 253 μm as shown in Fig. 5.14. It shows that the rate constant of leaching of pyrite increases with the decrease in particle size. A straight line is obtained from the plot ln (k) Vs ln (d) as shown in Fig. 5.15 which indicates that the order with respect to particle size is -0.225.

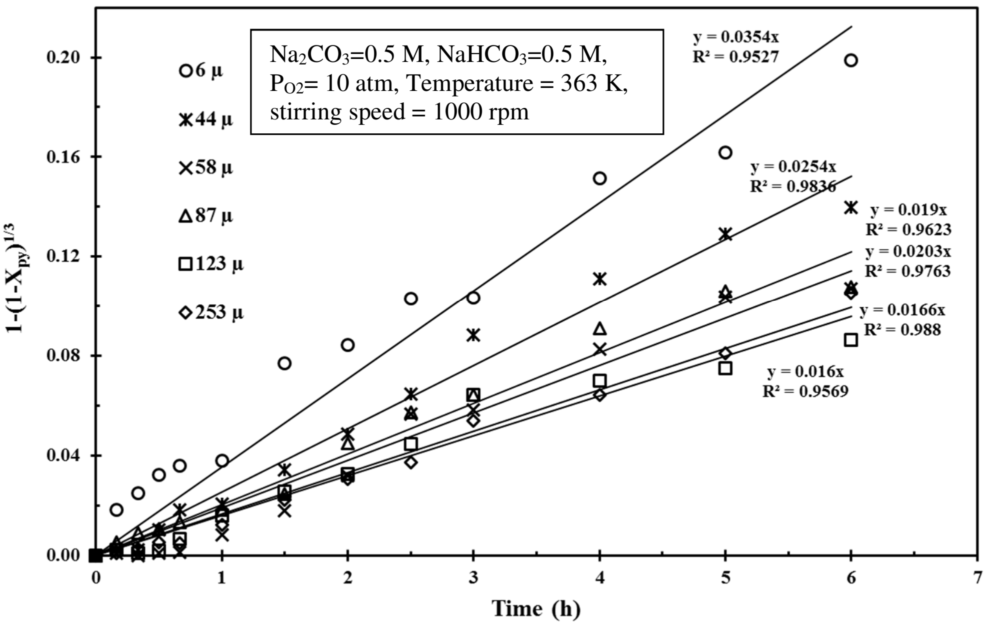

Fig. 5.14 Effect of particle size on pyrite oxidation, plotted according to topochemical model

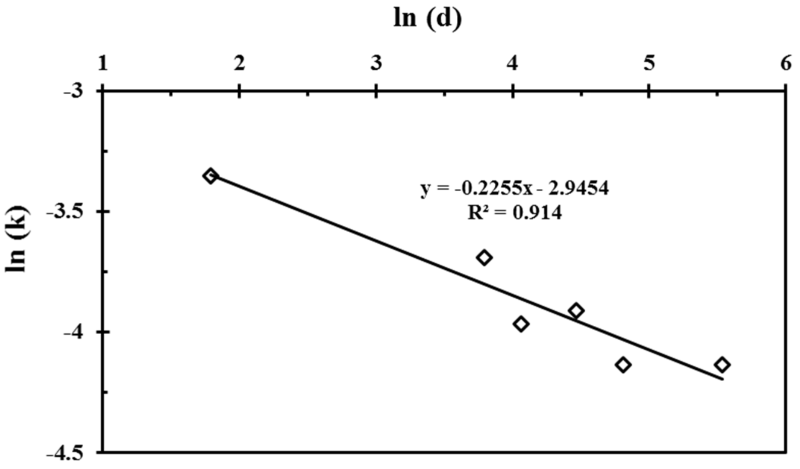

Fig. 5.15 Plot of ln (k) Vs ln (d) of pyrite leaching

<u>Effect of Temperature:</u> Experimental data of pyrite oxidation in carbonate solution is plotted according to topochemical model for the range of temperatures from 353 to 393 K, as shown in Fig. 5.16. It is observed that the rate constants of pyrite oxidation increases with the increase in temperature. A plot of ln (k) Vs 1/T results in a straight line as shown in Fig. 5.17. The activation energy calculated from slope of the line is 58 kJ/mol. Activation energy higher than 20.9 kJ/mol indicates that the leaching process predominantly follows chemical reaction control [142], which is in agreement with the initial assumption of chemical reaction controlled modeling in the present study for leaching of pyrite.

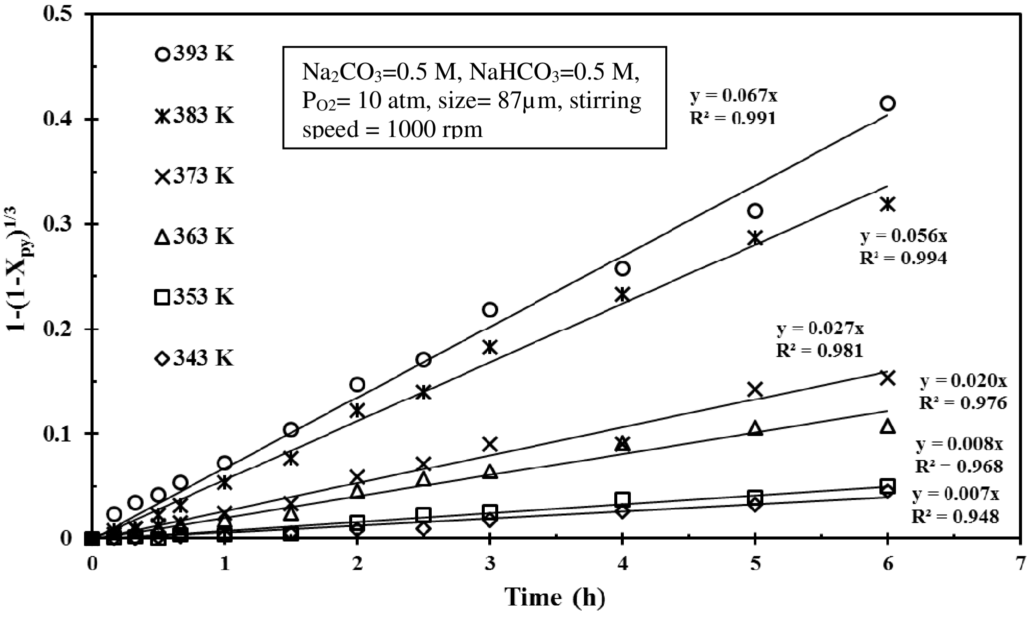

Fig. 5.16 Effect of temperature on pyrite oxidation in sodium carbonate solution, plotted according to topochemical model

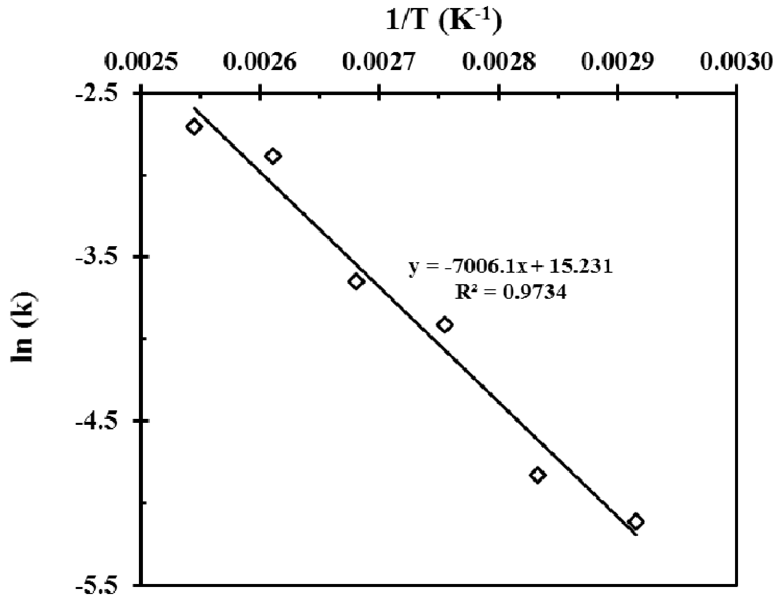

Fig. 5.17 Arrhenius plot of ln (k) Vs 1/T of pyrite leaching

<u>Effect of oxygen partial pressure:</u> Experimental data of pyrite oxidation in carbonate solution is plotted in Fig. 5.18 according to topochemical model for the range of pressures from 0.5 to 3 atm. It is observed that the rate constants of pyrite oxidation increases with the increase of oxygen partial pressure. The reaction order with respect to oxygen was estimated from the slope of a ln (k) Vs ln (P_{O2}) plot as shown in Fig. 5.19 is 0.2, indicating the leaching rate is proportional to 0.2 power of oxygen partial pressure. The fractional order suggests the leaching is chemical reaction controlled [92], which is in good agreement with the initial assumption of chemical reaction controlled model in the present study for pyrite leaching.

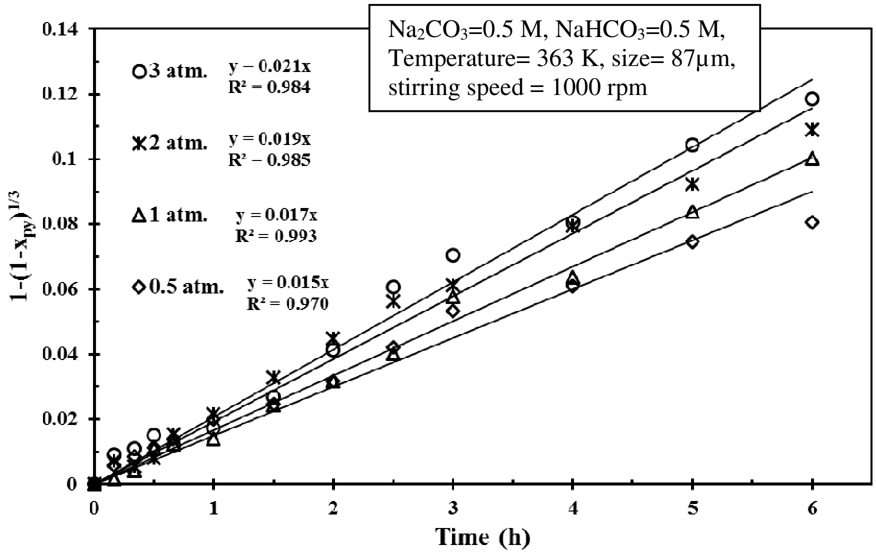

Fig. 5.18 Effect of oxygen partial pressure on pyrite oxidation in sodium carbonate solution, plotted according to topochemical model

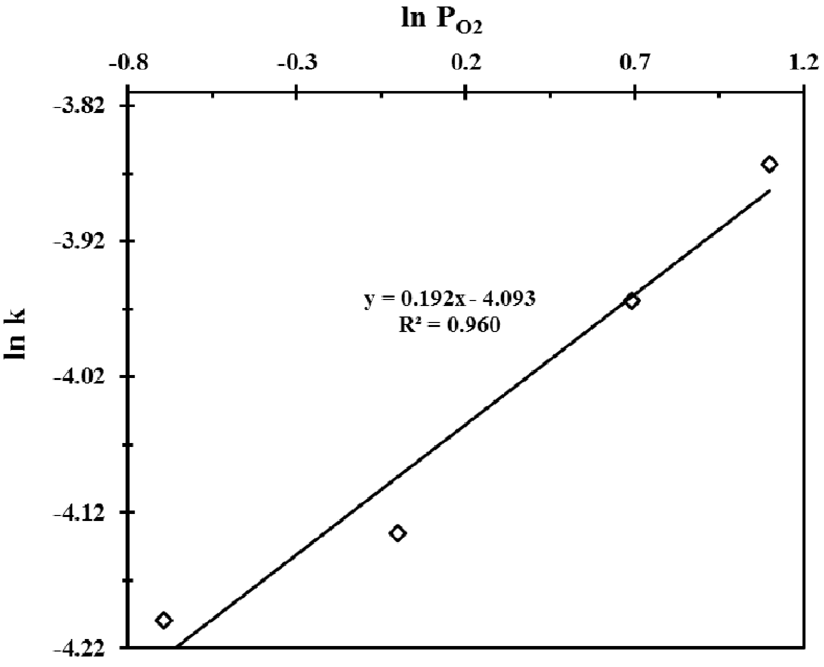

Fig. 5.19 Plot of ln (k) Vs ln (P_{O2}) of pyrite leaching

Determination of apparent rate constant (k_o): In order to find k_0, a linear fit is established between the $1\text{-}(1\text{-}X)^{1/3}$, and the product term, $p_{O_2}{}^{0.2}$ $[CO_3]^{0.8}$ $[HCO_3]^{0.2}$ $d^{-0.2}$ exp(-7006/T) t, for the range of concentrations of sodium carbonate and bicarbonate from 0 to 0.7 M at different values of variable parameters. The product term is changed to $p_{O_2}{}^{0.2}$ $[CO_3]^{-2.9}$ $[HCO_3]^{-2.1}$ $d^{-0.2}$ exp(-7006/T) t for range of concentrations of sodium carbonate and bicarbonate 0.7 to 1 M. The straight line relationships between $1-(1-X)^{1/3}$ and product terms are shown in Figs. 5.20 and 5.21. The slope of the line, k_0 is found to be 3 x 10^7 for range of concentrations of sodium carbonate and bicarbonate 0 to 0.7 M, and 2 x 10^6 for range of concentrations of sodium carbonate and bicarbonate 0.7 to 1 M.

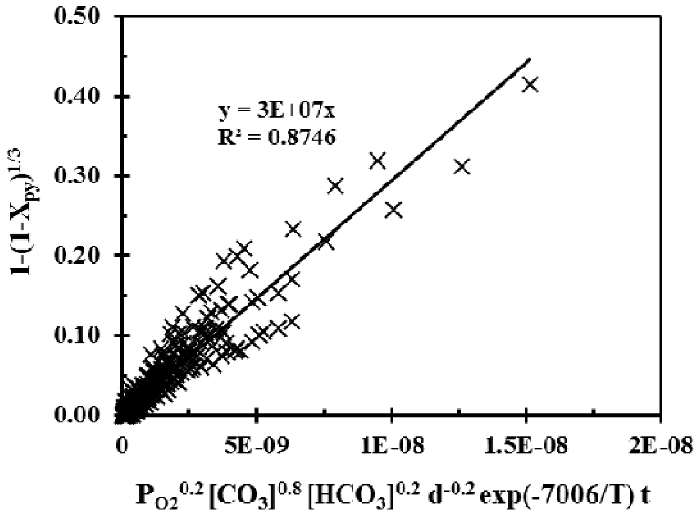

Fig. 5.20 Linear fit of $1-(1-X)^{1/3}$ against the product $Po_2{}^{0.2}$ $[CO_3]^{0.8}$ $[HCO_3]^{0.2}$ $d^{-0.2}$ exp(-7006/T) t for the range of concentration of carbonate and bicarbonate 0 to 0.7 M in pyrite leaching

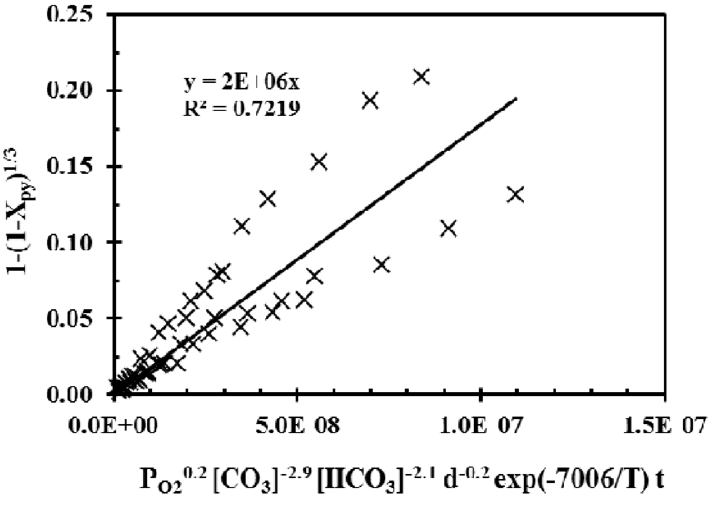

Fig. 5.21 Linear fit of $1-(1-X)^{1/3}$ against the product $Po_2{}^{0.2}$ $[CO_3]^{-2.9}$ $[HCO_3]^{-2.1}$ $d^{-0.2}$ exp(-7006/T) t for the range of concentration of carbonate and bicarbonate 0.7 to 1 M in pyrite leaching

__The overall kinetic model for leaching of pyrite:__ The rate equations for leaching of pure pyrite in alkaline sodium carbonate and bicarbonate solutions, at temperatures between 70°C and 120°C, oxygen partial pressure from 0.15 to 3 atm, average particle sizes from 6 to 253 μm in a time period of 0 to 6 h are found as Eqs. 5.9 and 5.10:

$$\mathbf{1-(1-X_{py})^{\frac{1}{3}} = 3\;x\;10^{7} x\; p_{O_2}^{0.2} d^{-0.2} e^{-\frac{7006}{T}}\,[CO_3]^{0.8}[HCO_3]^{0.2}\;t}$$

For 0 to 0.7 M concentration of Na_2CO_3 and $NaHCO_3$ [5.9]

$$\mathbf{1-(1-X_{py})^{\frac{1}{3}} = 2\;x\;10^{6} x\; p_{O_2}^{0.2} d^{-0.2} e^{-\frac{7006}{T}}\,[CO_3]^{-2.9}[HCO_3]^{-2.1}\;t}$$

For 0.7 to 1 M concentration of Na_2CO_3 and $NaHCO_3$ [5.10]

The hypothesis of chemical control is supported by the high magnitude of the activation energy (58 kJ/mol) and the fractional reaction orders with respect to oxygen partial pressure, sodium carbonate concentration, sodium bicarbonate concentration, particle size. The maximum possible conversion of pyrite by agitation leaching was about 80% at partial pressure of oxygen = 2.15 atm, average particle size = 87 μm, stirring speed = 1000 rpm, temperature = 393 K.

__Comparison with previous work reported in literature:__ The differences in the experimental conditions used in this study and the previously reported studies [92, 143] on pyrite oxidation make it difficult for extensive and direct comparisons. According to Ciminelli and Osseo-Asare [92], the oxidation of pyrite in 0.1 M Na_2CO_3 solutions, at a temperature range from 50 to 85°C and oxygen partial pressure from 0 to 1 atm is controlled by chemical reaction, with activation energy 60.9 kJ/mol. In the present work, the magnitude of the activation energy is found to be 58.25 kJ/mol. Ciminelli and Osseo-Asare [92] have indicated a reaction order of 0.1 with respect to hydroxyl ion concentration, fractional reaction order with respect to oxygen partial pressure. Fractional reaction orders with respect to concentrations of sodium carbonate, bicarbonate, and particle size and oxygen partial pressure are obtained in the present study also. These results are also in good agreement with a mechanism controlled by chemical reaction as cited in the literature by various authors, though the conditions of leaching are slightly different [92, 93, 143]. It is also indicated in the above mentioned literature that the rate of pyrite oxidation increases with the increase of pH, reagent concentration, and temperature, as found in the present study.

5.3 LEACHING STUDIES ON SYNTHETIC MIXTURE

Synthetic mixture of pure materials was used as feed in leaching experiments to generate kinetic data under ideal conditions. The composition of this feed material is chosen close and intermediate to the compositions of the two alkaline rock hosted Indian uranium ores, Tummalapalle and Gogi (composition of these two ores is reported in Tables 3.9 and 3.11). The synthetic mixture studied consisted of UO_2 as uranium bearing phase (to represent uraninite mineral in ores) and pyrite as the reactive gangue mineral that generally occur in uranium ores. Since calcite and dolomite have very similar chemical nature, only calcite is used along with pure UO_2, pyrite and silica for preparing synthetic mixture. The composition of this mixture used as feed in leaching experiments is given in Table 5.6.

Table 5.6 Composition of synthetic mixture of minerals used for leaching studies

Constituent	% wt
Pure UO_2	0.2
Pyrite (FeS_2)	5
Calcite ($CaCO_3$)	85
Silica (SiO_2)	9.8
Total	100

In all, four sets of experiments were carried out. (1) Sequential leaching experiments were carried out to develop a kinetic model. (2) Experiments were conducted to understand the critical influence of pyrite content in the feed solids. (3) Experiments were conducted to evaluate the effects of temperature and pressure and their interactional effect of leachability of UO_2 and pyrite. (4) Experiments were aimed to study the role of O_2 in leaching of uranium. Each leaching experiment was carried out using 35 g of accurately weighed synthetic mixture and 700 ml of alkaline lixiviant of predetermined concentration at a stirrer speed of 1000 rpm, unless stated otherwise.

5.3.1. Sequential experiments

The effects of concentration of Na_2CO_3 ($[Na_2CO_3]$), concentration of $NaHCO_3$ ($[NaHCO_3]$), particle size (d), temperature (T) and partial pressure of oxygen (P_{O2}) were studied in the range in which the leaching of both UO_2 and pyrite are most sensitive. The base levels and range were chosen based on a few screening experiments and the literature available on leaching of UO_2 and pyrite in carbonate medium. The plan of experiments conducted is given in Table 5.7.

Table 5.7 Scheme of experiments followed for alkaline leaching of synthetic mixture of pure materials

Parameter	Levels of parameters	Base level*
Concentration of Na_2CO_3, M	0, 0.1, 0.3, 0.5, 0.7, 1	0.5
Concentration of $NaHCO_3$, M	0, 0.1, 0.3, 0.5, 0.7, 1	0.5
Particle size, μm	6, 44, 58, 87, 123, 253	87
Temperature, K	373, 383, 393, 413, 428	413
Oxygen partial pressure, atm	8, 9, 10	10
* Constant value while other parameters are varied		

The fractional conversions of pyrite, (X_{py}), and UO_2, X_{UO2}, with time in each leaching experiment are calculated from the analysis of sulfate and U_3O_8 in the leach liquor at time t using the Eqs. 5.8 and 5.11, respectively.

$$X_{UO_2} = \frac{\text{Amount of } U_3O_8 \text{ formed in leach liquor at time t}}{\text{Total amount of } U_3O_8 \text{ in the feed}} \qquad [5.11]$$

Shrinking core model [39] is considered to fit the experimental data for leaching reactions of both uranium oxide and pyrite. Since experiments in the present study were conducted in an autoclave with continuous agitation, film diffusion does not control the leaching reaction as the film layer on the particles is continuously replaced due to agitation which leads to fast diffusion of solutes in the film.

The reaction products (reactions (2.4) and (2.5) in Section 2.1.3.1)) of uranium leaching are soluble in lixiviant without leaving any ash product. Hence, ash diffusion controlled mechanism is ignored, and thereby only the chemical reaction controlled model is attempted for the entire leaching period of 0 to 6 h.

In the case of leaching of pyrite, the change in rate of leaching of pyrite after 2 h is found to be small and the results of pure pyrite leaching, presented in Section 5.2.2, have shown that chemical reaction controlled shrinking core model is applicable. Hence, shrinking core model for reaction controlled mechanism is applied for the kinetic data on leaching of pyrite from synthetic mixture also for the leaching period of 0 to 2 h.

The governing equation of shrinking core model for chemical reaction controlled mechanism, already presented in Eqs. 5.6 and 5.7 for leaching of pure pyrite, is adopted again. The overall rate constant, k, is evaluated in each kinetic experiment according to Eq. 5.6 and the orders of the reaction with respect to each variable parameter, n, p, x, y and Arrhenius activation energy, E_a are calculated using Eq. 5.7 for leaching of both UO_2 and pyrite from the synthetic mixture.

<u>5.3.1.1 Kinetic model for leaching of uranium from synthetic mixture:</u> The plots to fit experimental data generated on alkaline leaching of uranium from synthetic mixture, to the chemical reaction controlled topochemical model, are given in Figs. 5.22 through 5.32 in the following Sections. Du Preez et al. [58] had also found pure UO_2 leaching by carbonate medium to follow chemical reaction controlled shrinking core model.

Effect of carbonate concentration:

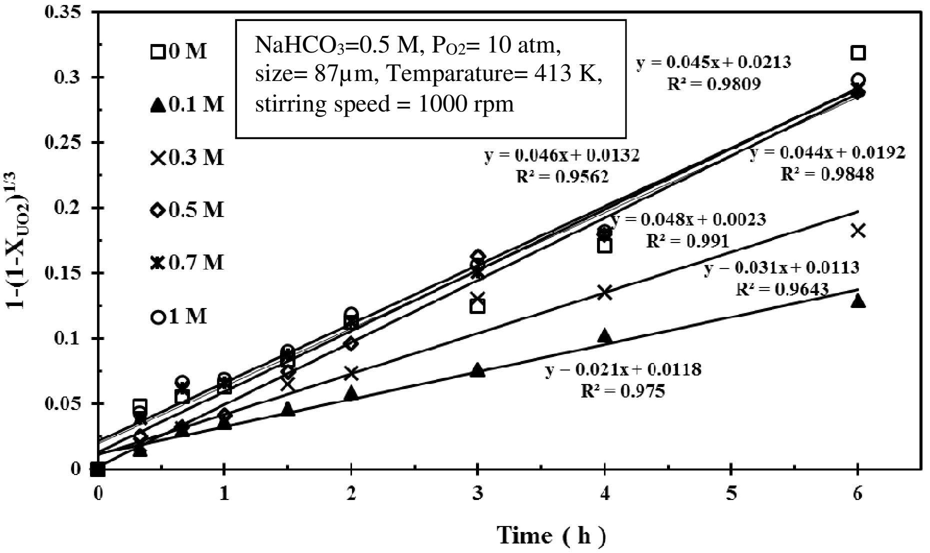

Fig. 5.22. Effect of sodium carbonate concentration on uranium leaching, plotted according to topochemical model

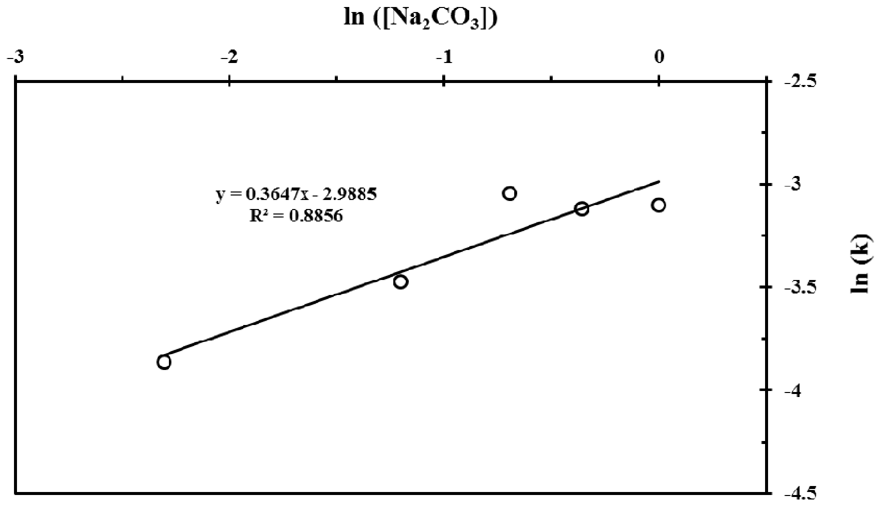

Fig. 5.23 Plot of ln (k) Vs ln[Na$_2$CO$_3$] of uranium leaching from synthetic mixture

The order with respect to the Na_2CO_3 concentration is found to be 0.4, indicating that the conversion of uranium increases, with increasing concentration of Na_2CO_3, as observed by other workers [37, 108].

<u>Effect of bicarbonate concentration:</u>

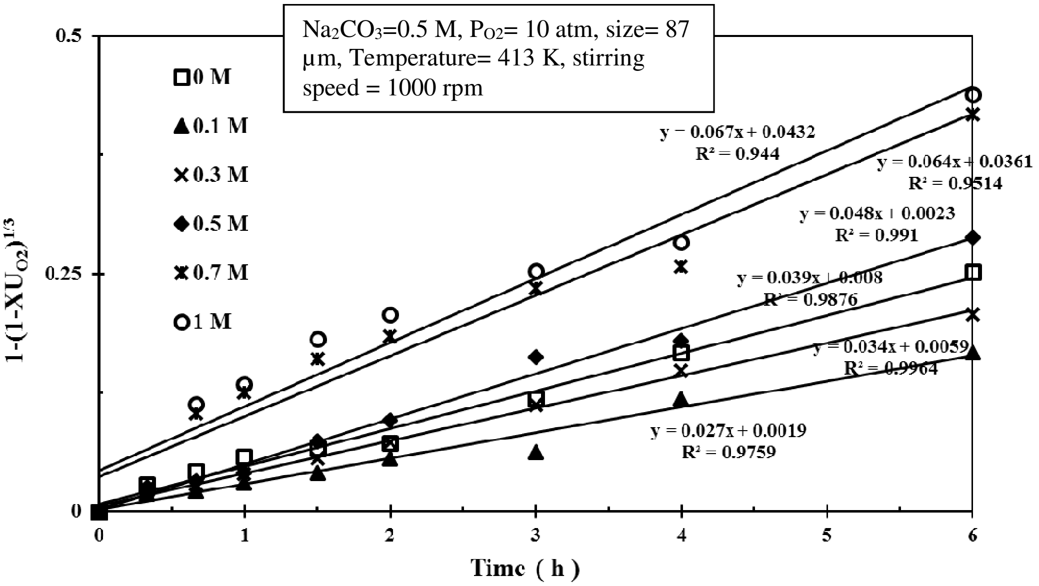

Fig. 5.24 Effect of sodium bicarbonate concentration on uranium leaching, plotted according to topochemical model

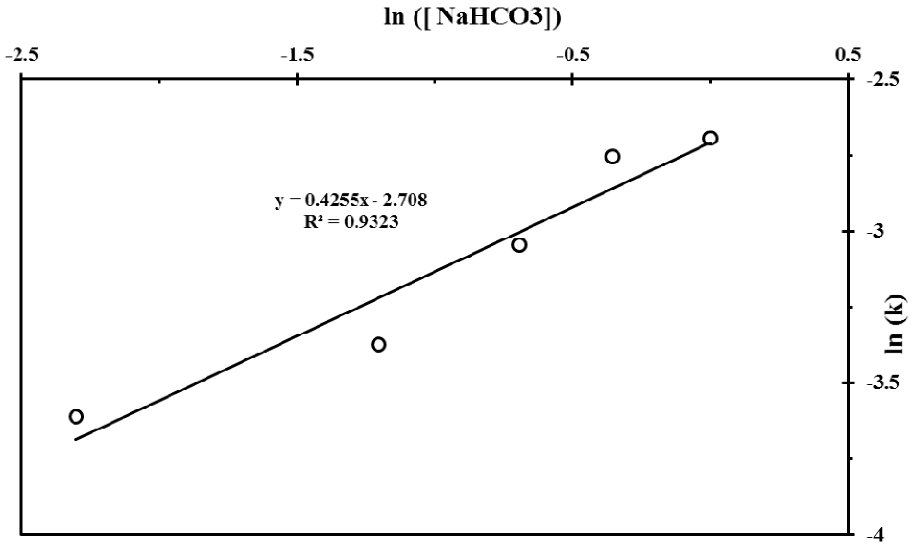

Fig. 5.25 Plot of ln (k) Vs ln[$NaHCO_3$] of uranium leaching from synthetic mixture

Effect of temperature:

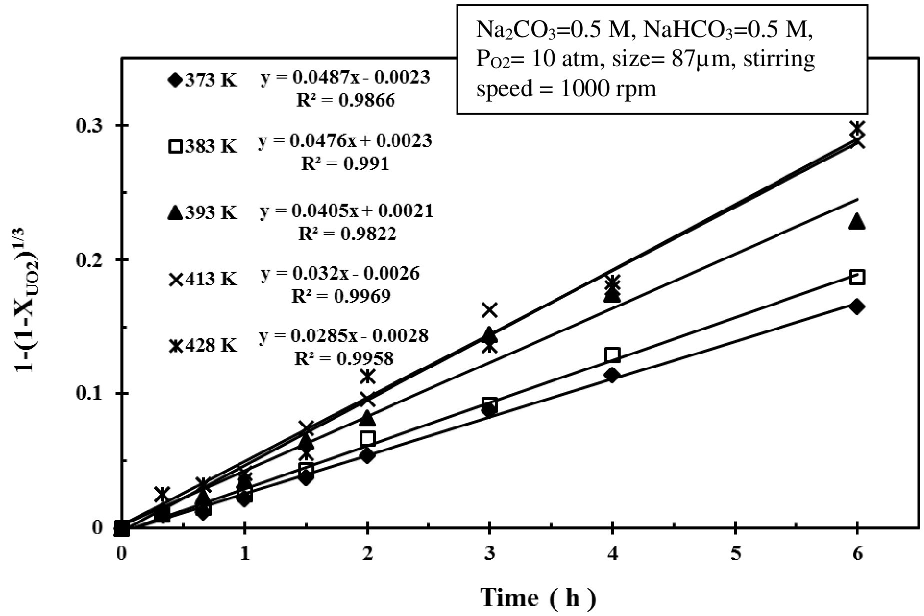

Fig. 5.26 Chemical reaction controlled model plot of dissolution of uranium at different temperatures

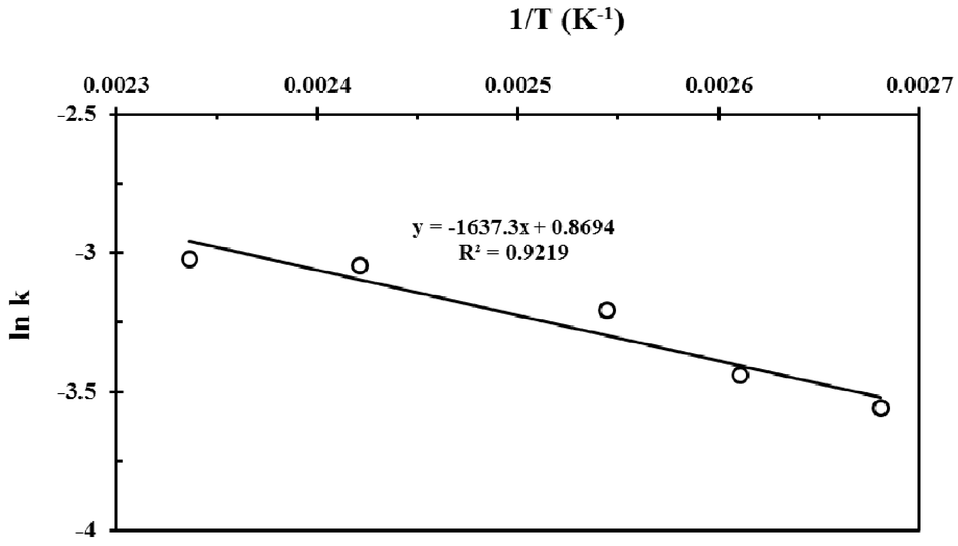

Fig. 5.27 Arrhenius plot of leaching of pure UO_2 from synthetic mixture

The Arrhenius activation energy of dissolution of UO_2 at 10 atm oxygen pressure is determined to be 13.4 kJ/mol from the slope of the straight line fitted in Fig. 5.27 whereas the

Arrhenius energy found by several other authors for dissolution of uraninite ranged from 29.2 to 54.34 kJ/mol [37, 38, 58, 91B]. The difference in Arrhenius activation energies found by different authors could be due to the difference in the origin and nature of pure uranium oxide (UO_2) used by different workers. The synthetic UO_2 used in the present study is obtained by crushing and grinding of a sintered material (as mentioned in Chapter 3).

__Effect of particle size:__

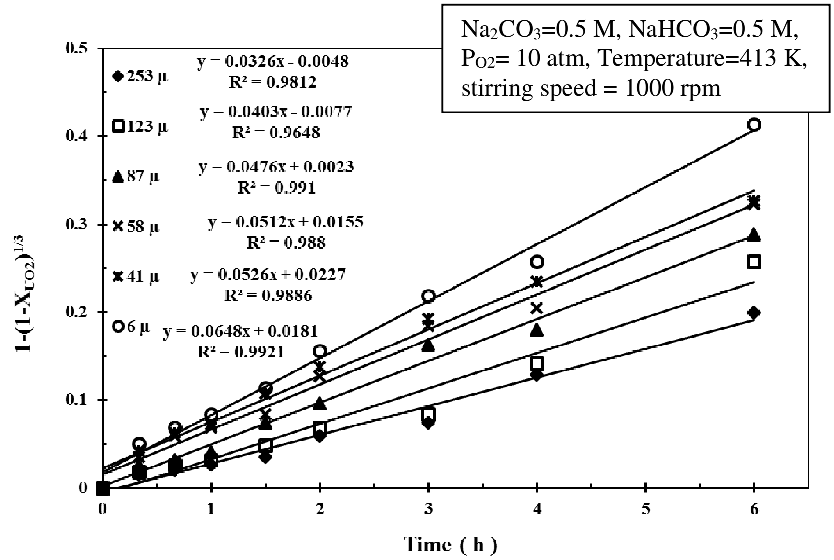

Fig. 5.28 Effect of particle size on uranium leaching, plotted according to topochemical model

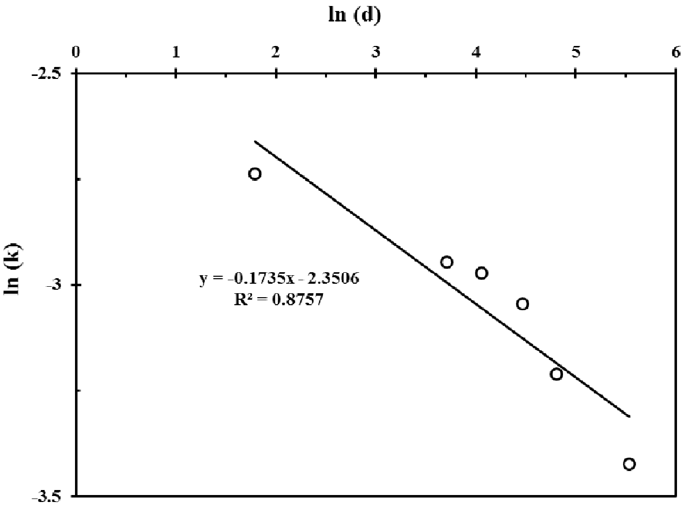

Fig. 5.29 Plot of ln (k) Vs ln (d) for uranium leaching from synthetic mixture

Effect of partial pressure of oxygen:

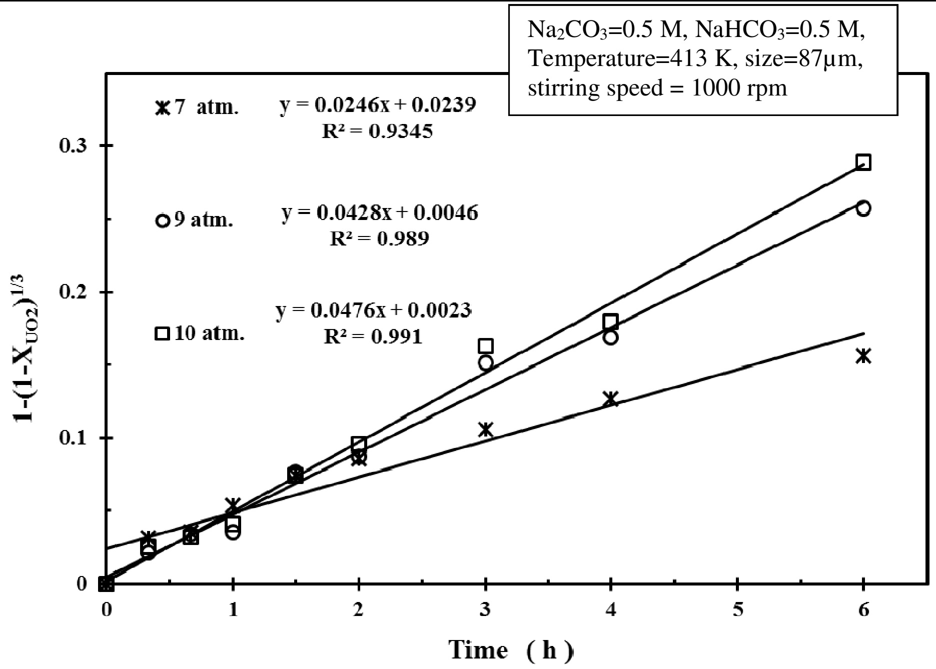

Fig. 5.30 Effect of P_{O2} on uranium leaching, plotted according to topochemical model

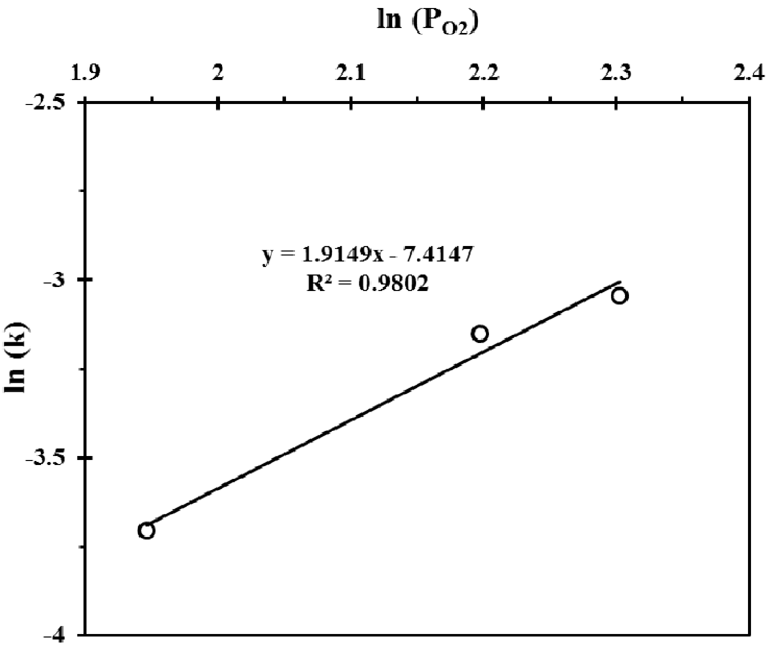

Fig. 5.31 Plot of ln (k) Vs ln [P_{O2}] for uranium leaching from synthetic mixture

The order of the leaching of uranium with respect to partial pressure of oxygen is observed to be 1.9, from the slope of the straight line obtained in Fig. 5.31, for agitation leaching conducted in the present study. De Pablo et al. [34] observed this value to be 1 using a thin layer flow-through reactor.

<u>Determination of apparent rate constant (k_o):</u> A linear fit is established between the 1-(1-X_{UO2})$^{1/3}$, and the product term $p_{O_2}{}^{1.9149}\,[Na_2CO_3]^{0.3647}\,[NaHCO_3]^{0.4255}\,d^{-0.1735}\,e^{-\frac{1637.3}{T}}$ t corresponding to all the experiments for the time duration from 0 to 6 h to determine the apparent rate constant, k_0, for uranium dissolution from synthetic mixture, using carbonate medium. The corresponding plot is shown in Fig. 5.32. The slope of the line, k_0, is found to be 0.1147. Thus, the overall rate equation for leaching of uranium is given by Eq. 5.12.

$$1-\left(1-X_{UO_2}\right)^{\frac{1}{3}} = 0.1147\,p_{O_2}{}^{1.9149}\,[Na_2CO_3]^{0.3647}\,[NaHCO_3]^{0.4255}\,d^{-0.1735}\,e^{-\frac{1637}{T}}\,t \qquad [5.12]$$

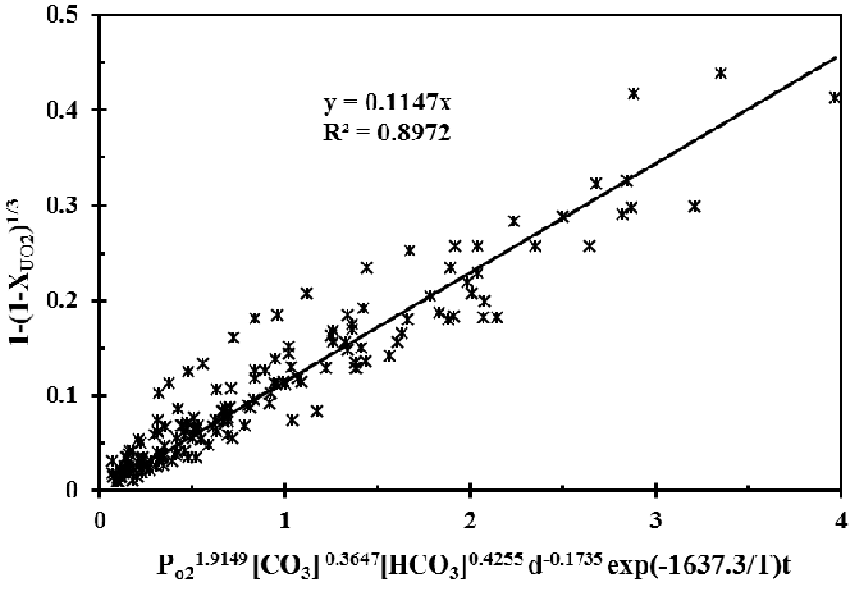

Fig. 5.32 Overall rate constant for the leaching of uranium from synthetic mixture

5.3.1.2 Kinetic model for leaching of pyrite from synthetic mixture: The plots to fit experimental data, generated on alkaline leaching of pyrite from synthetic mixture, to the chemical reaction controlled topochemical model for various leaching parameters are given in Figs. 5.33 through 5.42 in the following Sections.

Effect of concentration of sodium carbonate: The reaction order with respect to [Na_2CO_3] is estimated to be -0.314 from the slope of ln (k) Vs ln ([Na_2CO_3]) plot shown in Fig. 5.34. This could be due to higher temperature and pressure (base levels of temperature = 413 K and P_{O2} = 10 atm) at which the experiments on synthetic mixture were conducted. The decomposition of $NaHCO_3$ (reaction (2.9), Section 2.1.3.1) is high leading to higher concentration of Na_2CO_3, which could hinder the diffusion of oxygen gas by shrouding the reaction sites on the pyrite mineral as explained in Section 5.2.2. The negative order is also obtained in the case of leaching experiments conducted on pure pyrite at higher concentration (> 0.7 M) of Na_2CO_3 (Eq. 5.10; for the low temperature = 363 K and P_{O2} = 0.5 atm, the base levels). Thus, negative order of pyrite reaction in the case of synthetic mixture is in agreement with the negative order obtained for the case of pure pyrite rate equation Eq. 5.10.

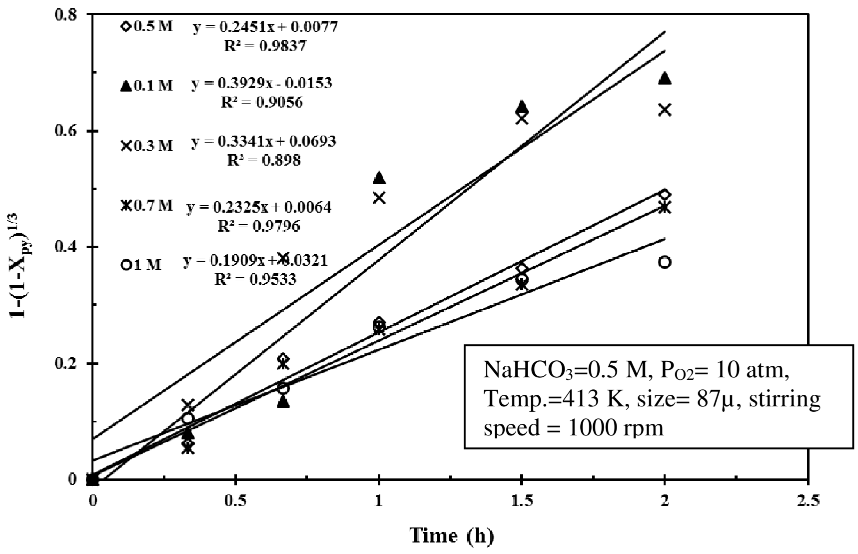

Fig. 5.33 Chemical reaction controlled model plot for dissolution of pyrite for variation of Na_2CO_3 concentration

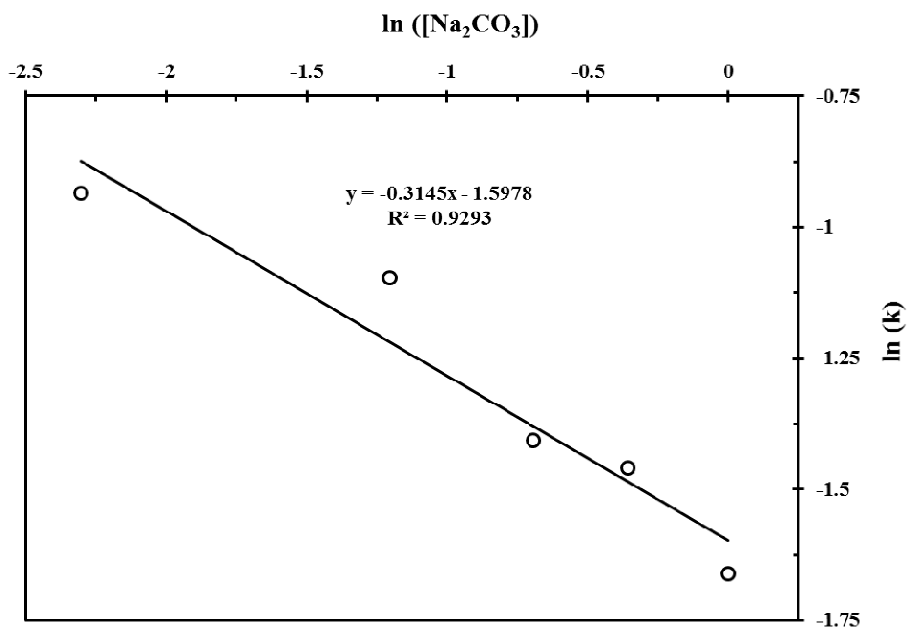

Fig. 5.34 Plot of order of dissolution of pyrite with respect to Na_2CO_3 concentration

Effect of concentration of sodium bicarbonate:

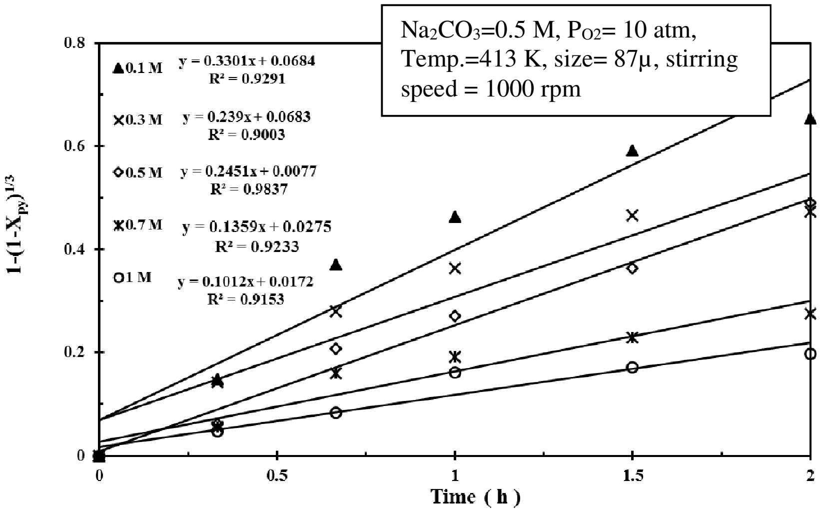

Fig. 5.35 Chemical reaction controlled model plot of dissolution of pyrite for variation of $NaHCO_3$ concentration

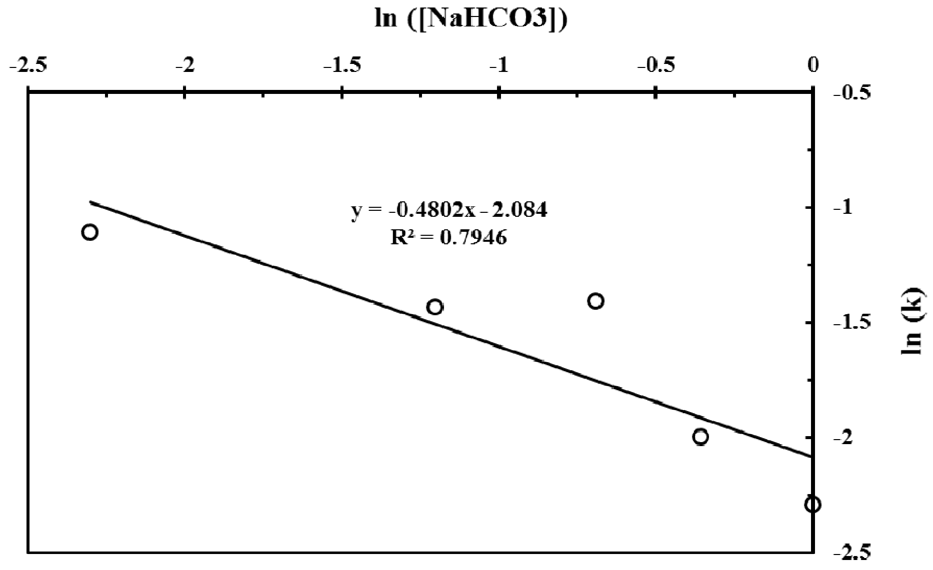

Fig. 5.36 Order of leaching of pyrite with respect to NaHCO₃ concentration

Effect of particle size:

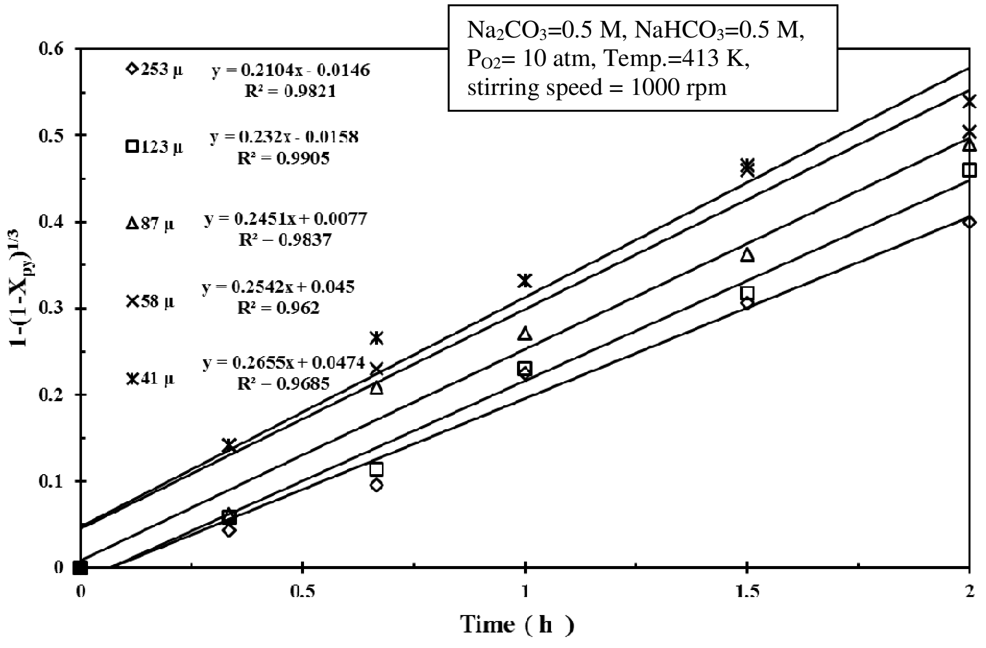

Fig. 5.37 Chemical reaction controlled model plot of leaching of pyrite for different particle sizes

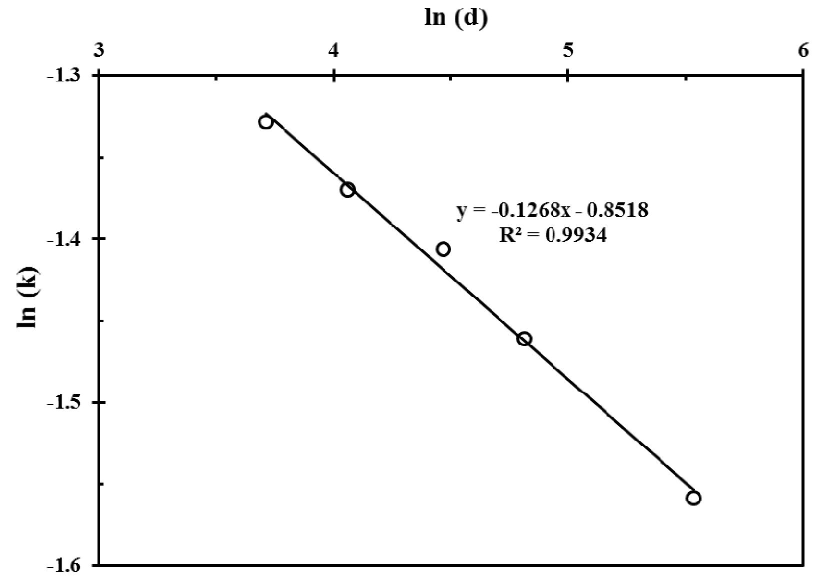

Fig. 5.38 Plot of order for dissolution of pyrite with respect to particle size

Effect of temperature:

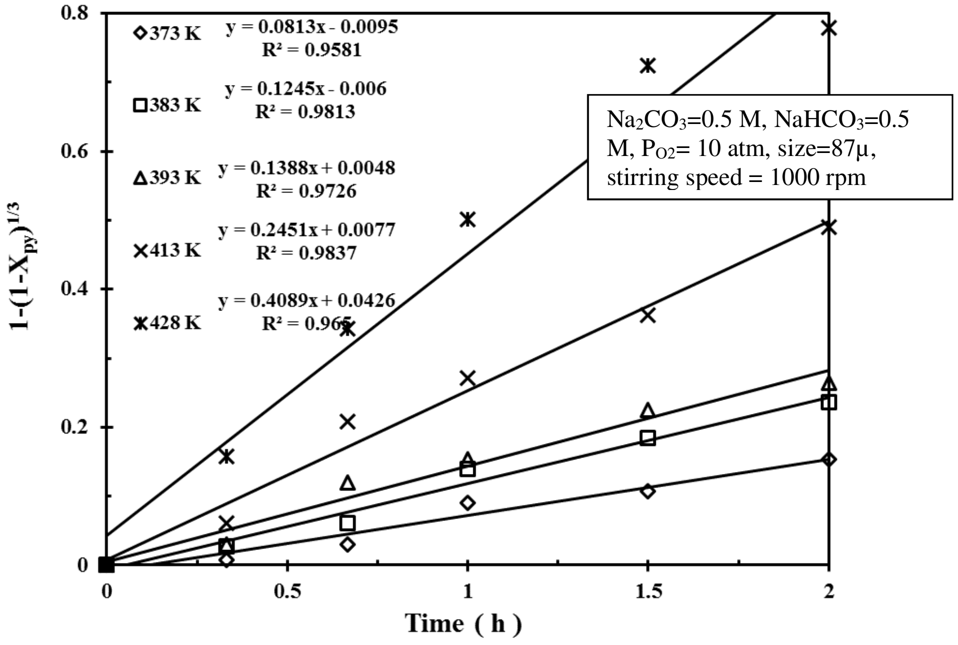

Na_2CO_3=0.5 M, $NaHCO_3$=0.5 M, P_{O2}= 10 atm, size=87μ, stirring speed = 1000 rpm

Fig. 5.39 Chemical reaction controlled model plot of dissolution of pyrite at different temperatures

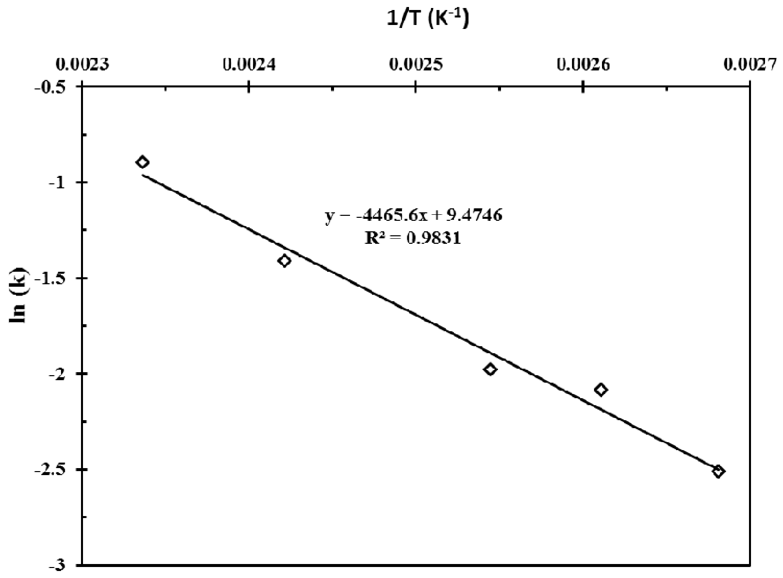

Fig. 5.40 Arrhenius plot of dissolution of pyrite from synthetic mixture

Effect of partial pressure of oxygen:

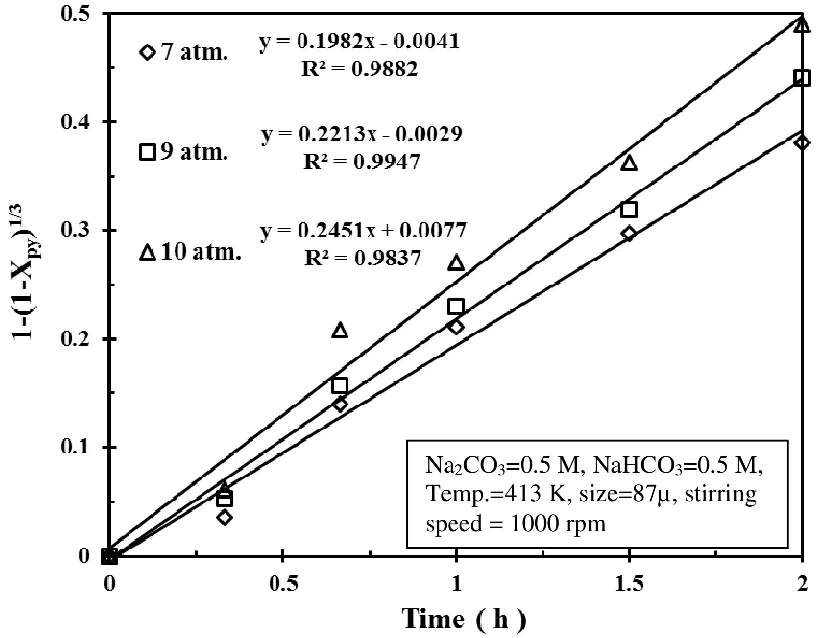

Fig. 5.41 Chemical reaction controlled model plot of dissolution of pyrite at different partial pressures of oxygen

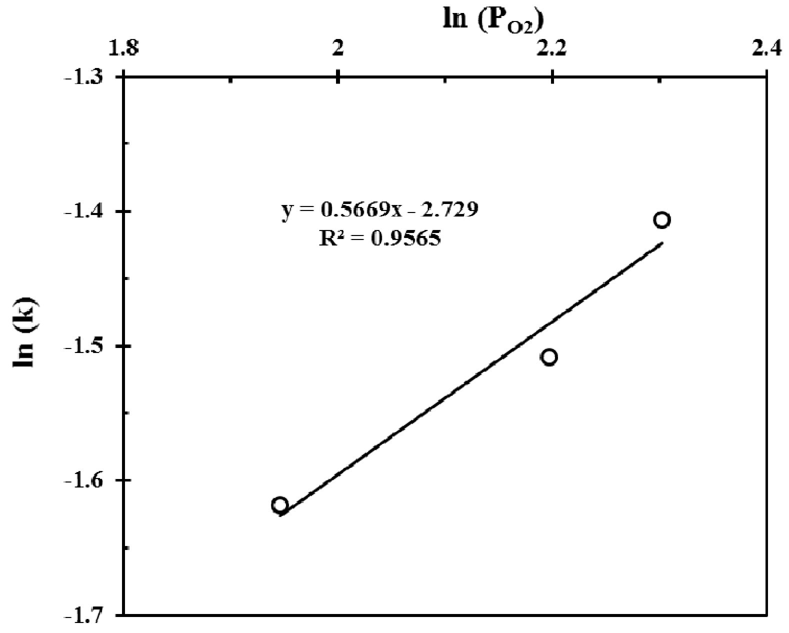

Fig. 5.42 Plot of order for dissolution of pyrite with respect to partial pressure of oxygen

Determination of apparent rate constant (k_o): A linear fit is established between the $1-(1-X_{py})^{\frac{1}{3}}$, and the product term ${p_{O_2}}^{0.5669}\,[Na_2CO_3]^{-0.314}\,NaHCO_3]^{-0.48}\,d^{-0.126}\,e^{-\frac{4465}{T}}$ t in all the experiments for the time duration from 0 to 2 h to determine the apparent rate constant, k_0, for pyrite dissolution, from synthetic mixture using carbonate medium. Plot is shown in Fig. 5.43. The slope of the line, k_0 is found to be 3489. Thus, the topochemical model developed for leaching of pyrite from synthetic mixture is given by Eq. 5.13.

$$1-\left(1-X_{py}\right)^{\frac{1}{3}} = 3489\,{p_{O_2}}^{0.5669}\,[Na_2CO_3]^{-0.31}\,[NaHCO_3]^{-0.4802}\,d^{-0.126}\,e^{-\frac{4465}{T}}\,\mathrm{t} \qquad [5.13\,]$$

The reasons for negative order with respect to bicarbonate concentration could be the same reasons applicable for negative order with respect to carbonate concentration as discussed in the above Subsection captioned ‘effect of carbonate concentration on leaching of pyrite from synthetic mixture’.

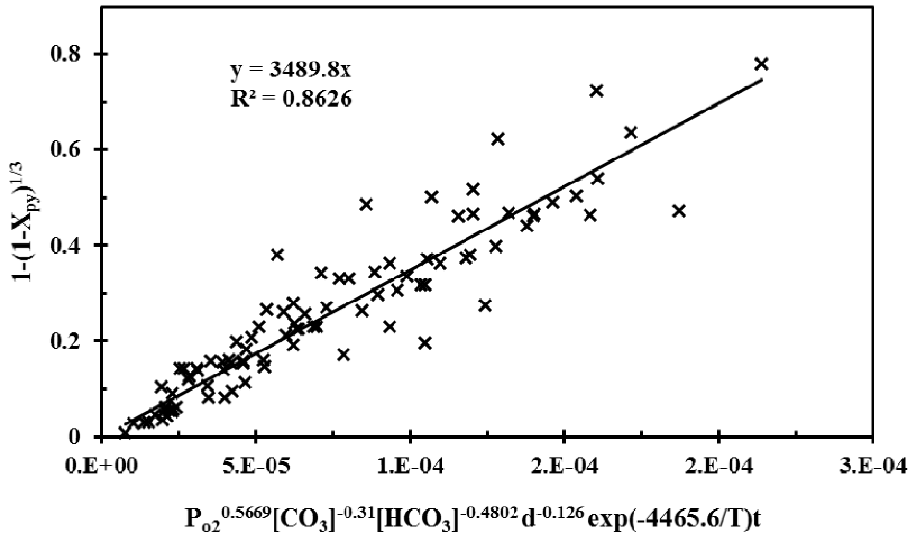

Fig. 5.43 Overall rate constant for pyrite leaching from synthetic mixture

5.3.2 Influence of pyrite content on the leaching of uranium and pyrite

Smaller content of pyrite plays beneficial role in oxidative alkaline leaching of uranium. However, when the same is present in excess, the leachability of uranium oxides is affected as both oxygen and carbonate ions essential for UO_2 solubilization are consumed by the sulphide gangue. The detailed discussion on this aspect is given in Section 2.1.3.1. The study reported here is an attempt to find rates of leaching of pyrite vis-a-vis that of uranium dioxide in carbonate solutions as the content of pyrite is increased in the leaching feed solids. The influence of pyrite content on the leaching behaviour of UO_2 has been clearly brought out. The study helps in delineating the leaching characteristics of uranium ores in carbonate host rocks which may have substantial content of pyrite.

Leaching experiments were carried out in a one-liter batch autoclave reactor (described in Section 4.1.1) on a synthetic mixture of minerals, using oxygen for a time period of 2 h. The pulp density in each experiment was maintained low at a pre-set value of 5% solids (35 g of synthetic mixture in 700 ml of distilled water), in order to minimize the effect of change in pulp density when liquor samples are withdrawn periodically during the experiment. The constant leaching conditions maintained in each of the experiments in the present study correspond to the optimum conditions of leaching of the Indian uranium ore, Tummalapalle, described in earlier published papers [28, 145]. The scheme of experiments including other details is given in Table 5.8.

Table 5.8 Experiments with coexistent system of materials consisting of UO_2 and FeS_2

<table>
<tr><td colspan="3">Constant conditions in each leaching experiment:
Amount of distilled water = 700 ml
Temperature = 398 K
Weight of Na_2CO_3 = 37.1 g
P_{H2O} = 2.3 atm. ; P_{O2} = 5.2 atm
Weight of $NaHCO_3$ =29.4 g
Average particle size = 87 µm
Stirrer speed =1000 rpm
Total weight of synthetic mixture of minerals = 35 g</td></tr>
<tr><td colspan="3">Feed solids: Silica = 9.8% (by wt), UO_2 = 0.2%(by wt);</td></tr>
<tr><td>Expt. code (SYM/PY/)</td><td>% Calcite</td><td>%Pyrite</td></tr>
<tr><td>1</td><td>89</td><td>1</td></tr>
<tr><td>2</td><td>88</td><td>2</td></tr>
<tr><td>3</td><td>87</td><td>3</td></tr>
<tr><td>4</td><td>86</td><td>4</td></tr>
<tr><td>5</td><td>85</td><td>5</td></tr>
<tr><td>6</td><td>84</td><td>6</td></tr>
</table>

The progress of dissolution of uranium dioxide at different time intervals is computed using uranium analysis (expressed as U_3O_8 assay) in the leach liquor. The FeS_2 leached is computed from the sulphate content in leach liquor at different time intervals and the stoichiometry of reaction (2.8) in Section 2.1.3.1. Back calculated feed values (in solids) of both FeS_2 and UO_2 from the assays of leach liquor and residue obtained at the end of each experiment (2 h) are found to be in agreement with >95% accuracy.

The carbonate leaching of uranium is a selective process compared to acid leaching, as few minerals in the ore other than those of uranium are attacked by the lixiviants. Of the three gangue minerals present in the synthetic mixture, calcite and silica are practically insoluble in carbonate medium at room temperature. Though, silica tends to dissolve appreciably at higher temperatures [53A], no significant dissolution of silica was observed under the leaching conditions of 125°C and 7.5 atm pressure applied in the present study. The leach liquors of a typical experiment (conducted with 3% FeS_2) analysed mere 3 mg/L SiO_2 and 4 mg/L Ca, which indicates that there is no appreciable dissolution of calcite and silica during the leaching. Hence, the presence of significant amounts of calcite and silica has no effect on the dissolution of either FeS_2 or UO_2.

5.3.2.1 Effect of pyrite content on leachability of UO_2: The kinetic data of dissolution of UO_2 is plotted in Fig. 5.44. using MS Excel (MSExcel®) linear regression plots, for the range of concentration of FeS_2 from 1% to 6% by weight. High R^2 values, obtained in these plots, represent that the data is well correlated by a linear relationship. The straight lines in Fig. 5.44 indicate that UO_2 is leached at constant rate. This implies that the leaching of UO_2 in alkaline media at T = 125°C and 5.2 atm. oxygen pressure follows shrinking core model for irregular shape particles ($X = kt$, where X is the conversion) [39, 146]. It is evident from Fig. 5.44 that the rate of dissolution of UO_2 increased from 0.223 to 0.494 mg/L-min with increase in FeS_2 content from 1% to about 3% and then decreased to 0.201 mg/L-min for 6% pyrite in the feed. Initial increase is due to effective neutralization of NaOH (formed during uranium dissolution reaction) by the $NaHCO_3$ generated in oxidation reaction of pyrite (reaction (2.8) given in Section 2.1.3.1). Neutralization of NaOH in turn avoids re-precipitation of dissolved uranium. Increase in FeS_2 content above 3% (by wt.) needlessly consumes reagents Na_2CO_3 and O_2 and generates excessive $NaHCO_3$ and Na_2SO_4, which results in lower pH of leaching slurry below 9. The pH values <9 decrease UO_2 leaching as postulated in the uranium species distribution diagram as a function of pH in Fig. 2.5. Other possible reasons for decrease of leaching rate of uranium when >3% pyrite is present in the feed, could be one or more of the following phenomena: (1) Higher concentration of soluble ions like sulfate and bicarbonate, may increase the viscosity of the solution which could decrease the rate of mass transfer of reaction species of uranium solubilization, (2) The excessive sulfate ions produced shall react with gangue mineral, calcite, and precipitate out gypsum ($CaSO_4.2H_2O$) that may coat on the surface of uranium mineral phases and inhibit the dissolution of uranium [40], (3) The products of pyrite reaction (2.8) namely $Fe(OH)_3$ and Fe_2O_3 may coat on the surface of uranium mineral phases and inhibit the dissolution of uranium.

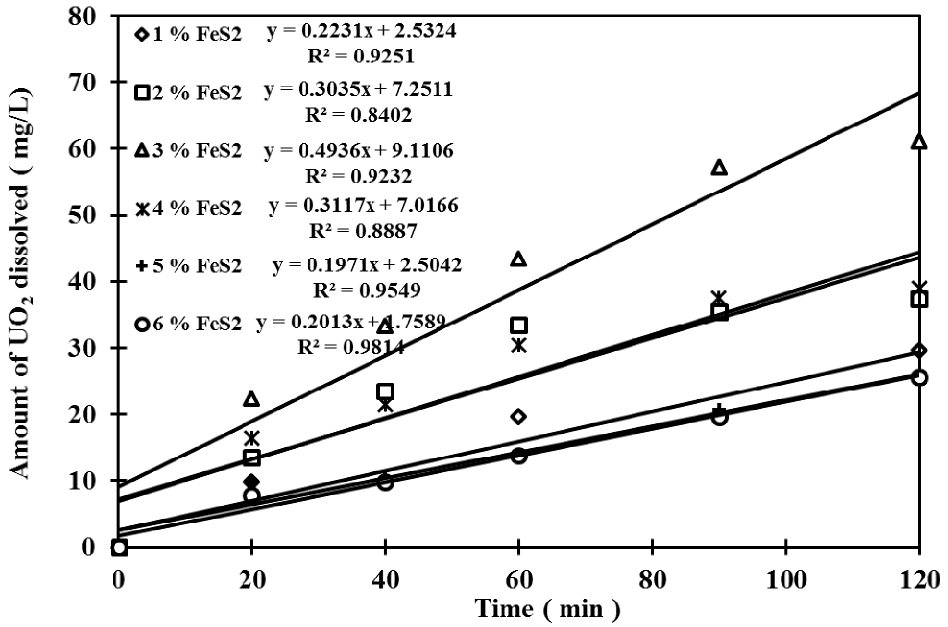

Fig. 5.44 Rate of leaching of UO_2 from synthetic mixtures of different pyrite content at 125°C and 5.2 atm oxygen pressure

<u>5.3.2.2 Effect of pyrite content on leachability of pyrite:</u> The amount of FeS_2 leached per unit volume of lixiviant at different time intervals for the range of concentration of FeS_2 from 1% to 6% by weight is plotted in Fig. 5.45. The data was tested for linear relation using Microsoft Excel (MSExcel®) regression plots. R^2 (coefficient of determination) ≥ 0.9 shows good linear relationship between amount of pyrite leached and the duration of leaching. This implies that the leaching of pyrite in alkaline media at T = 125°C and 5.2 atm oxygen pressure follows shrinking core model for irregular shaped particles ($X = kt$, where X is the conversion) [39, 146]. The slopes of fitted straight lines in this figure represent the rates of leaching of pyrite as mg/L/min. The rate of leaching of pyrite in turn was plotted against concentration of pyrite in the feed solids, on a log-log plot using Microsoft Excel (MSExcel®) linear regression in Fig. 5.46.

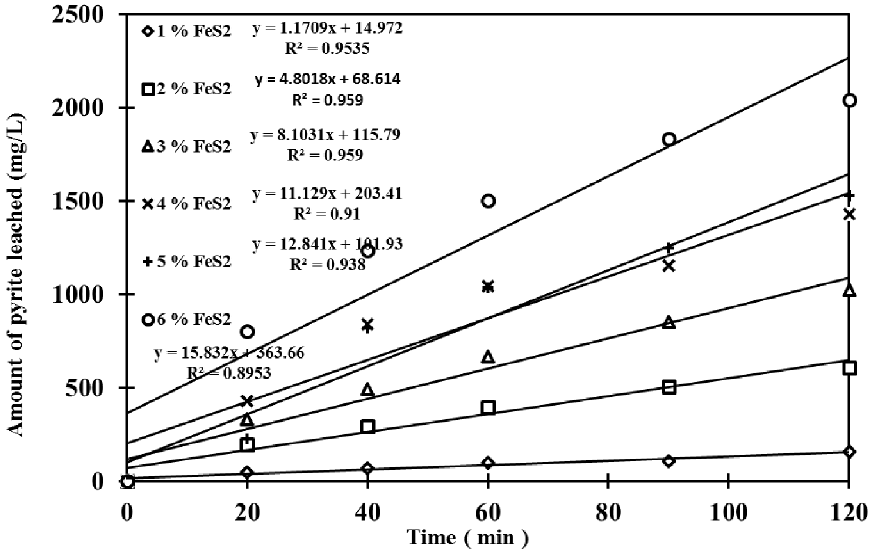

Fig. 5.45 Rate of leaching of iron pyrite from synthetic mixtures of different pyrite content at 125°C and 5.2 atm oxygen pressure

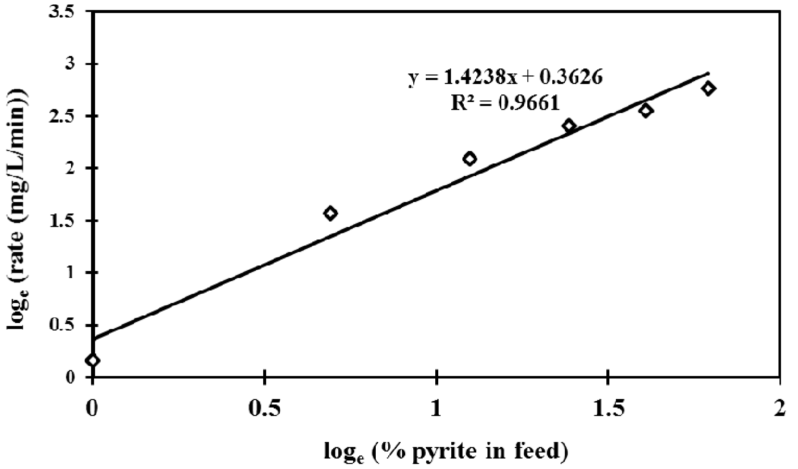

Fig. 5.46 Plot of order for leaching of pyrite with respect to pyrite concentration in feed

The R^2 value of the fitted straight line showed good linear relationship. The kinetic rate equation for leaching of pyrite can then be written as Eq. 5.14 from the slope and intercept of straight line equation obtained in Fig. 5.46. The Eq. 5.14 is simplified to Eq. 5.15.

$$\boldsymbol{ln\left(\frac{dC_{py}}{dt}\right) = 1.4238\, ln\,(W_{py}) + 0.3626} \qquad [5.14]$$

$$\boldsymbol{\frac{dC_{py}}{dt} = 1.437\, W_{py}{}^{1.5347}} \qquad [5.15]$$

Where *Wpy* is iron pyrite content in the solids (% wt.), t in minutes and C_{py} is amount of pyrite leached per unit volume of lixiviant (mg/L) in time t (min). The increasing rate of leaching of iron pyrite from 1.17 to 15.83 mg/L-min with increase in pyrite content; from 1 to 6% is due to the increase in available surface area for the reaction with O_2 and Na_2CO_3 reagents. The order of reaction (1.54) obtained from Fig. 5.46 is different from the stoichiometric constant in reaction (2.8) in Section 2.1.3.1. This indicates the non-elementary nature of the pyrite reaction.

5.3.3 Statistical modeling and optimization of alkaline leaching of UO_2

Phenomenological modeling of extraction of a metal through hydrometallurgical route involves searching for a reaction mechanism that best fits experimental data [39, 146]. Often, it is difficult to know which parameters influence the leaching efficiency, owing to the complex mechanisms involved in both desirable and undesirable chemical reactions. The classical, one factor at a time, methodology could be best applied when experimental data is processed to fit phenomenological type of models and there is no interaction between any two or more input variables. Interaction implies the dependence of relationship between an output variable and particular input variable on the value of another input variable. In other words, effect of one independent variable on the response depends on the value of another independent variable. Statistical design effectively addresses this issue of interaction of two input variables on response [148, 149]. A fractional factorial design requires fewer experiments than the full factorial design. Central Composite Design (CCD) is an effective alternative to factorial design, which was improved upon by Box and Hunter [150]. CCD gives almost as much information as a three-level factorial, requires many fewer tests than the full factorial design and has been shown to be sufficient to describe the majority of steady-state process responses [151]. This work is aimed at developing a mathematical model, using central composite design of experiments, to predict dissolution of uranium vis-a-vis that of pyrite; Optimum temperature and pressure at which uranium dissolution is maximum and the leaching of undesirable pyrite is minimal can be deduced from the model.

Batch leaching experiments were carried out according to two-factor central composite design using a synthetic mixture of pure uranium dioxide, pyrite, calcite and silica in the proportion in which they occur in Gogi uranium ore (0.2% U_3O_8, 5% Pyrite, 9.8% SiO_2 and 85% $CaCO_3$). The feed mixture of 35 g (size range: -150# + 200#) was leached with 700 ml of alkaline lixiviant (0.5 M of Na_2CO_3 and 0.5 M of $NaHCO_3$) in a one-liter autoclave reactor (described in Section 4.1.1.) maintaining temperature and pressure at pre-set values using oxygen gas as oxidant for 6 h. A few screening experiments were conducted to fix the range of temperature and pressure in which the leaching of both uranium and pyrite is most sensitive. Temperature was varied in the range 80 to 130°C and total pressure in the range 1 to 10 atm. The levels of two variables used in the central composite design adopted in the present study are given in Table 5.9.

Table 5.9 Levels of variables studied according to the central composite design

Factor	**Name**	**Units**	**Low Level**	**High Level**	**Low Alpha**	**High Alpha**
A	Temperature	°C	87.3223	122.677	80	130
B	Pressure	atm	2.318	8.682	1	10

The extractions of uranium dioxide and pyrite in all experiments are calculated using the U_3O_8 and SO_4 assays of leach liquors and the stoichiometry of reactions (2.4), (2.5) and (2.8) mentioned in Section 2.1.31. Results of the leaching experiments carried out are given in Table 5.10.

Table 5.10 Results of the leaching experiments conducted according to central composite design

Temperature (°C)	Pressure (atm)	%leaching of uranium dioxide	%leaching of pyrite
105	5.5	53	83
105	5.5	54	85.2
122.7	8.7	46.4	98
105	10	63.1	100
105	5.5	55.2	79.7
105	5.5	57	81.4
130	5.5	22.2	100
87.3	8.7	79.8	40
105	1	15.3	42
87.3	2.3	36.5	4
105	5.5	54.2	84
80	5.5	54.2	0.1
122.7	2.3	15.4	68

The analysis of variance Tables including linear effects and interactional effects on the leaching of both uranium and pyrite are given in Tables 5.11 and 5.12, respectively.

Table 5.11 Analysis of variance (ANOVA) for leaching efficiency of uranium dioxide

Source of Variation	Degrees of Freedom	Sum of Squares	Mean Squares	F Ratio	P Value
Model	5	4334.6236	866.9247	64.9612	1.03E-05
A:temperature	1	1248.0154	1248.0154	93.5175	2.67E-05
B:pressure	1	2520.5762	2520.5762	188.8742	2.55E-06
AB	1	38.8946	38.8946	2.9145	0.1315
AA	1	319.682	319.682	23.9547	0.0018
BB	1	275.8954	275.8954	20.6737	0.0026
Residual	7	93.4168	13.3453		
Lack of Fit	3	84.2586	28.0862	12.267	0.0174
Pure Error	4	9.1583	2.2896		
Total	12	4428.0404			

Table 5.12 Analysis of variance (ANOVA) for leaching efficiency of iron pyrite

Source of Variation	Degrees of Freedom	Sum of Squares	Mean Squares	F Ratio	P Value
Model	5	1.40E+04	2791.2073	86.4529	3.89E-06
A:temperature	1	8663.4188	8663.4188	268.3348	7.70E-07
B:pressure	1	2739.1506	2739.1506	84.8406	3.67E-05
AB	1	9.0199	9.0199	0.2794	0.6134
AA	1	2332.8087	2332.8087	72.2548	6.18E-05
BB	1	427.4529	427.4529	13.2396	0.0083
Residual	7	226.001	32.2859		
Lack of Fit	3	207.3368	69.1123	14.8117	0.0124
Pure Error	4	18.6642	4.6661		
Total	12	1.42E+04			

Analysis of variance (Tables 5.11 and 5.12) of both uranium and pyrite leaching shows that a model with 5 degrees of freedom is significant at 99.9% confidence level. The main effects are significant and the interaction effects are not significant at 99.9% confidence level in the range of temperature and pressure studied. Absence of the interactional effects validates the models developed using the kinetic data generated in sequential experiments (Sections 5.3.1 and 5.3.2). It can be observed from the values of Fisher ratio (F Ratio) that both leaching of uranium and pyrite follows the same order of effectiveness of the two factors studied: main effect of pressure > main effect of temperature > quadratic effect of temperature > quadratic effect of pressure.

The quadratic polynomial functions in terms of temperature (T, expressed in K) and pressure (P, expressed in atm) for fractional leaching of uranium dioxide (X_{UO2}) and that of pyrite (Xpy), developed by the analysis of variance method (ANOVA) using DOE++ software, are given below as Eqs. 5.16 and 5.17.

$$X_{uo_2} = \frac{[-191.8+4.15(T-273)+18.24(P)-0.0544(T-273)(P)-0.0217(T-273)^2-0.622(P)^2]}{100} \quad [5.16]$$

$$X_{py} = \frac{[-829.7+14.315(T-273)+17.135(P)-0.0267(T-273)(P)-0.0586(T-273)^2-0.774(P)^2]}{100} \quad [5.17]$$

The effects of temperature and total pressure on leaching of uranium dioxide and undesirable competing mineral, pyrite (FeS_2), calculated from Eqs. 5.16 and 5.17, are plotted in Figs. 5.47 to 5.50. Experimental values are also included in these figures to indicate accuracy of the models developed.

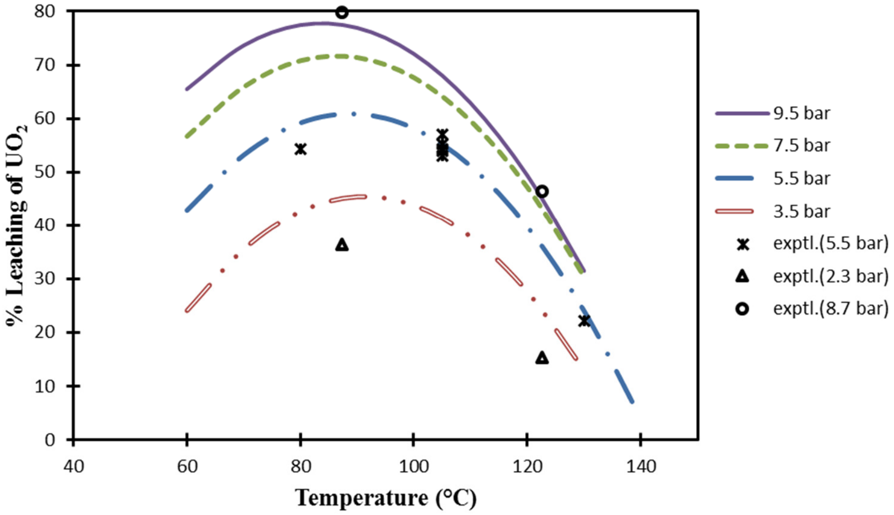

Fig. 5.47 Effect of Temperature on leaching of uranium dioxide at different total pressures

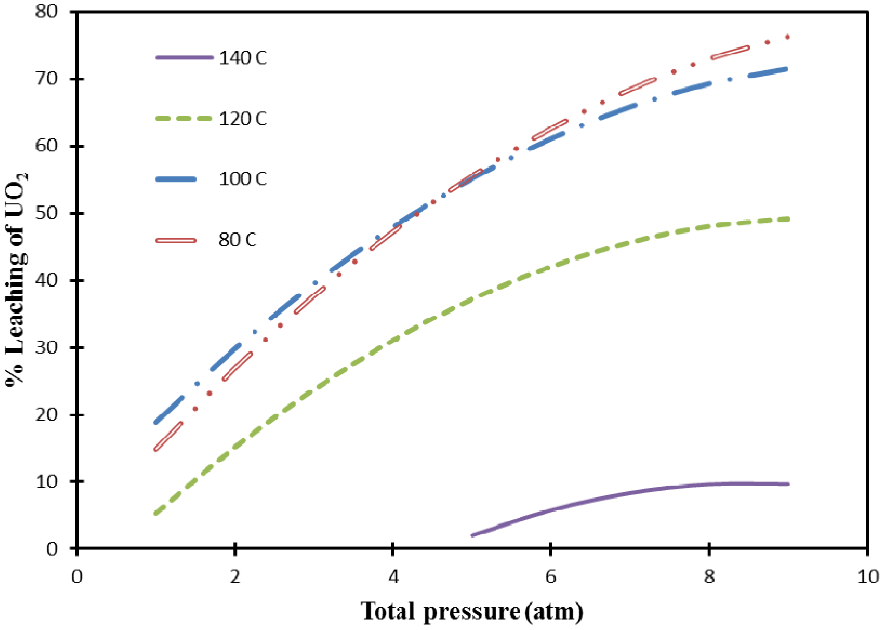

Fig. 5.48 Effect of total pressure on leaching of uranium dioxide at different temperatures

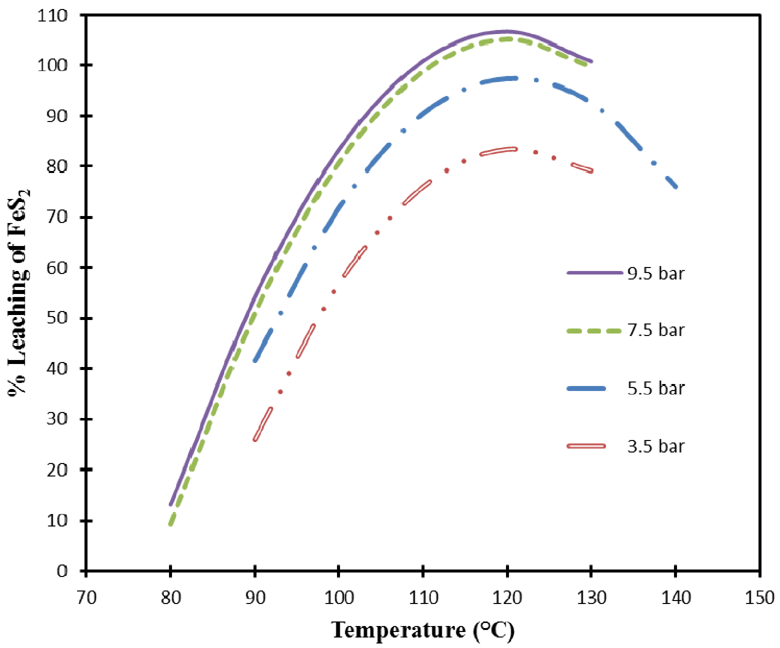

Fig. 5.49 Effect of Temperature on leaching of pyrite at different total pressures

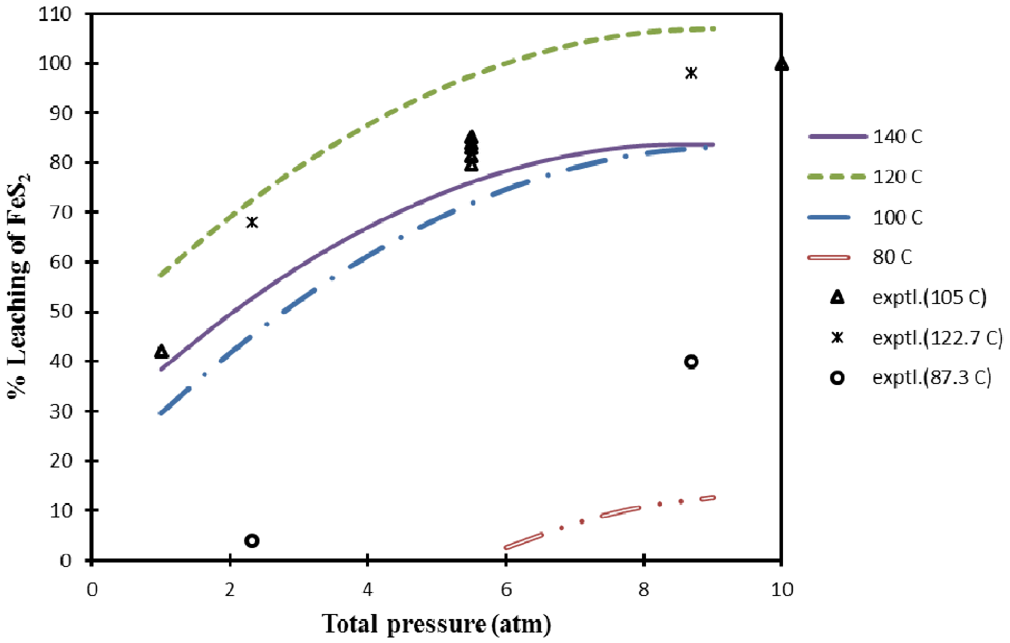

Fig. 5.50 Effect of total pressure on leaching of pyrite at different temperatures

It may be inferred from Fig. 5.47 that at fixed total pressure, uranium leachability increases with increasing temperature initially and decreases beyond a certain temperature (T_m). The decrease is due to increasing vapor pressure of water with increase in temperature rendering lesser oxygen partial pressure during leaching. The trends are in accordance with the reported literature [8]. Further, the value of T_m decreases with increasing total pressure. The shape of curves for leaching of pyrite with varying temperature remained same as shown in Fig. 5.49, which must be due to same reasons cited in case of uranium leaching. However, the maximum leachabilities for pyrite were observed at higher temperature of about 120°C, which could be due to higher activation energy of leaching reaction of pyrite than that of uranium. Figs. 5.48 and 5.50 show that the leachabilities of both uranium dioxide and pyrite increase with increase in total pressure at fixed temperature. This is due to increased partial pressure of oxygen at higher total pressures, which in turn increases solubility of oxygen in the lixiviant rendering higher amounts of oxygen available for reactions.

Taking advantage of quadratic programming, multi-objective optimization of leaching efficiencies of uranium and pyrite (described by Eqs. 5.16 and 5.17) has been performed using DOE++® software. The optimization of multiple responses involves use of desirability functions [152]. A temperature of 80°C and total pressure of 6.5 atm using oxygen gas have been determined as optimum levels to achieve maximum uranium dissolution of 65.4% and minimum undesirable pyrite dissolution of 5.4%.

5.3.4 Role of oxygen on leaching of UO_2 and pyrite

These experiments were conducted on synthetic mixture to confirm the oxidation of pyrite/uranium which occurs due to chemical reaction of O_2 only and not due to any other reactions / phenomena. For comparison, the temperature and pressure are varied according to the experiments conducted on actual ore from Tummalapalle (The experiments on actual ores are detailed in Section 6.1). The scheme of experiments conducted is given in Table 5.13.

Table 5.13 Scheme of leaching experiments on synthetic mixture using different gases

Parameter	Levels of parameters	Base level*
Temperature, °C	125, 140	125, 140
Partial pressure of Ar, atm	10,5.2	10,5.2
Partial pressure of CO_2, atm	10,5.2	1.3,5.2
Partial pressure of O_2, atm	0, 5.2,10	5.2,10
* Constant value while other parameters are varied		

It is clear from the Fig. 5.51 that small amounts (< 5%) of uranium values are leached in the absence of O_2 (conducted using CO_2 or Ar). The small amounts of uranium that got dissolved must be those present in +6 oxidation state which would have resulted from minor surface oxidation of the UO_2 powder during storage. The highest rate of dissolution of uranium was obtained with mixture of O_2 and CO_2 gases at 125°C as well as when oxygen alone was used at 140°C. Fig. 5.52 shows that the pyrite is also not leached in presence of either Ar or CO_2 at any pressure / temperature. As in the case of uranium, highest leaching of pyrite was obtained with mixture of O_2 and CO_2 gases at 125°C as well as when oxygen alone is used at 140°C. As expected from reactions (2.4), (2.5) and (2.8) given in Section 2.1.3.1, the leaching data presented in Figs. 5.51 and 5.52 shows that oxygen is essential for oxidation during leaching of either pure UO_2 or pure pyrite.

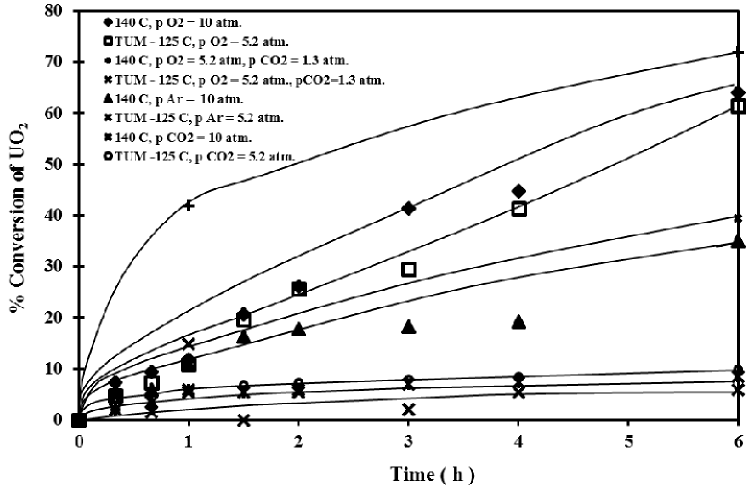

Fig. 5.51 Effect of different gases on leaching of uranium dioxide at different pressures and temperatures

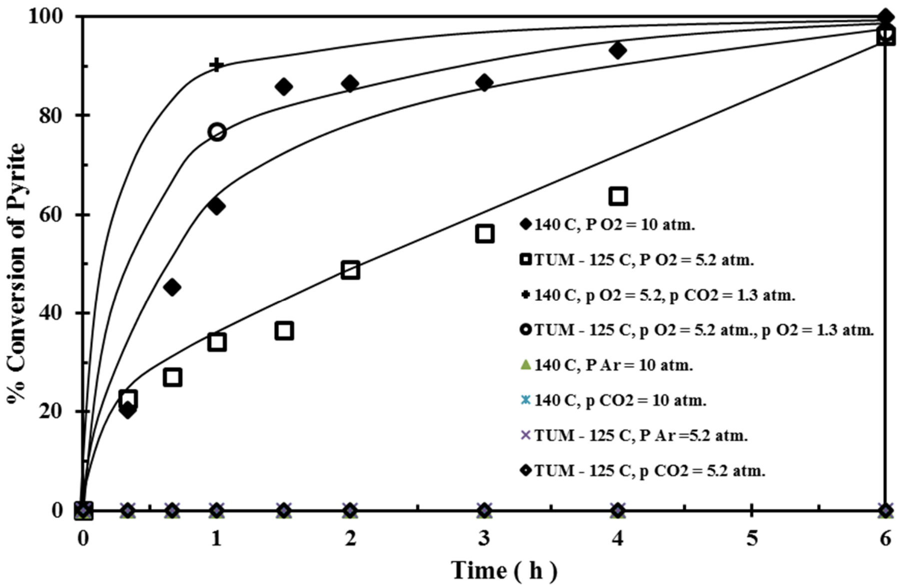

Fig. 5.52 Effect of different gases on pyrite leaching at different pressures and temperatures

5.4 Morphological changes during leaching of pure minerals

Since the leaching process is essentially a microscopic phenomenon controlled by diffusion and/or reaction of solvent molecules with those of solid [39, 146, 153], investigations on morphology were carried out to understand the leaching behavior of pure minerals viz., UO_2, FeS_2, calcite and silica, considered in the present study. The powders of these minerals before and after leaching were examined under Scanning Electron Microscope (SEM) attached with Energy Dispersive X-ray (EDX) spectroscope, using double sided carbon tape pasted on a brass disk according to the procedure described in Section 3.5. The purpose of morphological studies was to observe qualitative differences in morphology only and not the quantitative estimation of any of the components.

The scanning electron micrographs (along with EDX analyses) of all the four minerals used in the synthetic mixture before and after leaching at high temperature and pressure (125°C, 7.5 atm) are given in Figs. 5.53 to 5.56.

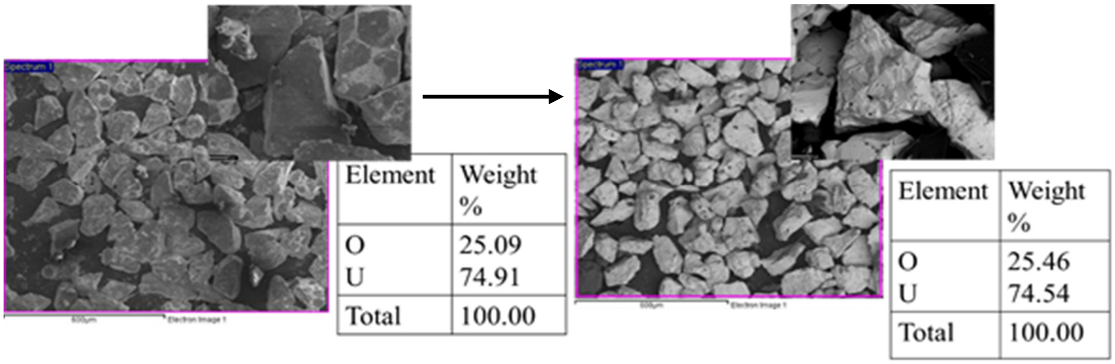

Element	Weight %
O U	25.09 74.91
Total	100.00

Element	Weight %
O U	25.46 74.54
Total	100.00

Fig. 5.53 Scanning Electron Micrographs of Uranium dioxide before and after leaching

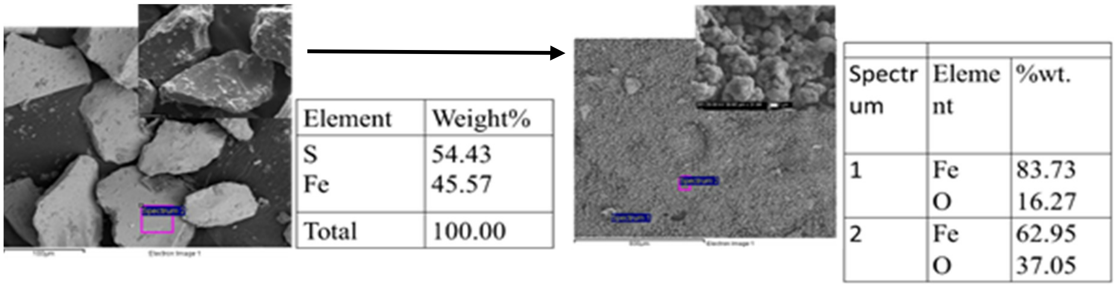

Element	Weight%
S Fe	54.43 45.57
Total	100.00

Spectrum	Element	%wt.
1	Fe O	83.73 16.27
2	Fe O	62.95 37.05

Fig. 5.54 Scanning Electron Micrographs of Iron pyrite before and after leaching

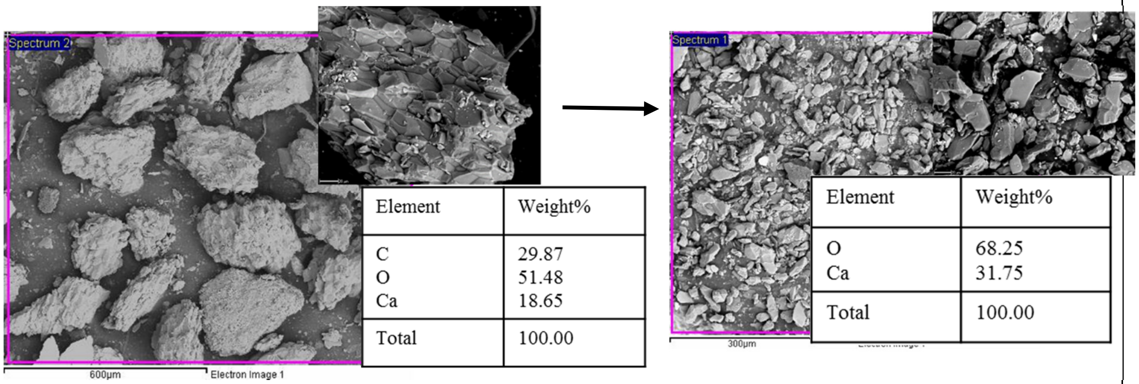

Element	Weight%
C O Ca	29.87 51.48 18.65
Total	100.00

Element	Weight%
O Ca	68.25 31.75
Total	100.00

Fig. 5.55 Scanning Electron Micrographs of pure Calcite before and after leaching

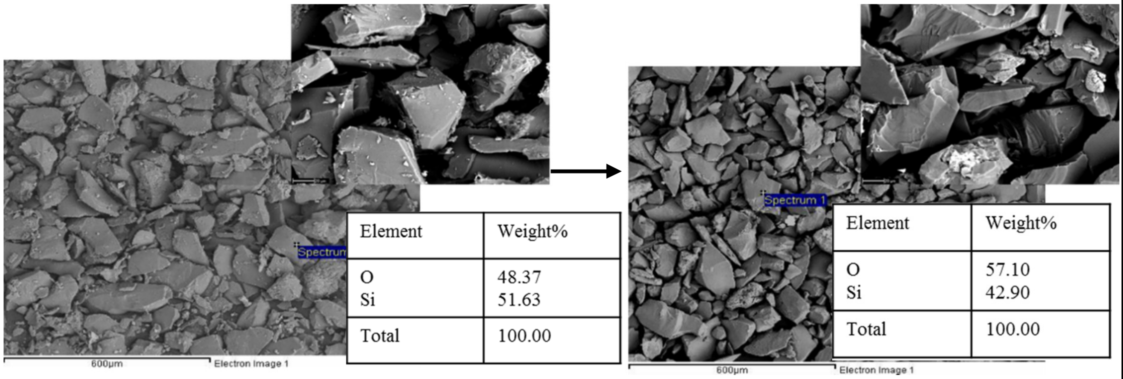

Element	Weight%
O Si	48.37 51.63
Total	100.00

Element	Weight%
O Si	57.10 42.90
Total	100.00

Fig. 5.56 Scanning Electron Micrographs of pure Silica before and after leaching

Fig. 5.53 suggests that pure UO_2 feed particles are in the size range 75 - 100 μm; they have a smooth surface and irregular shape. The SEM image of leached UO_2 particles shows rough surface, significant number of pits and micro cracks around them, indicating the dissolution of uranium dioxide. Since uranium reaction product is soluble (as given by reactions (2.4) and (2.5) in Section 2.1.3.1), it has not formed any new solid phase. Fig. 5.54 suggests that iron pyrite is chemically altered to iron oxide (a new solid phase) and is present in ultra-fine sizes. Formation of the pyrite reaction product, iron oxide, was also confirmed by X-ray diffraction study (according to the procedure described in Section 3.4) of pure pyrite and leach residue obtained after leaching at 125°C, 7.5 atm pressure. Characteristic peaks of pyrite and marcasite phases are identified in the feed material to leaching in Fig. 3.2 (in Section 3.4), while characteristic peaks of hematite mineral phase are identified in Fig. 5.57. The hematite (Fe_2O_3) could have formed from the decomposition, given as chemical reaction (5.18), of $Fe(OH)_3$ precipitated during the oxidation reaction (2.8) of pyrite stated in Section 2.1.3.1.

$$2Fe(OH)_3 \rightarrow Fe_2O_3 + 3H_2O \qquad [5.18]$$

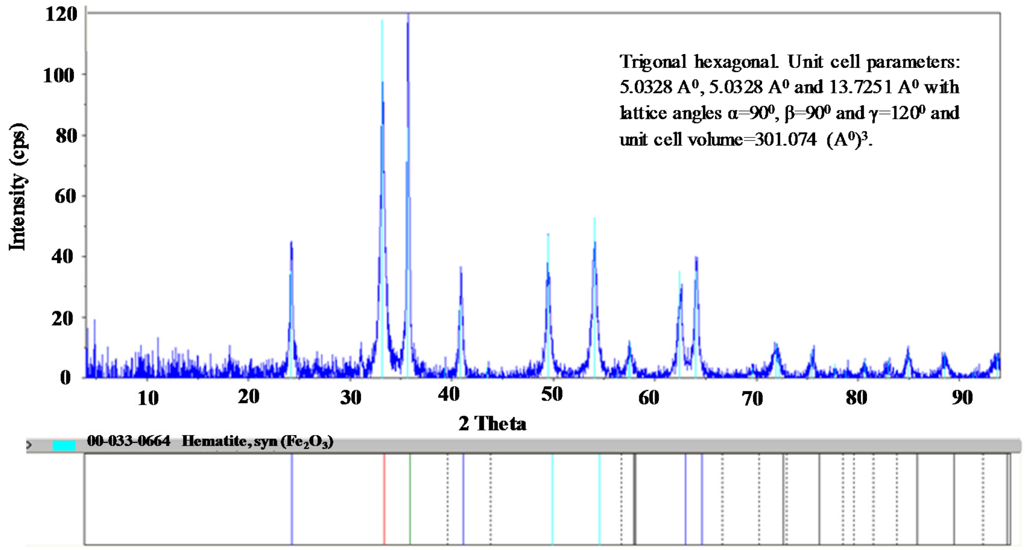

Fig. 5.57 X-ray diffractogram of residue obtained from leaching of pyrite at 125°C, 7.5 atm total pressure.

However, $Fe(OH)_3$ product was also identified in the leach residue of pyrite by visual observation under optical microscope as expected from the chemical reaction (2.8) given in Section 2.1.3.1. Since this phase is in amorphous form, it could not be detected by X-ray diffraction analysis. The observations indicate that a mixture of $Fe(OH)_3$ and Fe_2O_3 would have formed as products in the pyrite leaching experiments conducted in the present study. The formation of Fe_2O_3 during oxidation of pyrite in alkaline medium is also reported by Joshi et al. [93].

Calcite is not altered chemically, but disintegrated into smaller pieces (Fig. 5.55) which could be due to its low hardness of 3, presence of two sets of cleavable surfaces and agitation. Silica is neither chemically nor physically altered (due to higher hardness of 7) as seen in Fig. 5.56.

5.5 CONCLUSION

The leaching of pure UO_2 is described by a Michaelis–Menten type of rate equation and the pertinent empirical constants are determined in the present study. The order of leaching with respect to $[Na_2CO_3]$, $[NaHCO_3]$, and P_{O2} is determined to be 0.24, 0.1 and 0.6 respectively. The activation energy is found to be 36.8 kJ/mol. A topochemical rate equation is developed for alkaline leaching of pure pyrite. The order of P_{O2} and the activation energy are found to be 0.2 and 58.1 kJ/mol respectively. However, the orders of leaching with respect to $[Na_2CO_3]$ and $[NaHCO_3]$ are found to be positive (0.8 and 0.2 respectively) at the lower concentrations (< 0.7 M) and negative (-2.9 and -2.1 respectively) at higher concentrations (> 0.7 M) of carbonate and bicarbonate.

The leaching of pure UO_2 and pure pyrite from a synthetic mixture of pure materials are best described by topochemical type of rate equations. The order of UO_2 leaching with respect to $[Na_2CO_3]$, $[NaHCO_3]$, and P_{O2} is determined to be 0.4, 0.4 and 2 respectively. The activation energy is found to be 13.4 kJ/mol. The order of leaching of pyrite with respect to

$[Na_2CO_3]$, $[NaHCO_3]$, and P_{O2} is determined to be -0.3, -0.5 and 0.6 respectively. The activation energy is found to be 37 kJ/mol.

The difference in orders of different leaching parameters between the rate equations developed for UO_2 and pyrite in isolation (Eqs. 5.5 and 8.1) and for UO_2 and pyrite from synthetic mixture (Eqs. 5.12 and 5.13) can be attributed to the lower temperature and pressure conditions applied for leaching of pure materials (UO_2 and pyrite) in isolation than those applied for leaching of the same materials from synthetic mixture. The phenomenon is in congruence with the remarks of Sohn and Wadsworth [77] that the rate information obtained under a given set of conditions may not be applicable under another set of conditions.

The rate of leaching of pyrite increases with the pyrite content in the feed solids, while the rate of leaching of UO_2 increases with increase in pyrite content in the feed solids up to 3% and then decreases beyond 3%. The increase in uranium dissolution at lower levels of pyrite is due to the neutralization of NaOH produced by reaction (2.5a). The decrease in dissolution of uranium from the feed solids containing more than 3% pyrite is due to the decrease in pH of the lixiviant to below 9 due to formation of Na_2SO_4 and $NaHCO_3$.

The leaching experiments conducted on synthetic mixture according to central composite design methodology reveal that maximum and minimum extractions of UO_2 (desirable) and pyrite (undesirable) are 65.4% and 5.4% respectively at 353 K and 6.5 atm pressure using oxygen. It follows from the reactions (2.4), (2.5) and (2.8) that the extraction of UO_2 and pyrite requires oxygen. The leaching experiments carried out on synthetic mixture of pure materials using inert gases like Ar and CO_2 have also established that extraction of both uranium and pyrite is insignificant without the use of oxygen. Lastly, the leaching results are corroborated by morphological changes observed during leaching of synthetic mixture of major and important ore constituents: (1) UO_2, (2) pyrite, (3) calcite, and (4) silica.

CHAPTER 6

MODELING THE BATCH LEACHING KINETICS OF INDIAN URANIUM ORES (APPLIED STUDIES)

Leaching experiments carried out on two Indian uranium ores are presented in this Chapter. The study of role of oxygen and morphological changes during leaching formed part of the experiments. The last Section of this Chapter is dedicated to bring out the relation between leaching of pure minerals discussed in Chapter 5 and Indian uranium ores.

In India, alkaline leaching is adopted for Tummalapalle ore and is also expected to be adopted for Gogi ore for extraction of uranium in view of their high carbonate content. The reasons for choosing alkaline leaching for high carbonate content ores are elaborated in Section 2.1.3. Na_2CO_3 and $(NH_4)_2CO_3$ are the two commercial alkaline leachants available for uranium extraction. The latter is preferred for carbonate type of ores with high silica because of its high selectivity to uranium and lesser tendency to dissolve silicate minerals [57]. The former is preferred for ores with low silica since it is not only cheaper but also environmentally more benign than $(NH_4)_2CO_3$. It can be observed from the chemical analyses of the two ores, Tummalapalle and Gogi, given in Table 3.8, that they contain 19 and 25% SiO_2, respectively. Owing to their low silica content, Na_2CO_3 is selected for leaching uranium from both of the ores in the present study. Moreover, addition of $NaHCO_3$ is essential whenever Na_2CO_3 is used as leachant, as discussed in detail in Section 2.1.3.1. Therefore, a combination of Na_2CO_3 and $NaHCO_3$ is used as leachant for Tummalapalle ore. However, Na_2CO_3 alone is used for leaching of Gogi ore as the high pyrite present in the ore produces enough in-situ $NaHCO_3$ during leaching according to reaction (2.8) given in Section 2.1.3.1.

An oxidant is required along with the leachant to oxidize uranium from uranous state, U(IV) to uranyl state, U(VI) for forming a soluble complex. Of the oxidants suitable for alkaline leaching ($KMnO_4$, $CuSO_4$-NH_4OH, $K_3Fe(CN)_6$, NaOCl, Air, O_2, Pb_3O_4, PbO_2, $K_2S_2O_8$ and H_2O_2 [53B], oxygen and air are preferred for the cost and environmental friendliness even though the oxidation rates are low with them. When air is used instead of pure oxygen, the total pressure of the leaching system needs to be approximately increased by five times to get the desired partial pressure of oxygen requiring a structurally stronger leaching vessel. Considering the above fact, industrial oxygen of commercial grade (99.6% pure) from a cylinder, is used to maintain the required partial pressure of oxygen in the reaction vessel in the present studies.

6.1 TUMMALAPALLE URANIUM ORE

6.1.1 Materials and Methods

Leaching experiments were conducted using the five-liter autoclave (described in Section 4.1.1), according to the procedure described in Section 4.1.3. The constant parameters and levels of the variable parameters of present study were fixed around the optimum values observed in previous studies [28] on Tummalapalle ore. Experiments were conducted using 1 kg Tummalapalle ore and 900 ml of solution containing 50 g of each of Na_2CO_3 and $NaHCO_3$ reagents (maintaining pulp density at 50% by wt.). The variables studied were partial pressure of oxygen (p_{O_2}) in the range 4.5 to 6.5 atm, stirring speed (s) from 573 to 900 rpm, average particle size (represented in the present study by mean volume surface diameter), (d), between 25.8 to 34.76 μm and temperature (T) from 398 to 438 K. Three feed samples of different size distributions were generated by wet grinding of the rock pieces (-1/4" size) of the Tummalapalle ore for different time periods (25, 40 and 55 minutes) in a laboratory ball mill. The size distributions of these samples determined by wet sieving are given Table 6.1.

Table 6.1 Sieve analyses of three feed samples of Tummalapalle ore generated by wet grinding for three different time periods

Grinding time (min)	25	40	55
Size (μm)	Cumulative % wt. passing		
425	100.0	100.0	100.0
150	100.0	100.0	100.0
100	68.3	74.0	97.1
75	59.0	65.3	84.3
45	45.5	49.8	66.4
37	40.2	44.5	61.3
Surface mean volume diameter (μm)	25.8	32.36	34.76

6.1.2 Results

In all experiments the fractional conversion of uranium (α_{exp}) at different time intervals was calculated using the U_3O_8 concentration in leach liquor, measured by spectrophotometry described in Section 4.2.1.2, and the average back calculated feed assay of 480 ppm U_3O_8 (calculated from U_3O_8 concentration in residue and leach liquor obtained at the end of each experiment) of all the experiments using Eq. 6.1. Results of the leaching experiments are given in Table 6.2 along with the corresponding set of experimental conditions.

$$\alpha_{\exp} = \frac{C_{UO_2} V}{W f} \qquad [6.1]$$

$where, C_{UO_2} = \ Concentration\ of\ U_3O_8 in\ the\ leach\ liquor\ at\ time\ t\ (in\ \ g/L)$

$V = \ Volume\ of\ leach\ liquor = 0.9\ L$

$W = weight\ of\ feed = 1000\ g$

$f = average\ \%U_3O_8 in\ the\ feed = 0.048$

Table 6.2 Results of kinetic leaching experiments on Tummalapalle uranium ore

Expt. No. TUM/	Partial Pressure of O2, p_{O_2}	p_{H_2O} at temperature, T	Total pressure, P_{total}	Stirring speed, S	Particle size, D	Temp., T	Time, t	Concn. of U_3O_8 in leach liquor	Conversion of U_3O_8, α_{exp}
	(atm)	(atm)	(atm)	rpm	μm	K	(h)	mg/L	fraction
1	4.5	2.3	5.8	764	25.8	398	1	267	0.5
							2	283	053
							4	313	0.59
							6	326	0.61
2*	5.5	2.3	6.8	764	25.8	398	1	337	0.63
							2	379	0.71
							4	392	0.74
							6	397	0.74
3	6.5	2.3	7.8	764	25.8	398	1	346	0.65
							2	356	0.67
							4	401	0.75
							6	423	0.79
4	5.5	2.3	6.8	573	25.8	398	1	326	0.61
							2	365	0.69
							4	380	0.71
							6	386	0.73
5	5.5	2.3	6.8	900	25.8	398	1	356	0.67
							2	388	0.73
							4	404	0.74
							6	423	0.75
6	5.5	3.6	8.1	764	25.8	413	1	345	0.69
							2	394	0.74
							4	397	0.73
							6	404	0.75
7	5.5	7.0	11.5	764	25.8	438	1	358	0.78
							2	406	0.76
							4	434	0.81

Expt. No. TUM/	Partial Pressure of O_2, p_{O_2}	p_{H_2O} at temperature, T	Total pressure, P_{total}	Stirring speed, S	Particle size, D	Temp., T	Time, t	Concn. of U_3O_8 in leach liquor	Conversion of U_3O_8, α_{exp}
	(atm)	(atm)	(atm)	rpm	μm	K	(h)	mg/L	fraction
							6	436	0.82
8	5.5	2.3	6.8	764	34.76	398	1	229	0.43
							2	252	0.47
							4	254	0.48
							6	288	0.54
9	5.5	2.3	6.8	764	32.36	398	1	249	0.47
							2	293	0.55
							4	270	0.51
							6	294	0.55
*Base experiment, conducted at the constant values of each variable, when other parameters are changed									

6.1.3 Discussion

6.1.3.1 Mixed control model: The experimental data depicted in Table 6.2 is first fitted to two homogeneous rate models to test their applicability. Pseudo first order homogeneous model failed the test because the relationship between $-ln(1-\alpha)=kt$ and t is not linear. Avrami model [154], given by equation $-ln(1-\alpha)=kt^n$ is fitted to the data. Linear relation could not be obtained for the data of all the experiments when $ln[-ln(1-\alpha)]\ Vs\ ln(t)$ is plotted. Applicability of three heterogeneous rate equations of well-known shrinking core model was then tested for the leaching data. (1) Film diffusion controlled model given by equation, $\alpha = k\,t$ (2) Surface chemical reaction controlled, whose rate equation is given by $1-(1-\alpha)^{\frac{1}{3}}=k_c t$ and (3) Diffusion of reactants through ash / product layer (particle pore is assumed to be product layer in the present case) controlled, whose rate equation is given by $1-\frac{2}{3}\alpha-(1-\alpha)^{\frac{2}{3}}=k_D t$.

Film diffusion kinetics does not adequately represent physical system, due to absence of constant film layer over the particles, as the slurry is subjected to high agitation. Hence the data was not tested for this rate equation. Experimental data did not fit surface reaction and diffusion controlled rate equations. Hence, a "mixed control" behavior described by equation: $1-\frac{2}{3}\alpha-(1-\alpha)^{\frac{2}{3}}+\beta[1-(1-\alpha)^{\frac{1}{3}}]=kt$, is considered [155], the terms of which are defined as follows,

β =2D'/(k_c σ r_0) =Coefficient indicating surface chemical contribution to overall rate

k = $2D_{eff}C_{bulk}^nV/(r_0^2\sigma)$ = overall reaction rate constant [6.2]

D_{eff}=Effective diffusivity of leachant through the product layer

σ =Stoichiometry factor, moles solid reactant per mole of diffusing leachant

r_0 = Initial particle radius

C_{bulk} = Bulk leachant concentration

V = Molar volume of solid reactant

The above mixed control equation can be re arranged in the form of y = m x + c as

$$\frac{1-\frac{2}{3}\alpha-(1-\alpha)^{\frac{2}{3}}}{t}=-\beta\;\frac{[1-(1-\alpha)]^{\frac{1}{3}}}{t}+k \qquad [6.4]$$

y and x values were calculated using *α, t* values of each experiment results given in Table 6.2. The rate constant, k, given in Eq. 6.2 can be modified to include the effects of partial pressure of oxygen (P_{O2}), stirring speed (s), particle size (d) and temperature (T) using the Arrhenius expression [156] as following

$$k=k_0\;(P_{O_2})^n\;s^p\;d^q\exp(E_a/RT) \qquad [6.4]$$

The following Sections describe the determination of the rate constant, k, in each kinetic experiment according to Eq. 6.3, calculation of the orders of the reaction with respect to each variable parameter using Eq. 6.4, and finally the determination of k_0, the overall rate constant.

Effect of Partial pressure of oxygen: According to the results of experiments #TUM/1, #TUM/2 and #TUM/3 given in Table 6.2, the uranium concentration in the leach liquor is found to be increasing with time at different partial pressures. From the values of fractional conversion (α_{exp}) and time (t), y and x values are calculated according to Eq. 6.3 and plotted in Fig. 6.1. The y-intercepts of straight lines in Fig. 6.1 correspond to rate constant, k, which were found to be 0.002, 0.004 and 0.005 h^{-1} at P_{O2} = 4.5, 5.5 and 6.5 atm respectively. The rate constants of uranium extraction are found to be increasing with partial pressure of oxygen as the solubility of oxygen increases with pressure. The order of the leaching of uranium with respect to partial pressure of oxygen is determined to be 2.5 from the slope of the straight line obtained by plotting ln(k) Vs $ln(p_{O_2})$ in Fig. 6.2, according to Eq. 6.4.

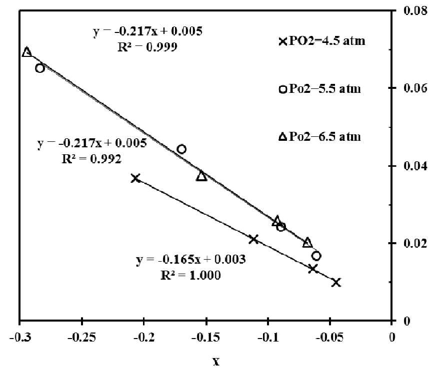

Fig. 6.1 Plot of Eq. 6.3, for calculating the values of rate constants (k) and β for experiments using different partial pressures of oxygen (constant values of other variables: stirring speed = 764 rpm, particle size=25.8 µm and temperature=398 K)

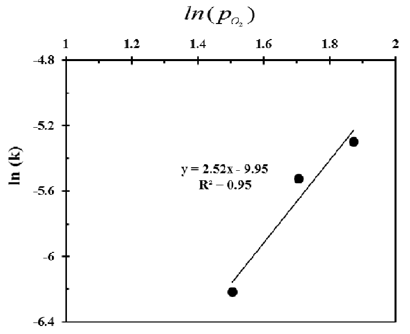

Fig. 6.2 Plot for reaction order with respect to partial pressure of oxygen for leaching of uranium from Tummalapalle ore

Effect of Stirring speed: Results of experiments #TUM/4, # TUM/2 and # TUM/5 given in Table 6.2 are plotted in Fig. 6.3 to elicit the effect of stirring speed. The rate constant, k, is found to be 0.0047, 0.0049 and 0.0052 h^{-1} at stirring speeds 573, 764 and 900 rpm respectively. The order of leaching of uranium with respect to stirring speed is found to be 0.21 from Fig. 6.4. The leaching rate increases with stirring speed marginally as the order of the reaction with respect to stirring speed is close to zero.

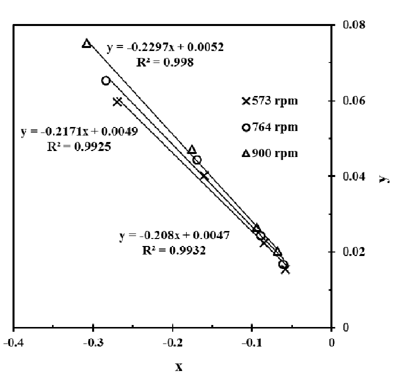

Fig. 6.3 Plot of Eq. 6.3, for calculating the values of rate constants (k) and β for experiments using different stirring speeds (constant values of other variables: P_{O2} = 5.5 atm, d=25.8 µm and T= 398 K)

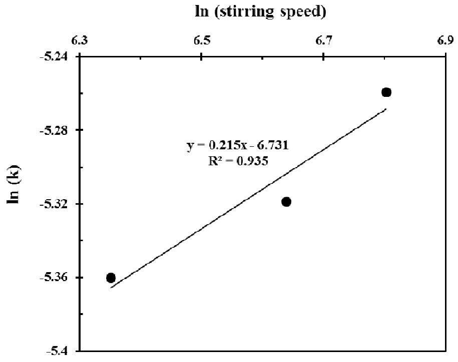

Fig. 6.4 Plot for reaction order with respect to stirring speed for leaching of uranium from Tummalapalle ore

Effect of Particle size: Results of experiments # TUM/8, # TUM/9 and # TUM/2 given in Table 6.2 are plotted in Fig. 6.5 to quantify the effect of particle size. The rate constant, k, is found to be 0.004, 0.001 and 0.001 h^{-1} at particle average particle sizes 25.8, 32.36 and 34.76 μ respectively indicating that the reaction rate decreases with increase in particle size. The order of leaching of uranium with respect to particle size is found to be -5.7 from Fig. 6.6. The leaching rate decreases with particle size significantly as the order of the reaction is very high.

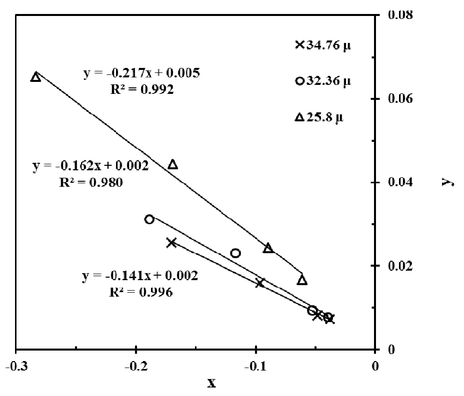

Fig. 6.5 Plot of Eq. 6.3, for calculating the values of rate constants (k) and β for experiments using different particle sizes (constant values of other variables: P_{O2} = 5.5 atm, s=764 rpm and T= 398 K)

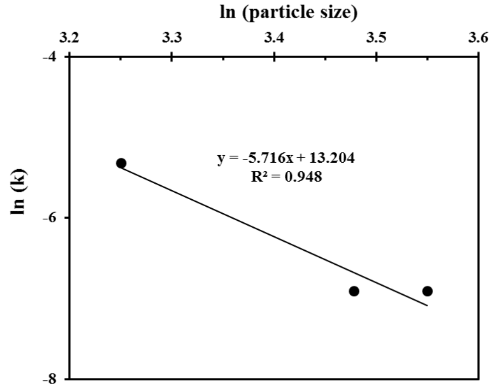

Fig. 6.6 Plot for reaction order with respect to particle size

Effect of Temperature: Results of experiments #TUM/2, #TUM/6 and #TUM/7 given in Table 6.2 are plotted in Fig. 6.7 to find the effect of temperature on rate of reaction. The rate constant, k, is found to be 0.0049, 0.0051 and 0.0081 h^{-1} at temperatures 398, 413 and 438 K respectively. The Arrhenius plot for uranium leaching is shown in Fig. 6.8. The activation energy is determined to be 18.8 kJ/mol, from the slope of straight line obtained in Arrhenius plot. As the activation energy obtained from Arrhenius plot is < 5 kcal/mol (20.9 kJ/mol), it can be concluded that the leaching predominantly follows diffusion control dissolution kinetics [142], though the rate equation is fitted to mixed control model with surface reaction and diffusion as limiting processes.

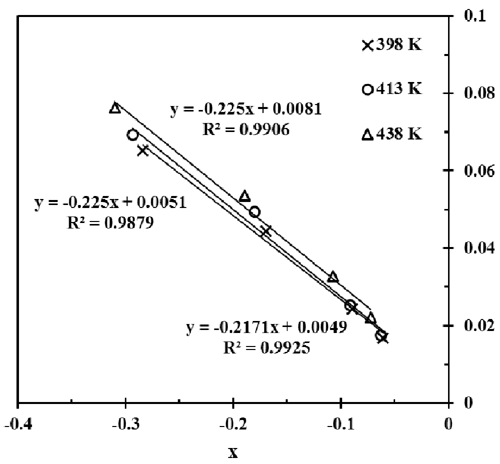

Fig. 6.7 Plot of Eq. 6.3, for calculating the values of rate constants (k) and β for experiments using different temperatures (constant values of other variables: P_{O2} = 5.5 atm, s=764 rpm and d= 25.8 μ)

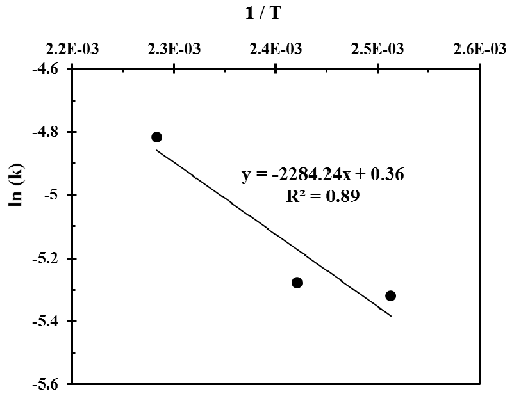

Fig. 6.8 Arrhenius plot for activation energy of leaching of uranium from Tummalapalle ore

<u>Overall rate constant of the mixed control leaching model:</u> If a linear fit can be established between the rate constant, k, and the product term $(p_{O_2})^n\ s^p\ d^q \exp(E_a / RT)$ at different values of variable parameters, the slope of such a linear fit would be the overall rate constant, k_O, employed in Eq. 6.4. The rate constant, k at different conditions of leaching variables, obtained from the Figs. 6.1, 6.3, 6.5, and 6.7, and the corresponding product term mentioned above, arranged as four groups of data, are summarized in Table 6.3. The straight line relationship between k and the product term is shown in Fig. 6.9. The slope of the fitted straight line, k_O, is found to be 40570.

Table 6.3 The rate constant (k) at different values of the variable parameters and the product term $(p_{O_2})^{2.5}\ s^{0.21}\ d^{-5.7} \exp(-18800 / RT)$

Variation in partial pressure of oxygen			Variation in stirring speed			Variation in particle size			Variation in temperature		
Speed = 764 rpm Particle size = 28.5 μ Temperature = 398 K			p_{O_2} = 5.5 kg / cm^2 Particle size = 28.5 μ Temperature = 398 K			p_{O_2} = 5.5 kg / cm^2 Stirring speed = 764 rpm Temperature = 398 K			p_{O_2} = 5.5 kg / cm^2 Stirring speed = 764 rpm Particle size = 28.5 μ		
p_{O_2}	k	product	speed	k	product	Size	k	product	K	k	product
4.5	0.002	5.2E-09	573	0.0047	8.02E-09	34.8	0.001	1.55E-09	398	0.0049	8.51E-09
5.5	0.004	8.5E-09	764	0.0049	8.51E-09	32.4	0.001	2.32E-09	413	0.0051	1.05E-08
6.5	0.005	1.3E-08	900	0.0052	8.02E-09	25.8	0.0049	8.51E-09	438	0.0081	1.43E-08

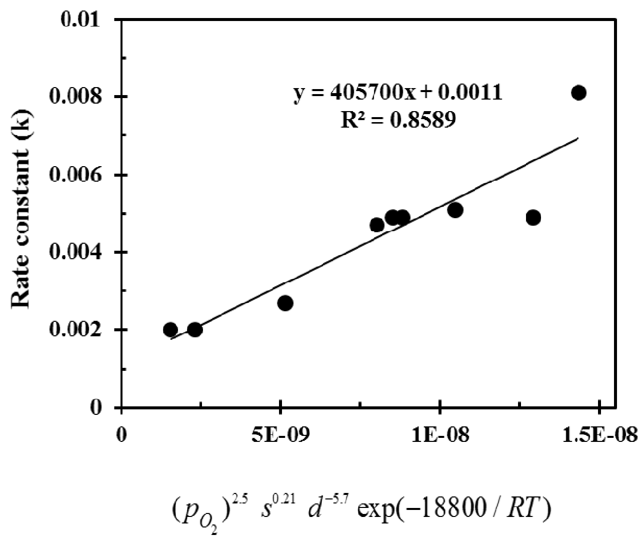

Fig. 6.9 Linear fit of rate constant (k) against the product term, $(p_{O_2})^{2.5}\ s^{0.21}\ d^{-5.7}\exp(-18800/RT)$, at different leaching conditions

Leaching kinetics indicate that both surface chemical reaction and diffusion through the inert particle pores are rate controlling steps according to shrinking core model of heterogeneous reactions. The overall rate equation is given by $1-\frac{2}{3}\alpha-(1-\alpha)^{\frac{2}{3}}+\beta[1-(1-\alpha)^{\frac{1}{3}}]=kt$ and $k=40570\,(p_{O_2})^{2.5}\ s^{0.21}\ d^{-5.7}\exp(-18800/RT)$. The rate of leaching is least affected by the stirring speed, decreases significantly with increase in particle size, and increases with increase in partial pressure of oxygen and temperature in the range of variables studied. The maximum possible uranium extraction from Tummalapalle ore by pressure alkaline line leaching is about 80% at partial pressure of oxygen = 6.5 atm, stirring speed = 764 rpm, particle size = 25.8 μm and temperature = 398 K.

6.1.3.2 Pore diffusion control model incorporating particle size distribution: If uranium minerals are fully liberated, the popular shrinking core model mechanisms (1) mass transport through the boundary layer fluid film surrounding each particle or (2) internal surface chemical reaction are applicable. If the product layer is porous, (3) core-shell (topochemical reaction model) diffusion, is applicable. Usually, the uranium minerals in the ground ore are fully / partially liberated by grinding. In high grade ores, even if uranium is partially liberated, the above mechanisms of shrinking core model generally fit the kinetic data. This is due to high rock permeability to the leachants [58, 119]. But for low grade and finely disseminated uranium ores like Tummalapalle ore, no single mechanism of shrinking core model was found to be applicable. Hence, a mixed controlled model, initially chemical reaction and later shell diffusion controlled, was fitted satisfactorily as delineated in the previous Section 6.1.3.1. This could be due to low permeability of the rock. Low permeability is evident from the low average specific surface area (0.42 m^2/g, given in Table 3.3) and low pore volume (0.02 cm^3/g, given in Table 3.3). Transport of dissolved metal in liquid within pores of rock particles is likely to be rate controlling step in overall extraction process, especially for low grade ores [157]. Counter current diffusion of uranyl anion out of the particle with CO_3^{-2} and O^{-2} ions of the fluid phase diffusing into the particle is involved. The diffusivity in turn is a function of porosity and tortuosity of the pores in the ground ore particles. Hence, a pore diffusion rate controlling extraction kinetic model is examined.

Murhammer et al. [158] showed that the error obtained by assuming uniform particle size distribution (= average of minimum and maximum size) is less than 5%, only if the ratio of maximum to minimum particle size is less than 5. Gbor et al. [126] showed that if coefficient of variation of particle size distribution following gamma function is more than 0.3, shrinking core model without considering particle size distribution would lead to substantial errors. Hence, the size distribution of ground ore particles of the three feed samples is considered for developing the kinetic model. Sieve analysis data given in Table 6.1 is fitted according to Gates-Gaudin-Schumann (GGS) relation, the most common representation of particle size distribution, given in Eq. 6.5 as shown in Fig. 6.10 [159].

$$y(R_i)=\left(\frac{R_i}{R_{\max}}\right)^m \qquad [6.5]$$

where, $y(R_i)$ is cumulative weight fraction finer than size R_i (radius of smallest uranium ore particle, µm) and R_{max} (radius of largest uranium ore particle, µm) is size of largest particle.

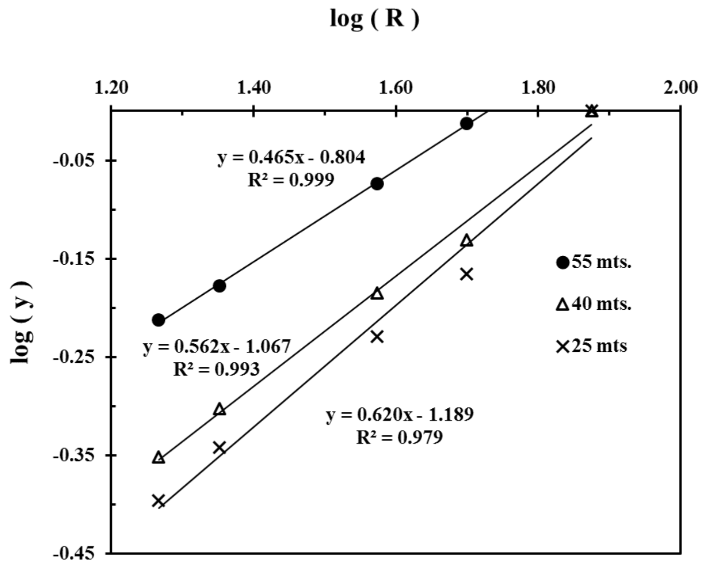

Fig. 6.10 Gates Gaudin Schuhmann plots of three feeds of Tummalapalle ore generated by grinding for different time periods

The plots of all the three products shown in Fig. 6.10 yielded a linear relation with high degree of correlation. From the slope and intercept values of straight lines obtained in Fig. 6.10, the values of m and R_{max} corresponding to three different sized feed samples are tabulated in Table 6.4.

Table 6.4 Particle size distribution parameters of Tummalapalle ore feed samples used in leaching experiments

R_{av} (µm)	Gates Gaudin Schumann distribution parameters	
	m	R_{max} (µm)
12.4	0.46	54
16.2	0.56	79
17.4	0.62	83

The fraction of uranium extracted, α_{sp}, from a single spherical particle of radius R_i in time t, is given by following Eq. 6.6 according to pore diffusion model [160, 161].

$$\alpha_{sp}(t,R_i)=1-\frac{6}{\pi^2}\sum_{K=1}^{\infty}\left(\frac{1}{K^2}e^{-K^2\pi^2 D_{eff}\,t/R_i^2}\right) \qquad [6.6]$$

where, K = 1,2,..... and D_{eff} = Effective diffusivity which can be described by Eq. 6.7.

$$D_{eff}=\frac{D_{AB}\,\varepsilon}{\tau_D} \qquad [6.7]$$

where, ε = porosity and the τ_D = tortuosity factor of the ground ore particle (usually ≈ 2) and D_{AB} = Diffusivity of solute A in solvent B. The weight fraction of material, $\Delta y(R_i)$, in size range between R_i and R_i-ΔR_i, can be obtained by differentiation of the Eq. 6.5.

$$\Delta y(R_i)=\frac{m\,R_i^{m-1}}{R_{\max}^m}\Delta R_i \qquad [6.8]$$

Sum of weight fractions of discrete size intervals between the smallest and largest size should be constrained to 1 as described by Eq. 6.9

$$\sum_{R_i=R_{\min}}^{R_{\max}}\Delta y(R_i)=1 \qquad [6.9]$$

The cumulative fraction extracted after an extraction time period t can be obtained from the Eq. 6.10, by summation of products of fraction extracted in each size R_i according to Eq. 6.6 and the fraction of material in small interval size R_i and R_i-ΔR_i according to Eq. 6.8,

$$\alpha_{cal}(t)=\sum_{R_i=R_{\min}}^{R_{\max}}\left(1-\frac{6}{\pi^2}\sum_{K=1}^{\infty}\left(\frac{1}{K^2}e^{-K^2\pi^2 D_{eff}\,t/R_i^2}\right)\right)\Delta y(R_i) \qquad [6.10]$$

Eq. 6.10 can be solved for the only unknown D_{eff} , given the fraction of uranium extracted (α_{exp}) for each set of leaching conditions. However, in order to fit the experimental data to this model equation, a computer program is written to find the effective diffusion coefficient, D_{eff}, in each experiment. Using m and R_{max} values of the feed sample used in each experiment, the value of $\Delta y(R_i)$ is computed according to Eq. 6.8 for each R_i, using 600 values of $R_i = R_{max}/600$ to R_{max}

with step size of $R_{max}/600$, and stored. The step size used was found to be lower enough to meet the constraint stated as Eq. 6.9. For a value of t, for which α_{exp} is available, sum of the terms of infinite series in Eq. 6.10 is approximated to a finite series sum such that values of K ranged from 1 to k where k is the least value of K whose term in the sum is less than 0.0005 of the cumulative sum of all previous terms. The omitted terms in the finite series make a negligible contribution to the sum. For each value of t, the cumulative conversion, $\alpha_{cal}(t)$, was computed by summing the product of $\alpha_{cal}(t,R_i)$ and $\Delta y(R_i)$ over all the values of R_i (no. of R_i values being 600 as indicated above). Value of D_{eff} is calculated to minimize the error given by Eq. 6.11 for each leaching experiment conducted,

$$Error = \sum_{1}^{N_m} (\alpha_{exp} - \alpha_{cal})^2 \qquad [6.11]$$

where α_{exp} is the experimental value of fractional conversion of uranium, α_{cal}, is the calculated value of fraction reacted using Eq. 6.10, and N_m is the total number of data, which is 4 in the present case, as α_{exp} in each kinetic experiment is available for four time periods of leaching.

The computed values of D_{eff} and the corresponding values of α_{cal} along with α_{exp} for the set of conditions in each experiment are given in Table 6.5. The predicted and experimental conversion values of uranium given in Table 6.5 are plotted as a parity plot in Fig. 6.11.

Table 6.5 The computed values of D_{eff} and the corresponding values of conversion of uranium, α_{cal} along with α_{exp}, for the set of conditions in each experiment on leaching of Tummalapalle ore

Expt. No. TUM/	D_{eff}x10^{11} (calculated)	Time, t	Experimental conversion of uranium, α_{exp}	Calculated conversion of uranium, α_{cal}
	(cm^2/s)	(h)	fraction	fraction
1	0.607	1	0.5	0.47
		2	053	0.53
		4	0.59	0.61
		6	0.61	0.65
2	2.43	1	0.63	0.61
		2	0.71	0.68
		4	0.74	0.76
		6	0.74	0.8
3	2.43	1	0.65	0.6
		2	0.67	0.68
		4	0.75	0.76
		6	0.79	0.8

Expt. No. TUM/	D_{eff}x10^{11} (calculated)	Time, *t*	Experimental conversion of uranium, α_{exp}	Calculated conversion of uranium, α_{cal}
	(cm^2/s)	(h)	fraction	fraction
4	2.025	1	0.61	0.59
		2	0.69	0.66
		4	0.71	0.74
		6	0.73	0.78
5	2.835	1	0.67	0.62
		2	0.73	0.7
		4	0.74	0.77
		6	0.75	0.81
6	2.835	1	0.69	0.62
		2	0.74	0.7
		4	0.73	0.77
		6	0.75	0.81
7	5.67	1	0.78	0.7
		2	0.76	0.77
		4	0.81	0.84
		6	0.82	0.88
8	0.957	1	0.43	0.36
		2	0.47	0.43
		4	0.48	0.51
		6	0.54	0.56
9	1.435	1	0.47	0.4
		2	0.55	0.48
		4	0.51	0.56
		6	0.55	0.61

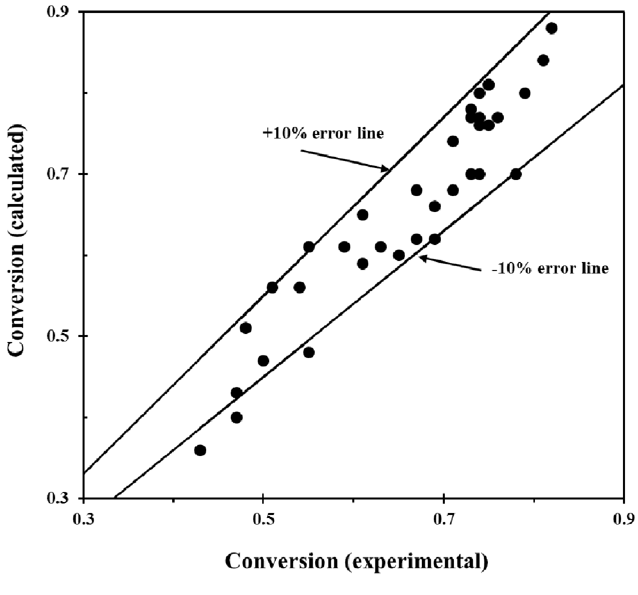

Fig. 6.11 Parity plot of calculated and experimental conversion of uranium in leaching of Tummalapalle uranium ore

Effect of partial pressure of oxygen: The effective diffusivity is found to be increasing from 0.61×10^{-11} cm^2/s to 2.43×10^{-11} cm^2/s when partial pressure of oxygen increased from 4.5 atm to 6.5 atm. This could be due to increase in solubility of oxygen with the increase in partial pressure of oxygen leading to increased concentration gradient between the bulk of the solution and the mineral surface.

Effect of stirring speed: Effective diffusivity is found to be increasing from 2.03×10^{-11} to 2.84×10^{-11} cm^2/s with increase in stirring speed from 573 to 900 rpm which could be due to increased rate of diffusion at higher agitation speeds.

Effect of temperature: Effective diffusivity is found to be increasing with increase in temperature. Arrhenius plot of $\log(D_{eff})$ Vs $1/T$, given in Fig. 6.12, has yielded activation energy (E_a) of 13.7 kJ/mol. Less than 5 kcal/mol (20.9 kJ/mol) of Arrhenius activation energy cross validates the assumption of diffusion controlled mechanism [142].

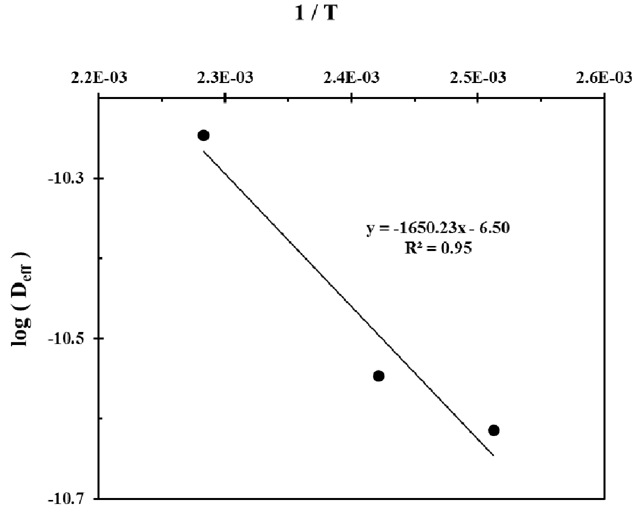

Fig. 6.12 Arrhenius plot of Diffusivity for leaching of uranium from Tummalapalle ore

Effect of particle size: The effective diffusivity is found to be decreasing with increase in particle size. The algebraic function is however incorporated in the leaching model given in Eq. 6.10.

6.1.4 Role of oxygen in leaching of uranium from Tummalapalle ore

In addition to the experiments stated in Section 6.1.1, a few more leaching experiments were carried out using inert gases such as Ar and CO_2 and / or oxygen gas to elicit the role of oxygen during leaching of Tummalapalle uranium ore. It was aimed to demarcate clearly the two portions of uranium present in the ore, (1) the portion (+6) extracted without the need of oxygen, and (2) the portion (+4) for which oxygen is essential for solubilization. The oxygen free environment in the reaction system was provided by using Argon and CO_2 as over pressure gases. An experiment using oxygen gas at optimum pressure and temperature conditions was also carried out for comparison. Each experiment was carried out in the 5-L autoclave (described in Section 4.1.1) according to the procedure described in Section 4.1.3.), using 1 kg dry ground ore (of the average size 25.8 μm with size distribution given in Table 6.1) and 900 ml of solution containing 50 g each of Na_2CO_3 and $NaHCO_3$, maintaining stirring speed at 764 rpm. Experiments were carried out varying temperature and pressure for a residence time of 6 h. The kinetic data of leaching of uranium from Tummalapalle ore at different temperatures and the partial pressures of different gases are plotted in Figs. 6.13 through 6.15.

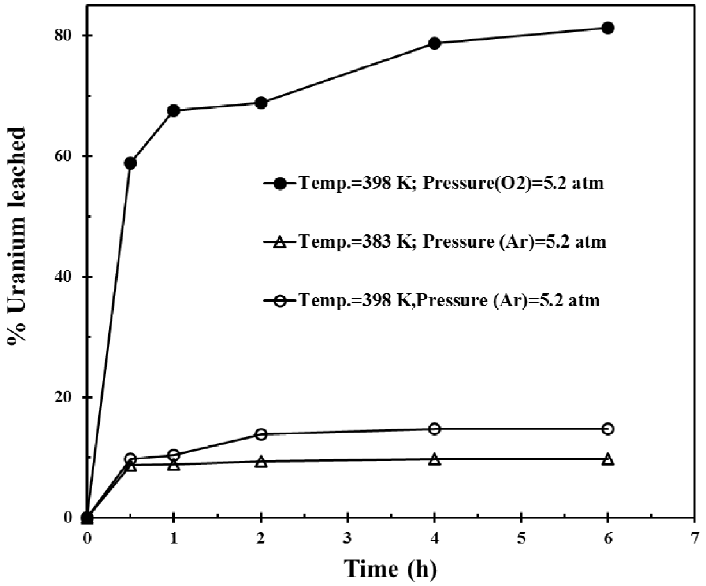

Fig. 6.13. Comparison of uranium extraction from Tummalapalle ore using oxygen and argon gas at different temperatures

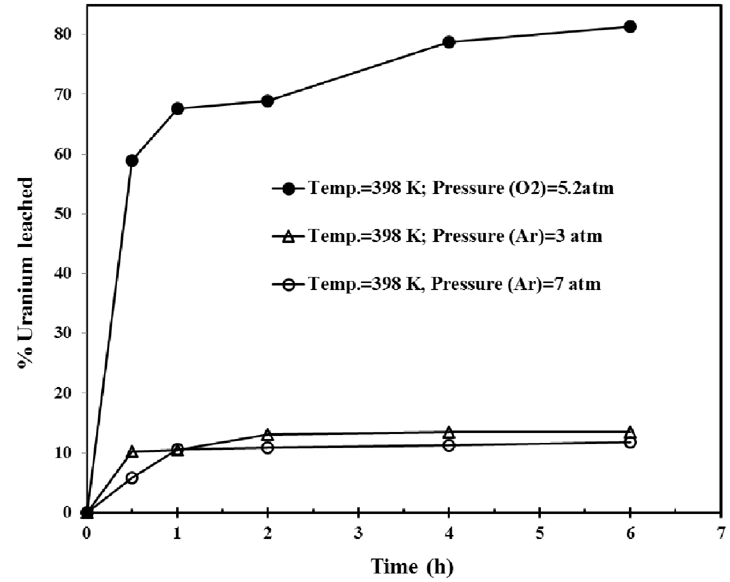

Fig. 6.14. Comparison of uranium extraction from Tummalapalle ore using oxygen and argon gas at different pressures

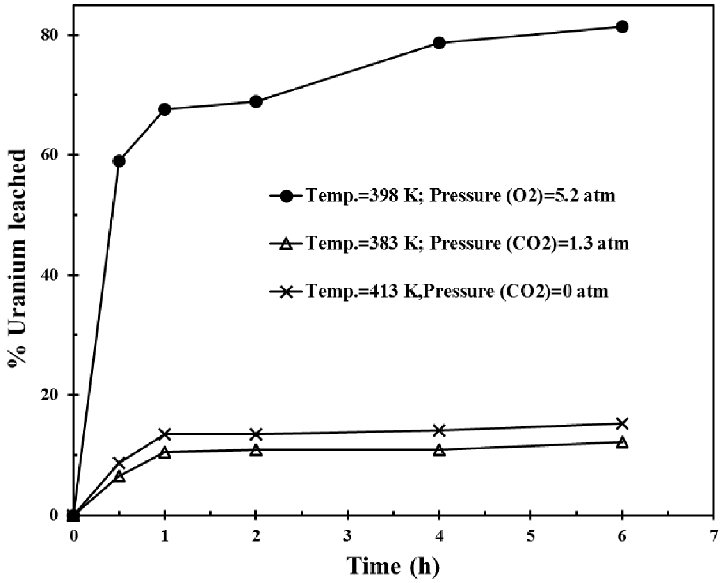

Fig. 6.15 Comparison of uranium extraction from Tummalapalle ore using oxygen and carbon dioxide gas at different temperatures and partial pressures

The leachability of uranium from Tummalapalle ore with oxygen gas under optimum conditions of P_{O2} = 5.2 atm and T=398 K (P_{H2O} = 2.3) is about 80%. When Argon (P_{Ar} = 5.2 atm) is used in place of oxygen, the leachability of uranium slumped to about 10% at temperatures 383 and 398 K (Fig. 6.13). Further, at an optimum temperature of 398 K, the extraction of uranium has not increased beyond 10% even when the partial pressure of Argon increased to 7 atm (Fig. 6.14). When CO_2 is used in place of oxygen, leachability of uranium remained at about 9% at 383 K and P_{CO2} = 1.3 atm (Fig. 6.15).

Ideally, if any ore contains all of its uranium in uranous state as UO_2, no uranium should get dissolved into leach liquor without oxygen gas / a chemical oxidant. However, low level of extraction of uranium is observed when Tummalapalle ore is leached with inert gases, Ar and CO_2, which could be due to presence of small proportion of uranium in uranyl state, as UO_3, in the uraninite present in the ore. Dissolution of UO_3 takes place, if the solution contains likes of ions SO_4^{2-} or CO_3^{2-}, without the need for an oxidizing agent, oxygen gas.

With regard to pyrite, no sodium sulfate is detected in the liquor obtained in the leaching experiments conducted with inert gases, either Ar or CO_2. This indicates that the pyrite has not been leached in the absence of oxygen. Whereas stoichiometric equivalent of sodium sulfate, for complete conversion of pyrite (according to reaction (2.8) in Section 2.1.3.1) present in the ore, is observed in the leach liquor of the experiment conducted with oxygen gas.

6.1.5 Morphological studies on leach residue of Tummalapalle ore

The leach residue of the Tummalapalle ore was concentrated by physical methods described in Fig. 3.4 of Section 3.5, to obtain uranium bearing phase. The Scanning Electron Micrograph of the concentrate is given in Fig. 6.16, along with X-ray spectrographic (EDX) elemental analysis. The uranium phase could not be traced in the leach residue, as was the case with the ore. The same reasons of low grade, low liberation size and fine dissemination of uranium in the ore (elaborated in Section 3.5.3) holds for uranium phase not appearing in the leach residue (in Fig. 6.16).

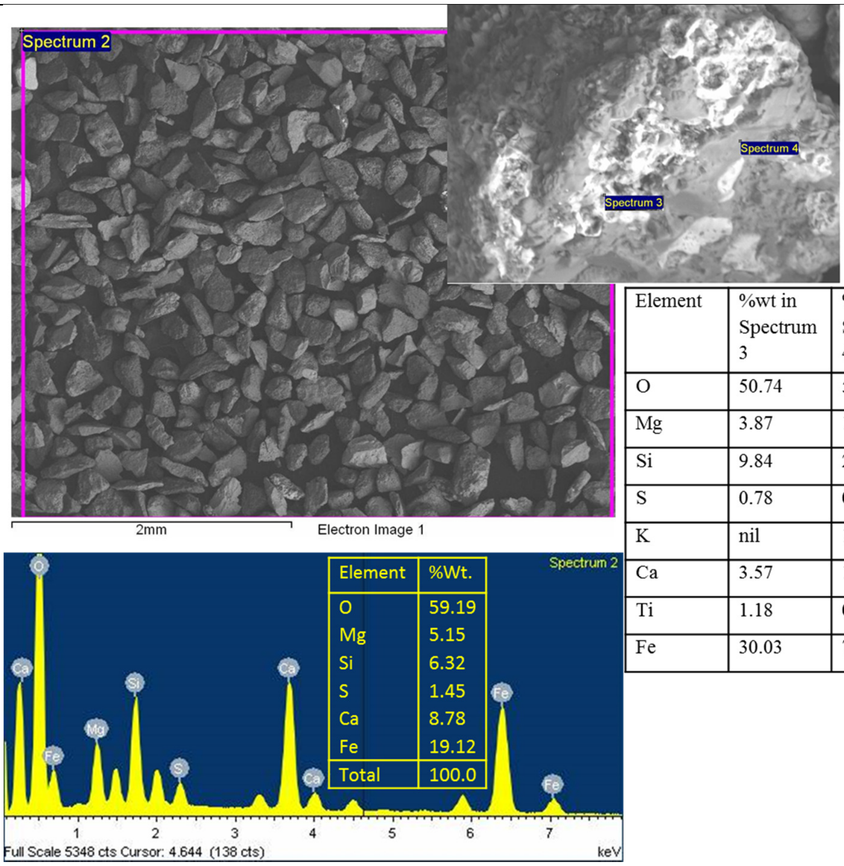

Element	%Wt.
O	59.19
Mg	5.15
Si	6.32
S	1.45
Ca	8.78
Fe	19.12
Total	100.0

Element	%wt in Spectrum 3	%wt in Spectrum 4
O	50.74	52.13
Mg	3.87	1.37
Si	9.84	21.44
S	0.78	0.17
K	nil	15.03
Ca	3.57	1.24
Ti	1.18	0.77
Fe	30.03	7.84

Fig. 6.16. Scanning Electron Micrograph of Methylene Iodide heavies-Non Magnetic (MIH and NM) portion of Tummalapalle leach residue concentrated by physical methods described in Fig. 3.4 in Section 3.5

Fig. 6.16 indicates that all the particles are irregular as in the feed. Dolostone and pyrite minerals are indicated by the presence of Mg, Ca, Fe and S. Magnified image of Fig. 6.16 (EDX of spectrum 3 and 4) shows that sulfur content is much less compared to that in the feed grains, 8.65% S, shown in Fig. 3.12[A] of Section 3.5.3, indicating near complete dissolution of pyrite mineral during leaching of Tummalapalle uranium ore.

6.1.6 Conclusion

The kinetic data of extraction of uranium from Tummalapalle ore using alkaline leaching was generated varying the parameters: partial pressure of oxygen, temperature, particle size, and stirring speed. The experimental data fitted well a leaching model with mixed control of surface chemical reaction and diffusion through the inert particle pores. Alternatively, a pore diffusion control model incorporating particle size distribution is developed. This model represents the reality of the leaching of Tummalapalle ore more closely. The conversions of pyrite and uranium in the absence of oxygen during leaching yielded 0 and <10%, respectively. This indicates that the U(VI) oxidation state in Tummalapalle ore could be <10%. The leaching studies indicate near complete (about 100%) and about 80% conversion of pyrite and uranium, respectively, at optimum conditions: temperature = 398 K and total pressure using oxygen = 7.5 atm. The uranium could not be traced in SEM images due its low concentration, low liberation, and fine dissemination. However, the near complete dissolution of pyrite is established by SEM pictures of the feed and leach residue.

6.2 GOGI URANIUM ORE

6.2.1 Materials and Methods

Leaching experiments were conducted using the 5-L autoclave, according to the procedure described in Section 4.1.3. The variables and their ranges considered for study were fixed based on previous studies [145]. Each experiment was conducted using 1 kg Gogi ore maintaining a pulp of 50% solids (by weight) concentration. The effects of variables studied are partial pressure of oxygen (p_{O2}) in the range 0.15 to 3 atm, stirring speed (s) from 573 to 900, average particle size (D) between 61 and 136 μm, concentration of sodium carbonate ([Na_2CO_3]) from 0.47 to 0.94 M and temperature (T) in the range 343 to 383 K. Three feed samples of different size were generated by wet grinding of the rock pieces (-1/4” size) of the Gogi ore for different time periods (15, 25 and 40 minutes) in a laboratory ball mill. The size distributions of these samples were determined by wet sieving, which are given in Table 6.6. The ore used in the present leaching experiments analyzed, on an average, 0.21% U_3O_8 and 2.7% S by fluorimetry and gravimetry respectively.

Table 6.6 Sieve analyses of three feed samples of Gogi ore generated by wet grinding for three different time periods

Grinding time (min)	15	25	40
Size (μm)	Cumulative % wt. passing		
425	100.0	100.0	100.0
150	63.6	73.6	93.9
100	53.2	60.9	81.5
75	46.9	54.7	71.8
45	38.4	44.5	59.2
37	35.2	41.0	54.5
Mean size (μm)	136	112	61

6.2.2 Results

The fractional conversion of uranium (α_{exp}) in each leaching experiment is calculated using the average back calculated feed assay (0.21% U_3O_8) and the leach liquor concentration of U_3O_8 measured at different time intervals. Results of leaching experiments are given in Table 6.7., along with the corresponding set of experimental conditions.

Table 6.7 Results of the leaching experiments on Gogi uranium ore

Expt. No. GOGI/	Partial Pressure of O_2, (P_{O_2})	Stirring speed, *(s)*	Average Particle size, *(D_{av})*	Temp., *(T)*	Concentration of sodium carbonate, (Na_2CO_3)	Time, *(t)*	Experimental Conversion of U_3O_8, (α_{exp})
	(atm)	rpm	μm	K	g mol/L	(min)	fraction
1*	0.15	764	112	363	0.66	60	0.64
						120	0.77
						240	0.82
2	0.15	764	112	343	0.66	60	0.52
						120	0.59
						240	0.69
3	0.15	764	112	353	0.66	60	0.54
						120	0.71
						240	0.74
4	0.15	764	112	373	0.66	60	0.69
						120	0.76
						240	0.83
5	0.15	764	112	383	0.66	60	0.73
						120	0.78
						240	0.83
6	0.15	764	136	363	0.66	60	0.58
						120	0.62
						240	0.70
7	0.15	764	61	363	0.66	60	0.76
						120	0.85
						240	0.90
8	0.5	764	112	363	0.66	60	0.81
						120	0.89
						240	0.91

Expt. No. GOGI/	Partial Pressure of O_2, (P_{O_2})	Stirring speed, *(s)*	Average Particle size, *(D_{av})*	Temp., *(T)*	Concentration of sodium carbonate, (Na_2CO_3)	Time, *(t)*	Experimental Conversion of U_3O_8, (α_{exp})
	(atm)	rpm	µm	K	g mol/L	(min)	fraction
9	1	764	112	363	0.66	60	0.83
						120	0.88
						240	0.91
10	2	764	112	363	0.66	60	0.73
						120	0.90
						240	0.90
11	3	764	112	363	0.66	60	0.66
						120	0.79
						240	0.82
12	0.15	573	112	363	0.66	60	0.50
						120	0.67
						240	0.70
13	0.15	900	112	363	0.66	60	0.63
						120	0.78
						240	0.85
14	0.15	764	112	363	0.47	60	0.62
						120	0.67
						240	0.71
15	0.15	764	112	363	0.94	60	0.75
						120	0.84
						240	0.89

*Base experiment, conducted at the constant values of each variable, when other parameters are changed

6.2.3 Discussion

6.2.3.1 Stochastic model: Since the dissolution reaction of uranium, given by reactions (2.4) and (2.5) in Section 2.1.3.1, are non-elementary, the rate equation cannot be written by mere stoichiometry. Hence, a rate equation (Eq. 6.12) for first order reaction for the case of batch leaching process carried out with excess leachant (solution of Na_2CO_3) is considered:

$$M\ (t) = e^{-kt} \qquad [6.12]$$

M(t) is the unleached mass fraction of uranium remaining in solids at time t. Many times, first order rate does not adequately represent the leaching kinetic data obtained in the experiments. Higher order reaction rate equations have little foundation other than analogy with that of first order rate equation [72]. In fact, the particles of the ground ore that are subjected to leaching are not identical but have the distributed properties like size, density, mineralogy, morphological properties, uranium content etc. Hence, it is appropriate to assume that these species with distributed attributes would have distributed first order rate constant,k, in Eq. 6.12.

A few population balance models addressing the heterogeneous nature of the leaching feed material are also available in literature [111, 112]. Several references are available in the literature on flotation kinetics following distributed first order rate constant [72, 162 – 164], from which analogy is drawn for developing model equation for batch leaching of Gogi ore with distributed first order rate constant. Eq. 6.12 can be extended to the multi particles with distributed rate constant, k, as Eq. 6.13 given below.

$$M(t) = \sum_{i=1}^{n} M_i(t) = \sum_{i=1}^{n} M_i(0) e^{-k_i t} \qquad [6.13]$$

$M_i(0)$ = Initial fraction of material with rate constant k_i, n is not known apriori and $k_i < k_{i+1}$

$\sum_{i=1}^{n} M_i(0) = M(0) =$ % uranium in the feed

The continuous distribution model of the Eq.6.13 takes the form of Eq.6.14, assuming that the rate constant, k_i, varies between 0 and infinity, and M is dependent on intrinsic property, rate constant (k) and external variable time, t. The first order rate applies for each mass fraction M, with corresponding rate constant, k.

$$M(k,t) = \int_{0}^{\infty} M(k,0) e^{-kt} dk \qquad [6.14]$$

The species distribution function, M(k,0) is assumed to be a gamma function, given by Eq. 6.15.

$$M(k,0) = \frac{1}{a^b \Gamma(b)} k^{b-1} e^{-\frac{k}{a}}, where\, k \geq 0, a\,(scale\ parameter) > 0\, and\, b(\,shape\ parameter) > 0 \qquad [6.15]$$

Substituting the above gamma distribution function in Eq. 6.14 and performing integration yields Eq. 6.16.

$$M(t) = \left(\frac{1}{1+at} \right)^{b} \qquad [6.16]$$

Interpolation is performed on the kinetic experimental data to generate more data points for developing accurate mathematical model of leaching. The set of 18 experimental values of M(t) generated for each experiment, by graphical interpolation of experimental results, is given in Table 6.8.

Table 6.8 The unleached mass fractions of uranium at different durations of time in the leaching experiments on Gogi ore

Time (h)		0	0.2	0.4	0.6	0.8	1	1.25	1.5	1.75	2	2.5	3	3.5	4	4.5	5	5.5	6
Expt. No. GOGI/	1	1	0.95	0.8	0.65	0.5	0.3614	0.32	0.29	0.25	0.2354	0.22	0.2	0.19	0.179	0.18	0.18	0.18	0.1833
	2	1	0.95	0.85	0.75	0.6	0.46	0.455	0.43	0.42	0.414	0.39	0.35	0.35	0.3127	0.3127	0.3127	0.3127	0.3127
	3	1	0.95	0.8	0.7	0.55	0.459	0.4	0.36	0.32	0.2927	0.285	0.285	0.285	0.2655	0.25	0.23	0.22	0.238
	4	1	0.93	0.8	0.6	0.5	0.3031	0.28	0.26	0.25	0.2404	0.21	0.2	0.18	0.1699	0.1699	0.1699	0.1699	0.1699
	5	1	0.88	0.78	0.6	0.4	0.2755	0.26	0.2	0.22	0.2169	0.2	0.19	0.18	0.1709	0.1709	0.1709	0.1709	0.1709
	6	1	0.88	0.7	0.55	0.45	0.3359	0.3	0.28	0.24	0.2016	0.19	0.18	0.17	0.1758	0.1758	1758	0.1758	0.1758
	7	1	0.84	0.7	0.6	0.4	0.2432	0.21	0.19	0.18	0.1471	0.14	0.13	0.11	0.0994	0.0994	0.0994	0.0994	0.0994
	8	1	0.83	0.65	0.54	0.35	0.1871	0.17	0.16	0.14	0.1152	0.1	0.09	0.08	0.0896	0.0896	0.0896	0.0896	0.0896
	9	1	0.81	0.72	0.53	0.33	0.1693	0.16	0.15	0.13	0.1242	0.12	0.1	0.095	0.0962	0.0962	0.0962	0.0962	0.0962
	10	1	0.88	0.75	0.59	0.4	0.2698	0.22	0.18	0.13	0.0979	0.0979	0.0979	0.0979	0.0979	0.0979	0.0979	0.0979	0.0979
	11	1	0.9	0.8	0.65	0.55	0.4195	0.4	0.4	0.39	0.3814	0.37	0.35	0.33	0.2966	0.28	0.27	0.26	0.2542
	12	1	0.89	0.8	0.7	0.6	0.5	0.47	0.42	0.38	0.335	0.32	0.31	0.335	0.3	0.3	0.3	0.3	0.3
	13	1	0.82	0.72	0.6	0.48	0.2735	0.26	0.24	0.21	0.188	0.17	0.14	0.12	0.1026	0.1026	0.1026	0.1026	0.1026
	14	1	0.84	0.74	0.62	0.51	0.381	0.37	0.36	0.34	0.3333	0.32	0.31	0.29	0.2857	0.2857	0.2857	0.2857	0.2857
	15	1	0.82	0.71	0.55	0.45	0.2475	0.23	0.21	0.18	0.1589	0.14	0.13	0.12	0.1147	0.1147	0.1147	0.1147	0.1147

Two constants of gamma species distribution, a (scale parameter) and b (shape parameter), are obtained by least square regression fitting of the nonlinear Eq. 6.16 to the experimental values, given in Table 6.8, of unleached fraction of uranium, M(t), at different time periods, t. The two parameters, computed using MATLAB® software, for each experiment are given in Table 6.9 along with the corresponding goodness of fit. The goodness of fit is found to be always greater than 0.92. High value of goodness of fit indicates that the popular gamma distribution of the leaching rate constant satisfactorily represents the kinetics of alkaline leaching of Gogi uranium ore.

Table 6.9 Computed shape and scale parameters (b,a) of gamma species distribution of rate constant of leach feed at different conditions of leaching

Expt. No. GOGI/	Shape parameter (b)	Scale parameter (a)	Goodness of fit (R^2)
1	1.167	0.9629	0.94
2	0.5616	1.706	0.94
3	0.7953	1.306	0.95
4	1.153	1.065	0.94
5	1.059	1.371	0.92
6	0.9605	1.548	0.96
7	1.983	0.6882	0.96
8	2.515	0.5996	0.96
9	2.342	0.6525	0.94
10	3.606	0.335	0.95
11	0.5494	2.242	0.95
12	0.5704	1.899	0.96
13	1.76	0.7164	0.97
14	0.4767	3.617	0.95
15	1.619	0.8786	0.96

In order to show the effect of the five leaching variables on the gamma species distribution of first order rate constant, the % mass fraction of leach feed with rate constant, k, as gamma distribution function is plotted in Figs. 6.17 through 6.21, using the parameter values tabulated in Table 6.9.

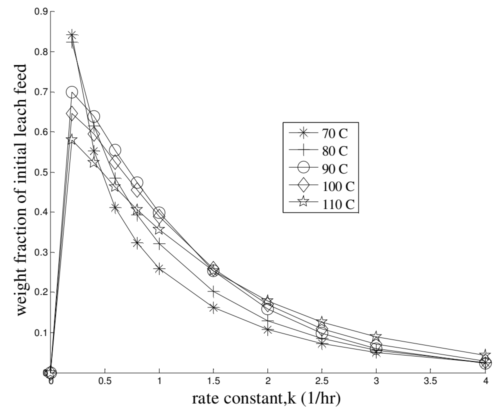

Fig. 6.17 Distribution of mass fraction of leach feed with rate constant at different temperatures of leaching

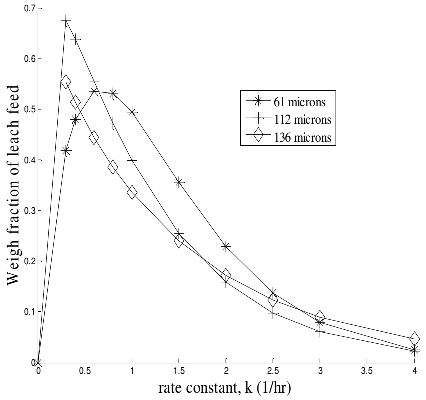

Fig. 6.18 Distribution of mass fraction of leach feed of different particle sizes with rate constant

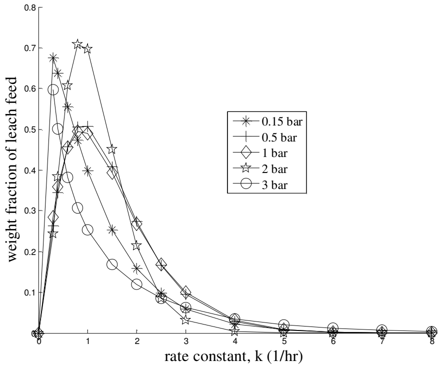

Fig. 6.19 Distribution of mass fraction of leach feed with rate constant at different partial pressures of oxygen during leaching

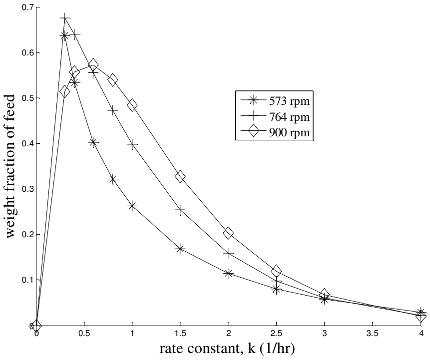

Fig. 6.20 Distribution of mass fraction of leach feed with rate constant at different stirring speeds during leaching

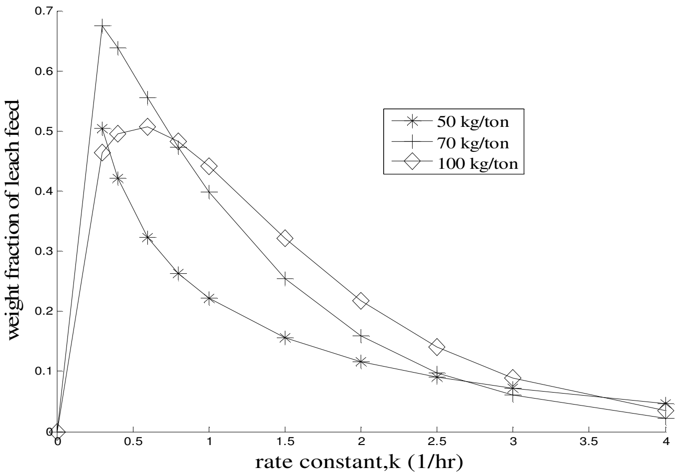

Fig. 6.21 Distribution of mass fraction of leach feed with rate constant at different reagent dosage of Na_2CO_3 during leaching

It is evident from Fig. 6.17, that at lower temperatures, more weight% of leach feed has lower rate constant which implies that average rate constant of all the material is increasing with increasing temperature. Similar observations from Figs. 6.18 to 6.21, reveal that the average rate constant is increasing with decreasing size, increasing partial pressure of oxygen, increasing stirring speed and increasing concentration of Na_2CO_3 in the lixiviant. The effects of temperature, particle size, partial pressure of oxygen, stirring speed and the lixiviant concentration on the gamma distribution of weight fraction of ore material with rate constant is found to be in good agreement with the theory of kinetics of leaching.

6.2.3.2 Topochemical model incorporating particle size distribution: Autoclave batch leaching of uranium ore particles may be represented by the conventional shrinking core model, the governing equation of which depends on one or more of the controlling mechanisms: (1) film diffusion (2) chemical reaction at the surface (3) ash diffusion of reactants/products [39]. In case of agitation leaching, as is the present case, the film layer on the particles is continuously replaced which leads to fast diffusion of solutes in the film. Hence film diffusion is not considered to be controlling the leaching reaction. Also, ash diffusion controlled mechanism is ignored, since all the reaction products, of uranium dissolution reactions (2.4) and (2.5) (given in Section 2.1.3.1), are soluble and leave no ash product. The leaching rate is investigated with surface chemical reaction control mechanism governed by Eq. 6.17 [165].

$$1-(1-\alpha)^{\frac{1}{3}}=k\,t \qquad [6.17]$$

where α = conversion at time t (min), and k = overall rate constant (min^{-1}). k is a function of concentrations of reactants, temperature, stirring speed, size of particles, and many other properties of the system. A plot of $1-(1-\alpha_{exp})^{\frac{1}{3}}\ vs\ t$ at different temperatures indicated that uranium dissolution does not follow the linear kinetic model of Eq. 6.17. Neither did it follow when changing other parameters such as partial pressure of oxygen, particle size, concentration of Na_2CO_3. Hence, an attempt has been made to fit the experimental data, incorporating particle size distribution into Eq. 6.17 using the procedure adopted by Gbor and Jia [126]. Few other authors also have published experimental evidence that leaching models without consideration of particle size distribution are prone to erroneous conclusions [112, 124, 125]. However, variation of particle shape is not included in the present study owing to the difficulty in obtaining the shape distribution. Hence, one of the limitations of the model presented here is that particles were assumed to be spherical.

For mono-sized particles of diameter D, undergoing shrinking core dissolution, the rate constant k is given by Eq. 6.18.

$$k = \frac{k_n}{D} \tag{6.18}$$

where k_n is independent of D. Eqs.6.17 and 6.18 may be combined to get the conversion, $\alpha(D,t)$, as a function of diameter, D and time, t to get

$$\alpha(D,t) = 1 - \left(1 - \frac{k_n}{D}t\right)^3 \tag{6.19}$$

For a group of particles of various sizes divided into discrete size ranges,

$$Fraction\ reacted = \sum_D \big(\alpha(D,t)\big)(Mass\ fraction\ of\ size\ D) \tag{6.20}$$

This equation transforms as the following for a continuous distribution of particles,

$$Fraction\ reacted = \int_0^{D_{max}} \big(\alpha(D,t)\big)(p(\,D))dD \tag{6.21}$$

where $p(D)$ is the particle size density function based on mass of particles. D_{max} is the size of largest particle in the system. As there could be always few particles less than certain size that react fully in a given time, an intermediate diameter, D_t is introduced such that

$$\alpha(D,t) = 1,\ \ 0 < D < D_t \tag{6.22}$$

Eq. 6.22 implies that at any time (t), all particles with sizes (D) less than D_t are fully reacted and thus have a conversion value of 1, which when substituted in Eq. 6.19 yields $D_t = k_n t$. But all the particles greater than D_t are partially reacted with a conversion given by Eq. 6.19 with the limits of particle size, *D*, as given in Eq. 6.23.

$$\alpha(D,t) = 1 - \left(1 - \frac{k_n}{D}t\right)^3 \; , \; D_t < D < D_{max} \qquad [6.23]$$

Popular Gates Gaudin Schuhmann (GGS) size distribution function is chosen for *p(D)* derived from *f(D)* given in Eq. 6.24 [159].

$$f(D) = \left(\frac{D}{D_{max}}\right)^m \qquad [6.24]$$

The GGS model fitted very well the three feed size distributions given in Table 6.6, as shown in Fig. 6.22. The parameters of the GGS model are given in Table 6.10.

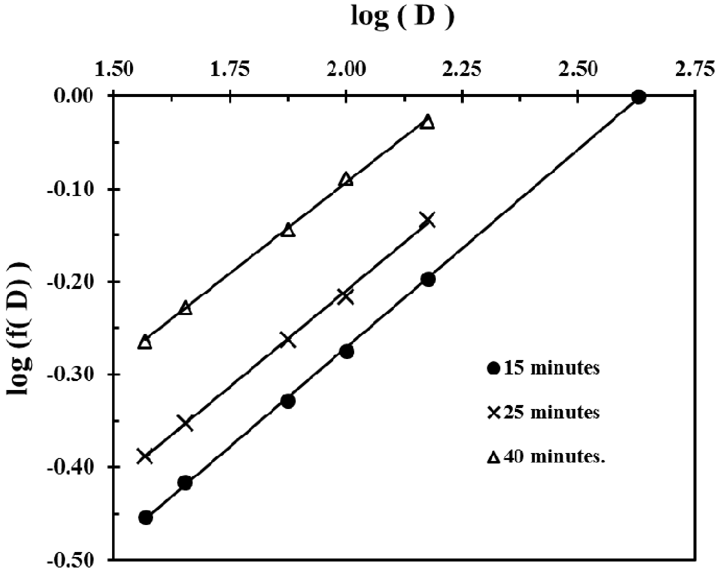

Fig. 6.22 Gates Gaudin Schuhmann plots of the three feed particle size distributions of Gogi ore generated by grinding for different time periods

Table 6.10 Particle size distribution parameters of three feed samples used in leaching experiments

D_{av} (μm)	Gates Gaudin Schumann distribution parameters	
	m	D_{max} (μm)
61	0.4	175
112	0.4	325
136	0.4	431

Differentiation of Eq. 6.24 yields *p(D)*:

$$p(D) = m\frac{D^{m-1}}{D_{max}^{m}} \qquad [6.25]$$

Substituting Eqs. 6.22, 6.23 and 6.25 into Eq. 6.21 gives

$$Fraction\ reacted = \alpha = \int_{0}^{D_t}(1)(m\frac{D^{m-1}}{D_{max}^{m}})dD + \int_{D_t}^{D_{max}}\left(1-(1-\frac{k_n}{D}t)^3\right)(m\frac{D^{m-1}}{D_{max}^{m}})dD \qquad [6.26]$$

where m and D_{max} can be calculated for a given sample and then be substituted for each of the experiments. If conversion, α, is known for given time t, Eq. 6.26 can be solved for the only unknown k_n which is unique to each experiment. However, to fit the leach data to Eq. 6.26, a MATLAB® program was written to find the value of k_n, which minimizes the error given by

$$Error = \sum_{1}^{N}(\alpha_{exp} - \alpha_{cal})^2 \qquad [6.27]$$

where α_{exp} is the experimental value of fraction reacted, α_{cal} is the calculated value of fraction reacted using Eq. 6.26, and N is the total number of data, which is 4 in the present case, as α_{exp} in each kinetic experiment is available for 0 and three time periods. k_n is fitted by trial and error method and α_{cal} is calculated from Eq. 6.26 for each experiment are given in Table 6.11.

Table 6.11 Results of laboratory kinetic leaching experiments along with computed reaction rate constant (k_n, µm/min) and conversion of U_3O_8

Expt. No. GOGI/	Time, *(t)*	Experimental Conversion of U_3O_8, (α_{exp})	Rate constant, (k_n)	Calculated Conversion of U_3O_8, (α_{cal})
	(min)	fraction	(µm/min)	fraction
1*	60 120 240	0.64 0.77 0.82	0.25	0.60 0.74 0.88
2	60 120 240	0.52 0.59 0.69	0.11	0.46 0.59 0.72
3	60 120 240	0.54 0.71 0.74	0.17	0.53 0.66 0.80
4	60 120 240	0.69 0.76 0.83	0.29	0.63 0.77 0.89

Expt. No. GOGI/	Time, (*t*)	Experimental Conversion of U_3O_8, (α_{exp})	Rate constant, (k_n)	Calculated Conversion of U_3O_8, (α_{cal})
	(min)	fraction	(μm/min)	fraction
5	60	0.73	0.32	0.65
	120	0.78		0.79
	240	0.83		0.92
6	60	0.58	0.2	0.49
	120	0.62		0.63
	240	0.70		0.77
7	60	0.76	0.23	0.72
	120	0.85		0.85
	240	0.90		0.96
8	60	0.81	0.59	0.77
	120	0.89		0.90
	240	0.91		0.98
9	60	0.83	0.6	0.78
	120	0.88		0.90
	240	0.91		0.98
10	60	0.73	0.47	0.73
	120	0.90		0.86
	240	0.90		0.96
11	60	0.66	0.29	0.63
	120	0.79		0.77
	240	0.82		0.89
12	60	0.50	0.13	0.48
	120	0.67		0.61
	240	0.70		0.75
13	60	0.63	0.25	0.60
	120	0.78		0.74
	240	0.85		0.88
14	60	0.62	0.17	0.53
	120	0.67		0.66
	240	0.71		0.80
15	60	0.75	0.42	0.71
	120	0.84		0.84
	240	0.89		0.95

A plot of conversion vs time showing actual data and model fit (intermediate times included), is shown in Fig. 6.23 for some key experiments: # GOGI/1 (base experiment), # GOGI/2(minimum conversion) and # GOGI/9 (maximum conversion). The predicted and experimental conversions of all the experiments plotted as a parity plot in Fig. 6.24, were in very good agreement. Small variations could be due to non-ideal conditions such as the irregular shape of particles, which is not considered in the present study.

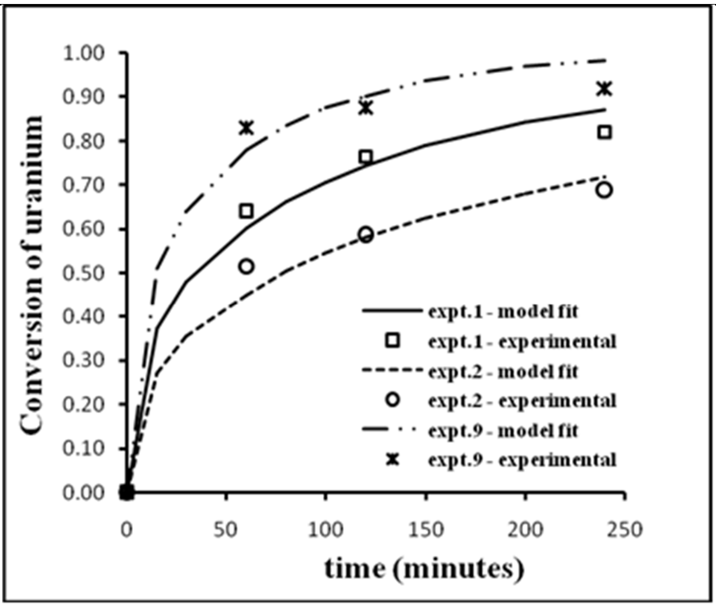

Fig. 6.23 Conversion vs. time plots of actual data and model fit for some key experiments

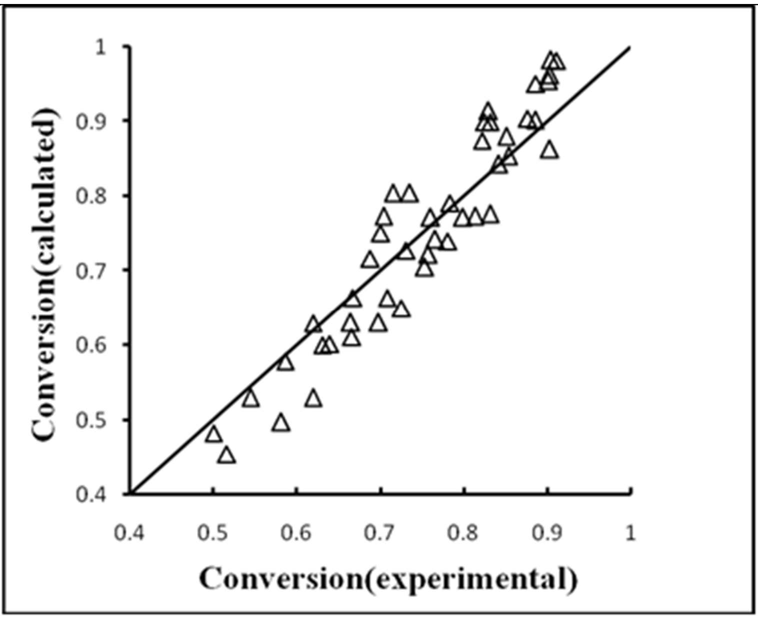

Fig. 6.24 Parity plot of calculated and experimental conversion of uranium in different experiments

The rate constant, k_n, which is independent of particle diameter D, can now be considered as a function of partial pressure of oxygen, temperature and concentration of Na_2CO_3. Effect of stirring speed is not included since the leaching is assumed to be chemical reaction controlled. The temperature dependent term of the function is assumed to be in the form of Arrhenius expression. The orders of the reaction with respect to each variable parameter can be calculated using the k_n values for each set of combination of variables using Eq. 6.28.

$$k_n = k_0(p_{O_2})^n[Na_2CO_3]^q e^{-\frac{E_a}{RT}} \qquad [6.28]$$

On a log-log plot, Eq. 6.28 would yield a straight line with p_{O_2} or [Na_2CO_3] or *1/T* as the X variable and k_n as the Y variable.

Effect of Stirring speed: The conversion of uranium with time at different stirring speeds was plotted in Fig. 6.25. The leaching rate increased with increase in stirring speed from 573 rev/min to 764 rev/min, whereas, further increase in stirring speed to 900 rev/min had not changed the dissolution of uranium significantly. Hence, it may be concluded that stirring speed of 764 rev/min is required to suspend solid particles and also sufficient to eliminate the external particle film resistance.

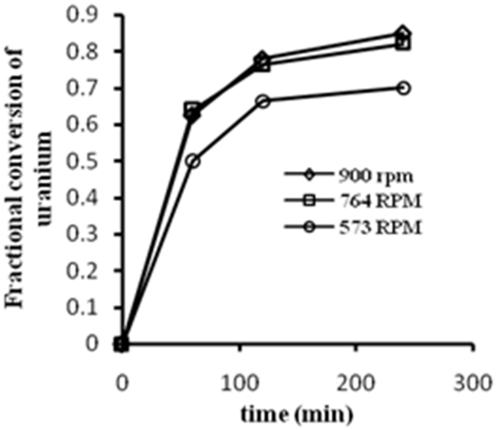

Fig. 6.25 Effect of stirring speed on uranium leaching from Gogi ore

Effect of particle size: The effect of particle size was incorporated in Eqs.6.18 and 6.25. The overall rate constant, $k=k_n/D$, is inversely proportional to the diameter of the particles while k_n is independent of the diameter of particle.

Effect of Temperature: Results of experiments #GOGI/1 through #GOGI/5 were plotted in Fig. 6.26 to find the effect of temperature on the rate of reaction according to the Arrhenius equation. The activation energy is determined to be 29.3 kJ/mol from the slope of the straight line obtained in the Arrhenius plot. As the activation energy is larger than 5 kcal/mol (20.9 kJ/mol), it may be concluded that leaching predominantly follows reaction-controlled dissolution kinetics [156]. The activation energy found by several other authors for dissolution of uraninite ranged from 33.6 to 54.3 kJ/mol [37, 38, 58, 91B]. The value recorded in present study is at the lower end of the range.

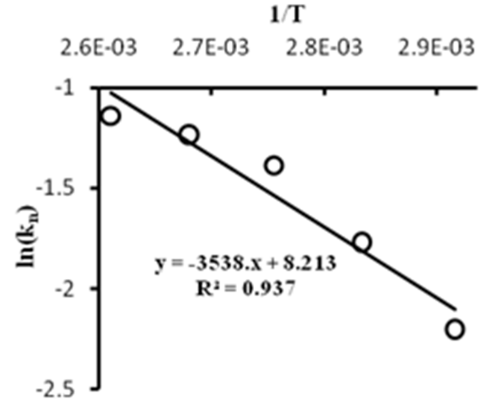

Fig. 6.26. Arrhenius plot for effect of temperature on leaching of uranium from Gogi ore

Effect of partial pressure of oxygen: Several authors have observed that the rate of dissolution of uranium mineral, present either in pure form or in ores, increased monotonously with increasing oxygen pressure, with a reaction order of 0.5 [36, 37, 85]. De Pablo et al. [34] observed the reaction order to be 1 using a thin layer flow-through reactor. However, the results of present study, of experiments # GOGI/1 and # GOGI/8 to # GOGI/11, shows that the rate constant, k_n, increased with the increase in partial pressure of oxygen up to about 1 atm, beyond which it decreased. This is due to the higher pyrite (5% by wt.) of the Gogi uranium ore than desirable limit of 0.045%. The desirable limit of pyrite for dissolution of total uranium in a given ore is calculated from the uranium content of the ore and the stoichiometry of reactions (2.5a) and (2.5b) (given in Section 2.1.3.1), considering the fact that the OH^- ion produced according to reaction (2.5a) would be neutralized by $NaHCO_3$ produced by pyrite (reaction 2.8) according to reaction (2.5b). The ores cited in literature had either no or lower pyrite than the desirable limit. The decreasing dissolution rate of uranium at increased partial pressures of oxygen beyond 1 atm is due to the higher dissolution of pyrite. Higher dissolution of pyrite consumes more sodium carbonate, which results in lower than minimum concentration of carbonate ions required for uranium leaching. The leach liquors in the experiments at more than 1 atm partial pressure were found to have pH values less than 9, indicating lower concentration of carbonate ions. It is reported in the literature that at these pH values, the rate of extraction of uranium is lower [108]. Consequently, the plot of $ln(k_n)$ Vs $ln(p_{O2})$, drawn in Fig. 6.27 to predict the order of reaction with respect to partial pressure of oxygen did not yield a straight line but a quadratic curve.

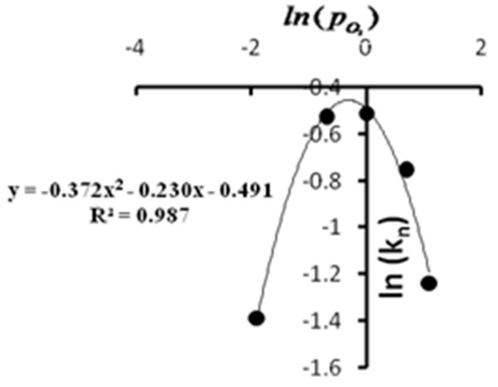

Fig. 6.27 Plot for reaction order with respect to partial pressure of oxygen

It is interesting to note that if one carries out leaching of Gogi ore between 0.5 atm and 1 atm partial pressure of oxygen at 90°C, dissolution of uranium is maximum and that of pyrite minimum. Minimal dissolution of pyrite obviates the removal of pyrite from the ore prior to leaching. The conversions of uranium and pyrite obtained at different oxygen pressures are given in Table 6.12. This is because uranium dissolves more rapidly than pyrite below 1 atm oxygen at 90°C, since the activation energy for dissolution of uranium is lower than that of pyrite. The activation energy of pyrite reported by Ciminelli and Osseo-Asare [92] is 14.6 kcal/mol (61 kJ/mol) under alkaline leaching conditions which are nearly the same as those used in the present study. High and low dissolution of uranium and pyrite minerals, respectively, is also evidenced by high and low differences in uranium and sulfur concentrations between the feed and leach residue, that can be seen from EDX analyses of scanning electron micrographs given in Figs. 3.13[A],[B] (in Section 3.5.3) and 6.32.

Table 6.12 Conversions of uranium and pyrite at different oxygen pressures (Leaching conditions: 0.66 g/L Na_2CO_3, temperature = 363 K, residence time = 240 min)

Oxygen pressure (atm)	Initial pH	Final pH	Conversion of uranium (%)	Conversion of pyrite (%)
< 0.5	10.5	>10	<90	<40
0.5 to 1	10.5	>10	>90	<40
> 1	10.5	< 9	<90	>40

Effect of the concentration of sodium carbonate: In Fig. 6.28, the rate constant, k_n, from experiment # GOGI/14, # GOGI/1 and # GOGI/15 was plotted against the Na_2CO_3 concentration. The order with respect to the Na_2CO_3 concentration was found to be 1.28, indicating that the conversion of uranium increases, with increasing concentration of Na_2CO_3, as observed by other workers [37, 108].

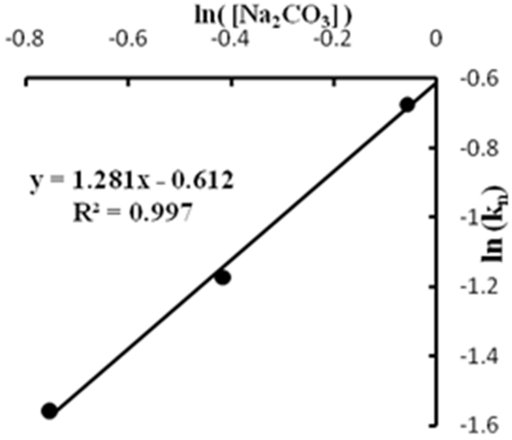

Fig. 6.28 Plot for reaction order with respect to concentration of sodium carbonate

Correlation of rate constant: The order of leaching reaction found for each variable from the plots in Figs. 6.26 through 6.28 transforms Eq. 6.28 to

$$k_n = k_0[Na_2CO_3]^{1.28}e^{-\ln(p_{O_2})(0.37\ln(p_{O_2})+0.23)}e^{-\frac{29300}{RT}} \qquad [6.29]$$

In order to find k_0 given in Eq. 6.29, a linear fit is established in Fig. 6.29 between the rate constant, k_n, and the product term $[Na_2CO_3]^{1.28}e^{-\ln(p_{O_2})(0.37\ln(p_{O_2})+0.23)}e^{-\frac{29300}{RT}}$ at different values of variable parameters. Slope of the straight line, k_0, was determined to be 17198.

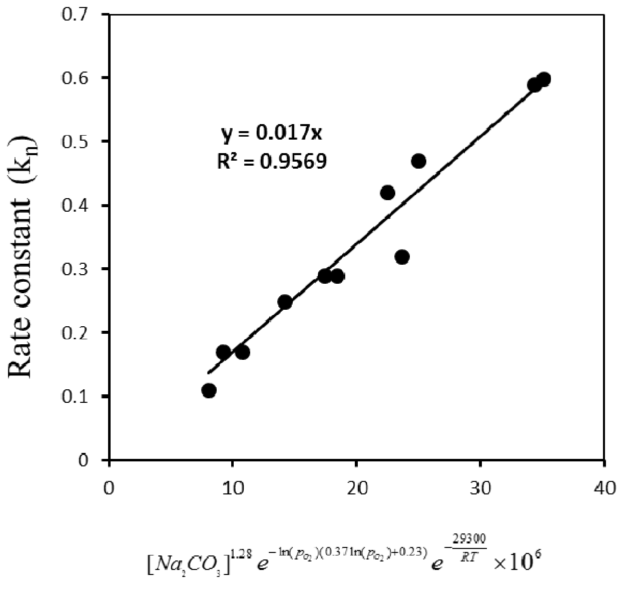

Fig. 6.29 Linear fit of rate constant (k$_n$) against the product term

Overall kinetic rate equation: Alkaline leaching kinetics of Gogi uranium ore indicate that surface chemical reaction is the rate controlling step modeled by the shrinking core model coupled with particle size distribution represented by Gates Gaudin Schumann density function. The overall equation for conversion of uranium is given by

$$Fractional\ conversion = \int_0^{D_t} (m\frac{D^{m-1}}{D_{max}^m})dD + \int_{D_t}^{D_{max}} \left(1-\left(1-\frac{k_n}{D}t\right)^3\right)(m\frac{D^{m-1}}{D_{max}^m})dD \qquad [6.30]$$

where $k_n = 17198\,[Na_2CO_3]^{1.28} e^{-\ln(p_{O_2})(0.37\ln(p_{O_2})+0.23)} e^{-\frac{29300}{RT}}$ and $D_t = k_n t$.

6.2.4 Role of oxygen on leaching of uranium from Gogi ore

The leaching experiments were conducted on dry ground Gogi ore (with average size of 112 µm and the size distribution given in Table 6.6) using inert gases CO_2 and Ar with a reference experiment using oxygen gas for an array of temperature and pressure conditions. These experiments were carried out in the 5-L autoclave (described in Section 4.1.1), following the procedure described in Section 4.1.3. The kinetic data of leaching of uranium from Gogi ore at different temperatures and the partial pressures of different gases are plotted in Figs. 6.30 and 6.31.

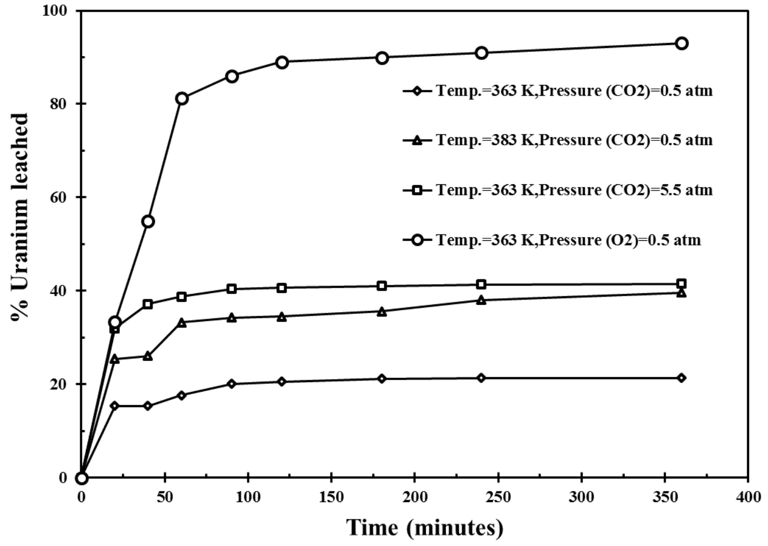

Fig 6.30 Effect of CO_2 and O_2 on leaching of uranium from Gogi ore at an array of temperatures and partial pressures of gases used

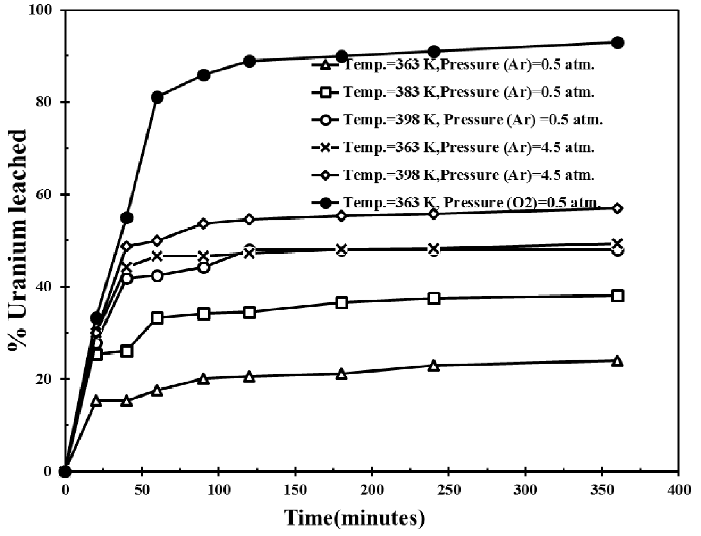

Fig. 6.31 Effect of Ar and O_2 on leaching of uranium from Gogi ore at an array of temperatures and partial pressures of gases used

Figs. 6.30 and 6.31 reveal that about 40-50% uranium could be leached from Gogi ore without the need of oxygen (using either Ar or CO_2 as the gases at different temperatures). However, leaching with O_2 at 363 K and $P_{O2} = 0.5$ atm (reference experiment) yielded highest dissolution of uranium.

With regard to leaching of pyrite at 363 K and 0.5 atm oxygen pressure, about 40% is leached as reported in Table 6.12 in Section 6.2.3.2. While, no sulfate is detected when Ar/CO_2 was used indicating no leaching of pyrite in the absence of oxygen gas.

6.2.5 Morphological studies on leach residue of Gogi ore

The leach residue of the Gogi ore was concentrated by physical methods described in Fig. 3.4 of Section 3.5, to obtain uranium bearing phase. The Scanning Electron Micrograph of the concentrate is given in Fig. 6.32, along with X-ray spectrographic (EDX) elemental analysis. Average elemental analysis by EDX indicates absence of uranium in the total leached solids sample (conditions of leaching: T= 363 K, P_{O2} = 0.5 atm. Many partially leached pyrite grains (eroded faces of pyrite lattices) are seen in Fig. 6.32, which is in agreement with the partial leaching of pyrite (about 40%) reported in Table 6.12. The leached particles captured in the image shown in Fig. 6.32 have the same irregular shape as those of unleached solids shown in Figs. 3.13[A] and [B] in Section 3.5.3. All leached particles have increased porosity which may be due to one or more processes such as leaching of uranium, leaching of pyrite, and agitation.

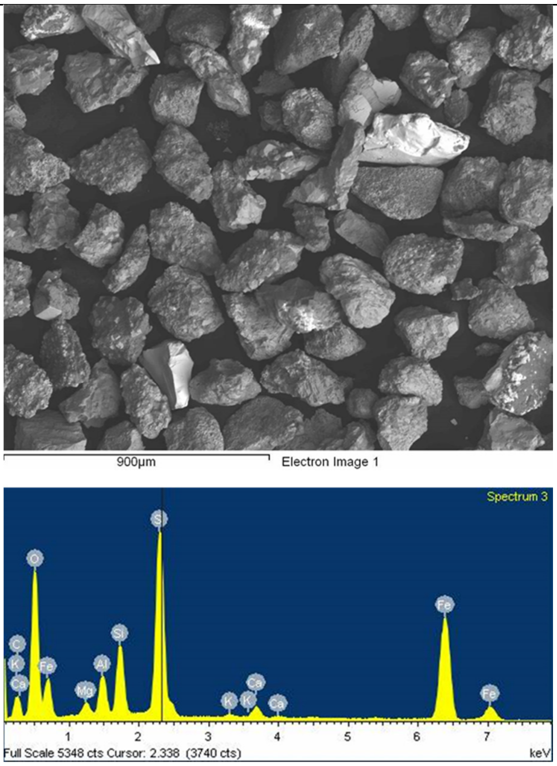

Element	Weight%
O	52.04
Mg	1.45
Si	9.83
S	11.17
Ca	4.59
Fe	20.92
Total	100.00

Fig. 6.32 Scanning Electron Micrograph of Methylene Iodide heavies - Non Magnetic (MIH and NM) portion of Gogi leach residue concentrated by physical methods described in Fig. 3.4 in Section 3.5

6.2.6 Conclusion

The kinetic data of extraction of uranium from Gogi ore using alkaline leaching was generated varying the parameters: partial pressure of oxygen, temperature, particle size, and stirring speed. The experimental data fitted well a stochastic leaching model with distributed rate constant according to gamma function. Alternatively, a topochemical leaching model coupled with particle size distribution is developed. This model represents the reality of the leaching of Gogi ore more closely. The conversions of pyrite and uranium in the absence of oxygen during leaching optimum yielded 0 and about 40 - 50%, respectively. This indicates that the U(VI) oxidation state in Gogi ore is high. The leaching studies also indicate partial (< 40%) and near complete (> 90%) leaching of pyrite and uranium, respectively, at optimum conditions: temperature = 363 K and oxygen pressure = 0.5 to 1 atm. SEM images of feed and leach residue too showed the partial and near complete leaching of pyrite and uranium, respectively, under these leaching conditions.

6.3 RELATING THE ALKALINE LEACHING OF INDIAN URANIUM ORES AND THEIR CONSTITUENTS

The results of leaching of pure materials studied under basic studies described in Chapter 5 and leaching of the two Indian uranium ores of alkaline host rocks origin reported in this Chapter have been compared to bring out relationship between them observed in certain aspects.

6.3.1 Role of oxygen in leaching of synthetic mixture of pure materials vis-à-vis Indian uranium ores

The naturally occurring uraninite (U_3O_8) consists of uranium in both in +4 and +6 oxidation states, the proportion of which varies from one ore to the other. Pure UO_2 used in synthetic mixture contained nearly all the uranium in +4 oxidation state (see complete chemical analysis given in Table 3.6 in Section 3.3) and X-ray diffractogram (shown in Fig. 3.2 in Section 3.4). The uranium values present in +6 oxidation state are readily soluble in suitable complexing aqueous medium (containing SO_4^{-2} or CO_3^{-2} ions) without the need of an oxidant (oxygen gas in the present study). However, the uranium in +4 oxidation state needs an oxidant for conversion to +6 state as well as the complexing aqueous medium.

The experiments on leaching of uranium from synthetic mixture (given in Section 5.3.4) without oxygen showed very low amounts of dissolution of uranium, <5%, in a range of temperatures and pressures maintained using either Ar/CO_2 gas. The low extraction of uranium indicates that nearly all the uranium is present in +4 oxidation state. The presence of all the uranium in +4 oxidation state in the pure UO_2 used, is also in agreement with the X-ray diffractogram and complete chemical analyses given in Fig. 3.2 and Table 3.6, respectively. The leaching experiments on Tummalapalle ore (Section 6.1.4) without oxygen (using either

Ar/CO_2 gas in a span of different temperatures and pressures) too indicated extraction of uranium as low as <10% (Figs. 6.13 through 6.15), it follows that Tummalapalle ore seems to contain uraninite with very low proportion of uranium in +6 oxidation state and most in +4 oxidation state. On the other hand, the experiments on Gogi ore (described in Section 6.2.4) without oxygen (using either Ar/CO_2 gas in a span of different temperatures and pressures) indicated extraction of uranium up to 50% (Figs. 6.30 and 6.31). It follows that Gogi ore appears to have uraninite with significant proportion of uranium in +6 oxidation state.

6.3.2 Comparison of uranium leaching from Indian uranium ores with that from pure UO_2

It is attempted to calculate the leaching efficiency of uranium from the two Indian ores for conditions of leaching given in Table 6.13. These conditions are close to the conditions under which uranium leaching efficiencies from pure UO_2 are reported in literature by Schortmann and DeSesa [37].

Table 6.13 The commonalities and the differences in the leaching conditions adopted for two Indian uranium ores and pure UO_2

Sl. No.	Leaching condition	Tummalapalle ore	Gogi ore	Pure UO_2 (After: [37])
1	Initial solid uranium concentration (g/L)	0.5	2	1
2	Average particle size of feed solids (μm)	25.8	112	<45
3	Concentration of Na_2CO_3 (M)	0.5	0.66	0.5
4	Concentration of $NaHCO_3$ (M)	0.5	0	0.5

The dissolution rates (in terms of mg/L-min) of uranium from Tummalapalle and Gogi ores under the constant conditions given in Table 6.13, at different temperatures in the range 343 to 383 K (at constant P_{O2} = 0.15 atm) and partial pressures of oxygen in the range 0.5 to 7.5 atm (at constant Temperature = 363 K) are calculated from experimental measurements and models developed in Sections 6.1 and 6.2 for conversion (α) values, in a time period of 1 h, using the relation given in Eq. 6.31.

$$\frac{dc}{dt} = \frac{\alpha\, w\, f}{100\, v\, t} \qquad [6.31]$$

where *c* is concentration of U_3O_8 in the leach liquor at time *t (min)*, *w* is weight of feed solids (1 kg), *f* is feed grade (0.21% U_3O_8 in Gogi ore, 0.048% U_3O_8 in Tummalapalle ore), *v* is volume of leachant (1 L in case of Gogi ore leaching and 0.9 L in case of Tummalapalle). For Tummalapalle ore, experimental conversion of 20% (obtained in a time period of 360 min, at P_{O2} = 0.15 atm, and 343 K) is used to calculate the rate of extraction of uranium at different temperatures (at constant P_{O2} = 0.15 atm) using Arrhenius activation energy (18.8 kJ/mol, found for Tummalapalle ore in Section 6.1.3.1) by the proportional relation given by Eq. 6.32.

$$\frac{dc}{dt} \propto e^{-\frac{2284}{T}} \qquad [6.32]$$

Section 6.1.3.1 established that the order of uranium extraction with respect to partial pressure of oxygen is 2.5. Accordingly, the dependence of rate of extraction of uranium on the oxygen pressure can be given by Eq. 6.33, keeping all parameters constant except partial pressure of oxygen. An experimental value of 58.7% at P_{O2}=5 atm, T = 363 K is extrapolated to predict conversions at different oxygen pressures (at constant temperature of 363 K) using Eq. 6.33.

$$\frac{dc}{dt} \propto {P_{O_2}}^{2.5} \qquad [6.33]$$

In the case of Gogi uranium ore, experimental conversions in experiments #GOGI/1 through #GOGI/5 and (for temperatures from 343 to 383 K at constant P_{O2} = 0.15 atm.) #GOGI/8 through #GOGI/11 (for oxygen pressures from 0.5 to 3 atm at constant temperature = 363 K), given in Table 6.7 in Section 6.2.3.1 are used. The predicted values for these experiments are calculated using the topochemical model developed (given by Eq.6.30). The same model is extrapolated to predict leaching efficiencies at oxygen pressures > 3 atm.

For the case of pure UO_2 leaching, since the leaching model developed in Section 5.1.2 is applicable only for the UO_2 powders generated from sintered material, with very low specific surface area of about 0.01 m^2/g (reported in Table 3.2, Section 3.1), the leaching efficiencies that can be predicted by this model are not used for comparison with those of Indian uranium ores. However, leaching rates of pure UO_2, under the temperature and pressure conditions used for Indian uranium ores are taken from the work of Schortmann and DeSesa [37] and used for comparison with that of Indian uranium ores.

The dissolution rates of uranium from Tummalapalle ore, Gogi ore and pure UO_2 are normalized for initial solid uranium concentration of 2 g/L by the proportional relation represented by Eq. 6.34, deduced by Schortmann and DeSesa [37]. The dissolution rate plots of two Indian uranium ores and pure UO_2 at different temperatures and oxygen pressures are shown in Figs. 6.33 and 6.34, respectively.

$$\frac{dc}{dt} \propto \mathit{initial\ solid\ uranium\ concentration} \qquad [6.34]$$

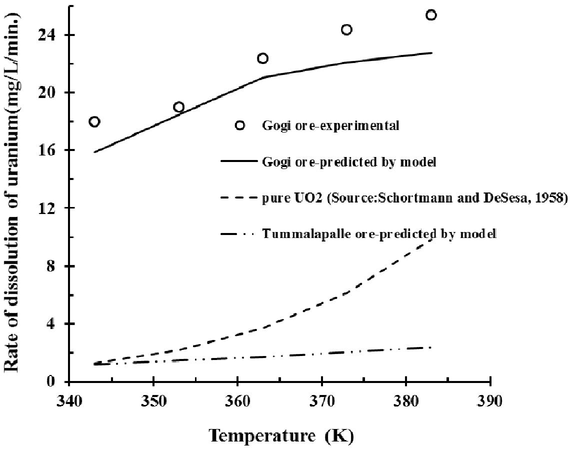

Fig. 6.33 Dissolution rates of uranium from Tummalapalle (predicted), Gogi ore (experimental and predicted) and pure UO_2 (model) as a function of temperature at P_{O2} = 0.15 atm in a time period = 60 minutes

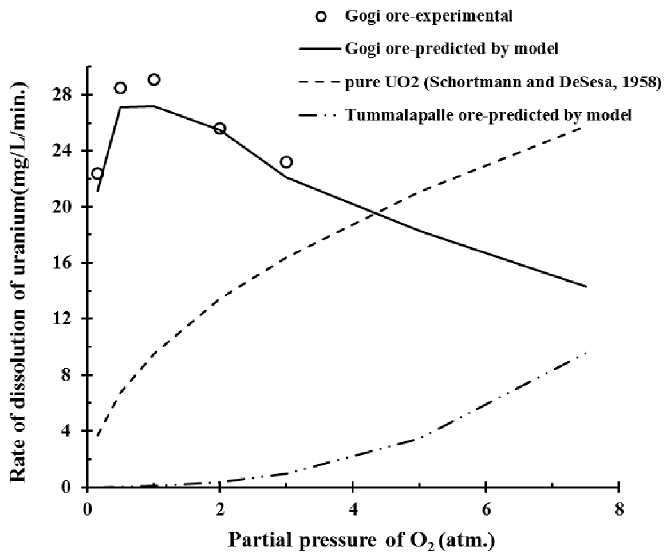

Fig. 6.34. Dissolution rates of uranium from Tummalapalle ore (predicted), Gogi ore (experimental and predicted) and pure UO_2 (model) as a function of partial pressure of oxygen at temperature = 363 K in a time period = 60 minutes

Much higher dissolution rates of uranium from Gogi ore (Figs. 6.33 and 6.34) than pure UO_2 is due to the presence of significant amount of U^{+6} in pitchblende (U_3O_8) occurring in Gogi ore. The uranyl (U^{+6}) form of uranium readily dissolves whereas uranous (U^{+4}) form needs to be first oxidized. Lower dissolution rates of uranium from Tummalapalle ore (Figs. 6.33 and 6.34) than pure UO_2 could be due to the insufficient liberation or exposure of uranium to leachant and also due to the absence of uranium +6 oxidation state. Higher ($\approx$ 50%) and lower (<10%) proportion of uranium in +6 oxidation state in Gogi and Tummalapalle ores respectively are also concluded from the results of leaching experiments described in Section 6.3.1. The leaching rate of uranium goes through a maximum in Fig. 6.34 is due to pyrite reaction discussed in Section 6.2.3.2.

6.3.3 Effect of pyrite content on leaching of uranium from synthetic mixture vis-à-vis Indian uranium ores

It is reported by several authors that the variation of leaching rate of UO_2 to be first order with respect to surface area [34, 85, 91B]. Hence, it is justifiable to represent rate of leaching in terms of surface area, as mg/(m^2-s). It is presumed in the present study also that the rate of leaching of both UO_2 and FeS_2 is proportional to the surface area and the specific rates of leaching of UO_2 and FeS_2 are calculated in terms of surface area as mg/(m^2-s) using Eqs. 6.35 and 6.36, for easy comparison with other published data, and plotted in Fig. 6.35.

$$\boldsymbol{Specific\, rate\, of\, dissolution\, of\, UO_2\left(\frac{mg}{m^2-s}\right)=\frac{Rate\, of\, dissolution\, of\, UO_2 * V}{60 * w * f_{UO2} * S_{p,UO2}}} \qquad [\mathbf{6.35}]$$

where the rate of dissolution of UO_2 (as mg/L/min), at each %FeS_2 content in the feed, is obtained from the slope of corresponding fitted straight line in Fig. 5.44. (Section 5.3.2.1, Chapter 5), V=volume of lixiviant = 0.7 L, w = weight of the feed sample = 35 g, f_{UO2} = weight fraction of UO_2 in feed = 0.002, and $S_{p,UO2}$ = specific surface area of UO_2 powder used = 0.01 m^2/g (as reported in Section 3.1, Table 3.2).

$$\boldsymbol{Specific\, rate\, of\, dissolution\, of\, FeS_2\left(\frac{mg}{m^2-s}\right)=\frac{Rate\, of\, leaching\, of\, FeS_2 * V}{60 * w * (P/100) * S_{p,FeS2}}} \qquad [\mathbf{6.36}]$$

where the rate of leaching of FeS_2 (as mg/L/min), at each %FeS_2 content in the feed, is obtained from the slope of corresponding fitted straight line in Fig. 5.45 (Section 5.3.2.2), V=volume of lixiviant = 0.7 L, w = weight of the feed sample = 35 g, P = %wt. of FeS_2 in feed = 1 to 6, $S_{p,FeS2}$ = specific surface area of FeS_2 powder used = 0.077 m^2/g (as reported in Section 3.1, Table 3.2).

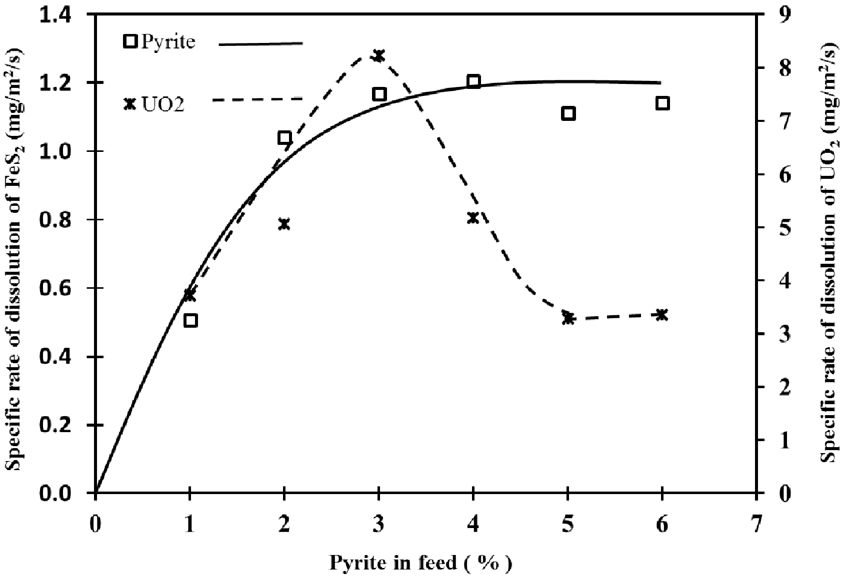

Fig. 6.35 Specific rates of leaching of Iron pyrite and UO_2 from synthetic mixtures with varying pyrite content in the feed solids

The reasons are clearly brought out in Section 5.3.2, for the initial increase in rate of dissolution of UO_2 with increase in FeS_2 content from 1% to about 3% and the decrease of dissolution rate of UO_2 with further increase in pyrite content beyond 3%.

The Tummalapalle uranium ore in India contains about 1.5% pyrite [166]. The dissolution of pyrite is necessary to extract all the uranium since it is present as composite with pyrite [130, 167]. The complete dissolution of pyrite and maximum uranium leachability of about 80% could be obtained at high temperature and pressure: 398 K and 5.2 atm oxygen pressure [168]. Fig. 6.35 also shows that the leaching of uranium from synthetic mixture, containing same amount of pyrite (1.5%) as that of Tummalapalle ore, is high and the uranium leachability is aided by presence of pyrite.

Whereas, Gogi uranium ore in India contains about 5% pyrite [169]. If high temperature and pressure (398 K and 5.2 atm. oxygen pressure) are applied in leaching of this ore, the dissolution of UO_2 reduces due to high dissolution of pyrite as reported in Table 6.12 in Section 6.2.3.2. Fig. 6.35 also shows that the leaching of synthetic mixture containing high pyrite (5%

by wt.), as much as in Gogi ore, resulted in high dissolution of pyrite and lower dissolution of uranium dioxide at high temperature and pressure. However, since the uranium is available in liberated and discrete form in Gogi ore [132, 170], it is feasible to obtain maximum leaching of uranium at 363 K and 0.5 atm oxygen pressure with partial dissolution of iron pyrite (< 40%) as reported in Table 6.12 in Section 6.2.3.2.

6.3.4 Morphological changes during leaching of synthetic mixture vis-à-vis Indian uranium ores

The morphological changes during leaching of synthetic mixture, Tummalapalle and Gogi uranium ores have already been discussed in Sections 5.4, 6.1.4 and 6.2.4 respectively. The observations are compared and main points are summarized in Tables 6.14 and 6.15.

Table 6.14 Morphological correlation between leaching of uraninite and reactive gangue mineral, pyrite, from the actual ores vis-a-vis synthetic mixture (Leaching conditions: Synthetic mixture and Tummalapalle ore at 398 K and P_{O2}=5 atm; Gogi ore at 363 K and P_{O2}=0.15 atm)

Feed solids	Uranium dioxide/Uraninite		Iron Pyrite	
	Feed to leaching	Leach residue	Feed to leaching	Leach residue
Synthetic mixture	Size: 75-100 µm, Smooth surface. No cleavages or fractures. The UO_2 grains are angular and anhedral in shape and display gray color and isotropism under reflected light (Fig. 3.5 in Section 3.5.1).	Partially leached. Rough surface; significant number of pits and micro cracks on UO_2 grains.	Pure Iron pyrite grains are yellowish white with high reflectance and isotropism. No cleavages or fractures.	Completely leached and chemically altered and produced a new solid phase, identified to be iron oxide, in ultra fine sizes.
Tummalapalle ore	Pitchblende in intimate association with pyrite segregations. Uranium is also in variable concentration associated with dolomicrite, ferruginous or pigmented carbonates, microstylolite prisms, and cellophane. Liberation size of uranium: 20-60 µm (source: [130]).	Uranium phase could not be tracked either by optical microscope or scanning electron microscope due to very low concentration, fine dissemination, low liberation size.	The minute segregated inclusions in micrite (Fig. 3.10[B]) and the euhedral pyrite with overgrowths (Fig. 3.10[D]) indicate syngenetic origin, whereas fractured (Fig. 3.10[C]) and brecciated pyrite represent pre-deformational hydrothermal phase.	Magnified image of Fig. 6.16 (EDX of spectrum 3 and 4) shows that sulfur content is much lesser compared to that in the feed grains in Fig. 3.12[A] (8.65% S) of Section 3.5.3, indicating near complete conversion of pyrite mineral.
Gogi ore	Coffinite occurs as independent grains (Fig. 3.11 [B]) and also in	Average elemental analysis by EDX indicates	Spectrum 1 in Fig. 3.13 [B] shows a prominent face of	Many partially leached pyrite grains (eroded

Feed solids	Uranium dioxide/Uraninite		Iron Pyrite	
	Feed to leaching	Leach residue	Feed to leaching	Leach residue
	intimate association with pitchblende (Fig.3.11 [C]) and pyrite. Spectrum 2 in Fig.3.13[B] shows that a particular portion of a particle contains as much as 39% U indicating that it is not liberated completely with respect to uranium.	absence of uranium in the total leached solids sample. (Fig. 6.32)	pyrite (cubic system) having a crystalline outline. While vein type pyrite is free and liberated (spectrum 4 in Fig. 3.13[B]).	faces of pyrite lattices) are seen. Particles have increased porosity which may be due to leaching of pyrite mineral and/or agitation. (Fig. 6.32).

Table 6.15 Morphological correlation between leaching of inert minerals: calcite and silica from the actual ores vis-a-vis synthetic mixture (Leaching conditions: Synthetic mixture and Tummalapalle ore at 398 K and P_{O2}=5 atm; Gogi ore at 363 K and P_{O2}=0.15 atm)

Feed solids	Calcite		Silica	
	Feed to leaching	Leach residue	Feed to leaching	Leach residue
Synthetic mixture	Calcite grains observed under transmitted light are colorless, showing change of relief on rotation with rhombohedral cleavage. They appear to be mechanically interlocked. (Fig. 3.5 in Section 3.5.1)	Not altered chemically, but disintegrated into smaller pieces (which must be due to low hard ness = 3). Two sets of cleavable surfaces identified. (Fig. 5.55 in Section 5.4)	Quartz grains are anhedral granular, colorless and display no variation in indices of refraction on rotation under the transmitted light of the optical microscope. They have faceted microstructure. (Fig. 3.5 in Section 3.5.1)	Neither chemically nor physically altered. (Fig. 5.56 in Section 5.4)
Tummalapalle ore	Cherty lime stone is found with quartz-calcite vein. (Fig. 3.8 in Section 3.5.2.1)	Dolostone appeared to be un altered during leaching. EDX of the SEM image (Fig. 6.16) indicated the presence of Mg and Ca.	Contains fine clasts of detrital quartz as impurity (Fig. 3.9[F]). Quartz is present in the form of chert.	Not altered due to leaching. (Fig. 6.16)
Gogi ore	The feed-rock is formed by fractured lime stones composed of micrite and sparite in varying proportions with minor quartz and dolomite. (Fig. 3.9)	Size reduced and chemically unaltered due to leaching.	Contains fine clasts of detrital quartz as impurity (Fig. 3.9[F]) in the form of chert.	Not altered due to leaching.

CHAPTER 7

Modeling, Simulation and Experimental Validation of Continuous Leaching of an Indian Uranium Ore

The use of continuous leaching reactor is indispensable and highly beneficial for commercial uranium mills where high throughputs (few thousand tons per day) of ores are processed. Better product quality control is possible through automation in continuous production as there are fewer opportunities for human error. One of the important steps in designing the commercial scale leaching process is finding relation between operating conditions of laboratory batch process and continuous process. In the present study, batch kinetic data of uranium leaching from Tummalapalle uranium ore was obtained from a laboratory scale reactor. The batch data is scaled to multiple continuous stirred tank reactors using the Residence Time Distribution (RTD) model. A graphical approach for scale up reported by Sarkar [117] was improved for better predictions of the observed experimental results. The scaling is also used to predict the temperature rise in a continuous reactor, which happens mostly due to conversion of pyrites present in the ore. The temperature of the reactor contents is essential to calculate thermal stresses for mechanical design of the reactor. The scaling obtained with the modified model is compared with measurements of uranium conversions and reactor temperatures in a pilot scale continuous reactor having three stirred tanks (effective volumes of the tanks holding the leach slurry are 267, 170 and 113 liters) in series.

The results of the present study serve as a reference for predicting the leaching efficiency as a function of time, inlet stream temperature and pyrite content of the ore. The simulation of residence time and heat absorption/evolution for continuous leaching from the laboratory data could predict the conversions of uranium, pyrite and the reactor temperatures of the 680 m^3 size continuous autoclave at the recently set up alkaline leaching plant at Tummalapalle in India.

7.1 BATCH LEACHING

The batch kinetic leaching test was carried out in a 5 L capacity cylindrical laboratory autoclave (described in Section 4.1.1), according to the procedure described in Section 4.1.3. The ground Tummalapalle uranium ore with an average assay of 0.04% U_3O_8 was used as feed to the leaching experiment. The dry ore used in the test was chosen as 0.35 kg so that the leaching pulp occupies about 65% of the reactor volume at an arbitrarily chosen low pulp density of 10% solids by weight. Pulp density was purposely chosen low to minimize the effect of change in pulp density due to the removal of leach liquor samples periodically. The optimum leaching parameters published by Suri et al. [28] are used in this study. These parameters are: particle size = 85% (by wt.) passing 75 µm size, leachant concentrations = 50 and 70 g/L of sodium carbonate and sodium bicarbonate, temperature = 398 K, total pressure, using oxygen = 7.5 atm. and residence time = 7 h. Samples, each of 5 ml, were drawn periodically through the sample draining port of the autoclave. The samples were filtered and analyzed for dissolved concentrations of U_3O_8 and sodium sulfate contents by spectrophotometry (Section 4.2.1.2) and gravimetry (Section 4.2.2.2) respectively. The leaching test was repeated twice to check reproducibility of results. At different cumulative time intervals, the uranium leached was computed from the concentration of U_3O_8 in the leach liquor and the pyrite reacted was computed from the concentration of Na_2SO_4 in leach liquor using the stoichiometry of reaction (2.8). The batch leaching kinetic curves for both pitchblende and pyrite are shown in Fig. 7.1. They indicate that the pitchblende reacts faster than the pyrite up to 1.5 h. Later, the pyrite continues to react to near completion in about 4 h while pitchblende reaction slackens with maximum of 82% recovery. The high rate of dissolution of uranium in the initial period could be due to presence of some amount of uranium in already oxidized form (+6 oxidation state), in the pitchblende mineral, as it is soluble easily according to reaction (2.5) without the need of reaction (2.4). However, the above two kinetic curves are independent and cannot be compared as they represent intrinsic behaviour of two different minerals proceeding with different reaction mechanisms. The residence time needed and heat effects in continuous leaching with multiple tanks are computed from this batch kinetic data.

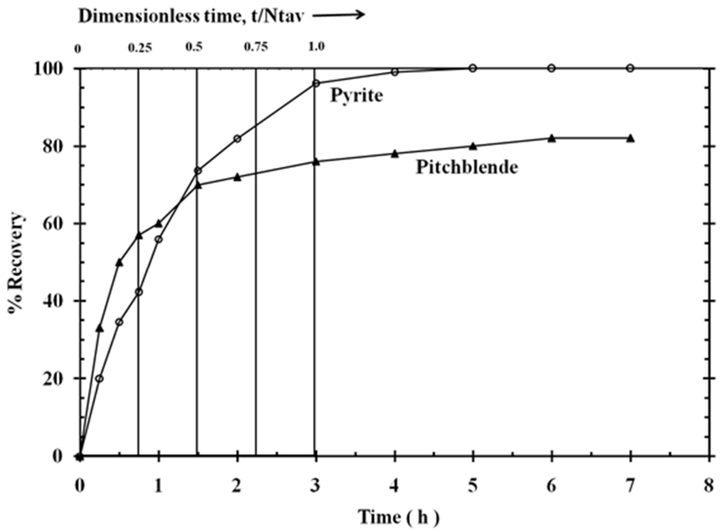

Fig. 7.1 Rate curves for batch leaching of pitchblende and pyrite from Tummalapalle uranium ore using carbonate solution

7.2. MODELING AND SIMULATION OF CONTINUOUS LEACHING

Several scale up methods are already discussed in Section 2.3.4 for designing continuous leaching from laboratory batch kinetic data. Among these, the method developed by Sarkar [117] does not assume a rate equation for batch leaching. It involves dividing batch kinetic curve, obtained from experiments, into small intervals of dimensionless time and applying residence time distribution equation for N stirred tanks in series. This method is adopted in the present study, with modification, to find residence time for continuous leach reactor from batch kinetic data generated on leaching of uranium using sodium carbonate and bicarbonate solution.

7.2.1 Residence time scale up for continuous leaching from batch process

Residence time in a batch leach reactor is same for all the particles participating in chemical reactions. However, this time is distributed in a continuous reactor due to non-ideal flow patterns that include short circuits and dead zones [146]. Perry [161] discussed two ways of mitigating these detrimental effects: (1) increasing the residence time in continuous leaching to exceed that of batch leaching and (2) decreasing the possibility of early discharge, caused by short-circuiting, by increasing the number of leaching stages. This increase is achieved by having multiple identical tanks in series, maintaining the total volume of all the tanks constant. The reactor contents flow from one tank to the next in series; in each tank the contents are perfectly mixed.

One of the theoretical estimates for different residence times spent by different fractions of the feed pulp (solids+leachant) in a continuous stirred tank reactor is based on Residence-Time Distribution (RTD) equation [39]. The cumulative weight percent pulp discharge of original feed, M_t, from a series of N continuously stirred reactors (N-CSTRs) of identical size in an elapsed time t, is given by,

$$M_t = \left[1 - \left[\sum_{N=1}^{N} \frac{1}{(N-1)!}\left(\frac{t}{t_{av}}\right)^{N-1}\right] e^{-\frac{t}{t_{av}}}\right] \times 100 \qquad [7.1]$$

t_{av} is average retention time per reactor and Nt_{av} is total retention time in N tanks. A dimensionless time period, t/Nt_{av}, is used for relating leaching efficiency in batch process, at different time periods, to that in continuous process as described by Sarkar [117] with a minor modification.

The values of M_t for different, arbitrarily chosen values of dimension less time, t/Nt_{av}, were computed from Eq. [7.1] for one, two, three, four, six, eight and ten tanks in series. These values are given in Table 7.1 which can be combined with the recovery of uranium in batch process. The batch leaching recovery ($\%Y_{batch}$) at different time periods can be obtained by interpolation through superimposing t/Nt_{av} values from 0 to 1 on x-axis of batch curve for particular Nt_{av} (=3 h in the present case) as shown in Fig. 7.1. Model calculations are shown in

Table 7.2 for N = 2 and 3 and Nt_{av} = 3 h and 4 h. For a batch time of 0-0.3 h (for the case of Nt_{av} = 3 h), the recovery (Fig. 7.1) varies from 0 to 36.4%, as shown under the column $\%Y_{batch}$ in Table 7.2. In the present study, average recovery during this period, 18.2%, is considered to represent continuous leaching efficiency. Sarkar [117] considered the highest recovery, 36.4%, for this purpose in his original methodology. This average recovery multiplies with $d(M_t)$ = 1.8 (for N=2) to give a differential recovery of 0.3%; similarly for a batch time of 0.3-0.475 h, the differential recovery is 3.4%. Similar calculations are made for other times and the differential recoveries are added to give the cumulative recoveries for N=2. The final computed recovery of uranium in continuous leaching, Y_{UO2}, for N, varying from 2 to 10, at different plant residence times (Nt_{av}) from 2 to 8 h are plotted in Fig. 7.2.

Table 7.1 Reactor discharge, M_t, as cumulative weight percentage of original feed for different values of dimensionless time, t/Nt_{av} and number of tanks in series, N, calculated from Residence Time Distribution (RTD) equation (Eq. 7.1)

t/Nt_{av}	M_t, %						
	$N = 1$	$N=2$	$N=3$	$N=4$	$N=6$	$N=8$	$N=10$
0	0.0	0.0	0.0	0.0	0.0	0.0	0.0
0.1	9.5	1.8	0.4	0.1	0.004	0.0002	0.00001
0.25	22.1	9.0	4.1	1.9	0.4	0.1	0.03
0.50	39.3	26.4	19.1	14.3	8.4	5.1	3.2
0.75	52.8	44.2	39.1	35.3	29.7	25.6	22.4
1.00	63.2	59.4	57.7	56.7	55.4	54.7	54.2

Table 7.2: Model computation of recovery (%R) of U_3O_8, calculated from values of M_t and Y_{batch} (%yield from batch kinetic curve) at different dimensionless times (t/Nt_{av}), for series of N tanks in continuous leaching system with Nt_{av} = 3 and 4 h

Nt_{av}, (h)	t/Nt_{av}	t, (hr)	$\%Y_{batch}$	Average $\%Y_{batch}$	$N=2$				$N=3$			
					$(M)_t$	$d(M_t)$	$d(\%R)$	%R	$(M)_t$	$d(M_t)$	$d(\%R)$	%R
3	0 - 0.1	0 - 0.3	0-36.4	18.2	1.8	1.8	0.3		0.4	0.4	0.1	
	0.1 - 0.25	0.3 - 0.75	36.4-57	46.7	9.0	7.3	3.4		4.1	3.7	1.7	
	0.25 - 0.5	0.75-1.5	57-70	63.5	26.4	17.4	11.1		19.1	15.1	9.6	
	0.5 - 0.75	1.5-2.25	70-73	71.5	44.2	17.8	12.7		39.1	20.0	14.3	
	0.75 - 1.0	2.25-3.0	73-76	74.5	59.4	15.2	11.3		57.7	18.6	13.9	
	1.0 - ∞	3.0 - ∞	76-82	79.0	100.0	40.6	32.1	70.9	100.0	42.3	33.4	72.9
4	0 - 0.1	0-0.4	0-42	21.0	1.8	1.8	0.4		0.4	0.4	0.1	
	0.1 - 0.25	0.4 - 1	42-60	51.0	9.0	7.3	3.7		4.1	3.7	1.9	
	0.25 - 0.5	1 - 2	60-72	66.0	26.4	17.4	11.5		19.1	15.1	9.9	
	0.5 - 0.75	2 - 3	72-76	74.0	44.2	17.8	13.2		39.1	20.0	14.8	
	0.75 - 1.0	3 - 4	76-78	77.0	59.4	15.2	11.7		57.7	18.6	14.3	
	1.0 - ∞	4 - ∞	78-82	80.0	100.0	40.6	32.5	72.9	100.0	42.3	33.9	74.9

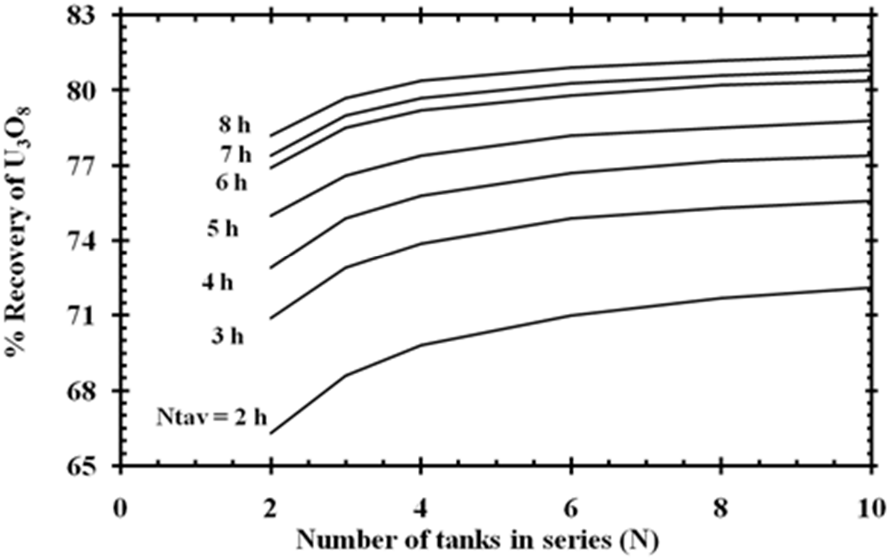

Fig. 7.2 Predicted variation of recovery of U_3O_8 with number of tanks in continuous leaching system for different plant residence times (Nt_{av})

Fig. 7.2 shows that to achieve 78% recovery, either 5 hours of plant residence time with 6 tanks in series, or 6 hours of residence time with three tanks in series are required. The batch leaching yielded 78% recovery in 4 h residence time (see Fig. 7.1). Therefore, the residence time scale up factor for three tanks in series is 1.5 and for 6 tanks in series is 1.25. The working volume of the plant scale continuous reactor can be calculated by multiplying desired slurry volumetric flow rate by plant residence time (Nt_{av} = 6 h for three stages and 5 h for six stages).

The conversion of pyrite, Y_{FeS_2}, for different residence times in a three stage continuous reactor is also calculated according to the above procedure based on the batch kinetic data of pyrite shown in Fig. 7.1. The predicted conversions of both the pitchblende (Y_{UO_2}) and the pyrite (Y_{FeS_2}) in continuous leaching are given in Table 7.3. These values are combined with energy balance equations to calculate the heat effects in the succeeding Section 7.2.2.

Table 7.3: Predicted conversions of pitchblende and pyrite from the batch kinetic data shown in Fig. 7.1, for different residence times in pilot scale continuous reactor having three stirred tanks in series

Residence time (h)	Conversion of UO_2 (Y_{UO2}) (%)	Conversion of FeS_2 (Y_{FeS2}) (%)
0	0	0
0.25	36.7	33.4
0.5	48.8	41.9
0.75	54.6	47.8
1	58.8	54.5
2	68.6	73.5
3	72.9	84.6
4	74.9	90.1
5	76.6	93.2
6	76.9	95.3
7	79	95.9

7.2.2 Simulation of heat effects in continuous leaching

Heat effects play a vital role in the operation of a commercial scale continuous leach reactor. Paphane et al. [171] has shown the complexity in the kinetics of exothermic reactions proceeding via some intermediates before formation of products from a sulfide concentrate in a five-compartment continuous autoclave. The temperature of all the exiting streams from the reactor is influenced by inlet temperature of entering streams and the heats of reactions [116]. Following main reactions are considered for the heat balance calculations: (1) dissolution of pitchblende, the uranium mineral, and pyrite (exothermic), (2) decomposition of sodium bicarbonate (endothermic). These reactions are already mentioned in Section 2.1.3.1, which are re-written below along with the heats of reactions at Standard Temperature and Pressure (STP) [62].

$$2UO_2 + O_2 \rightarrow 2UO_3 \ , \Delta H^0_{UO_2} = -543.41\, kJ / kg\, UO_2 \qquad [2.4]$$

$$UO_3 + Na_2CO_3 + 2NaHCO_3 \rightarrow Na_4UO_2(CO_3)_3 + H_2O \ , \ \Delta H^0_{UO_3} = -3469.41\, kJ / kg\, UO_3 \qquad [2.5]$$

$$4FeS_2 + 15O_2 + 16Na_2CO_3 + 14H_2O \rightarrow 16NaHCO_3 + 4Fe(OH)_3 + 8Na_2SO_4 \ , \Delta H^0_{FeS_2} = -15451.17\, kJ / kg\, FeS_2 \qquad [2.8]$$

$$2NaHCO_3 \rightarrow Na_2CO_3 + CO_2 + H_2O \ , \ \Delta H^0_{NaHCO_3} = 512.5 kJ\ /\ kg\ NaHCO_3 \qquad [2.9]$$

The rate of generation of heat in continuous leach reactor is calculated by combining the simulated conversions of pitchblende and pyrite, given in Table 7.3, with the heats of reactions (2.4), (2.5), (2.8) and (2.9).

Energy balance on the reactor shows that enthalpy of stream leaving the reactor equals sum of enthalpy of the entering feed and the heat generated/absorbed due to chemical reactions, assuming that the reactor is well insulated and kinetic and potential changes are negligible.

$$Rate\ of\ enthalpy\ of\ feed\ entering\ the\ reactor = (\dot{M}_{solids} C_{p,solids} + \dot{M}_{liquid} C_{p,liquid})\ T_{in} \qquad [7.2]$$

$\dot{M}_{solids}$ (kg/h), $\dot{M}_{liquid}$ (kg/h) are the mass flow rates of solids and liquid entering the reactor. $C_{p,solids}$ (kJ/kg-°C), $C_{p,liquid}$ (kJ/kg-°C) are their heat capacities. Since the reacting species, pitchblende and pyrite, together constitute small weight fraction (< 1%) of the total mass fed to the reactor, stream leaving the reactor is assumed to be same as that of feed for energy balance purpose. Hence,

$$Rate\ of\ enthalpy\ of\ stream\ leaving\ the\ reactor = (\dot{M}_{solids} C_{p,solids} + \dot{M}_{liquid} C_{p,liquid})\ T_{out} \qquad [7.3]$$

The feed pulp density of the continuous system mentioned in Section 4.1.4 is 50% solids (by wt.), Hence,

$$\dot{M}_{liquid} = \dot{M}_{solids} \qquad [7.4]$$

The total heat generated by reactions (2.4), (2.5), (2.8) and (2.9) is given by,

$$\begin{aligned} heat\ generated\ due\ to\ reactions = {} & \Delta H_{UO_2}\, \dot{m}_{UO_2} \frac{Y_{UO_2}}{100} + \Delta H_{UO_3}\, \dot{m}_{UO_3} \frac{Y_{UO_3}}{100} \\ & + \Delta H_{FeS_2}\, \dot{m}_{FeS_2} \frac{Y_{FeS_2}}{100} - \Delta H_{NaHCO_3}\, \dot{m}_{NaHCO_3} \frac{Y_{NaHCO_3}}{100} \end{aligned} \qquad [7.5]$$

ΔH_{UO_2}, $\dot{m}_{UO_2}$, Y_{UO_2} are enthalpy of UO_2 (kJ/kg of UO_2), mass flow rate of UO_2 (kg/h) and %

conversion of UO_2 respectively. Similar nomenclature holds for other reactants in Eq. 7.5 too. The enthalpy of all the reactions at the operating temperature and pressure range of continuous reactor, ΔH , is assumed to be not varying significantly from that at standard temperature and pressure (ΔH^0). It may be noted that Y_{UO_2} , Y_{UO3} , Y_{FeS_2} and Y_{NaHCO_3} are functions of residence time of the slurry in the reactor. Individual terms of Eq. 7.5 are calculated as below.

$$\Delta H_{UO_2}\,\dot{m}_{UO_2}\frac{Y_{UO_2}}{100} = 543.41\dot{M}_{solids}\,(\frac{0.05}{100})(0.98)(\frac{Y_{UO_2}}{100}) \qquad kJ/h \qquad [7.6]$$

as the feed grade used in continuous leaching is 0.05% U_3O_8 (as mentioned in Section 4.1.4) and the conversion factor from U_3O_8 to UO_2 is 0.98. The dissolution of UO_3 is assumed to be instantaneous and nearly complete (98%) [79], hence $Y_{UO_3} = Y_{UO_2}\,(0.98)$.

$$\Delta H_{UO_3}\,\dot{m}_{UO_3}\frac{Y_{UO_3}}{100} = 3469.41\dot{M}_{solids}\,(\frac{0.05}{100})(0.98)(\frac{Y_{UO_2}}{100})(0.98) \qquad kJ/h \qquad [7.7]$$

$$\Delta H_{FeS_2}\,\dot{m}_{FeS_2}\frac{Y_{FeS_2}}{100} = 15451.17\dot{M}_{solids}\,(\frac{W_{py}}{100})(\frac{Y_{FeS_2}}{100}) \qquad kJ/h \qquad [7.8]$$

Wpy is the % pyrite in the feed solids.

$$\Delta H_{NaHCO_3}\,\dot{m}_{NaHCO_3}\frac{Y_{NaHCO_3}}{100} = 512.5\left\{\frac{\dot{M}_{solids}}{1.05}(\frac{70}{1000}) + \dot{M}_{solids}(\frac{W_{py}}{100})(\frac{Y_{FeS_2}}{100})(\frac{4}{120})84\right\}(\frac{25}{100})\,kJ/h \qquad [7.9]$$

In Eq. 7.9, the mass flow rate of $NaHCO_3$, $\dot{m}_{NaHCO_3}$, comprises original $NaHCO_3$ present in the feed liquid (70 g/L, as mentioned in Section 4.1.4) and $NaHCO_3$ produced from reaction (2.8) from the pyrite. The decomposition of $NaHCO_3$ is considered to be 25% at the operating temperature and pressure of the reactor [59, 172]. Hence, the overall heat balance equation, Eq. 7.10, is obtained by combining Eqs. 7.2 to 7.9.

$$\dot{M}_{solids}(C_{p,solids} + C_{p,liquid})\,(T_{out} - T_{in}) = 0.01936\,\dot{M}_{solids}\,Y_{UO_2} + 1.5092\dot{M}_{solids}(W_{py})(Y_{FeS_2}) - 8.542\,\dot{M}_{solids} \qquad [7.10]$$

The heat capacities of solid and liquid streams are assumed to be constant in the range of operating temperature and equal to 0.5 kJ/kg-°C (that of Tummalapalle ore) and 4 kJ/kg-°C (that of water), respectively. The rise in temperature of the pulp, $T_{out} - T_{in} = \Delta T$, can be calculated as,

$$\Delta T = 0.0043 Y_{UO_2} + 0.3354 (W_{py})(Y_{FeS_2}) - 1.898 \tag{7.11}$$

Low pyrite in uranium ores is beneficial in alkaline leaching, as described in Section 2.1.3.1 in Chapter 2. But, high pyrite in the ore needlessly consumes leaching reagents (see reactions). Hence, it is usual practice to "float-out" pyrite from ores with high pyrite content. The pyrite rich concentrate (float) and the tails are treated separately by acid and alkaline leaching, respectively, for recovery of uranium [62]. Hence for both low and high pyrite containing ores, the feed to alkaline leaching contains less amounts of pyrite. Therefore, detailed analysis of heat effects due to pyrite content of carbonate uranium ores is not necessitated and not reported in the literature.

The ore in the present study, however, contains pyrite in the intermediate range, - 0.5% in the laboratory experiments and 1.5% in the pilot plant studies. Hence these ores are treated by direct alkaline leaching route without separating out the pyrite. Further, composition of actual ore fed to a commercial plant may vary from place to place within the mine and may contain even higher pyrite. Since pyrite reaction releases largest amount of heat compared to other reactions and pyrite concentration is orders of magnitude higher than uranium, the heat production is mainly governed by the pyrite reaction.

Fig. 7.3, plotted using Eq. 7.11, shows that the reactor temperature rises steeply initially due to fast kinetics of pyrite conversion. The rise in temperature is higher for ores containing larger amounts of pyrites. Y_{UO_2} and Y_{FeS_2} values for Fig. 7.3 are taken from Table 7.3. This Figure can be used to predict maximum temperature rise as a function of pyrite content of the ore. Alternatively, one can calculate the permissible limit of pyrite content of the ore for a given feed inlet temperature and the design temperature of the autoclave from Eq. 7.11. For example, if the feed enters autoclave at 110°C, and the maximum design temperature of the reactor is 200°C (as in the case of pilot scale reactor), then pyrite content of the ore should be < 3%.

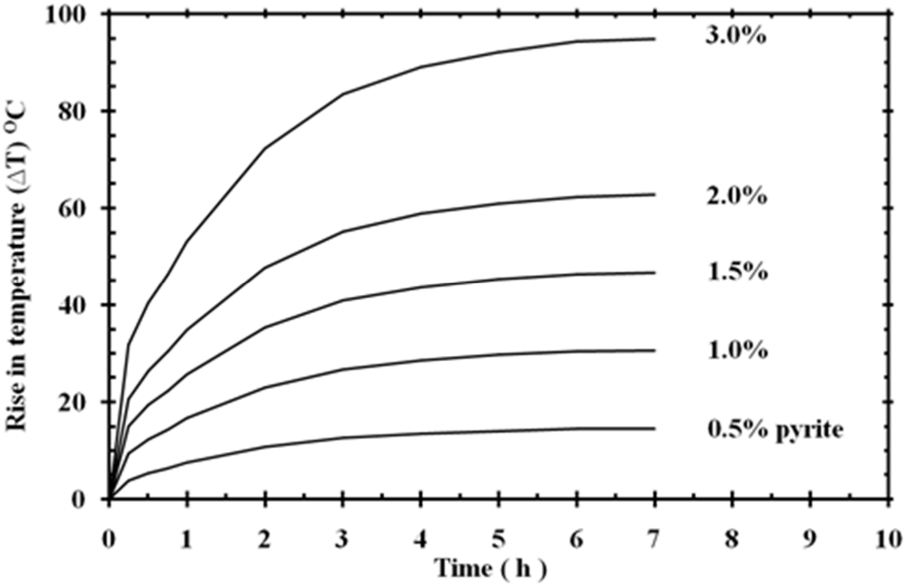

Fig. 7.3 Predicted rise in temperature of the slurry, for different pyrite concentrations of the ore, in pilot scale continuous reactor with residence time distribution

If the reactor temperature surges above the optimum value, 125°C in the present study, not only the design temperature of the reactor (in the present study) would be exceeded but also leaching efficiency of pitchblende would be reduced. This efficiency is lower at temperatures higher than the optimum value [8]. Higher temperatures raise water vapor pressure and thus lower partial pressure of oxygen for a fixed total reactor pressure, 7.5 atm in the present study, which in turn reduces the solubility of oxygen. As less oxygen is available for leaching reaction, the efficiency of uranium leaching is lowered.

7.3 CONTINUOUS LEACHING EXPERIMENTS

The continuous leaching tests were carried out in a pilot scale reactor described in Section 4.1.3, according to procedure described in Section 4.1.4. (Most of the conditions in continuous leaching were maintained identical to those of batch leaching, except those such as feed grade of uranium and pyrite, which cannot be controlled). Results of the tests conducted at different flow-rates and inlet temperatures of feed pulp, under fixed operating conditions, mentioned in Section 4.1.4, are given in Table 7.4. About 79% of uranium was leached in 7.86 h in the Continuous Leach Reactor (CLR). However, closer look at the progress of reaction in each of the CLR's compartments reveals interesting observations. The residence times in the first tank at lower flow rate (3.8 h residence time with 70 L/h) and in the last tank at higher flow rate (3.93 h residence time with 140 L/h) are close and the recoveries of uranium in these tanks at different flow rates also have been found to be nearly equal. For all the residence times obtained by different flow rates and different volumes of the reactor (from the data given in Table 7.4), a single monotonously increasing curve of Recovery *Vs* Residence time (which is included in Fig. 7.4 in the succeeding Section 7.4.1) is obtained. Hence, flow rate seems to have no effect not only on final recovery but also on rate of conversion.

Table 7.4 Uranium leached from Tummalapalle ore at different feed flow rates and inlet temperatures of the slurry in continuous pilot-scale reactor having three stirred compartments connected in series. Samples for chemical analyses were taken 20-30 h after steady state was reached

Flow rate (L/h)	Feed inlet temperature (°C)	Compartment1 (pulp volume = 267 L)		Compartment2 (pulp volume = 170 L)		Compartment3 (pulp volume = 113 L)	
		Cumulative Time (h)	%U_3O_8 Leached	Cumulative Time (h)	%U_3O_8 Leached	Cumulative Time (h)	%U_3O_8 Leached
340	95	0.79	NA	1.29	NA	1.62	53.4
240	90	1.11	NA	1.82	NA	2.29	70.0
140	90	1.91	66	3.12	72	3.93	72.5
70	85	3.8	75	6.24	77.7	7.86	78.6

Fixed operating conditions: 50% solids wt./wt., 125° - 130°C reactor temperature, 7.2 - 7.5 atm (g) over-pressure, 50 g/L Na_2CO_3 and 70 g/L$NaHCO_3$.
NA = Not Available.

7.4 EXPERIMENTAL VALIDATION

7.4.1. Experimental validation of residence time scale up

Fig. 7.4 shows good agreement between the predicted conversions of the pitchblende and the experimental data obtained from the pilot plant, for several residence times. The predicted recoveries by the modified method are closer to the recoveries obtained in actual continuous leaching than those predicted by the original method developed by Sarkar [117].

This closeness is because the average leaching recovery within the small intervals of time, considered in the modified method here, represents the actual recovery (Y_{batch}) more closely within particular time interval than the recovery at the end of the interval. The recoveries from continuous plant are lower than the batch experiments because of residence time distribution in the former. The predicted conversions also compared well with those in a commercial scale reactor (not shown here).

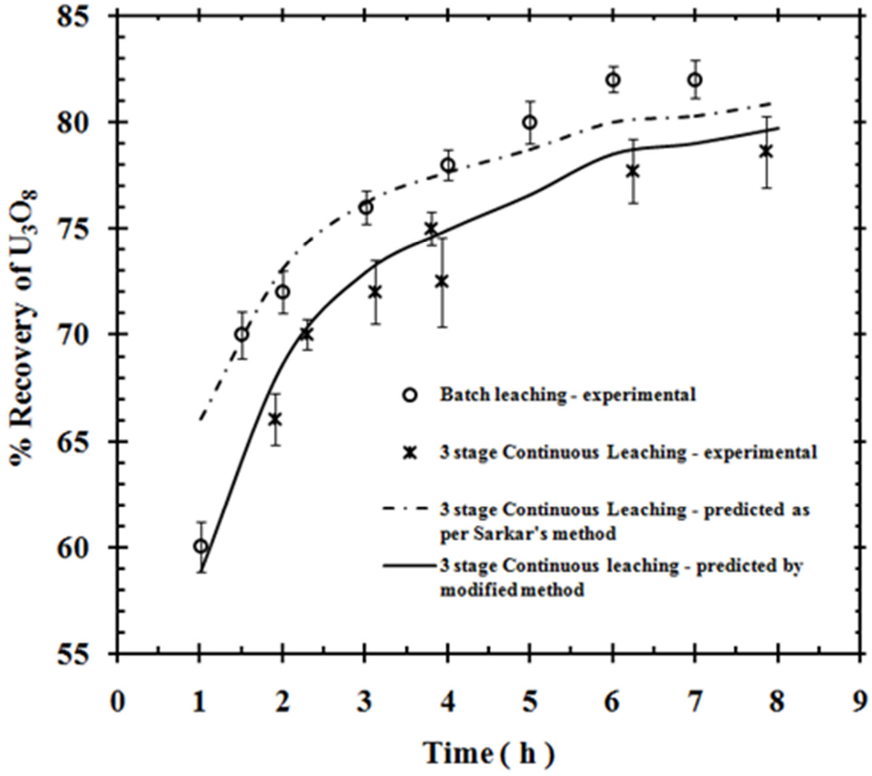

Fig. 7.4 Comparison of recovery of uranium in pilot scale continuous reactor with three stirred compartments and predictions. Recovery in batch scale (5L) is shown for reference. Experimental points are mean values with error bars

7.4.2. Experimental validation of heat effects

The slurry temperature, at different residence times, can be calculated from Eq. 7.11 by substituting pyrite content (Wpy = 1.5%) of the ore treated in continuous leaching (as mentioned in Section 4.1.4),

$$T_{out} = T_{in} + 0.0043 Y_{UO_2} + 0.403 Y_{FeS_2} - 1.898 \qquad [7.12]$$

Using Y_{UO_2} and Y_{FeS_2} at different residence times from Table 7.3, slurry temperature, T_{out} , *Vs* residence time is predicted and shown in Fig. 7.5. The three inlet temperatures (85°C, 90°C and 95°C) at which continuous leaching experiments were carried out are considered. The measured temperatures at three different pulp flow rates compared well with predicted temperatures. Hence the scale-up using residence time distribution can estimate the reactor size for continuous leaching and the temperature rise in the reactor.

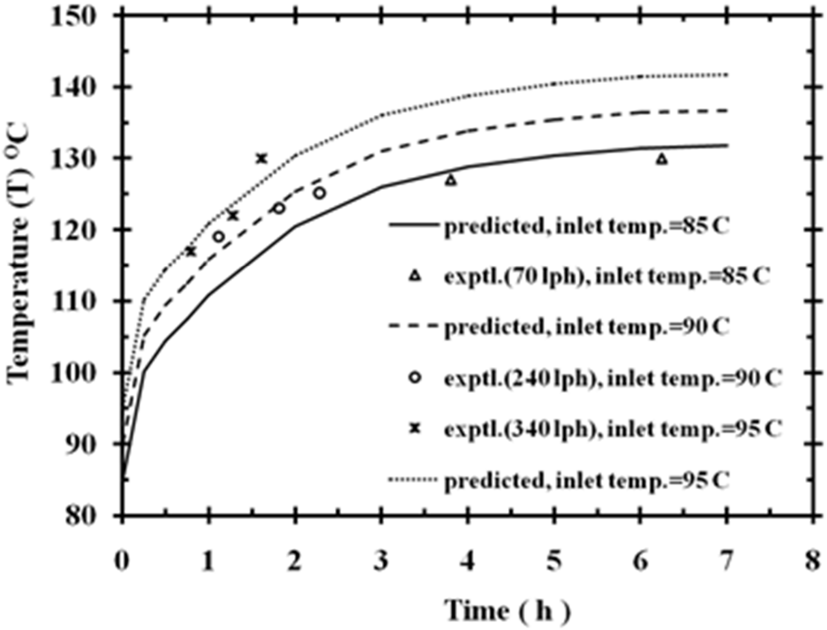

Fig. 7.5 Predicted and experimental temperatures of pulp at different residence times for a pilot scale continuous reactor operated with Tummalapalle ore containing 1.2% pyrite and inlet temperature of 85°C, 90°C and 95°C

7.5 CONCLUSION

A batch leaching experiment was conducted on Tummalapalle uranium ore in a 5 L autoclave under the optimum conditions: particle size = 85% (by wt.) passing 75 μm size, leachant concentrations = 50 and 70 g/L of sodium carbonate and sodium bicarbonate, temperature = 398 K, total pressure, using oxygen = 7.5 atm. and residence time = 7 h. The conversions of UO_2 and FeS_2 for different time periods obtained in this experiment formed the basis for simulation of leaching in series of continuous stirred tank reactors using residence time distribution equation. The predicted conversion of pitchblende for different residence times in three stage continuous autoclave of 850 L capacity, operated under the above mentioned optimum leaching conditions, is in good agreement with the experimental measurements (Fig. 7.4). Since the exothermic heat of two reactions (pyrite and pitchblende with leachant) exceeds the endothermic heat third reaction (decomposition of sodium bicarbonate), the temperature of the feed slurry to the continuous autoclave increases. The rise in temperature of the reactor contents is calculated using heat balance equations across the 850 L capacity continuous leach reactor and the predicted conversions of pitchblende and pyrite from residence time distribution equation. The acceptable upper limit of the pyrite content of the Tummalapalle uranium ore is calculated to be about 3% for maintaining a continuous autoclave temperature below a design value of 200°C for a feed slurry inlet temperature of 110°C (Fig. 7.3). The predicted outlet temperatures of the leached slurry are very close to the measured values for different slurry flow rates in the 850 L continuous autoclave (Fig. 7.5). The conversions of pitchblende and pyrite, and the rise in temperature of contents of 680 m^3 capacity commercial reactor could also be predicted.

CHAPTER 8

Conclusions and Scope for Further Research

India has set up its first commercial uranium mill using alkaline processing technology at Tummalapalle, Cuddapah district, Andhra Pradesh. The committed and forthcoming uranium ore processing plant at Gogi in Karnataka is also based on alkaline leaching route. Thus the techno-economics of alkaline leaching technology has become important for India. The present study focuses on modeling the kinetics of alkaline leaching, the central process in the extraction of uranium, from the Tummalapalle and Gogi uranium ores.

The investigations on actual uranium ores have been supported with the basic leaching studies on their constituents, in their pure form. The studies carried out on morphological variations of the ores during their leaching have added new dimension to the findings presented in this thesis.

The batch leaching kinetics (obtained in a 5 L capacity autoclave) of Tummalapalle uranium ore has been scaled to multiple continuous stirred reactors using an improved Residence Time Distribution (RTD) model. The scaling is used to predict the temperature rise in continuous reactor, which happens mostly due to conversion of pyrites present in the ore. The predicted uranium and pyrite conversions, and reactor temperatures are in good agreement with experimental measurements obtained for several different operating conditions of the pilot scale continuous reactor (850 L capacity) having three stirred tanks in series. The RTD model could also predict the conversion of uranium and reactor temperature in a commercial scale (680 m^3) reactor at Tummalapalle. The leaching models developed in the present study are useful for the design of new uranium mills, plant expansions and process improvements at Gogi and Tummalapalle deposits in India in particular, and high carbonate content ores elsewhere in general.

8.1 MAJOR OUTCOMES OF THE STUDY

The leaching of pure UO_2 (synthetic origin) using 1% (w/v) solids in sodium carbonate and bicarbonate solutions, at temperatures between 353 K and 413 K (base level=353 K), oxygen partial pressure from 0 to 10 atm (base level=10 atm), Na_2CO_3 and $NaHCO_3$ concentrations between 0.05 and 0.7 M (base level=0.5 M), average particle sizes 41 to 172 µm (base level=87 µm), in a time period of 0 to 360 min, can be described by the rate equation, Eq. 5.5 deduced in Section 5.1.2.

$$\frac{\mathrm{d}C_{UO_2}}{\mathrm{dt}} = \frac{99.1 \times [\mathrm{Na^2CO^3}]^{0.24} \times [\mathrm{NaHCO^3}]^{0.09} \times \mathrm{Po_2}^{0.58} \times d^{-0.2762} \times \, e^{-\frac{4440.8}{T}}}{(3 \text{ x } 10^{-7} \times [\mathrm{Na^2CO^3}]^{0.24}) + (1.5\text{x}10^{-4} \times [\mathrm{NaHCO^3}]^{0.09}) + (1.9\text{x}10^{-5} \times \mathrm{Po_2}^{0.58})} \quad [5.5]$$

Where, C_{UO2} is the concentration of UO_2 in mg/L and t is the leaching time in minutes. The high magnitude of the activation energy and the fractional orders with respect to carbonate concentration and bicarbonate concentration indicate a reaction mechanism limited by chemical reaction on the surface of UO_2.

The reaction of pure pyrite mineral in sodium carbonate and bicarbonate solutions (base concentration levels = 0.5 M) with 1% solids (w/v), at temperatures between 343 K and 393 K base level = 363 K), oxygen partial pressure from 0.15 to 3 atm (base level = 0.5 atm), average particle sizes from 6 to 253 µm (base level = 87 µm), in a time period of 0 to 6 h can be described by the rate equation (combined form of Eqs. 5.9 and 5.10) formulated in Section 5.2.2:

$$1 - \left(1 - X_{py}\right)^{\frac{1}{3}} = k_o \;\; p_{O_2}^{0.2} d^{-0.2} e^{-\frac{7006}{T}} \, [CO_3]^x [HCO_3]^y \, t \qquad [8.1]$$

Where, $k_o = 3\text{x}10^7$, x = 0.8 and y = 0.2 for 0 to 0.7 M concentration of Na_2CO_3 and $NaHCO_3$; and $k_o = 2\text{x}10^6$, x = -2.9 and y = -2.1 for 0.7 to 1 M concentration of Na_2CO_3 and $NaHCO_3$.

The increase in rate of reaction of pyrite with increase in concentrations of Na_2CO_3 and $NaHCO_3$ at lower concentrations (up to 0.7 M) can be explained by the law of mass action. On the other hand, leaching of pyrite decreases beyond 0.7 M concentrations of Na_2CO_3 and $NaHCO_3$. The leaching of pyrite at high concentrations of reagents and the decreasing trend of leaching rate at those concentrations has not been reported in the literature. However, the lowering of leaching rate could be due to the excessive concentrations of Na_2CO_3 and $NaHCO_3$ that may hinder the diffusion of oxygen gas to the sites of reaction on the surface of pyrite mineral. An analogy is available in literature in the case of leaching of gold ores that the rate of reaction decreases when the concentrations of competing reactants increases beyond certain limit [140, 141]. It may be calculated from the rate equation mentioned above, that the maximum possible conversion of pyrite by agitation leaching is about 80% at partial pressure of oxygen = 2.15 atm, average particle size = 87 μm, stirring speed = 1000 rpm, temperature = 393 K.

The leaching of pure UO_2 (in a time period of 0 to 6 h) and pure pyrite (in a time period of 0 to 2 h) from a synthetic mixture (with composition similar to that of actual Indian uranium ores) in sodium carbonate and bicarbonate solution (using 5% solids (w/v)), at temperatures between 373 K and 428 K (base level = 413 K), oxygen partial pressure from 7 to 10 atm (base level = 10 atm), Na_2CO_3 and $NaHCO_3$ concentrations between 0.1 M and 1 M (base level=0.5 M), average particle sizes 6 to 253 μm (base level = 87 μm) can be described by the rate equations, Eqs. 5.12 and 5.13, developed in Section 5.3.1:

$$1-\left(1-X_{UO_2}\right)^{\frac{1}{3}} = 0.1147\, {p_{O_2}}^{1.9149}\, [Na_2CO_3]^{0.3647}\, [NaHCO_3]^{0.4255}\, d^{-0.1735}\, e^{-\frac{1637}{T}}\, \mathrm{t} \qquad [5.12]$$

$$1-\left(1-X_{py}\right)^{\frac{1}{3}} = 3489\, {p_{O_2}}^{0.5669}\, [Na_2CO_3]^{-0.31}\, [NaHCO_3]^{-0.4802}\, d^{-0.126}\, e^{-\frac{4465}{T}}\, \mathrm{t} \qquad [5.13]$$

The difference in orders of different leaching parameters between the rate equations developed for UO_2 and pyrite in isolation (Eqs. 5.5 and 8.1) and for synthetic mixture (Eqs. 5.12 and 5.13) is essentially due to the difference in base levels of leaching parameters studied. The temperature and pressure conditions applied for leaching of pure materials (UO_2 and pyrite) are much lower than those applied for leaching of the same materials from synthetic mixture. The phenomenon is in congruence with the remarks of Sohn and Wadsworth [77] that the rate information obtained under a given set of conditions may not be applicable under another set of conditions. In particular, with reference to leaching of pure pyrite in isolation, the orders with respect to carbonate and bicarbonate reagents is negative at high concentrations of Na_2CO_3 and $NaHCO_3$ (Eq. 8.1; for the base level of temperature = 363 K and the base level of P_{O2} = 0.5 atm). On the other hand, since the experiments conducted on synthetic mixture are at higher temperature and pressure as the base levels (temperature = 413 K and P_{O2} = 10 atm), the decomposition of $NaHCO_3$ (reaction (2.9), Section 2.1.3.1) is high leading to higher concentration of Na_2CO_3 in the leach liquors of these experiments. The higher concentration of Na_2CO_3 could be the reason for negative orders of carbonate and bicarbonate reagents in Eq. 5.13 (developed for leaching of pyrite from synthetic mixture) as predicted by Eq. 8.1 (developed for pure pyrite in isolation). Thus Eqs. 8.1 and 5.13 are in agreement with reference to negative reaction orders of carbonate and bicarbonate reagent concentrations.

In another set of leaching experiments conducted on synthetic mixture with varying pyrite content in alkaline media revealed that both FeS_2 and UO_2 are leached at constant rate at temperature = 398 K and partial pressure of oxygen (P_{O2}) = 5.2 atm (total pressure = P_{O2} + P_{H2O} = 7.5 atm). The kinetic rate equation of pyrite oxidation is given by Eq. 5.15 (Section 5.3.2).

$$\frac{dC_{py}}{dt} = 1.437\, W_{py}{}^{1.5347} \qquad [5.15]$$

Where W_{py} is iron pyrite content in the solids (%wt) and C_{py} is amount of pyrite leached per unit volume (mg/L) in time t (min). The rate of dissolution of pyrite increased from 1.17 to 15.83 mg/L-min with increase in pyrite content from 1% to about 6%. The rate of dissolution of UO_2 increased from 0.223 to 0.494 mg/L-min with increase in pyrite content from 1% to about 3% and then decreased beyond 3%. The plots of rates of dissolutions of UO_2 and pyrite (represented in terms of surface area) as a function of pyrite content of synthetic mixture have been shown in Fig. 6.35 (Section 6.3.3). Smaller content of pyrite plays beneficial role in oxidative alkaline leaching of uranium due to the neutralization of NaOH produced by reaction (2.5a). However, when the same is present in excess, the leachability of uranium dioxide decreases which could be due to excessive consumption of dissolved oxygen and carbonate ions (required for UO_2 solubilisation) by FeS_2 and the decrease in pH of the lixiviant to below 9 due to formation of Na_2SO_4 and $NaHCO_3$.

From the results of central composite design of leaching experiments conducted on synthetic mixture, quadratic equations were developed for percent leaching of uranium dioxide (Xu_{O2}) and that of pyrite (Xpy). These equations are valid in the range of temperature from 353 to 403 K and total pressure using oxygen gas in the range of 1 to 10 atm. (Section 5.3.3).

$$X_{UO_2} = \frac{[-191.8 + 4.15(T-273) + 18.24(P) - 0.0544(T-273)(P) - 0.0217(T-273)^2 - 0.622(P)^2]}{100} \qquad [5.16]$$

$$X_{py} = \frac{[-829.7 + 14.315(T-273) + 17.135(P) - 0.0267(T-273)(P) - 0.0586(T-273)^2 - 0.774(P)^2]}{100} \qquad [5.17]$$

A temperature of 353 K and total pressure of 6.5 atm using oxygen gas have been determined as optimum levels to achieve maximum uranium dissolution of 65.4% and minimum extraction (5.4%) of undesirable pyrite from synthetic mixture of minerals.

The characterization studies on Tummalapalle ore revealed that the ore contains about 80% carbonate minerals and the grains of pitchblende are in intimate association with pyrite segregations. About 95% of uranium is present in lighter minerals of the ore as obtained by heavy media separation (Bromoform and Methylene Iodide Lights). The ultra-fine dissemination of uranium in lighter minerals in Tummalapalle calls for fine size grinding for adequate exposure of uranium to the lixiviant during leaching.

The characterization of Gogi ore revealed that the ore contains about 62% calcite along with high pyrites (about 6%), coffinite and pitchblende uranium minerals. Spectrum 1 in Fig. 3.13 [B] of Chapter 3 shows a prominent face of pyrite (cubic system) having a crystalline outline within the gangue minerals, calcite and dolomite. Vein type pyrite is free and liberated (spectrum 4 in Fig. 3.13[B]) in Gogi ore. Spectrum 2 in Fig. 3.13[B] showed a particular portion of a particle containing as much as 39% uranium.

Leaching kinetics of Tummalapalle uranium ore indicated that a mixed control model of both surface chemical reaction and diffusion through the inert particle pores is applicable. The overall rate equation is given by $1-\frac{2}{3}\alpha-(1-\alpha)^{\frac{2}{3}}+\beta[1-(1-\alpha)^{\frac{1}{3}}]=kt$ and $k=40570\,(p_{O_2})^{2.5}\,s^{0.21}\,D^{-5.7}\exp(-4.5/RT)$, where α=fraction of uranium leached, P_{O2}, s, D, T and t expressed as atm, rpm, µm, K and h respectively (Section 6.1.3.1 of Chapter 6).

Alternatively, a pore diffusion model coupling particle size distribution, which represents physical system of Tummalapalle ore leaching more closely, has been applied to the kinetic leaching data generated (Section 6.1.3.2). The effective diffusion coefficient of reactants in leaching of Tummalapalle uranium ore was found to be in the range 0.6×10^{-11} cm^2/s to 5.67×10^{-11} cm^2/s under various conditions of leaching. The effective diffusivity is found to be increasing with increase in partial pressure of oxygen increased from 4.5 to 6.5 atm, which could be due to increased solubility of oxygen at higher partial pressures of oxygen. The diffusivity increased with increase in stirring speed, decrease in particle size. The diffusivity is found to be increasing with increase in temperature with an Arrhenius activation energy (E_a) of 0.78 kJ/mol.

The popular gamma distribution of the leaching rate constant was found to be satisfactorily representing the experimental kinetic data of alkaline leaching of Gogi uranium ore (Section 6.2.3.1). The goodness of fit was found to be always greater than 0.92. The average rate constant of leaching was found to be increasing with increase in temperature, decreasing particle size, increasing partial pressure of oxygen up to a certain limit, increasing stirring speed and increasing Na_2CO_3 concentration. Alternatively, a topochemical model coupling particle size distribution, which represents physical system of the Gogi ore leaching more closely, has been evaluated (Section 6.2.3.2). The overall equation for leaching of uranium is given by

$Fraction\ of\ uranium\ leached = \int_0^{D_t}(m\frac{D^{m-1}}{D_{max}^m})dD + \int_{D_t}^{D_{max}}\left(1-\left(1-\frac{k_n}{D}t\right)^3\right)(m\frac{D^{m-1}}{D_{max}^m})dD,$ where $k_n = 17198\,[Na_2CO_3]^{1.28}e^{-\ln(p_{O_2})(0.37\ln(p_{O_2})+0.23)}e^{-\frac{29300}{RT}}$ and $D_t = k_n t$. The kinetic model fit is in close agreement with the experimental data and possibly can be applied to ores with low silica, high pyrite content and mineralogy similar to Gogi uranium ore. The activation energy of 29.3 kJ/mol supports a reaction controlled mechanism. The rate of leaching of uranium from Gogi ore increased with increasing agitation, concentration of sodium carbonate and temperature. However, there is an optimum oxygen partial pressure. The extraction of uranium is >90% and dissolution of pyrite is <40% at <1 atm oxygen pressure and 90°C. This phenomenon is due to increased dissolution of pyrite at higher than 1 atm pressure of oxygen. Morphological studies using scanning electron microscope with EDX of unleached and leached Gogi ore samples affirmed near complete leaching of uranium and partial leaching of pyrite mineral at 90°C and below 1 atm oxygen pressure.

The leachability of uranium dioxide as well as that of pyrite from the synthetic mixture was insignificant (Figs. 5.51 and 5.52) in the absence of oxygen in a range of temperature (125 to 140°C) and pressure (0 to 10 atm) conditions. In the case of the leaching of actual uranium ore samples, pyrite has not been leached from both Tummalapalle and Gogi uranium ores without oxygen. Leachability (without using oxygen) of uranium has been very low from Tummalapalle ore and high from Gogi ore. This difference between the leachability of two different ores is attributed to the variation in the proportions of U(IV) and U(VI) valence states of uranium in the uranium phases occurring in the ores.

The leachability of uranium from Tummalapalle ore in absence of oxygen was < 10% (Figs. 6.13 through 6.15) at temperatures (90 to 125°C) and pressures (P_{Ar} = 5.2 to 7 atm; P_{CO2} = 1.3 atm). Leachability of uranium from Tummalapalle ore with oxygen gas under optimum conditions of P_{O2} = 5.2 atm and T=125°C is about 80%. Figs. 6.30 and 6.31 reveal that about 40 - 50% uranium could be leached from Gogi ore without the need of oxygen (using either Ar or CO_2 as the inert gases at different temperatures: 90 to 125°C and pressures: 0.5 to 5.5 atm), which indicates high proportion (about 40-50%) of uranium in U(+6) oxidation state, which does not require oxidation for solubilisation. However, leaching of Gogi ore with O_2 gas at 90°C and P_{O2} = 0.5 atm (Figs. 6.30 and 6.31) yielded dissolution (>90%) of uranium.

The experimental and predicted rate of leaching of uranium from pure UO_2 was compared with that from the two Indian uranium ores. The rate of leaching of uranium from Gogi ore has been found to be much higher (Figs. 6.33 and 6.34) than from pure UO_2; the rate of leaching of uranium from Tummalapalle ore has been found to be much lower (Figs. 6.33 and 6.34) than from pure UO_2. Higher (about 50%) and lower (<10%) proportion of uranium in +6 oxidation state in Gogi and Tummalapalle ores respectively are also concluded from the leaching experiments conducted with inert gases (without oxygen) described in Section 6.3.1.

The limitations of the kinetic rate models developed for batch leaching process in the present study are as follows: (1) Different models developed are applicable only for the range of leaching parameters and their base levels indicated for each of the rate equations. It may be noted that the orders of various leaching parameters are sensitive to the base levels at which experiments were conducted, (2) The origin of the UO_2 used for leaching studies on pure materials is sintered UO_2 pellets and not the naturally occurring mineral. Since, the sintered materials may have low specific surface area leading to lower dissolution rates [138], the absolute leaching rates of UO_2 measured in the present study are lower than those given in literature (more details on comparison of leaching rates is given in Section 5.1.2). However, the trends of dissolution rates obtained with UO_2 used in the present study are similar to those of UO_2 reported in the literature, (3) The shape of the particles is assumed to be spherical for all the leaching models developed.

Chapters 5 and 6 included the studies on morphological changes during leaching of synthetic mixture as well as ores. Scanning Electron Micrographs (SEMs) and X-ray diffractograms suggest that alkaline leaching chemically alters pyrite to mainly iron oxide, Fe_2O_3. The conversion of pyrite was near complete at 398 K, $P_{O2} = 5$ atm. in the case of leaching of both synthetic mixture of pure materials and Tummalapalle ore. Partial leaching (< 40%) of pyrite was observed in the case of leaching of Gogi ore at 363 K and $P_{O2} = 0.15$ atm. The SEM image of pure UO_2 particles after leaching revealed number of pits and micro cracks. Unlike pyrites, no new solid phase was observed during leaching of UO_2 as the reaction products of uranium dissolution reaction are soluble. Calcite was found to disintegrate into smaller pieces, while chemically remained unaltered during alkaline leaching. Silica was neither chemically nor physically altered due to leaching.

Finally, a residence time distribution model has been used to relate the conversions of pitchblende and pyrite in laboratory scale batch reactor (5 L) to continuous reactor having multiple stirred tanks connected in series (Chapter 7). Specifically, this relation is applied to predict conversions on pilot scale for a reactor (850 L) having three tanks. The predicted conversion of pitchblende with time in three stirred tank reactors is in good agreement with the measurements on the pilot scale (Fig. 7.4). The recovery of uranium in laboratory batch leaching with Na_2CO_3 (50 g/L) and $NaHCO_3$ (70 g/L) at 125°C and 7.5 atm pressure in a five-liter capacity autoclave in 4 h residence time is 78%. About 77.7% of U_3O_8 values could be leached in three continuous stirred tank reactors in 6.2 h residence time with a flow rate of 140 L/h. Under the same conditions, Residence Time Distribution (RTD) model adopted in the present study predicted a uranium recovery of 78.5%. The predicted conversions of uranium and pyrite were combined with the heat of reactions to calculate the temperatures of the reactor contents. It is predicted that the pyrite content of the Tummalapalle uranium ore should not exceed 3% for maintaining a continuous autoclave temperature below a design value of 200°C for a feed slurry inlet temperature of 110°C (Fig. 7.3). The predicted temperatures of pulp at different residence times matched well with measurements on a pilot scale continuous reactor operated with Tummalapalle ore (Fig. 7.5). The residence time scale model could even predict the leaching efficiencies of uranium and pyrite values, and temperature of the contents in a commercial reactor, about 800 times the size of pilot scale reactor (volume = 850 L). The predictions are useful not only to design continuous leaching of uranium ore on a commercial scale but also to find the limit on pyrite content of the ore to operate commercial reactors below design temperature.

8.2 SCOPE FOR FURTHER RESERACH

The studies carried out under the present doctoral work revealed that a few future studies could be conducted in continuation of the studies presented in this thesis. They are listed below.

- An attempt was made in the present doctoral work to relate the leaching behavior of synthetic mixture of minerals (ideal conditions) to that of actual ores of Indian origin (Section 6.3). Though certain relationships could be identified, scope exists to further examine the differences and the commonalities between the UO_2 in isolation and present in the ore. One can examine the possibility of developing a universal leaching model which can predict leaching of uranium from any ore by plugging in the appropriate characteristics of a given uranium ore. Two properties that influence uranium leaching have been identified in the present study (1) pyrite content of the ore (2) proportion of uranium in +6 oxidation state. Influence of other characteristics of ores such as porosity, active surface area, grain size of uranium minerals and the gangue minerals and their association could be explored.
- Alkaline leaching model for most commonly found uranium mineral, Uraninite, is developed in the present study. As a follow up, other uranium minerals such as

Coffinite, Brannerite likely to occur in uranium ores, may also be studied to develop the corresponding leaching models and compare their rates of dissolution.

- In the present study, particle size distribution is coupled with topochemical leaching model and pore diffusion controlled model developed for Gogi and Tummalapalle ores respectively. However, the particle shape is assumed to be spherical. A shape factor may be attempted to be included in the models developed.
- The loss of sulfur from the leaching feed solids should indicate the corresponding stoichiometric loss of sodium carbonate also according to the reaction (2.8). However, actual values of sodium carbonate present in the leach solutions have found to be much higher indicating production of significant sodium carbonate by the reaction (2.9) [59]. Laboratory and pilot plant studies carried out on Tummalapalle uranium ore in the present work, also have indicated higher concentrations of sodium carbonate in the leach liquors than predicted by reaction (2.8) alone. In this thesis, 25% decomposition of $NaHCO_3$ (at 398 K and $P_{O2} = 5.2$ atm) was considered for predicting the temperature rise in pilot scale leaching of Tummalapalle ore (in Eq. 7.9 of Section 7.4). The value of percent decomposition used in heat balance calculations was excerpted from the literature [59, 172]. There is not much study reported on what fraction of Na_2CO_3 is decomposed according to reaction (2.9). This must be dependent on temperature and pressure during leaching determined by phase equilibrium (Pourbaix) diagrams and decomposition kinetics of sodium bicarbonate. It is worth investigating on this aspect, especially to predict the leach liquor composition with respect to proportion of carbonate-bicarbonate under different conditions of elevated temperatures and pressures.
- In the present study, modeling and simulation of continuous leaching of Tummalapalle uranium ore of Andhra Pradesh, has been illustrated. Similar theoretical exercise can

be carried out using batch leaching kinetic data of Gogi uranium ore at Karnataka in India. The scale up of Gogi uranium leaching from batch to continuous reactor will be of immense use to set up the forthcoming and commited uranium mill at Gogi deposit in India.

- Leaching rate of uranium from synthetic mixture is compared with that from the two Indian uranium ores at Tummalapalle and Gogi (Figs. 6.33 and 6.34). Similar comparison of leaching rate of pyrite from these two ores and that from synthetic mixutre may also be undertaken. Since the reaction of pyrite is exothermic, understanding of the leaching rates of pyrite would help in heat balance calculations to predict the rise in temperature of commercial leach reactor processing the uranium ore.

To summarize, the alkaline leaching process has been modelled for two potential Indian uranium ores. Certain relations have been obtained between the leaching behaviour the actual uranium ores and their constituents in the pure form. An improvised RTD model was used to scale up kinetics of batch leaching process generated in 5 L laboratory autoclave to a three stage pilot plant scale continuous reactor of 850 L capacity. The batch and continuous leaching models developed in the present study will be useful in the design of commercial uranium mills for treating pyritic high carbonate ores.

REFERENCES

1 Pasternak Alan D., 2000. Global Energy Futures and Human Development: A Framework for Analysis, UCRL-ID-140773, US Department of Energy, Lawrence Livermore National Laboratory.

2 Anon, 2015. World Nuclear Association website. http://www.world-nuclear.org (Last accessed in February 2015).

3A Bryndza, A., 2012. 2012 Global Nuclear Markets after Fukushima, LLC: The Ux Consulting Company. http://www.uxc.com (Last accessed in August 2015).

3B Bajaj, S.S., Gore, A.R., 2006. India's Reactors: Past, Present, Future: The Indian PHWR. Nuclear Engineering and Design, Vol 236, 701 – 722.

4 Anon, 2006. Integrated Energy Policy: Report of the Expert Committee. Planning Commission Document, Government of India. http://planningcommission.nic.in/reports/genrep/rep_intengy.pdf (Last accessed in August 2015).

5 Anon, 2015. World Nuclear Association website, http://www.world-nuclear.org/info/Country-Profiles/Countries-G-N/India/ (Last accessed in February 2015).

6 Ganguly C., Slezak J., 2009. IAEA activities on uranium resources and production and databases for the nuclear fuel cycle. URAM 2009, IAEA, Vienna.

7 Yan D. and Connelly D., 2008. Implications of Mineralogy in Uranium Ore Processing. ALTA 2008 Uranium Conference, Perth, Western Australia.

8 Merrit R C., 1971. The Extractive Metallurgy of Uranium, Colorado School of Mines Research Institute, Golden Colorado, United States Atomic Energy Commission, Colorado, 576.

9 Nikkhah Khosrow, H.A., 1998. Autoclave Design and Scale-up from Batch Test Data: A Review of Sizing Methods and Their Bases. SME Preprint Number 98-149, Simons Ltd., http://technology.infomine.com/hydrometmine/papers/K.Nikkhah-autoclave.pdf (last accessed on 29/05/2015).

10 Clark, D.L., Neu, M.P., Runde, W., Keogh, D.W., 2006. Uranium and Uranium Compounds, Kirk-Othmer Encyclopedia of Chemical Technology. John Wiley and Sons, Inc.

11 Peehs, M., Walter, T., S. and Zemek, M., 2007. Uranium, Uranium Alloys, and Uranium Compounds. Ullmann's Encyclopedia of Industrial Chemistry, John Wiley and Sons Inc.

12 Nash J.T., Granger H.C., Adams S.S., 1981. Geology and concepts of genesis of important types of uranium deposits, Economic Geology 75th Annual Volume, 63-116.

13 Dahlkamp Franz J., 1993. Uranium Ore Deposits. Springer-Verlag Berlin Heidelberg, 460.

14 Cuney M., 2009. The extreme diversity of uranium deposits. Mineral Deposita, Vol 44, 3-9.

15 Cuney M., 2010. Evolution of uranium fractionation processes through time; driving the secular variation of uranium deposit types. Economic Geology, Vol 105, 553-569.

16 Cumming GL, Krstic D, 1992. The age of unconformity-related uranium mineralization in the Athabasca basin, northern Saskatchewan. Canadian Journal of Earth Sciences, Vol 29, 1623-1639.

17 Kotzer, T. G., Kyser, T.K., 1993. O, U, and Pb isotopic and chemical variation in uraninite: Implications for determining the temporal and fluid history of ancient terrains. American Mineralogist, Vol 78, 1262-1274.

18 Susan Hall, Coleman Margaret, 2013. Critical analysis of world uranium resources: U.S. Scientific Investigations Report 2012–5239, http://pubs.usgs.gov/sir/2012/5239/sir2012-5239.pdf (Last accessed in August 2015), 7.

19 Anon, 2009. World Distribution of Uranium Deposits (UDEPO) with Uranium Deposit Classification. IAEA-TECDOC-1629, 117.

20 Suri A.K., 2008. Uranium processing – a new alkaline route, Transactions of Indian Institute of Metals, Vol 61 (No. 1), 1-6.

21 Anon, 2014. Uranium 2014: resources, production and demand. A Joint Report by the Organization for Economic Co-operation and Development (OECD) Nuclear Energy Agency and the International Atomic Energy Agency. OECD 2014 NEA No. 7209, 18.

22 Anon, 2015. https://infcis.iaea.org/UDEPO/ (Last accessed in May 2015).

23 Anon, 2014. Web page of Atomic Minerals Directorate for Exploration & Research. http://www.amd.gov.in/regions/sr.htm (Last accessed on 20/12/2014).

24 Anon, 2014. World Nuclear Association website. http://www.world-nuclear.org/info/Nuclear-Fuel-Cycle/Mining-of-Uranium/World-Uranium-Mining-Production/ (Last accessed on 11/12/2014).

25 Parihar P.S., 2013. Uranium and thorium resources in India: UNFC system, Proceedings of National Conference on Sustainable Mining and the United Nations Framework Classification (UNFC) - Challenges and Opportunities in India, New Delhi, India.

26 Taraknath V.K., Woddi, Charlton, Villiam S., Nelson, Paul, 2009. India's Nuclear Fuel Cycle: Unraveling the Impact of U.S.–India Nuclear Accord. Morgan and Claypool publishers, 27.

27 Rai, A.K., Zakaullaa, S., Chaki, A., 2009. Proterozoic strata bound carbonate rock (dolostone) hosted uranium deposits in Vempalle formation in Cuddapah basin, India. International Symposium on Uranium Raw Material for the Nuclear Fuel Cycle, Vienna, Austria, IAEA-CN-175/27, URAM 2009.

28 Suri, A.K., Padmanabhan, N.P.H., Sreenivas, T., Anand Rao, K., Singh, A.K., Shenoy, K.T., Mishra, T., Ghosh, S.K., 2010. Process development studies for low-grade uranium deposit in alkaline host rocks of Tummalapalle. Proceedings IAEA Technical Meeting on Low-grade Uranium Deposits at Vienna, 29–31.

29 Shrivastava, V.K., Parthasarathy, T.N., Sinha, K.K., 1992. Geochemical study of the uraniferous granites from Lambapur area, Nalgonda district, Andhra Pradesh, India. Exploration and Research for Atomic Minerals (EARFAM), Vol 5, 41–52.

30 Padmanabhan N.P.H., A.K. Suri, Ghosh S.K., 2010. R&D input to extraction of uranium from different primary and secondary resources in India. Proceedings of the

XI International Seminar on Mineral Processing Technology (MPT-2010), NML Jamshedpur, 628–641.

31 Chaki, A., Panneerselvam, A., Chavan, S.J., 2005. Uranium exploration in the upper Proterozoic Bhima basin, Karnataka, India: a new target area. Proceedings of International Symposium on Uranium Production and Raw Materials for the Nuclear Fuel Cycle Supply and Demand, Economics, the Environment and Energy Security. International Atomic Energy Agency (IAEA), Vienna, (IAEA-CN-128), 183–194.

32 Civin, V. and Belsky, M., 1966. Status Report from Czechoslovakia, Proceedings of low-grade uranium ores, Panel Proceedings Series. IAEA, Vienna.

33 De-Xin Ding, Hai-Ying Fu, Yong-Jun Ye, Nan Hu, Guang-Yue Li, Jian-Bin Song, Yong-Dong Wang, 2013. A fractal kinetic model for heap leaching of uranium ore with fractal dimension of varied particle size distribution. Hydrometallurgy, Vol 136, 85-92.

34 De Pablo Joan, Ignasi Casa, Javier Gimenez, Mireia Molera, Miquel Rovira, Lara Duro, and Jordi Bruno, 1999. The oxidative dissolution mechanism of uranium dioxide. I. The effect of temperature in hydrogen carbonate medium. Geochimica Acta 63 (No. 19/20), 3097-3103.

35 Giammara Daniel, .E, Cerratoa Jose, M., Vrajesh Mehtaa, Zimeng Wanga, Yin Wanga, Troy J Peppinga, Kai-Uwe Ulricha, Juan S Lezama-Pachecob, and John R Bargar, 2012. Effect of diffusive transport limitations on UO_2 dissolution. Water Research, Vol 46, 6023-6032.

36 Habashi, F., Thurston, G.A., 1967. Kinetics and mechanism of the dissolution of uranium dioxide. Energia Nucleare, Vol 14 (4), 238–245.

37 Schortmann, W.E., DeSesa, M.A., 1958. Kinetics of the dissolution of uranium dioxide in carbonate–bicarbonate solution. Proc. 2nd United Nations Int. Conf. on the Peaceful Uses Atomic Energy, 3. United Nations, Geneva, 333–341.

38 Sharma J.N., Bhattacharya K., Swami R.G., Tangri S.K., Mukherjee T.K., 1996. Studies on the kinetics of UO_2 dissolution in carbonate-bicarbonate medium using sodium hypochlorite as oxidant, Journal of Radioanalytical and Nuclear Chemistry, Letters, 214 (3), 223-233.

39 Levenspiel, O., 2001. Chemical Reaction Engineering. John Wiley & Sons, New York.

40 Galkin, N.P., Sudarikov, B.N., Veryatin, U.D., Shishkov Yu.D., Maiorov A.A., 1966. Technology of Uranium. Israel Program for Scientific Translations Ltd., IPST Cat. No. 1530, S.Monson printers, Jerusalem.

41 Chaki A., 2010. Uranium Occurrences and Exploitation Experience in India, 2010. Proceedings of 3rd International Conference on Uranium & 40th Annual Hydrometallurgy Meeting, Uranium-2010 (CIM), Saskatoon, Saskatchewan, Canada.

42 Gribble, C.D., 2005. Rutley's Elements of Mineralogy, 27th Edition, CBS Publishers, India.

43 Ford William E., 2006. Dana's Textbook of Mineralogy. 4th Edition, CBS Publishers, India.

44 Berry L.G., Brian Mason, 2004. Mineralogy. 1st Edition, CBS Publishers, India.

45 Anon, 2015. http://en.wikipedia.org/wiki/Uraninite (Last accessed in August 2015).

46 Anon, 2015. http://www.miningandmetallurgy.com/mining/uranium-process-flowsheet (Last accessed in August 2015).

47 Sen S., Murthy T.K.S., 1980. Ore processing and refining of uranium in India. Proceedings of an advisory group meeting, Paris, International Atomic Energy Agency, Vienna

48 Anon, 1999. Developments in uranium resources, production, demand and the environment, Proceedings of a technical committee meeting held in Vienna, June 1999, IAEA-TECDOC-1425.

49 Gupta C.K., Singh, H., 2003. Uranium resource processing – secondary resources. Springer.

50 Botella T., Gasos P., 1989. Recovery of uranium from phosphoric acid: An overview, IAEA-TECDOC-533, IAEA, Vienna.

51 Ragheb Magdi, Khasawneh Mohammed, 2010. Uranium fuel as byproduct of phosphate fertilizer production. Proceedings of the 1st International Nuclear and Renewable Energy Conference (INREC10), Amman, Jordan.

52 Mattus A.J., Torma A.E., 1980. A comparison of carbonate leaching of a low-grade uranium ore at atmospheric and increased pressures, Hydrometallurgy, Vol 5, 179-190.

53A Clegg J.W., Foley Dennis D, 1958. Uranium ore processing, Addison- Wesley.

53B Haque, K.E. and Ritcey, G.M., 1982. Comparison of oxidants for the leaching of uranium ores in sulphuric acid. CIM Bulletin, Vol 75 (841), 127-133.

54 Brookins, Douglas G., 1988. Eh-pH Diagrams for Geochemistry, Springer-Verlag, New York.

55 Roodt J., Sandenbergh R.F., 2003. Characterization of the leaching properties of a uranium leaching pulp. The Journal of the South African Institute of Mining and Metallurgy, Vol 103, 111-112.

56 Filippov, A.P., Kanevskii, E.A., 1964. Oxidation-reduction potentials and the degree of uranium leaching in sulphuric acid solutions. Journal of Nuclear Energy, Vol 19, 575–580.

57 Anon, 1993. Uranium Extraction Technology. Technical reports series no. 359, International Atomic Energy Agency, Vienna, 80.

58 Du Preez, J.G.H., Morris, D.C., Van Vuuren, C.P.J., 1981. The chemistry of uranium, part XXVII. Kinetics of the dissolution of uranium dioxide powder in a solution containing sodium carbonate, sodium bicarbonate and potassium cyanide. Hydrometallurgy, Vol 6, 197–201.

59 Du Preez J G H, Morris D C, Van Vuuren C P J, 1981. The chemistry of uranium, part XXVIII. The development of a combined gold and uranium leach of randfontein ore, Hydrometallurgy, Vol 6, 203.

60 Caldeira, C.L., Ciminelli, V.S.T., Dias, A., Osseo-Asare, K., 2003. Pyrite oxidation in alkaline solutions: nature of the product layer. International Journal of Mineral Processing. 72, 373-386.

61 Anon, 2001. Manual of acid in situ leach uranium mining technology. IAEA-TECDOC-1239, IAEA, Vienna.

62 Anon, 1990. Manual on Laboratory Testing of Uranium Ore Processing. Technical reports series no. 313, International Atomic Energy Agency, p 45, 107.

63 Anon, 2015. https://en.wikipedia.org/wiki/Uranyl (Last accessed in August 2015).

64 McKay A. D., Miezitis Y., 2001. Australia's uranium resources, geology and development of deposits. In: AGSO-Geoscience Australia, Mineral Resource Report 1, 119.

65 Anon, 2015. http://www.aph.gov.au/ (Last accessed in August 2015).

66 Anon, 2011. Mining Activity in Wiluna – MidWest Development Commission, A report published by Urbis Pty Ltd, Australia. http://www.wiluna.wa.gov.au/Assets/Documents/Document-Centre/Public-ocuments/Mining-in-Wiluna-Economic-Report.pdf (Last Accessed in August 2015).

67 Anon, 2015. http://www.mining-technology.com/projects/trekkopje-mine/ (Last accessed in August 2015).

68 Gupta R., Pandey V.M., Pranesh S.R., Chakravarty A.B., 2004. Study of an improved technique for precipitation of uranium from eluted solution. Hydrometallurgy, Vol 71, Issues 3-4, 429-434.

69 Suri A.K., Sreenivas T., 2012. Developments in processing of conventional uranium ore resources of India. Proceedings of XXVI International Mineral Processing Congress (IMPC 2012), New Delhi, India, 5282.

70 Anon, 2015. http://www.ucil.gov.in/turamdihmill.html (Last accessed in August 2015).

71 Hossain Mohammad Mohsin, Ella Ekeroth, Mats Jonsson, 2006. Effects of HCO_3 - on the kinetics of UO_2 oxidation by H_2O_2. Journal of Nuclear Materials, Vol 358, 202-208.

72 Harris C.C. and Chakravarti A, 1970. Semi-Batch Froth Flotation Kinetics: Species Distribution Analysis. Trans. Am. Inst. Min. Engrs., Vol. 247 p 162.

73 Demirkiran Nizamettin and Kunkul Asim, 2007. Dissolution kinetics of ulexite in perchloric acid solutions. International Journal of Mineral Processing, Vol 83, 76-80.

74 Burkin, A.R., 2001. Chemical Hydrometallurgy, Imperial College Press, London, 271.

75 Ruitenberg R., Hansford G.S., Reuter M.A., Breed A.W., 1999. The ferric leaching kinetics of arsenopyrite. Hydrometallurgy, Vol 52, 37-53.

76 Song Jian, Gao Ling, Lin Jianqun, Wu Hongbin, Lin Jianquiang, 2013. Kinetics and modeling of chemical leaching of sphalerite concentrate using ferric iron in a redox-controlled reactor. Chinese Journal of Chemical Engineering, 21 (8), 933-936.

77 Sohn H.Y., Wadsworth Milton E., 1979. Rate Processes of Extractive Metallurgy, Plenum Press, New York.

78 Sylvie C. Bouffard, Berny F. Rivera-Vasquez, David G. Dixon, 2006. Leaching kinetics and stiochiometry of pyrite oxidation from a pyrite-marcasite concentrate in acid ferric sulfate media. Hydrometallurgy, Vol 84, 225-238.

79 Forward, F.A., Halpern, J., Peters, E., 1953. Studies in the carbonate leaching of uranium ores. The Canadian Mining and Metallurgical Bulletin, 634-644.

80 Peters E., Halpern J., 1953. Kinetics of the dissolution of pitchblende. Canadian Mining and Metallurgical Bulletin, Vol 56, 350-354.

81 Needes C.R.S. Nicol M.J. and Finkelstein N.P., 1975. Electrochemical model for the leaching of uranium dioxide: 2 - alkaline carbonate media. In Leaching and reduction in Hydrometallurgy, (ed) Burkin A.R., London, Institution of Mining and Metallurgy (IMM), 12-9.

82 Shane M. Peper, Lia F. Brodnax, Stephanie E. Field, Ralph A. Zehnder, Scott N. Valdez, Wolfgang H. Runde, 2004. Kinetic study of the oxidative dissolution of UO_2 in aqueous carbonate media. Ind. Eng. Chem. Res., Vol 43, 8188-8193.

83 Kweto B., Groot D.R., Stassen E., Suthiram J. and Zeevaart J.R., 2014. Kinetic study of uranium residue dissolution in ammonium carbonate media, Journal of Radio Analytical and Nuclear Chemistry, Vol 302, 131-137.

84 Smith S.C., Peper S.M., Douglas M., Ziegelgruber K.L., Finn E.C., 2009. Dissolution of uranium oxides under alkaline oxidizing conditions, Journal of Radio Analytical and Nuclear Chemistry, Vol 282 (2), 617-621.

85 Hiskey, J.B., 1979. Kinetics of uranium dioxide dissolution in ammonium carbonate. Trans. Inst. Min. Metall., C145–C152.

86 Hiskey, J.B., 1980. Hydrogen peroxide leaching of uranium in carbonate solutions. The Institution of Mining and Metallurgy, C145-C152.

87 Clarens F., de Pablo J., Casa I., Gimenez J., Rovira M., Merino J., Cera E., Bruno J., Quinones J., Martinez-Exparza A., 2005. The oxidative dissolution of unirradiated UO_2 by hydrogen peroxide as a function of pH. Journal of Nuclear Materials, Vol 345, 225-231.

88 Pearson, R.L., Wadsworth, M.E., 1958. A kinetic study of the dissolution of UO_2 in carbonate solution. Trans. Metall. A.I.M.E., Vol 212, 294-300.

90 Casas Ignasi, Borrel M., Sanchez L., De Peblo J., Gimenez J., Clarens F., 2008. J Determination of $UO_2(s)$ dissolution rates in a hydrogen peroxide medium as a function of pressure and temperature. Journal of Nuclear Materials, Vol 375 (Issue 1), 151-156.

91A Magno P.J., DeSesa M.A., 1957. Oxidants in carbonate leaching of uraninferous ores. USAEC Report WIN-86, National Lead Co., Inc.

91B Grandstaff D.E., 1976. A kinetic study of the dissolution of uraninite. Economic Geology and the Bulletin of the society of economic geologists, Vol 71 (No.8), 1493-1506.

92 Ciminelli, V.S.T., Osseo-Asare, K., 1995. Kinetics of pyrite oxidation in sodium carbonate solutions. Metallurgical and Materials Transactions B, Vol 26 B, 209-218.

93 Joshi J.B., Shah Y.T., Albal R.S., 1982. Effect of pH on the removal of pyritic sulphur from coal by oxydesulfurization. Ind. Eng. Chem. Process. Des. Dev., Vol 21, 594-600.

94 Guilinger Terry R., Robert S. Schechter, Larry W. Lake, 1987. Kinetic study of pyrite oxidation in basic carbonate solutions, Ind. Eng. Chem. Res., Vol 26, 824-830.

95 Nicholson, R.V., Gillham, R.W., Reardon, E.J., 1988. Pyrite oxidation in carbonate-buffered solution: 1. Experimental kinetics. Geochimica et Cosmochimica Acta, Vol 52, 1077–1085.

96 Hood, T. A., 1991. The kinetics of pyrite oxidation in alkaline systems. Ph. D. thesis, University of Miami, United States.

97 Evangelou V. P. B., 1995. Pyrite oxidation and its control. CRC Press, Inc., Boca Raton, Florida, 293 p.

98 Evangelou V. P., Huang X., 1994. Infrared spectroscopy evidence of an iron(II)-carbonate complex on the surface of pyrite. Spectrochim. Acta 50A, 1133–1340.

99 Descostes M., Beaucaire C., Mercier F., Savoye S., Sow J., Zuddas P., 2002. Effect of carbonate ions on pyrite (FeS2) dissolution. Bull. Soc. Geol. Fr., Vol 173, 265–270.

100 Bailey L. K., Peters E., 1976. Decomposition of pyrite in acids by pressure leaching and anodization: the case for electrochemical mechanism. Canadian Metallurgical Quarterly, 15, 333–344.

101 Wei D. and Osseo-Asare K., 1997. Semiconductor electrochemistry of particulate pyrite: mechanisms and products of dissolution.J. Electrochem. Soc., Vol 144, 546–553.

102 Mishra K. K., Osseo-Asare K., 1988. Aspects of the interfacial electrochemistry of semiconductor pyrite (FeS2). Journal of Electrochemical Society, Vol 135, 2502–2509.

103 De Andrade Lima L.R.P., 2004. A mathematical model for isothermal heap and column leaching, Brazilian Journal of Chemical Engineering, Vol 21, No. 03, 435-447.

104 Abrahan Barriga Vilca, 2013. Studies on the curing and leaching kinetics of mixed copper ores. Thesis, Master of Applied Science, The university of British Columbia, Vancouver.

105 Mason C.F.V., Turney W.R.J.R., Thomson B.M., Longmire N.LU.P.A., Chisholm-Brause C.J., 1997. Carbonate leaching of uranium from contaminated soils. Environmental Science and Technology, Vol 31, 2707-2711.

106 Ping Zhon, Baohua Gu, 2005. Extraction of oxidized and reduced forms of uranium from contaminated soils: Effects of carbonate concentration and pH. Environmental Science and Technology, Vol 39 (12), 4435-4440.

107 Trygve E. Eriksen, David W. Shoesmith, Mats Jonsson, 2012. Radiation induced dissolution of UO_2 based nuclear fuel – A critical review of predictive modelling approaches. Journal of Nuclear Materials, Vol 420, 409-423.

108 Torma, A.E., Pendleton, N.R. and Fleming, W.M., 1985. Sodium carbonate-bicarbonate leaching of a new mexico uranium ore and removal of long half-life radio nuclides from the leach residue. Uranium 2, 17-36.

109 Henein, H., Biegler, L.T., 1988. Optimization of Reactor Volumes for Topochemical Reactions. Trans. Inst. Min. Metall., Vol 97, C215-223.

110 Pritzker, M.D., 1993. Reactor design for topochemical leaching reactions taking into account simultaneous depletion of solid and aqueous reactants. Transactions of Institution of Mining and Metallurgy (Section C: Mineral Processing and Extractive Metallurgy), Vol 102, C149-C158.

111 Peters, E., 1991. The Mathematical modelling of Leaching systems. Journal of Metals, 20-26.

112 Dixon David, G., 1995. Improved methods for the design of multistage leaching systems, Hydrometallurgy, Vol 39, 337-351.

113 Crundwell F.K., Bryson A.W., 1992. The modeling of particulate leaching reactors-the population balance approach. Hydrometallurgy, Vol 29, 275-295.

114 Crundwell F.K., 1995. Progress in the mathematical modeling of leaching reactors, Hydrometallurgy, Vol 39, 321-335.

115 Crundwell, F.K., Preez, N. Du., Lloyd, J.M., 2013. Dynamics of particle-size distributions in continuous leaching reactors and autoclaves. Hydrometallurgy, Vol 133, 44-50.

116 Rubisov, D.H., Papengelakis, V.G., 1995. Model-based analysis of pressure oxidation autoclave behavior during process upsets. Hydrometallurgy, Vol 39, 377-389.

117 Sarkar, K.M., 1985. Selection of autoclaves in hydrometallurgical operations. Mineral Processing and Extractive Metallurgy, 94C.

118 Bouffard Sylvie, C., Dixon David, G., 2007. Evaluation of kinetic and diffusion phenomena in cyanide leaching of crushed and run-of-mine gold ores. Hydrometallurgy, Vol 86, 63-71.

119 Bartlett Robert, W., 1972. Pore diffusion-limited metallurgical extraction from ground ore particles. Metallurgical Transactions, Vol 3, 913-917.

120 Vu, H., Bernardi, J., Jandova, J., Vaculikova, L Golias, V., 2013. Lithium and rubidium extraction from zinnwaldite by alkali digestion process: Sintering mechanism and leaching kinetics. International Journal of Mineral Processing, Vol 123, 9-17.

121 Wang Xiaolong and Maroto-Valer M Mercedes, 2011. Dissolution of serpentine using recyclable ammonium salts for CO_2 mineral carbonation. Fuel, Vol 90, 1229-1237.

122 Fabiano, M.F., Santos, Pablo S Pina, Rodrigo Porcaro, Victor, A., Oliveira, Carlos, A., Silva, Versiane A Leao, 2010. The kinetics of zinc silicate leaching in sodium hydroxide. Hydrometallurgy, Vol 102, 43-49.

123 Christine Chin Choy, George P. Korfiatis, XiaoguangMeng, 2006. Removal of depleted uranium from contaminated soils, Journal of Hazardous Materials, Vol 136, 53–60.

124 Nunez, C. and Espiell, F., 1985. Kinetic model for the chemical dissolution of multi particle systems. Metallurgical Transactions B, Vol 16B, 449-454.

125 Suni, J., Henein, H., Warren, G.W. and Reddy, D., 1989. Modelling the leaching kinetics of a sphalerite concentrate size distribution in ferric chloride solution. Hydrometallurgy, Vol 22, 25-38.

126 Gbor Philip K., Jia Charles Q., 2004. Critical evaluation of coupling particle size distribution with the shrinking core model. Chemical Engineering Science, Vol 59, 1979-1987.

127 Grenman Henrik, Malin Ingves, Johan Warna, Jukka Corander, Dmitry Yu. Murzin, Tapio Salmi, 2011. Common potholes in modeling solid-liquid reactions – methods for avoiding them, Chemical Engineering Science, Vol 66, 4459-4467.

128 Mathew, K. J., Burger, S., Vogt, S., Mason, P., Morales-Arteaga, M.E., Narayanan, U.I., 2009. Uranium assay determination using Davis and Gray titration: an overview and implementation of GUM for uncertainty evaluation. Journal of Radio analytical & Nuclear Chemistry, Vol 282 Issue 3, 939.

129 Sunitha V., Muralidhara Reddy B., Ramakrishna Reddy M., 2014. Mineral Resources of Cuddapah Basin. Journal of Biological and Chemical Research, Vol 31 (1), 226-235.

130 Minati Roy, Dhana Raju, R., 1999. Mineragraphy and electron microprobe study of the u-phases and pyrite of the dolostone-hosted uranium deposit at tummalapalle, cuddapah district, Andhra Pradesh and its implication on genesis and exploitation. Journal of Applied Geochemsitry, Vol 1 (No.2), 53-75.

131A Anon, 1926. Operating manual of Frantz Isodynamic separator model L-1, serial no. 1926.

131B Malghan, S. G., Van Dillen, J. P., 2007. TECHNICAL NOTE - Influence of Process Variables in the High Gradient Separation of Uranium Ores. Mining Engineering, Vol 7.

132 Srikantappa, C., Govindaiah, S., 2010. Nature and composition of basement and basinal fluids in the Proterozoic U-bearing sediments around Deshnur, Kaladgi Basin, Karnataka. The Indian Mineralogist, Vol 44 (1), 1–7.

133 Vogel, A.I., 1961. A text-book of Quantitative Inorganic Analysis including elementary instrumental analysis. 3rd edition, Longman group limited, London.

134 Sandell E.B., 1959. Colorometric Determination of Traces of Metals. Interscience Publishers, Inc., New York.

135 Potts P.J., 1992. A Handbook of Silicate Rock Analysis, Springer, United States.

136 Anand Rao, K., Suri, A.K., 2014. Application of a topochemical reaction model to predict leaching behaviour of high carbonate uranium ores in alkaline solutions: an experimental case study. Hydrometallurgy, Vol 141, 67–75.

137 Balaceanu, Jean C., Fernand Coussemant, Fernand, Mouret, 1958. Oxidizing Lixiviation of Pitchblendes and Precipitation of the Uranium with Hydrogen. Proceedings of 2nd International conference on the peaceful uses of Atomic Energy, Vol 3, 363-377.

138 Olivia Roth, 2005. Physical and Chemical aspects of Radiation Induced Oxidative Dissolution. Licentiate Thesis, School of Chemical Science and Engineering, Royal Institute of Technology, Stockholm, Sweden.

139 Mahabub Alam Bhuiyam, Shamina Choudhury, Shaik Manjura Hoque, 2012. Validation of transport properties and apparent density of soft nickel ferrite. Journal of Bangladesh Academy of Sciences, Vol 36 (No.1), 137-142.

140 Marsden and House, 1992. The chemistry of gold extraction. Society for Mining, Metallurgy, and Exploration, Inc (SME), 260-295.

141 Parga J.R., Valenzuela J.L., Cepeda F., 2007. Pressure Cyanide Leaching for Precious Metals Recovery. Journal of Metals, Vol 10, 43-47.

142 Laidler, K.J., 1965. Chemical Kinetics, Second ed., McGraw-Hill Book Co., New York.

143 Burkin, A.R., Edwards. A.M., 1963. Proceedings of the 6th International Congress on Mineral Processing, Cannes, pp 159-169.

145 Padmanabhan N. P.H., Sreenivas T., Anand Rao K., Manmadha Rao M., Rajan K.C., Serajuddin Md., and Karthikayini P., 2010. Process Development Studies for the Recovery of Uranium from the Gogi Limestone-type Ore, An Unpublished Internal Report, Mineral Processing Division, Bhabha Atomic Research Centre, Hyderabad, 104.

146 Fogler, H. Scott., 2004. Elements of Chemical Reaction Engineering. Prentice-Hall, U.S.A., 3rd Edition, 811.

147 Maria Gavrilescu, Lucian Vasile Pavel, and Igor Cretescu, 2009. Characterization and remediation of soils contaminated with uranium. Journal of Hazardous Materials, 163, 475-510.

148 Douglas C. Montgomery, 2013. Design and Analysis of Experiments, 8th Edition, Wiley India.

149 Box G.E.P., Hunter J.S. and Hunter W.G., 2005. Statistics for Experimenters Design Innovation and Discovery. 2nd Edition, John Wiley and Sons, New York.

150 Box G.E.P., Hunter J.S., 1957. Multi-factor experimental design for exploring response surfaces. Annals of Mathematical Statistics, Vol 28, 195–241.

151 Obeng D.P., Morrell S., Napier-Munn T.J., 2005. Application of central composite rotatable design to modelling the effect of some operating variables on the performance of the three-product cyclone. International Journal of Mineral Processing, Vol 76, 181–192.

152 Derringer G., Suich R., 1980. Simultaneous Optimization of Several Response Variables. Journal of Quality Technology, Vol 12, 214-219.

153 Mari Lundstrom, Jari Aromaa, Forsen O., 2011. Microscopy and XRD investigations of the product layer formed during chalcopyrite leaching in copper(II) chloride solutions. Physicochemical Problems of Mineral Processing 46, http://www.dbc.wroc.pl/Content/10110/46_2011.pdf (Last accessed in August 2015), 263.

154 Nizamettin Demirkiran etal, 2007. Dissolution kinetics of ulexite in perchloric acid solutions. International Journal of Mineral Processing, Vol 83, 79.

155 Shaohua Ju, Tang Motang, Yang Shenghai, Li Yingnian, 2005. Dissolution kinetics of smithsonite ore in ammonium chloride solution, Hydrometallurgy, Vol 80, 67-74.

156 Prosser Alan P., 1996, Review of uncertainty in the collection and interpretation of leaching data. Hydrometallurgy, Vol 41, 133.

157 Roach,G,I,D., Prosser,A,P., 1978. Prediction of rates of chemical processes for treatment of low-grade materials: theory and tests for mass transfer controlled reactions. Institution of Mining and Metallurgy, C129-C137.

158 Murhammer, D., Davis, D., Levenspiel, O., 1986. Shrinking core model/reaction control for a wide size distribution of solids. Chemical Engineering Journal, Vol 32, 87-91.

159 Kelly,E,G., Spottiswood,D,J., 1982. Introduction to Mineral Processing, John Wiley, 26.

160 Jost, W., 1960. Diffusion in solids, liquids, gases. Academic Press Inc., New York, 46.

161 Perry, J.H., 1999. Chemical Engineers Handbook, McGraw-Hill, USA, p 23-15.

162 Kapur P. C., Mehrotra S.P., 1974. Estimation of the flotation rate distributions by numerical inversion of the laplace transform, Chemical Engineering Science, Vol 29, 411-415.

163 Imaizumi, T., Inoue, T, 1965. Kinetic considerations of froth flotation. Proceedings 6th International Mineral Processing Congress, Pergamon Press, New York, pp 581-593.

164 Inou, T., Imaizumi, T., 1968. Some aspects of flotation kinetics. Paper S-15, 8th International Mineral Processng Congress, Leningrad, Russia.

165 Regina, O., Ajemba and Okechukwu D Onukwuli, 2012. Application of the shrinking core model to the analysis of alumina leaching from ukpor clay using nitric acid. International Journal of Engineering Research & Technology, Vol 1, Issue 3, 1-13.

166 Reddy L. S .R., 2007. An Unpublished Internal Report of Atomic Minerals Directorate for Exploration and Research, Department of Atomic Energy, Government of India, (Report No.: AMD / PET/HYD / ODG - 17/ 2007).

167 Minati Roy, 2000. Petromineralogical studies of a carbonate rock-hosted uranium deposit at Tummalapalle, Cuddapah district, A.P., Visakha Science Journal, Vol 4 (1), 67.

168 Suri A.K, Sreenivas T., Anand Rao K., Rajan K.C., Srinivas K., Singh A.K., Shenoy K.T., Mishra T., Padmanabhan N.P.H., Ghosh S.K., 2014. Process development studies for the recovery of uranium and sodium sulfate from a low grade dolostone hosted stratabound type uranium ore deposit. Mineral Processing and Extractive Metallurgy (Trans. Inst. Min. Metall. Sec. C), Vol 123 (Issue 2), 104-115.

169 Latha A., Sharma A. K., Vishwamohan K., 2009. An unpublished Internal Report of Atomic Minerals Directorate for Exploration and Research, Department of Atomic Energy, Government of India, (Report No.: AMD / PET/12/ 2009).

170 Latha A, Sharma A K, Fahmi S and Shivakumar K, 2012. Mineralogical characterisation of mine sample of Gogi uranium ore deposit, Karnataka. Journal of Applied Geochemistry, Vol 14 (3), 316.

171 Paphane B.D., Nkoane B.B.M., Oyetunji O.A., 2013. Kinetic studies on the leaching reactions in the autoclave circuit of the Tati Hydrometallurgical Demonstration Plant. The Journal of The Southern African Institute of Mining and Metallurgy, Vol 113, 485 - 489.

172 Padmanabhan, N.P.H., Sreenivas, T., Anand Rao, K., Manmadha Rao M., Rajan, K.C., 2009. An unpublished internal report on process development studies for the recovery of uranium from Tummalapalle deposit. Mineral Processing Division, Bhabha Atomic Research Centre, Hyderabad, 35.